Contract 950327

CONSOLIDATED SYSTEMS

A FEASIBILITY STUDY OF THE MASS SPECTROMETER INSTRUMENTATION FOR THE ANALYSIS OF THE MARTIAN ATMOSPHERE

Prepared for

JET PROPULSION LABORATORY

CALIFORNIA INSTITUTE OF TECHNOLOGY

By

CONSOLIDATED SYSTEMS CORPORATION

Space Sciences Department

7 September 1962

CONSOLIDATED SYSTEMS CORPORATION
1500 SO. SHAMROCK AVE., MONROVIA, CALIFORNIA

CONSOLIDATED SYSTEMS CORPORATION
1500 SOUTH SHAMROCK AVENUE, MONROVIA, CALIFORNIA

Telephone ELliott 9-9111
TWX: MONR 8319-U

7 September 1962

Jet Propulsion Laboratory
4800 Oak Grove Drive
Pasadena 3, California

Attention: Mr. Charles S. Chuh
Cognizant Contract Negotiator

Subject: Contract No. 950327 under NAS 7-100
CSC Register No. 41-3494

Reference: Final Report on Design Study of Mass Spectrometer Instrumentation for the Analysis of the Martian Atmosphere

Gentlemen:

Enclosed please find ten (10) copies and one (1) reproducible of the Final Report on CSC Register No. 41-3494.

If we can be of assistance in answering any questions you may have concerning this report, please contact us.

Sincerely,

CONSOLIDATED SYSTEMS CORPORATION

W. J. Whistler
Manager
Space Sciences

WJW:gb

enclosures

ABSTRACT

11743

The feasibility of a mass spectrometer analysis of the Martian atmosphere was investigated. The mass spectrometer system must yield accurate analytical data in the presence of imposing restrictions on instrument size, weight, power, and magnetic fringe field; sample time and conditions; and transmitting channel capacity. The proposed analyzer is the Paul instrument known as quadrupole mass filter. A general theoretical analysis of the quadrupole analyzer was carried out discussing resolution, transmission efficiency, and power requirements. Theoretical analyses were also performed on the electron bombardment and alpha ion sources; thermal and perfect imaging focal systems; Knudsen flow, getter ion pumping, electrometer detectors, and data handling techniques. Several new getter ion pumps were also investigated.

An experimental analyzer was constructed with r_o = 0.100" and the rod length equal to 6". This was mated with a non-magnetic parabolic electron trajectory ion source. An experimental logarithmic electrometer with a dynamic range of 10^5 and 10^{-13} amp sensitivity was also built and tested. In addition a weak magnetic field getter ion pump was tested and looks promising. A means was developed for producing an inlet leak with molecular flow properties across a pressure drop of 140 mb. The conclusions reached are that a system can be built along the lines indicated by the experimental work which will meet the analytical requirements. This system will weigh around seven pounds and demand an average power of less than eight watts.

TABLE OF CONTENTS

TABLE OF CONTENTS (Continued)

TABLE OF CONTENTS (Continued)

1.0 STATEMENT OF THE PROBLEM

1.10 BOUNDARY CONDITIONS[1]

The environment of the Martian atmosphere, the general requirements for compatibility with the space capsule, and the performance required can be considered to form a set of boundary conditions which are applied to the system variables to arrive at a workable solution. These boundary conditions are stated below.

1.11 Information Requirements

One or more samples of the Martian atmosphere are to be examined to determine the constituents and their relative abundances. A mass range of 12 a.m.u. to 50 a.m.u. is considered adequate for this purpose. It is also expected that the mass spectrometer would furnish data on the absolute pressure. This can be used as a cross check on the other pressure measuring devices. The accuracy of these measurements is expected to be ±10% on 1% components and ±5% or better on 80% components.

The detectible limit is set at 0.1 volume percent.

The 1% resolution is to be $\frac{M}{\Delta M} = 25$ or better.

1 Most of this information is taken from JPL Statement of Work SW-2751 January 12, 1962

1.12 Assumed Model of Martian Atmosphere

The important parameters of the Martian atmosphere are listed below with their expected values:

Pressure at surface: $40\ mb < P_s < 140\ mb$

Composition (volume %):

$0 < H_2O < 0.1\%$ (vapor)

$0 < N_2 < 100\%$

$0 < CO_2 < 15\%$

$0 < O_2 < 10\%$

$0 < Ar < 20\%$

Temperature at surface: $200°K < T_s < 300°K$

Density at the surface: $4.6 \times 10^{-5}\ gm/cm^3 < P_s < 2.4 \times 10^{-4}\ \frac{gm}{cm^3}$

The capsule will fall through the atmosphere with a velocity between 50 to 150 ft./sec.

1.13 Sampling Limits and Measurement Duration

1.13.1 Falling Through Atmosphere

It is expected that the required information will be obtained while the capsule is falling through the atmosphere. The maximum analysis plus data transmission time will be no more than 20 minutes and not less than 5 minutes. The time taken to scan a spectrum must be in the range 20 to 60 seconds. The probable range in the sampling limits during the fall is expected to be:

P = 15 mb to 140 mb

T = 150°K to 300°K

$\rho = 3.5 \times 10^{-5}$ gm/cm^3 TO 2.4×10^{-4} gm/cm^3

The change in composition of the atmosphere over the sampling height is expected to be negligible with the possible exception of H_2O.

1.13.2 After Impact

It is hoped that the capsule will remain operative after impace in which case it is expected that the mass spectrometer would continue sampling. However, it is realized that the probability of surviving intact is not too high and therefore, it is important that as much data as possible is extracted during free fall.

1.14 Available Power

The average power requirement of the mass spectrometer system is not to exceed 6 watts during operation. The peak power at any time during operation may exceed this value by a factor of 10 or 50. The forms of power available on the space craft are:

a. 28v d-c.

b. 2400 cps, 100v p-p square wave with a voltage regulation of ±2%.

c. 26v rms, 400 cps, 3 phase sinusoidal wave.

1.15 Size and Weight

The mass spectrometer package including all support equipment such as a pump, detector, etc., should weigh no more than 5 pounds. The volume of the unit shall not exceed 800 cc/pound.

This is equivalent to 245 cubic inches for a five pound package. The package should have a rectangular shape with a reasonable length/width ratio (2:1).

1.16 Environmental Constraints

The scientific package must be designed to survive the following environmental extremes:

a. Sterilization - bake out at 135°C for 28 hours. Non-operative during this time.

b. Vibration - white gaussian noise, 15-1500 cps in three orthoganal directions. Sequentially, 15G for 6 sec., 10G for 180 sec., 4 1/2G for 360 sec.

c. Shock - 200G for 0.5-1.5 milliseconds, thermal peak, sawtooth shocks in three orthogonal directions.

d. Temperature - 150°K to 400°K.

e. Transit Time - 6 months.

1.17 Channel Capacity

The total number of binary data bits assigned to the mass spectrometer output which can be transmitted from the capsule during its fall is 1000. Two of the spectra will be telemetered back to earth, therefore, there will be

only 500 bits available per scan. The output of the mass spectrometer may be either analog or digital but a voltage range of 0-5 volts is required.

1.18 Magnetic Leakage Field

Because there is a magnetometer on the space bus, the magnetic leakage field from the mass spectrometer package cannot exceed 1 gamma (10^{-5} gauss) at three feet. This is a very strict requirement and strongly suggests a non-magnetic system be designed.

1.20 FIRST ORDER REQUIREMENTS

From the boundary conditions of the problem which have been stated in the preceding section a number of the system variables are partially or wholly determined. These requirements are discussed in this section.

1.21 Speed of Measurement

From the Schilling[2] report, the value for the scale height of the Martian atmosphere near the surface has been calculated to be the order of 19 kilometers.

The rate of fall is stated to be between 50 and 150 ft./sec. If it is assumed that the larger value is for the maximum sample height and the smaller rate is near ground height it can be shown that the rate of change of density will lie between 0.035 and 0.08%/second.

2 G. F. Schilling, Rand Report RM-2782-JPL, June 22, 1962.

In order to accomplish an analysis within a period of less than 5% change in density, the analysis time would have to be less than or equal to 62 seconds. One minute would be a reasonable scan time.

For the mass range m/e 12 to 50, the analysis could conceivably be done by; a) simultaneous analysis of the peaks of interest; b) spectrum stepped from peak to peak; c) selected peaks stepped according to a preset estimate of composition; d) by scanning the complete spectrum. If the spectrum is scanned linearly with time in a total time of 60 seconds there would be 1.58 sec./peak. However, at the stated resolution of 1/25 the peak base width at mass 12 is about half the above value or 0.75 sec. The detector response time would have to be 0.1 to 0.2 sec., the exact value depending upon the peak shape.

For stepped or selected data, the time per peak would be T/N where N is the number of peaks selected. For 1% reading accuracy $\tau = (1/5)(T/N)$. If 38 readings are made in 60 seconds, τ = 3.16 sec. Actually, more than 1 reading per mass position may be taken. If 50 readings are made, this would imply τ = 0.25 sec. It is apparent that the stepped mode of operationis somewhat less restrictive upon the detector time constant. The simultaneous analysis of the peaks would place a less rigid requirement on the detector; however, this would imply selected peaks with one detector per monitored mass. Neither of these requirements is very appealing, the first from the

standpoint of possible restrictionof data and the second from the standpoint of additional weight and power required for N detectors. Based upon these considerations, a stepped system appears to be the most advantageous.

1.22 Type of Pumping

Because of required sampling time desirability of more than one sample and the minimum value to which the incoming flow can be restricted, it is evident that a pumping mechanism will be required. The possible means of pumping which might be considered are: mechanical, cryogenic, gettering or getter-ion pumping. Mechanical pumping must be ruled out on the basis of weight and power considerations in addition to a general aversion to moving mechanical parts. Cryogenic pumping was also considered but even if it were practical during the transit to Mars it is felt that during the fall through the atmosphere the low temperature could not be maintained. Any increase in temperature would liberate part of the gas absorbed during transit.

Gettering is an effective means of pumping provided that a large surface area is available and the only gases which are to be pumped are active. The expected abundance of argon implies that simple gettering cannot be relied upon to maintain a low total pressure. The only pumping method which appears to be effective for active and inert gases and at the same time falls within the weight and power requirements is getter-ion pumping. This

technique employs the positive pumping action of ionization and sputtering in combination with sustained gettering to produce a stable pumping action.

Presently used commercial getter-ion pumps employ strong magnetic fields to obtain electron trapping and thereby a high efficiency. The presence of such a field would require a great deal of shielding to meet the specification on the magnetic fringe field, and it is doubtful that the resulting weight can be tolerated. For this reason, it appears highly desirable to develop a non-magnetic getter-ion pump. Ion pumping has been observed in ionization vacuum gauges but the speeds are only of the order of 0.1 to 1 cc/sec. and 1 liter/sec. would be necessary. Additional study was required.

1.23 Sample Flow

In standard mass spectroscopy a pressure divider system is employed to introduce the sample from a relative high pressure region into the low pressure ionization and analyzer section. The first pressure drop occurs across a viscous leak and the second across a molecular leak. The region between the two leaks is maintained at an intermediate pressure by a combination roughing pump and diffusion pump. This type of system is clearly not applicable to the system which is under study. This implies that the entire pressure drop from external pressure to the internal working pressure must occur across a single restriction. In addition, the flow through this restriction must be

held to the lowest possible level in order to reduce the gas load upon the pump.

Several types of flow are possible. The most common practice is to employ a long restriction to reduce thegas flow across a large pressure drop. Such a leak is known as a viscous leak because the rate of flow is controlled by the viscosity of the gas. This type of leak has several disadvantages. First, the rate of flow is proportional to the square of the external pressure thus increasing the dynamic range of the system and making total pressure measurement difficult. Second, the sample which is actually analyzed in a viscous leak system is related to the actual external composition through the viscosity of the gas mixture. This greatly increases the difficulty of reconstructing the actual composition.

Critical flow through a thin aperture was investigated but it was found that this condition was not realizable because the resulting size of the aperture dictated that molecular flow would be reached first. Molecular flow is much more desirable than viscous flow because the flow increases linearly with pressure and the sample is related to the actual environment by the atomic masses of the component gases. This increases the ease of analysis. Although molecular flow is the desired flow mechanism, it is extremely difficult to achieve across a large pressure drop due to the small size of the aperture. A diameter on the order of 0.3 μ is necessary.

The technical aspects of manufacturing such small leak apertures were investigated. It is also possible that near molecular flow can be obtained into the transition region between molecular and viscous flow. This possibility was investigated.

There are several other aspects of the sample inlet problem which should be mentioned. If an accurate pressure measurement is expected, the use of a buffer cavity between the actual inlet leak and the external atmosphere is recommended to counteract the effects of turbulence, Bernoulli's law, and the ram effect. In addition, a filter must be employed to portect the inlet leak from clogging by dust or other foreign particles. The resulting gas volume between the filter restriction and the inlet leak must be kept small if a noticeable time constant in the gas flow system is to be avoided. The possibile condensation of CO_2 and H_2O upon entering the ion source should be guarded against. The best means of preventing this is to heat the inlet leak and the immediately surrounding surface area. If a filament electron emitter is used it is proposed that instead of wasting valuable power that the filament dissipation be made use of.

One final point to be made is that if an accurate pressure measurement is to be obtained the temperature of the inlet system must be accurately known. This may require an additional temperature monitor which had not been previously anticipated.

1.24 Data Handling and Output Measurements

Because of the serious limitation in the number of data bits available for sending the mass spectrometer output readings, the method of handling this information becomes extremely important.

1.24.1 Log Implied Output

There are two factors which dictate that the analog output be logarithmic in form. The first is that a range of several decades must be compressed into a 0 to 5v scale. It would be impossible for a digital device to read from decades in a linear scale from 0 to 5v with the necessary accuracy. The second factor is that the percentage error encountered in digitizing the output of a logarithmic device is constant. This can be shown as follows:

$$V = 5 - K \log i/i_o$$

from which

$$dV = -K \frac{di}{i}$$

This says that a given dV error always corresponds to the same percentage error (di/i).

1.24.2 Dynamic Range

The dynamic range is determined by taking into account several factors. The maximum current which will be read is the total ion current. The minimum constituent level should be 0.1% of this maximum. Therefore, a range of 10^3 is needed to include these extremes. Variation in density during the sampling period

accounts for another factor of 2 and the H_2O reading should be a factor of 2 above the noise level. Allowing for an additional safety factor of 2.5 the total necessary dynamic range is seen to be 10^4. It is somewhat arbitrary to assume that the H_2O reading will be a factor of two above the noise level since this will be determined by the source sensitivity and the detector sensitivity, however, a factor of 2 should be allowed for actually it might be possible to squeeze by with a dynamic range of 4×10^3, but all of the considerations handled here will be for the larger value.

1.24.3 Accuracy

Since the logarithmic analog readout will be a constant error system the accuracy must be set at the maximum value stated in the specifications. It is expected that the total error will be divided into three parts:

±2% error in analyzer output

±1% error in amplifier calibration

±2% error in digitizing

±5% total error.

It is also expected that at the low output end of the spectrum where ±10% accuracy is needed that noise on top of the peak will account for the additional ±5% allowed error. A total error of ±2% reading accuracy corresponds to a ±10 mv error in reading the log amp output. In order to see 10 mv in a five volt range, nine binary bits are necessary. This is the same number of bits required

if a linear output were read and a digital scaling technique was employed.

1.24.4 Sampling Methods

During the fall of the capsule through the atmosphere, the data contained in two scans will be telemetered back to earth. There will be 1000 binary bits available for this data or 500 bits per scan. It is assumed that 50 of these bits might be used for peripheral data such as total current reading, emission check, etc. This leave 450 bits for digitizing the analog scan data. As determined in the previous section, it takes up to 9 bits to read out to the desired accuracy. If the data is read serially, a marker bit would also be used to indicate those sample positions at which data is read and those at which it is not. This is assuming that all sample positions will not be read out but only those points at which data above the noise level is indicated. Perhaps five positions would be chosen where mass peaks were not expected to be present and these would serve as zero check points. Hopefully, three fo these positions would be mass free. These considerations indicate that a maximum of 10 bits per sample point would be needed, and if every position were read out, the available number of sample points is 45. There are several ways of making use of these sample positions.

a. Synchronized System

The easiest readout technique from the standpoint of data handling is the synchronized method in which each sample point

corresponds to the center (plus or minus some allowable variation) of a known mass peak. If this method is used only 38 sample points would be needed, thus allowing a greater reading accuracy to be used. If flat topped peaks are obtained at the log amp output then a reading anywhere across the top of the peak would be sufficiently accurate. The disadvantage of this method lies in the fact that the r.f. voltage must be precisely controlled. At a fixed frequency dV/V = dm/m. If the peak top to base width ratio is defined as (t/b), then dV/V = $\pm 0.5(t/b)\frac{dm}{m}$

For dm/m = 1/25 dV/V = $\pm 2(t/b)$ %

For t/b = 0.5 dV/V = ±1% which may be attainable.

b. Non-Synchronized

If a non-synchronized sampling system is used, the r.f. voltage does not have to beas accurately controlled but the full number of bits must be used. If discreet jumps of constant mass are used, the total number of sample points needed to insure sampling the top of every peak is 2x38/(t/b). The factor of 2 results from the fact that unit resolution is obtained at m/e 25 so that at m/e 12 the peak base is about half a mass unit wide. For a rectangular peak, the required number of sample points would be 74 which is considerably more than theavailable number of 45. This method cannot be used. If the width of the jumps is allowed to vary with mass,

the factor of two can be eliminated in which case it is found that t/b = 38/45 = 0.845. It is extremely doubtful that such a high ratio can be obtained without a severe loss in sensitivity.

It must be remembered that these calculations have assumed that the full number of allowed sample points will be telemetered. This will not be true since the logic can be designed to read out of memory only those readings which have a level above some fixed value. A position marker would be read at all points where data was not read out so that the serial nature of the output is maintained. If there are 20 peaks present, then t/b = 20/43 = 0.465 which says that a 50% top to base width would be sufficient. It is difficult to know exactly how many peaks will be present. This problem can be partially handled by gating the memory output at two different levels for the two scans which are to be sent. The gate level would be dropped to zero at those points where the zero level is to be checked.

The gating process could also be accomplished at the input to memory by allowing the electrometer to read in only those positions at which a reading above a fixed level is obtained.

1.25 Type of Analyzer and Pump

Meeting the weight specification on this experimental package will be a difficult task and the situation will not be improved if a great deal of magnetic shielding is required. Not only the shielding but the magnets themselves would add notibly to the weight. If an

entirely non-magnetic system can be realized the difficulties in meeting the weight limit will be greatly reduced. Therefore, one of the important considerations in the design of the ion source and analyzer. The only practical non-magnetic analyzers appear to be the time of flight or the quadrupole mass filter. The time of flight has the disadvantage that accurate, high speed circuitry is required. The reliability of such circuitry after a six month transit period is questionable. On the other hand, the quadrupole analyzer requires more power for the r.f. drive than is required by the T.O.F. Both analyzers would be light and both appear to be easily capable of meeting the performance specifications.

Three important requisites of the ion source are:

a. That is have a high differential pumping factor. This is necessary to reduce the effects of unequal pumping of various gases and outgasing in the larger analyzer section. The higher the differential pumping the lower will be the background relative to the sample.

b. The source should be free of mass discrimination in the event that a mass scan is used.

c. The source sensitivity and maximum exit angle should be independent of temperature effects. This implies that a perfect imaging rather than a thermal imaging source is desirable.

The balance of sensitivity, resolution and accuracy may make special demands upon the detector and data handling methods. If sensitivity

is low, a multiplier may be required or perhaps digital counting techniques will be necessary. As an example of the balance of requirements, it should be noted that if a non-magnetic ion source is used, a loss in sensitivity will be sustained.

1.26 In Flight Operations

There are several operations which should be carried out during the transit between the Earth and Mars. These are discussed below.

1.26.1 Pump Out

One of the fundamental limitations on the performance of a mass spectrometer is the ability to detect small ion concentrations in the presence of background gases. This limitation is most evident when the gases of interest fall within the mass range of the background gases. The normal approach to this problem involves the use of high speed pumps, ion sources with high differential pumping ratios, and high temperature bakeout. Under normal laboratory conditions, all of these conditions can be met and a low background spectra maintained by continuous pumping.

Experience has shown that after lengthy pumping periods and extended high temperature bakeout, the residual gas pressure in a sealed system will rise continually until an equilibrium pressure is reached. The ultimate pressure is generally determined by the size of the system, the materials used, the previous history of the system, storage temperature and is likely to be significant in any system.

The most logical method of conbating the out gassing problem is to take advantage of the long transit time and the high pumping speed of inter planetary space to pump out the system. This would require a break off mechanism to open the system to space after the Earth's atmosphere had been penetrated. Then before entering the Martian

atmosphere the pump out tube would have to be sealed leaving only the sample inlet leak to admit the Martian atmosphere. This apparatus would require additional weight, but since a breakoff mechanism is necessary in any event, the resealing device would not add appreciably to it.

1.26.2 Filament Turn On

Before entering the sample range it is advisable to turn on the filament and allow thermal equilibruim to be reached. At the same time, the ion pump should be turned on so that a pressure build up does not occur. After an equilibruim condition is reached a scan of the background should be taken so that a comparison can be made with the sample measurement. If the filament dissipation is used to heat the inlet leak to prevent condensation of H_2O or CO_2 this would also reach equilibrium well before entering the atmosphere of Mars.

2.0 SELECTED STUDY PROGRAM

2.10 CHOICE OF ANALYZER

The study program which was pursued centered around the type of analyzer which was decided upon. The quadrupole mass filter appeared to have several advantages which combined made it the most desirable type of analyzer. Most important of these is that this analyzer is non-magnetic thereby leading the way toward the realization of a non-magnetic system. Because it is not magnetic it is light in weight, consisting only of a thin walled outer tube with four rods and their suspension mounted inside. Another advantage of the quadrupole is that it is a flexible instrument in that resolution, size, power, and sensitivity can be traded for one another. Therefore, it can be easily adapted to varying demands placed upon it. Furthermore, the quadrupole mass filter may be used with a frequency scan which implies that the source voltages can remain constant thereby allowing a discrimination free source if a non-magnetic source is employed. In addition to these features the quadrupole can be operated to give 100% transmission efficiency, and is thereby eliminated as a source on system inaccuracy.

2.20 OUTLINE OF STUDY PROGRAM

The following outline constitutes the proposed study program:

2.21 Theoretical System Study (System Analysis)

Calculation and preliminary evaluation of component functions of the system and their interrelationships. Several potential instrument systems are expected to evolve from the preliminary analysis to serve as guidance in specific areas of the study.

2.22 Mass Spectrometer Analyzer and Ion Source

a. Calculations for a preliminary optimum of the analyzer design.

b. Evaluation of pumping speed and differential pumping of several possible ion sources.

c. Design and construct one experimental model of the analyzer and one ion source for experimental evaluation. To be used for evaluation of: 1) sensitivity, and 2) resolution, under expected boundary conditions.

2.23 Sample System

a. Theoretical study of inlet system to obtain best analytical conditions in view of pumping capabilities.

b. Study of controlled techniques for producing molecular and viscous leaks compatible with flow rate.

c. Construction and evaluation of one or more sample systems based on study of techniques.

2.24 Pumping

a. Investigations of potential ion pumping systems.

b. Construct and evaluate properties of most promising design.

2.25 Detector System

a. A study of the relative merits of: 1) direct analog measurement of ion current, and 2) single ion pulse counting using an electron multiplier.

b. Investigation of detector components and circuits.

2.26 Support Electronics

Study and experimental evaluation of more difficult circuits required for operation of system components.

2.27 Optimization of the System

a. Reduction of previous studies into an optimum design.

b. Submission of designs and results of the studies in the form of a final report.

3.0 METHOD OF SOLUTION OF THE PROBLEM

In the investigation of a complex system such as this one it is important that all of the facets of the problem are examined in a logical manner. This study must include a detailed analysis of the system components so that their operating properties and their effect upon other components are understood. Then these elements must be combined in such a way that an optimum system is the result. In order to aid this process, a logic diagram was constructed which is shown in Figure 3.10. This diagram shows the various subsystems along with their variables and the relationship between these variables to one another.

There are several possible solution paths which may be followed. The choice of path depends in part upon which of the system requirements is considered to be the most important. This results from the fact that starting at one point in the logic diagram and working through it places increasing restriction upon those variables which remain. As an example, if the resolution and transmission efficiency of the quadrupole analyzer are initially set then the variables affecting the quadrupole supply and ion source are determined. The requirements of the quadrupole supply determine the total power drawn by the quadrupole subsystem. The ion source design implies the sensitivity of the detector, and the detector design necessary

to achieve this sensitivity. At the same time the peak shape at the output of the analyzer implies the time constant of the detector and the means used to handle the output data. The design of the ion source determines the differential pumping which in turn affects the sample flow and pumping systems. Other paths may be followed which may result in different conclusions. Care must be taken that the problem is attacked from several standpoints so that the best overall result can be obtained.

In addition to the choice of the proper solution logic, the problems must be classified into the following categories:

a. Those which will not be investigated.

b. Those which will be given only preliminary investigation.

c. Those which will receive a thorough theoretical investigation.

d. Those which will be investigated experimentally.

e. Those which should be followed up later when time and money allow.

4.0 VARIABLES OF SUBSIDIARY ELEMENTS

With the boundary conditions, first order requirements, and approach outlined, each of the elements which make up the system is discussed in theory, and the resulting variables are examined.

4.10 THE QUADRUPOLE MASS FILTER

4.11 Fundamental Considerations

The potential distribution of a quadrupole field is given by:

$$\phi = (V_{dc} + V_{ac} \cos \omega t)(x^2 - y^2)/r_o^2 \qquad (1)$$

Such a field is established in the region between four hyperbolic electrodes when voltages are applied to them as shown in Figure 4.11. However, it has been shown[1] that this field distribution is approximated to a high degree of accuracy by electrodes with circular cross-sections, provided that the proper ratio between rod diameter and rod spacing is employed. If the rod spacing is $2r_o$, the rod diameter should be $2.32\ r_o$.

The motion of a singly charged ion in a quadrupole field is described by the two independent differential equations:

$$m\ddot{x} + 2e(V_{dc} + V_{ac} \cos \omega t)x/r_o^2 = 0 \qquad (2)$$

and

$$m\ddot{y} - 2e(V_{dc} + V_{ac} \cos \omega t)y/r_o^2 = 0 \qquad (3)$$

---

[1] Dayton, Shoemaker, and Mozley, RSI, 25 (1954)

where:

$$m\ddot{z} = 0 \tag{4}$$

Upon making the following simplifying substitions:

$$a = \frac{8eV_{dc}}{mr_0^2\omega^2}, \quad q = \frac{4eV_{ac}}{mr_0^2\omega^2}, \quad \omega T = 2\xi; \tag{5}$$

the above equations may be placed in the recognizable form of Mathier's equations,

$$x'' + (a + 2q\cos 2\xi)x = 0, \tag{6}$$

and

$$y'' - (a + 2q\cos 2\xi)y = 0. \tag{7}$$

The standard form of Mathieu's equation is

$$u'' + (a - 2q\cos 2\xi)y = 0, \tag{8}$$

where a and q may assume either positive or negative values. These parameters play a fundamental role in the theoretical investigation of the quadrupole mass filter, since the solutions of Mathieu's euqation are stable or unstable depending upon the particular values which they assume. For a stable solution, the variable u remains bounded for all values of ξ while in the case of an unstable solution, u is unbounded as $\xi \rightarrow \infty$.

Equations (6) and (7) place two simultaneous stability requirements upon the motion of an ion in the mass filter which correspond to two simultaneous restrictions upon the values of a and q. When these conditions are superimposed, a stability diagram results which, for a small region of interest, is shown in Figure 4.12. The mass filter is operated by scanning either voltage or frequency in such

a manner that the a/q ratio remains constant and motion along a "scan line" through the stable region results. As the voltage or frequency is scanned, the path followed by ions of a given mass will slowly be altered. As the scan progresses from $q = 0$ to $q > 0$, the path will at first be stable in the X-Z plane, but unstable in the Y-Z plane. Hence, the ions will not be transmitted. As the scan continues, the instability of the Y motion will diminish and finally, at the boundary of the stability diagram, ion motion will become stable in both planes of motion. In this region, the ions will be transmitted through the quadrupole section. Then, as the operating point changes such that q increases farther, the motion will become unstable in the X direction and the ions will again be cut off.

The solution of the equations of motion is a tedious job since the paths cannot be expressed in closed form.

The solution of equation (8) is expressible in the complex Fourier series:

$$u = Ae^{\mu\xi} \sum_{n=-\infty}^{+\infty} C_{2n} e^{2in\xi} + Be^{-\mu\xi} \sum_{n=-\infty}^{+\infty} C_{2n} e^{-2in\xi} \quad (9)$$

where μ is a function of a and q which may be real, imaginary or complex, depending upon their value. Imaginary values of $\mu (\mu = i\beta)$ correspond to stable solutions which may be expressed as an infinite sine and cosine series. The stability of a path is not affected by the values of A and B which are determined by the initial conditions of the particle.

The X and Y motions in a quadrupole field are fundamentally different. This is the result of the fact that in the X direction, the d-c field has a stabilizing action and the a-c field a destabilizing one, while the opposite is true in the Y direction. The paths may be approximately described as follows: The Y motion appears as a product of two sine waves, one with frequency ω and the other with frequency $\frac{1}{2}\beta_y\omega$. The X motion has the appearance of a 100% modulated sine wave with a high frequency of $\frac{1}{2}\omega$ and a modulating frequency of $\frac{1}{2}\omega(1-\beta_x)$. Brubaker[2] has carried out an actual plot on a digital computer of the motion in the X and Y planes for a given set of initial conditions. His results confirm the above description.

4.12 Controlling Variables

The quantities which control the desired operating conditions of the mass filter are:

a. Resolution

b. Transmission efficiency (peak top width)

c. Scan mode

d. Power

The variables which can be manipulated to optimize these quantities are:

a. V_{ac}/V_{inj} = r.f./injection voltage ratio

b. V_{ac}/V_{dc} = r.f./d-c voltage ratio

---

[2] W. M. Brubaker, "The Quadrupole Mass Filter," presented at Congres International Des Techniques et Applications Du Vide Paris, 20-24, June 1961

c. ω = angular frequency

d. r_o = rod spacing parameter

e. l = rod length

f. r_c = collector aperture radius

g. r_e = entrance aperture radius

h. α = entrance angle

i. V_I = injection energy

j. ΔV_I = energy spread

The last four variables are controlled by the ion source since, as will be shown, the design of the mass filter is intimately associated with the nature of the entering ion beam.

4.12.1 Resolution

The basic essentials of the theory discussed thus far indicate that the resolving properties of the quadrupole filter are based upon the stability or instability of the ion path as determined by the operating point in the stability diagram. While this is true, it must not be forgotten that the physical boundaries of the system actually determine whether a given ion will be transmitted and therefore, these boundaries play an important role in the determination of the resolving properties of the quadrupole mass filter. Both aspects of the problem are discussed below.

a. Width of Bandpass Characteristic

The most fundamental factor in determining the resolution of the quadrupole mass filter is the width of the bandpass characteristic. This may be expressed in terms of the stability

diagram as the width of the stable region at the point where the scan line makes its intersection. The initial conditions of an ion as it enters the quadrupole field are also important in determining if it is transmitted, however, this does not effect the fundamental peak width since somewhere in the distribution of initial conditions will occur those for which the boundaries of the theoretical stability diagram from the actual bandpass limits. Tails may occur on the peak which fall outside of the predicted frequency range. These will be discussed subsequently.

From equation (5), the maximum frequency at which a mass, m, is transmitted is given by:

$$f_{max}^2 = \frac{K}{q_{min}\, m} \tag{10}$$

and similarly, the minimum frequency at which the same mass is transmitted is given by:

$$f_{min}^2 = \frac{K}{q_{max}\, m} \qquad m \text{ in a.m.u.} \tag{11}$$

The quantities q_{min} and q_{max} are fixed by the slope of the scan line. For the particular definition of resolution used here, two adjacent masses are theoretically resolved if they are not transmitted at the same frequency; i.e.,

$$f_{min}^{(m)} \geq f_{max}^{(m+1)} \tag{12}$$

Use of equation (10) and (11) yields:

$$\frac{q_{min}}{q_{max}} \geq \frac{m}{m+1} \tag{13}$$

Defining:

$$\Delta q = q_{max} - q_{min} \tag{14}$$

equation (13) may be put in the form:

$$\Delta q \leq \frac{q_{max}}{1 + m} \tag{15}$$

The stated requirement is unit resolution at mass 25. If the apex value of q_{max} is assumed, the result is:

$$\Delta q \leq 0.02720 \tag{16}$$

This relation places a restriction upon the range of values which the ratio V_{dc}/V_{ac} may assume, since the scan line must cross the stable region between the apex and the point where $\Delta q = 0.02824$. From the stability diagram, this range is seen to be:

$$0.1617 \leq \frac{V_{dc}}{V_{ac}} \leq 0.1678 \tag{17}$$

This is clearly a small range of variation and points up the fact that the d-c to a-c voltage ratio should be tightly controlled.

b. Peak Tails

The bandpass characteristic of the stability diagram does not control the actual tails which may occur on a mass peak when it is scanned. These tails are caused by the fact that an ion with an unstable trajectory may still pass through the quadrupole section and be collected provided that its path becomes unbounded at a slow enough rate.

The rate at which a path becomes unbounded is controlled by the initial conditions and the operating point on the stability diagram. As the initial radius or initial radial velocity is increased, unstable paths will grow at a faster rate for a given position on the Z axis. At the same time, the farther that the operating point lies from the region of X-Y stability, the faster will be the increase in amplitude with distance. Let us consider ions of mass m and follow a scan through the region of X-Y stability. As the scan point approaches the stability border, the degree of instability decreases. Hence, an increasing number of mass m ions can pass through to the collector by virtue of the fact that the requirements on initial conditions become less severe. The number of mass m ions which get through the quadrupole section at a given point on the scan line is governed by the ratio $r_o/\int$ and the injection energy V_I. The smaller the ratio $r_o/\int$, the more severe are the restrictions on initial conditions since the slower must be the rate of increase in amplitude. The smaller the value of V_I, the greater the increase in amplitude of the envelope of an unstable trajectory per unit length. Consequently, the smaller V_I, the longer the rods appear to be. Once the stability border is reached, the paths become stable. At this point, the envelope of the trajectory changes from an exponential to a sine function with zero frequency ($\beta = 0$). As the scan point moves into the region of X-Y stability, the frequency of the envelope function increases. In crossing

the stability border, a fundamental change takes place in the transmission determining factors. Transmission is no longer principally dependent upon r_o/ℓ or V_I because of the periodic nature of the stable solution. There is a lesser dependence upon these variables which appear in the form of ripple or spikes superimposed on the peak. This will be discussed later.

Verification of these dependences is given by the fact that von Zahn[3] has experimentally determined a relation that says, in effect, that if the resolution predicted by the bandpass characteristic (equation 15) is to be realized, then the ions must remain in the quadrupole field for a number of cycles which is given by:

$$n = 3.5\sqrt{\frac{M}{\Delta M}} \qquad (18)$$

where

n = number of cycles of a-c voltage

$\frac{M}{\Delta M}$ = half-height resolution as theoretically set by the position of the scan line.

This equation may not be applied directly to our problem since $\frac{M}{\Delta M}$ is the half-height resolution, while we are interested in 1% peak height resolution. Conversion of the equation for complete separation depends upon the general form of the peak. It was stated that the result was obtained at a bandpass resolution of 100 which indicates that the peaks were nearly triangular in shape. (See discussion of transmission efficiency.) The half-height peak width is approximately one-half of the base

[3] U. von Zahn, Diplomarbeit Bonn (1956)

height peak width and the resolution becomes:

$$n = 5\sqrt{\frac{M}{\Delta M}} \tag{19}$$

where now $\frac{M}{\Delta M}$ is the 1% peak height resolution. Because of our assumption (above) on peak shape and by considerations of minima in the modulation envelope, it was decided to allow for a margin of safety. Hence, we have used:

$$n \geq 2\pi\sqrt{\frac{M}{\Delta M}} \tag{20}$$

The number of cycles occurring during the traversal of the rod length is given by:

$$n = \frac{fl}{V_z} \tag{21}$$

where:

V_Z = axis velocity

f = frequency

l = rod length

The Z axis velocity is given approximately by:

$$V_z \approx \sqrt{\frac{Ze\,V_I}{M}} \tag{22}$$

where a cosine factor was neglected. From equation (5):

$$f^2 M = \frac{e\,V_{ac}}{\pi^2 r_0^2 q} \tag{23}$$

Combining euqations (20), (21), and (22):

$$\frac{V_{ac}}{V_I} \geq 8\pi^4 q \left(\frac{r_0}{l}\right)^2 \frac{M}{\Delta M} \tag{24}$$

In this equation, q is considered to be a constant at its apex value of 0.706. The system considered in this report will use a frequency scan as will be discussed later. In such a system,

V_{ac} is held constant during the scan. As V_{ac} is set at a higher and higher value, the frequency must go up accordingly for the same mass (see equation 23). In terms of the actual path followed, higher frequency is reflected in terms of greater instability in the region where one of the motions is unstable (outside of the stability diagram). Then it is seen that the result of increasing V_{ac} is to make the paths more unstable (relative to Z distance traveled) and thereby decrease the tails. The factors V_I and r_o/ℓ appear in the form discussed previously.

The dependence on $\frac{M}{\Delta M}$ in equation (24) can be explained by noting that if two adjacent masses are to be resolved, the relative effect of tails becomes greater as the mass at which unit resolution is to be obtained increases. This comes about because the tails which appear on a peak are not a function of the mass of the peak. When the V_{dc}/V_{ac} ratio is increased, unit resolution is obtained at a higher mass but only if the tails are also reduced in proportion to the decrease in Δq. Therefore the $\frac{M}{\Delta M}$ dependence is necessary.

When 1% peak height resolution is desired, the tails necessarily play a much greater role than in the case of half-height resolution. This indicates that more detailed knowledge of the tails is needed if an exact quantitative relation between the controlling variables and resolution is to be obtained. The transformation involved in going from equation (18) to equation (19) may contain a greater error than was adjusted for in

equation (20) because such detailed information was not available. Work by Wedemeyer[4] described methods of reducing tailing effects, however, the nature of his study was such that it finds no application to the present problem. This report was concerned for the most part with an experimental study of the effect of initial conditions on the resolving power of the system. Particular emphasis was placed on the effect of molecular energies in the ion source.

Two means were considered for controlling the tail size. The first was to bias the exit aperture electrode with respect to the quadrupole rods. It was thought that this would give the incoming ions an electrical jog which would cause their initial conditions to be diverse enough that the peak tails would be significantly reduced. This method was experimentally tested. The second means which was proposed was to mask off the entrance aperture areas near the X and Y axes. This could be accomplished by a small ring with a cross in it which would be positioned over the aperture. Such a mask could be easily fabricated by present day metal etching techniques.

4.12.2 Transmission Efficiency

A second important aspect of the quadrupole operation is its transmission efficiency. This is defined as the ratio of the number of ions of a given mass collected to the number of ions of that mass entering the quadrupole section at any instant of time. (It is

---

[4] R. Wedemeyer, Inaugural-Dissertation, "Ein Molekularstrahldetektor Mit Elektronenstoss-Ionisierung Und Vierpol-Massenfilter, Juli 1961

here assumed that the transit time down the axis is negligible.)

The importance of transmission efficiency arises from the fact that flat-topped mass peaks at the output of the instrument are obtained only by operating the quadrupole in such a manner that 100% transmission is obtained over some portion of the frequency range for which a mass is being passed. Flat-topped peaks are a necessity in view of the limited number of bits available for transmitting the output data.

Another demanding reason for having flat-topped peaks is that the accuracy of peak amplitude measurements is greatly increased. This comes about since during the scan period at which 100% transmission occurs, the peak height is not controlled by the analyzer. In addition, small changes in the V_{dc}/V_{ac} ratio are not reflected in sensitivity changes. This is a desirable condition since this ratio may be difficult to control accurately. The burden of accuracy is then thrown upon the ion source which, if non-scanning, should produce optimum stability of the ion beam.

Just as the initial conditions on an ion entering the quadrupole section play an important roll in their transmission when their paths are unstable, they are also important when their paths are stable. Ions which enter the quadrupole section following a stable trajectory may still fail to reach the collector because their amplitude of motion is too large and they strike the rods.

The maximum amplitude of motion for an ion is determined by its

initial radial velocity, the phase angle of the rf voltage, and the operating point on the stability diagram. The larger the initial radius or entrance angle of an ion, the larger will be its range motion. At the same time, the farther that the operating point progresses from the edges of the regions of instability, the greater is the allowable range of entrance conditions because of the greater stability of the path. It is this phenomena which controls the shape of a peak. In addition, the phase of the rf voltage controls the path amplitude, but since the rate of scan is extremely low compared with rf frequency, ions of a given mass will experience all possible phase angles, and therefore, an average effect is noted.

Ions which enter the quadrupole section following a stable trajectory may still fail to reach the collector because the amplitude of the motion is too large.

The detailed analysis of transmission efficiency and its effect upon peak shape is extremely involved because of the lengthy numerical calculations which are necessary. Paul Reinhard and von Zahn[5] have partially treated this problem and come up with some useful results for design. They started with the general solution to the Mathieu equation (equation (9)) and expressed the arbitrary constants A and B in terms of the initial conditions. Then, by use of the orthogonal properties of the Fourier series, they were able to express the maximum amplitude in terms of a function of these initial conditions multiplied by the summation of the absolute values of the coefficients

---

[5] W. Paul, H. P. Reinhard, and U. von Zahn, Zeitschrift für Physik, Bd. 152, S. 143-182 (1958)

C_{2n}. If the maximum amplitude is set equal to r_o, then the restrictions on initial position, angle, phase, and operating point can be determined. It was found that the transmission limits could be expressed as a family of ellipses when plotted on the X_o, X'_o plane, with ξ_{1o} and β_x as parameters. Continuing from this point, they were able to express the ratio of the maximum amplitude to initial amplitude as a function of phase angle ξ_{1o} with β as a parameter for the case of initial radial velocity equal to zero. From this data, it was then possible to replace the iso-β lines on the stability diagram with lines of constant restriction on initial position. The result of their work is shown in Figure 4.13. This data is not sufficient to solve our problem since we are concerned not only with initial position, but initial radial velocity as well. It was necessary to find an approximate method of extending the available data to include this more general case since its exact numerical solution would be too time consuming.

This was accomplished by making use of the work of Brubaker[2] in which an appropriate expression for the Y-Z plane motion was derived. This expresion may be expressed as:

$$y = A\sin(\alpha T + \delta)[1 - 0.35\cos(\omega T + \phi)] \quad (25)$$

where:

$$\alpha = \tfrac{1}{2}\beta_y \omega \quad (26)$$

ϕ = phase angle of rf voltage

$A+\delta$ = arbitrary constants expressible in terms of initial conditions

Letting:

$$f_1(\phi) = 1 - 0.35\cos\phi \tag{27}$$

$$f_2(\phi) = 0.35\sin\phi \tag{28}$$

the expressions for initial position and velocity are found to be:

$$y_0 = A f_1(\phi)\sin\delta \tag{29}$$

$$V_0 = A\left[\alpha f_1(\phi)\cos\delta - \omega f_2(\phi)\sin\delta\right] \tag{30}$$

These equations may be solved for A:

$$A = \left\{\frac{y_0^2}{f_1^2(\phi)} + \frac{1}{\alpha^2 f_1^2(\phi)}\left[V_0 + y_0\omega\frac{f_2(\phi)}{f_1(\phi)}\right]^2\right\}^{1/2} \tag{31}$$

The maximum value of y is given by:

$$y_{max} = 1.35A \tag{32}$$

and for transmission it is required that:

$$y_{max} \leq r_0 \tag{33}$$

then,

$$r_0 \geq 1.35\left\{\frac{y_0^2}{f_1^2} + \frac{4}{B_y^2 f_1^2}\left[\frac{V_0}{W} + y_0\frac{f_2}{f_1}\right]^2\right\}^{1/2} \tag{34}$$

Where equation (26) has been substitued for α.

The indications from the work of Fischer and Paul's group are that the most severe restrictions on initial conditions occur at $\phi = \pi/2$, in which case:

$$f_1\left(\frac{\pi}{2}\right) = 1 \quad \text{and} \quad f_2\left(\frac{\pi}{2}\right) = 0.35 \tag{35}$$

It is desirable to eliminate the variable ω.

This is accomplished by the use of equation (5) along with:

$$v_o = \sqrt{\frac{2eV_I}{m}}\ \sin\alpha \tag{36}$$

from which is obtained:

$$\frac{v_o}{\omega} = r_o \sin\alpha \sqrt{\frac{V_I}{V_{ac}}\frac{q}{2}} \tag{37}$$

Making these substitutions:

$$r_o \geq 1.35\left\{y_o^2 + \frac{4}{B_y^2}\left[r_o \sin\alpha\sqrt{\frac{V_I q}{V_{ac}}} + 0.35\, y_o\right]^2\right\}^{1/2} \tag{38}$$

This expression now has r_o on both sides. Solving for r_o/y_o yields:

$$\frac{r_o}{y_o} \geq \frac{1.4\sin\alpha\sqrt{\frac{q}{2}\frac{V_I}{V_{ac}}}}{\frac{B_y^2}{1.82} - 2q\frac{V_I}{V_{ac}}\sin^2\alpha} + \sqrt{\frac{\left[1.4\sin\alpha\sqrt{\frac{q}{2}V_I/V_{ac}}\right]^2}{\left[\frac{B_y^2}{1.82} - 2q\frac{V_I}{V_{ac}}\sin^2\alpha\right]^2} + \frac{B_y^2 + 0.488}{\frac{B_y^2}{1.82} - 2q\frac{V_I}{V_{ac}}\sin^2\alpha}} \tag{39}$$

For the special case of zero entrance angle

$$\frac{r_o}{y_o} \geq 1.35\sqrt{\frac{B_y^2 + 0.488}{B_y}} \tag{40}$$

By comparing equation (40) to the results obtained by Paul, Reinhard, and von Zahn, the values of B_y corresponding to the "tents" of Figure 4.13. These values for B_y can then be substituted into equation (39) giving a new set of "tents" which correspond in position, but not in value, to the old ones. The value will depend upon the assumed maximum values for α and V_I/V_{ac}.

The value of q in equation (39) is set at its apex value of 0.706. The results of numerical calculation are shown in Figures 4.14 and 4.15. The parameter γ is defined to be:

$$\gamma = \sqrt{\frac{V_I}{V_{ac}}}\ \sin\alpha \tag{41}$$

The set of tents shown in 4.14 are for $\gamma = 0.01$. It is seen that even for the relatively small value, the transmission characteristics

of the quadrupole are greatly impaired.

It is of interest to check the accuracy of equation (39). Returning to equation (34) and setting $y_o = 0$, and making substitutions (35), the following result is obtained:

$$r_o \geq 1.35 \times \frac{2 V_o}{B_y \omega} \tag{42}$$

which can be put in the form:

$$V_o \leq 0.74 r_o \alpha \tag{43}$$

This is identical to Brubaker's expression which neglected completely the effects of the rf phase angle. It should be pointed out that equation (39) is only intended to give an approximate solution to the problem. The actual values of $F_1(\varphi)$ and $F_2(\varphi)$ which pose the worst restriction on entrance conditions depend upon the relative values of y_o and V_o. Since fixed values were assumed, the results will not be entirely correct. This problem is no greater in significance than that produced by the field distortion due to the presence of the entrance aperture structure. In view of thes these considerations, it is felt that equation (39) can be used only as an approximate guide for design. Although these results were obtained for y motion only, they may be extended to the case of X motion since, although the nature of the path is somewhat different, the stability criterion is essentially the same. Again, the exact choice for worse case phase angle is not known, but the error should not be appreciably different from the y motion case.

Another phenomenon, which appears in the form of spikes on the sides of the peak, is attributed to varying transmission effects. These spikes arise because during portions of the scan over a peak, the X and Y motions peak and zero at different times relative to one another. If the injection velocity is too high, the ions passing through the quadrupole section may not be eliminated by a rod collision at those points in the scan where the phase of X and Y maxima and zero crossings are just right. At such points in the scan, there will be a spike on the peak. Such spikes cannot occur on the top of a peak provided that the operating point is set for 100% transmission efficiency and therefore should not be a significant bother.

There are two important conclusions which can be drawn from this discussion of transmission efficiency. The first is that the sensitivity of the instrument is not governed directly by the quadrupole section. This is true because the mode of operation is such that the transmission efficiency of the quadrupole is 100% over some portion of each peak. It is indirectly controlled by the quadrupole analyzer since it is analyzer conditions which set the maximum size of r_e. Since it is really the ratio r_o/r_e which is of importance, it may be necessary to adjust r_o instead of r_e if the source sensitivity is marginal.

The second conclusion is that the peak shape in a quadrupole analyzer is controlled in a different method than in a conventional magnetic instrument. In a conventional mass spectrometer, the peak width

is controlled by the width of the collector slit and the initial conditions or aberrations on the ions as they enter the analyzer. The width of the base of the peak is proportional to the width of the beam plus the width of the slit. The width of the peak top is proportional to the slit width minus the beam width. As the beam is narrowed down, the base of the peak is narrowed and the top of the peak is widened. In the case of the quadrupole analyzer, the base width of the peak (neglecting tails) is controlled by the slope of the scan line while the top width is controlled by the initial conditions. This means that resolution and peak shape can be independently controlled. These considerations are pointed out in Figure 4.16.

It should also be pointed out that another mode of operation exists for the quadrupole. As the slope of the scan line is increased for a fixed r_o and fixed entrance condition limits, a region will be entered in which the transmission efficiency does not reach 100%. As the scan line is raised further, the resolution continues to improve due to the decreasing width of the stable region, but at the same time the peak transmission falls off and triangular shaped peaks are obtained. This mode of operation would be desirable under three conditions:

a. If source sensitivity is marginal, the overall sensitivity can be increased by opening up r_e to increase the number of ions entering the quadrupole. Improved sensitivity would be obtained only up to the point at which the ions admitted by a farther increase in r_e all have initial conditions which are too diverse

for the quadrupole to accept.

b. If an extremely high resolution instrument was desirable, then this mode of operation would be assumed. Since $\frac{M}{\Delta M} \propto \frac{1}{I^+}$ ion source beam density would have to be high and detector sensitivity would have to be maximized.

c. This mode of operation could only be tolerated if enough data bits were available to transmit the output under conditions of pointed peaks.

4.13 Scanning Mode

There are two modes of scanning the peaks in a quadrupole mass filter. One is by scanning the voltage applied to the rods, and the second is by varying the frequency of the rf. From Figure 4.12 and equation (5), it is clear that if V_{dc}/V_{ac} remains constant, motion along a linear scan line in the a-q plane is obtained by either technique.

The principle factor governing the technique to be used is the application to which the instrument is to be put.

It is apparent from equations (24) and (39) that resolution and transmission characteristics are functions of the ratio V_{ac}/V_I. Therefore, if these quantities are to remain constant over the mass spectrum, which is necessary for a true analytical instrument, this ratio must also remain constant.

If the mass spectrometer is applied to a satellite application in which all of the incoming particles have essentially the same

velocity:

$V_o = K$ = constant.

Then:

$V_o = \frac{1}{2}\left(\frac{m}{e}\right)v_o^2$ is the equivalent initial energy.

This equivalent initial voltage is likely to be fairly appreciable compared with the applied injection voltage and therefore, to keep the V_{ac}/V_I ratio constant voltage must be scanned with mass.

In the case at hand, the mass spectrometer is analyzing a thermal gas in which case energy is constant, independent of mass. In this situation, V_I = constant and therefore, V_{ac} must be kept constant. This dictates that a frequency scan be employed.

There are other advantages obtained in scanning frequency instead of voltage. These are discussed elsewhere.

4.14 Power

One of the primary differences between the quadrupole mass filter and conventional types of mass spectrometers is that the operating characteristics of the instrument (size, resolution, and transmission efficiency) can be directly related to the rf power needed to drive the quadrupole rods. For this reason, in power limited applications such as the one under consideration, power becomes an important parameter. This is good from the standpoint that it allows an extra dimension in optimizing the operation of the instrument. At the same time, however, it is likely to create more of a problem in meeting the power requirements than would be encountered on

other types of instruments.

The power loss in the quadrupole is due to the copper loss in the inductor which must be placed in parallel with the quadrupole capacity in order to obtain a high efficiency resonant circuit. The impedance of a LC parallel circuit at resonance is:

$$R_r = \omega_o L Q \tag{44}$$

The power dissipated in this circuit is then:

$$P = \frac{1}{2} \frac{V^2}{R_r} \tag{45}$$

An examination of Figure 1 shows that

$V = 2V_{ac}$ and therefore the result is: $P = 2 \frac{V_{ac}^2}{\omega_o L Q}$ (46)

At this point, it is common practice to substitute the quadrupole scan line equation in such a manner that voltage is eliminated. The result is:

$$P = \frac{6.5 \times 10^{-4} M_{A,M,u}^2 F_{mc}^5 r_{ocm}^4 C_{pf}}{Q} \quad \text{watts} \tag{47}$$

This equation is extremely misleading if it is applied without careful consideration of its true meaning. In the first place, in a frequency scanned system, mass varies at the same time that frequency does, and therefore, the equation does not give power directly as a function of mass. In the second place, in this system, capacity is a function of frequency and therefore one or the other cannot be arbitrarily varied. In the third place, V_{ac}, which affects resolution and transmission efficiency, does not even appear in the equation, and consequently, it is not immediately clear what is happening to these important quantities as f, r_o, C, or Q are varied.

In view of this, let us first eliminate frequency from the equation in favor of voltage which may then be set at a value necessary to accommodate adequate resolution and transmission efficiency. By substitution of equation (23), the above expression becomes:

$$P = 4\sqrt{\frac{e}{M}}\,\frac{V_{ac}^{5/2}}{q^{1/2}}\,\frac{C}{r_o Q} \quad \text{watts} \qquad (48)$$

If the frequency scanning is accomplished by the use of a variable capacitor in parallel with the quadrupole capacity, then it is clear that:

$$\frac{M}{C} = \frac{M_o}{C_o} = \text{constant} \qquad (49)$$

and substitution of this result yields:

$$P = 4.64 \times 10^{-6}\, V_{ac}^{5/2}\,\frac{M}{M_o}\,\frac{C_o}{r_o Q} \quad \text{watts} \qquad (50)$$

where

M_o = lowest mass in scan range (amu)

C_o = minimum capacity (pf)

M = mass (amu)

Q = quality factor of turned circuit

Even this equation is somewhat misleading because if V_{ac} is fixed, then r_o is related to C_o. To further clear up this issue, the following sequence of substitutions is used. Let M and V_{ac} be fixed. Then from equation (14):

$$r_o = K/f \qquad (51)$$

but:

$$f^2 = \frac{K}{LC} \quad \text{and} \quad Q = \frac{\omega L}{R_L} \qquad (52)$$

and therefore:

$$P = K R_L \frac{C}{L} \qquad (53)$$

This equation is of great significance because it says that r_o can be varied at will and the power will remain constant provided that $\frac{R_L C}{L}$ remains constant. For example, increasing V_o means decreasing f which means increasing C and L. If they are increased such that C/L remains constant, then power will remain constant if R_L remains constant. Since the inductance has increased, more turns will be required and therefore it would be expected that the copper loss would go up. However, at the same time, the frequency has dropped by the same factor by which the inductance has increased. Consequently, the skin depth of current flow has increased by the square root of the frequency since:

$$\delta = \frac{6.62}{\sqrt{F}} \qquad \text{for copper} \qquad (54)$$

and the conducting area has therefore increased nearly enough to make up for the added length. (Since the region of interest is the low megacycle range, δ will be considerably less than the radius of the wire.) In addition, other losses caused by dielectric heating in the ceramic supports and eddy currents in the surrounding shielding will decrease with frequency. The only factor which works against this decrease in R_L is the effects of the self-capacitance of the coil.

The apparent inductance can be expreesed as:

$$L_{ap} = L(1 + C_o/C) \qquad (55)$$

where

L = actual inductance

C_o = interwinding capacity

C = turning capacity.

It is seen that dropping frequency required C to go up, and hence, L must increase slightly more than would be anticipated, thus adding extra coil length. At the same time, however, C_o will also increase thereby counteracting the increase in C. It must be assumed that the overall volume of the coil and shield has not increased since it will be desirable to maximize this volume at any frequency. Therefore, increasing L requires closer spaced turns, and a greater C_o. The net result of all this appears to be that as frequency drops, R_L will decrease, even though L and the number of turns has increased. Consequently, the act of increasing r_o may actually reduce power instead of increasing it. This is a very important discovery, although it must be realized that it is valid only for some limited range of frequency.

Other conclusions which can be reached concerning power are that it is always desirable to minimize V_{ac} and C_o and maximize Q. Decreasing V_{ac} is limited by the rod capacity of the quadrupole, wiring capacity, and the minimum capacity of scanning capacitor. This may be expressed as:

$$C = C_Q + C_i \gamma_{lo} + C_s \qquad (56)$$

where

C_Q = stray wiring and end capacity of rods

C_S = residual capacity of scanning capacitor

$\frac{C_2}{\ell_o}$ = capacity/unit length of rods

The overall capacity is essentially independent of r_o, while a large portion of it is proportional to length. Therefore, it is advantageous from the power standpoint to minimize length, but this can only be done by sacrificing performance. The principle factor limiting Q is the size of the volume which the coil, along with its shield, is restricted to. For this reason, it is likely that the overall volume requirement may be pushed to the limit.

It is actually average power which is important and therefore, it is necessary to relate instantaneous power to average power over the scan. For the scan mode under consideration:

$$P = K\sqrt{\frac{M}{e}} \tag{57}$$

It is assumed that mass is scanned linearly with time.

$$P_{AV} = K\int_{12=(M/e)_1}^{50=(M/e)_2} \sqrt{\frac{M}{e}}\, d\left(\frac{M}{e}\right) \Big/ \int_{12}^{50} d\left(\frac{M}{e}\right) \tag{58}$$

In the Martian application, the mass range is 12 to 50:

$$P_{MAX} = K\sqrt{\frac{M_{50}}{e}} \qquad P_{MIN} = K\sqrt{\frac{M_{12}}{e}} \tag{59}$$

$$P_{AV} = 0.77\, P_{max} \qquad P_{AV} = 1.57\, P_{MIN} \tag{60}$$

By the use of these equations, it is now possible to relate power to the other design parameters.

Once the diameter of the quadrupole rods has been determined, it is interesting to see what the relationship between the remaining variable is. This is shown in Figure 4.17 in which an r_o values of

0.100 and 0.200 inches has been assumed. Plotted on plane of voltage vs. frequency are lines of constant mass and lines of constant PQ/C. A frequency scan corresponds to moving horizontally on this diagram. As the scan progresses from mass 12 to mass 50, PQ/C decreases. This is true because C is increasing faster than power.

4.20 ION SOURCE

Since the ion current delivered to the detector carries the desired analytical information, the magnitude of this current to a large extent controls the noise content of the information. The ion source plays a key part in producing the maximum ion current for transmission to the detector and for this reason should receive a major emphasis in the design.

Not only is it necessary that the ion source be matched to the quadrupole analyzer in the size of the source exit aperture (r_e), the half-angle (α), the injection energy (qV_I), and the energy spread of the ion beam ($q\Delta V_I$), but it also controls the ionization process, which is an independent variable to be optimized, and partially controls gas flow and thus pressure, a second independent variable.

The approach taken in this section is to: 1) discuss the ion focusing system in relation to exit aperture and angle; 2) discuss various types of ionization methods, and 3) establish an equation relating the ion current emission to other parameters of the ion source.

4.21 Ion Focusing

Numerous references are available which discuss electron optics and which are equally applicable to ion optics. While the theory of particle motion through an arbitrary field is well established mathematically, the solutions are seldom in closed form, nor applicable to thick apertures. However, the chief difficulty is that

there is little or no insight offered from available equations for synthesis of a desired lens system. Until a method is available for converting a selected particle motion to a set of fields and hence, to a set of electrodes as a process of synthesis, the design of ion and electron lenses will continue to be based upon experience and iterative procedure.

The first step in establishing a lens design is the determination of the desired optical properties based upon geometric light optics as applied to thin lenses. From these rays, the general form of ion motion can be interpreted. While in mass spectrometry an object-image relationship is not necessary in focusing ions from the source, an understanding of the ion distribution at the final slit and also as a function of angle is very useful for the proper design.

Figures 4.21 and 4.22 show several useful types of ray patterns based on light optics. The object (O) is considered to be a thin source of ions passing through thin lenses at H_1, H_2, etc., to an aperture (A). In some cases, an image I is formed. Ions with initial energy transverse to the direction of ion flow create aberrations which are shown as rays divergent from central rays at the origin. These rays are arbitrarily labeled + and - to clarify their path through the lens. Ions formed with initial energy along the direction of ion flow create the equivalent of chromatic aberration, however, this is generally not a serious aberration in the source and thus is not considered here.

In order to convert from the true ion path to the optical equivalent, Figure 4.21(a) shows the ion paths (i) formed with transverse energy (qV_r) in a field E_1, following parabolic paths $y = (4V_r \underline{Z}_1/E_1)^{1/2}$ and reaching the plane H_1 with an angle $dy/dz = (V_r/E_1\underline{Z}_1)^{1/2}$. These have an apparent origin at $\underline{Z}_o = 2\underline{Z}_1$ following paths (O). While, in general, this example cannot be easily extended beyond the first aperture and the uniform field, some insight is gained into the transformation necessary for use of a light-optic analogy. It is not always possible (or in some cases desirable) to have a uniform field in the ionizing region since in the general case, the field is curved due to electron and ion space charge and leakage field from other lenses. However, for the purposes here it is an adequate representation.

Reference to Figure 4.21(b) shows a single, weak, positive lens, focusing parallel rays to a point at the focal distance, f. The angle of emission is thus, $\alpha = \tan^{-1} y_o/f$ (1) a function of the initial position. The distribution of density over the aperture is dependent upon the magnitude of the initial ion energy transverse to the axis of the lens. In a typical situation, the gas is in thermal equilibrium with the walls of the ion chamber thus having, from the Maxwell-Boltzmann distribution law, a radial distribution function:*

$$f(v_r) = (m/4\pi kT)\, e^{-mv_r^2/2kT}$$

* Note: For the case of a circular aperture discussed here, discrimination against thermal energies must be considered for two independent $\underline{X}$ and $\underline{Y}$ initial motions of the molecule. Thus, the radial distribution function is the product of the two distribution functions, however, normalized by integration over radial velocities from 0 to ∞, rather than from $-\infty$ to ∞ in the orthogonal case.

where m is the molecular mass, k, Boltzmann constant, T, the absolute temperature, and v_r, the radial velocity. In terms of initial radial energy, qV_r, this becomes:

$$\psi(V_r) = (m/4\pi kT)e^{-qV_r/kT} \qquad (2)$$

From thin lens optical considerations, the image of this distribution function appears at the final aperture with a radius

$$\rho = F(V_r) = f(V_r/V_c)^{1/2} \qquad (3)$$

where f is the focal length of the lens,

qVr, the initial radial energy, and

qVc, the ion energy at the first aperture potential.

Since the size of this image is dependent upon initial gas temperature, we may label this the thermal image.

Washburn and Berry[7] have demonstrated the characteristic effects of initial energies as well as thermal energy and Berry[8] has calculated transmission through a slit system using the one dimensional distribution. He gives the change in transmission due to initial energies as the forward accelerating voltage is scanned for a magnetic instrument or as the ion source temperature is changed. The arguments he presents make it desirable to avoid using a thermal image if the accelerating voltage is varied during a spectral scan or if the ion source temperature is not controlled. In certain special cases, a variation of ion source temperature will cause a

---

[7] H. W. Washburn and C. E. Berry, Phys. Rev. 70, 559 (1946)

[8] Clifford E. Berry, Phys. Rev. 78, 597 (1950)

variation in the absolute level of ion current, but not change the compositional analysis. This is discussed in Section 4.21.1. In the situation where the ion beam passes from the strong field E_2 into a field free region in leaving the final aperture, a defocusing action takes place. This is indicated in Figure 4.21(c) where the defocusing action is used to place the focus in the final aperture. The example shown is for a field free region between an electrode at the plane H_2 and the aperture at A. The half angular divergence through A is then the value α as seen by the analyzer. It is noted that the effect of the final divergence is to magnify the thermal image.

In order to establish the form of the transmission function, let the initial radial energy be a factor ϕ of the characteristic thermal energy of $q\bar{V} = 3/2\,kT$ such that ρ is equal to the radius r_e of the final aperture. This allows energies less than

$$V_r' = \phi\bar{V} = r_e^2 V_c / f_2 \qquad (4)$$

to be transmitted. If the ionizing region is illuminated to an ion "cathode" density of J^+, current/unit area, and the area of the ion object is πy_o^2, then the ion current formed is $\pi y_o^2 J^+$ and the source current emitted is:

$$I_s^+ = \pi y_o^2 J^+ \int_0^{\phi\bar{V}} \psi(V_r)\, dV_r \qquad (5)$$

Substituting from (1) and (4), where $y_o = f \tan\alpha$ and

$$f^2 = r_e^2 V_c / \phi\bar{V},$$

$$I_s^+ = \pi r_e^2 J^+ \frac{V_c}{\phi \bar{V}} \tan^2\alpha \int_0^{\phi\bar{V}} f(V_r)\, dV_r$$

Since πr_e^2 is the area of the exit aperture and since V_e is an established fraction, k_1*, of the injection voltage when designed for a focal distance of f,

$$I_s^+ = A_e J^+ \frac{k_1 V_I}{\phi \bar{V}} \tan^2\alpha \int_0^{\phi\bar{V}} f(V_r)\, dV_r \qquad (6)$$

Stated as a transmission efficiency,

$$\theta_s = \frac{A_e}{A_o} \frac{k_1 V_I}{\phi \bar{V}} \tan^2\alpha \int_0^{\phi\bar{V}} f(V_r)\, dV_r \qquad (7)$$

It would appear that by increasing V_I, the ion source efficiency could be increased indefinitely. Such is not the case, however, since by the manner in which the problem was set up, the limit of the integration ϕ could be increased in proportion to the applied voltage to maintain $\rho = r_e$. Thus, an increase in transmission will accrue due to an increase in the integration limit up to a plateau which includes all thermally energetic particles. It can be shown that at small ϕ, this increase is proportional to $V_I^{\frac{1}{2}}$, considering only a single direction of thermal motion or as V_I for two directions of motion, as considered here.

*Note: In a cylindrically symmetric system, the focal distance of this type lens is given by $f = 4V_c/E_{z_1} - E_1$. If the focus is at the second aperture, then $k_1 = \frac{1}{(5 + f/z_1)}$ where symbols are as defined previously.

Equations (6) and (7) are the general form of a limiting condition applied to any ion source focused on the thermal image. When upper limits are placed upon A_e and $\tan^2\alpha$ by effects in the analyzer, then sensitivity can only be increased by an increase in V_I up the previously discussed limits or in J^+. Brubaker[9] has shown that J^+ is further limited by non-linearity with pressure when electron and ion space charge reach limiting values. This is discussed further in Section 4.22.1.

A similar limit on system efficiency exists when an ion source such as shown in Figure 4.22(a) is used. In this case, a true ion optical image of the "cathode" is obtained at the final aperture. In so doing, the illumination of the aperture and hence the source transmission, are independent of initial energies. As in the light-optical sense, every point in the image corresponds to a point in the object without regard for the direction of the initial ray (within the limits of the lens boundary).

This type of ion source is used in a satellite mass spectrometer[10] for the purpose of focusing particles of high kinetic energy due to satellite motion, without altering the reading of particle density. The importance of this factor is that the spectrometer may be calibrated in the laboratory using gases at low thermal energies and yet be expected to read the correct densities in orbit.

---

[9] W. M. Brubaker, J. App. Phys. 26, 1007 (1955)

[10] L. G. Hall, P. f. Howden, and T. F. Iwasaki, ASTM, Comm. E-14, 27 June 1960 (unpublished)

While the thermal image ion source has a constant exit angle and a distributed exit aperture density, the opposite is characteristic of the true imaging source since here the exit angle displays the distribution function of initial energies. For this reason, it is necessary that the analyzer accept and transmit angles up to the desired value in the distribution.

The source exit angle is obtained by application of Abbe's sine law.[11] This states that a ray emitted from an object at position y, with an energy qV at the object plane, and with an angle θ to the lens axis, will reach the image plane at angle θ', if the energy is qV' and the position y' at the image plane, by the following relationship:

$$(V)^{1/2} y \sin\theta = (V')^{1/2} y' \sin\theta' \qquad (8)$$

This law applies for paraxial rays between object and image space without regard for the intervening lens system. Since y'/y is the magnification M,

$$\sin\theta' = (V/V')^{1/2} \frac{\sin\theta}{M} \qquad (9)$$

With reference to Figure 4.21(a), we assume in the worst case that particles with initial energy qV_r emerge from the object at $\theta = \pi/2$, reaching the image plane at half-angle $\alpha = \theta'$. Thus,

$$\sin\alpha = (V_r/V_I)^{1/2}/M \qquad (10)$$

---

[11] c.f. O. Klemperer, Electron Optics, p.14, Cambridge University Press, 1953

where qV_I is the injection energy. The transmission function is simply obtained as follows: If the object is illuminated at ion current density J^+, the density at the final aperture is $J^{+\prime} = J^+/M^2$, and the emitted source current is

$$I_s^+ = A_e J^+/M^2 \tag{11}$$

dependent only upon J^+. The object area from which this is drawn is $A_o = \pi y_o'^2 = A_e/M^2$, which should encompass only the central part of the available lens opening if good imaging properties are to be obtained. If the transmission efficiency is given as $\Theta_s = I_s^+/I^+_{formed} = A_e J^{+\prime}/A_o J^+$, then the transmission efficiency is 1 if $A_o = \pi y_o'^2$ is considered the available object or less by $y_o'^+/y_o^2$, if y_o is the lens radius and considered to be the available object.

This argument tacitly assumes that the magnification may be reduced without limit to obtain high source current where, in fact, $\sin^2\alpha$ must increase in proportion to I^+_s for a given initial radial energy. If the analyzer can only transmit angles up to some limiting value α_m, then the fraction of particles transmitted is

$$N/N_{TOT.} = \int_o^{V_r'} \phi(V_r)\, dV_r$$

where $V_r' = V_I M^2 \sin^2\alpha_m$. If the analyzer does not limit in any other manner, then the net transmission is,

$$I_s^+ \; N/N_{TOT.} = I_s^+ \Theta_A = \frac{A_e J}{M^2} \int_o^{V_r'} \phi(V_r)\, dV_r$$

Substituting for M^2 and letting $V_r' = \phi \bar{V}$ as in euqation (4),

$$I_s^+ \theta_A = A_e J^+ \frac{V_I}{\phi \bar{V}} \sin^2 \alpha_m \int_0^{\phi \bar{V}} f(V_r) dV_r \quad (12)$$

The similarity of (6) and (12) indicate that approximately equal limitations are placed on system sensitivity whether a thermal image or true image ion source is used.

It is noted that the lens action of Figure 4.22(a) is to image the central ray of each bundle parallel to the axis. It is not necessary to form parallel bundles in order to form an image, however, the analysis of angles in the non-parallel case requires more detailed knowledge of the lens system.

The lens of Figure 4.22(b) is noteworthy in that this is a mode of operation of two commonly used ion sources.* These sources may be adjusted over a wide range of focal power to provide a tradeoff between angle and intensity.

4.21.1 Ion Lens Considerations for Use With the Quadrupole

In the previous section, the value of matching the ion source aperture and the angle of injection to the quadrupole was discussed. Several other unusual considerations pertain to matching the ion source to this type of analyzer which can control the type of lens used.

In some types of ion sources (c.f., Figure 4.22(b)), it is possible to inject the ion beam with sufficient correlation of angle and

* Note: Both the lens system of A. O. Nier and the CEC Isatron operate in the so-called focused mode to produce this lens action.

position, that the beam appears to come from an object smaller than the slit. In conventional systems, the analyzer can be focused on the apparent object to produce a smaller image of the collectors and, while a corresponding loss in intensity occurs, a higher resolution can be obtained. The nature of the fields in the quadrupole, however, preclude the use of an apparent object to reduce the image width. Ions emergent up to the full value of exit radius, r_e, are captured by the fields and hence, the effective object radius is always r_e.

With reference to the discussion of quadrupole variables, it is seen that there is no electrical control in those euqations which can make the effect of r_e smaller. Consequently, it is important to carefully match this variable in the ion source and quadrupole if the highest performance is to be obtained.

Paul further makes the exit aperture in the form of a nozzle extending along the axis of the quadrupole. While von Zahn[12] from his work on a 6-meter instrument, believes that this nozzle may not be necessary, a desirable control which we wish to apply is the biasing of the final source aperture. We believe that in this case it may be necessary to have a narrow snout to reduce leakage field into the quadrupole. Consequently, it becomes difficult to produce the type of focusing shown in Figure 4.22(a) where other electrodes cannot be placed close to the exit plate.

---

[12] U. von Zahn, Private communication

Consideration of sample flow dictates that the lens openings be held as small as possible. Since the desired apertures for flow are smaller than those indicated for producing the desired ion source sensitivity, the lens opening should be long in the direction of ion flow to reduce gas loss. This further restricts to weak lens action. In the design of these apertures, grazing incidence of the ions should also be avoided so that deposits within the aperture are not formed.

As a consequence of these considerations, the focusing action shown in Figure 4.21 becomes the more practical thus resulting in a thermal image at the exit aperture. While nearly all ion sources are designed and operated with the thermal image to obtain high sensitivity, nevertheless, this mode poses questions on source voltage change and temperature. Since frequency scanning of the quadrupole was chosen to avoid scanning the source voltages, the only remaining question is that of operation in environment of unknown temperature.

It appears that the conceivable gases of the Martian atmosphere could be analyzed on the basis of the parent peak of the spectrum where the only important initial energies would be due to translational velocity at ion chamber temperature. This effect would cause all parent peaks to change in the same proportion with temperature and thus, not necessitate temperature control of the ion sources for measurement and composition. If a more accurate measurement of density is needed to correlate with other measurements, then a measurement of the temperature of the environment near the ion source would suffice to make a correction of the data.

4.22 Electron Bombardment Sources

The most common source of mass spectrometer ionization is by electron bombardment. Figure 4.23 shows several configurations of ionizing techniques which are potentially applicable to this problem.

Figure 4.23(a) shows a magnetically aligned electron beam. The magnetic field, B, constrains the electrons to flow from the filament, f, through the electron aperture, a, and the ion chamber to the anode, A. The field created between the repeller, R, and the ion aperture is set to produce the optimum focusing in the lens system and for operation of the spectrometer. A shield behind the filament is biased negative with respect to the filament to prevent flow of electrons in the opposite direction of the magnetic field and also to provide some measure of focusing.

The advantages of the magnetically aligned beam are: 1) the spacings and source dimensions can be quite compact, thus providing a minimum of volume in the ionizing region; 2) a high percentage of electrons pass through the chamber (compared to total emission) without the use of complex electron beam focusing electrodes; and 3) the ionizing beam maintains a relatively stable position when ion source voltages are scanned. The chief disadvantage is that the presence of the magnetic field causes a small mass separation in the ion source leading to mass discrimination. Only when the voltage, V, is scanned to observe mass, m, by the relationship $mV = \text{const.}$, is discrimination eliminated. This relationship is generally true only for a magnetic deflection spectrometer.

If magnetic fields are to be avoided for a non-magnetic instrument or for other reasons, then several other types of electron bombardment sources may be used. Figure 4.23(b) shows a parabolic trajectory source using the same electrode elements as in the magnetic source. If a parallel electron beam is injected at an angle of 45° through the repeller, the uniform ion accelerating field opposes the electron flow, producing a parabolic trajectory. Parallel rays at the same energy reach the same amplitude of motion in the trajectory and thus, as shown in the inset, produce a one-dimensional, first order focus of the beam. A thin region of ionization in the direction of ion flow results.

When loss of sample gas or electron beam is more important than the effect of sample reacting with the filament, then the filament may be mounted within the ion chamber as shown in (c). The problem of this mounting position is that gases may disassociate at the filament surface leading to a distorted composition in the ionizing region. Sample gas leakage can be minimized by using a dense, non-porous, ceramic for spacing and mounting of anode and electrodes. Filament leads may be sealed into a separate ceramic plate or into the source spacer ring. It is believed, however, that containment of the filament in the ionizing region should be avoided.

Another means of focusing the electron beam, which appears to be new with this report, is shown in Figure 4.23(d). The repeller, R, is made in the shape of a spherical dome, while the accelerator, (Acc.), is a spherical cup. A parallel electron beam injected

through the aperture, a, will then focus in two dimensions to (in theory) a point over the ion aperture. Space charge must be considered, however, which will prevent such a high electron density, and as Robinson[13] has shown, shift the focus along the electron orbit in the direction of flow. This effect could be compensated for by injecting the beam on a convergent path to produce the minimum dimensions over the aperture.

In each of the non-magnetic systems, a more elaborate electron gun than shown would be needed. Typically, a Pierce-type[14] electrode system would be used to produce the parallel beam. If the filament is placed outside the ionizing region, the electron gun design becomes very important in obtaining the highest ionizing current with a minimum of gas loss.

As is discussed in Section 5, a combination of an electron bombardment ion source and a weak magnetic getter ion pump (which also requires an electron beam) is an attractive possibility for saving emitter power. Either of two methods could be used to utilize the same electron beam. The beam passing through the ionizing region could exit through an aperture in place of the anode and thus be used in the ion pump. This, however, creates two openings in the ion chamber causing excessive gas loss. A more efficient method appears to be by use of emission from both sides of the filament.

---

[13] C. F. Robinson, Rev. Sci. Instr. 20, 745 (1949)

[14] J. R. Pierce, Theory and Design of Electron Beams, D. Van Nostrand

Since in a Pierce-type gun, the emission from the back of the emitter returns to the emitter, this method would require a slight increase in filament temperature, but without additional avenues for sample loss.

Returning now to Figure 4.23(b), the field, E_1, required for operation of the trajectory source is given when the components of velocity in the +Z direction reaches zero due to the opposing field; i.e., $q E_1 Z_o = q V_o \sin^2 \phi$

or

$$E_1 = \frac{V_o \sin^2 \phi}{Z_o} \tag{13}$$

Since the velocity in the X direction is unchanged by the field, the ionizing energy at the closest approach to the aperture is

$$q V_i = q V_o - q E_1 Z_o = q V_o (1 - \sin^2 \phi) \tag{14}$$

For $\phi = \pi/4$, $\sin^2 \phi = 1/2$,

$$E_1 = V_o / 2 Z_o \tag{15}$$

and

$$V_1 = V_o / 2 \tag{16}$$

Also, for this angle of injection $X_o = 2 Z_o$ and

$$\Delta V_{Rep\text{-}Acc.} = V_1 Z_1 / Z_o$$

As an example, if the desired ionizing voltage is $V_i = 70$ v , then the injection voltage, V_o, is 140 volts and $E_1 Z_o = V_i = 70$ volts. The size can be made any appropriate value to establish E_1.

For example, if X_o = 0.5 cm, Z_o = 0.25 cm and E_1 = 70v/0.25 cm = 280v/cm. This is in a desirable range of field strength for the ionizing region.

In the spherical beam configuration, electrons are injected at equilibrium energy and are on a circular orbit when

$$q E_o = m v_e^2 / r_o = 2 q V_i / r_o$$

where r_o = orbit radius, E_o = orbit field, v_e = electron velocity, and qV_i the electron ionizing energy. Thus, assuming V_i = 70 volts on radius r_o = 0.5 cm, then $E_o = 2\ V_i/r_o$ = 280v/cm.

4.22.1 Ionization Density of Electron Bombardment Sources

The limits of ionization density depend upon the degree of non-linearity of ion current vs pressure or electron current and upon the degree of ion-molecule collision which can be tolerated. Brubaker's calculations on space charge effects in an ion source demonstrate how space-charge limited conditions may arise with excessive pressure or electron current. Since these calculations are based upon an infinite sheet of charge however, it is difficult to connect these aberrations into conditions where a concentrated electron beam controls the attractive or repulsive field of the charge.

In view of the complex conditions in typical ion sources, the only accurate way to establish the degree of non-linearity for a given ion source is by direct measurement under known conditions. However, some indication of the operating conditions for linear

operation may be obtained from published data[15], where the electron currents, ionizing fields and size of the ionizing electron beam are comparable to that desired here. From this data (R+H, Figure 2) one obtains a field in the ionizing region of 330v/cm to 68v/cm in scanning from m/e 12 to 58. From Figure 8, linearity is obtained for CH_4 at m/e 16 up to 200 microamps at .05 microns Hg in the source.

From Brubaker's results, we find that charge, dimensions, and potential may be increased or decreased providing these changes are made in such a way as to hold all fields of the same relative strength. This allows some latitude for variation even though it must be done in a strict manner and from at least one known set of conditions. If we assume no dimensional changes are considered, from his work we may say that

$$I^- = K_1 E_i \tag{17}$$

and

$$n = \frac{K_2}{Q}\left(\frac{E_i}{M}\right)^{1/2} \tag{18}$$

where I^- = ionizing electron current

E_i = field in the ionizing region

n = molecular density

Q = molecular cross section

M = molecular weight of ions creating the space charge

K_1 and K_2 = constants relating to known conditions of linearity with regard to I^- and n respectively

---

[15] C. F. Robinson and L. G. Hall, Rev. Sci. Instr., 27, 507, (1956)

These equations state, for instance, that if E_i is changed from known conditions, I^- must be changed in proportion and density by $E_i^{\frac{1}{2}}$ in proportion to maintain ion and electron space charge effects constants. Thus, from cited conditions for CH_4 and using MKS units, the constants are approximately,

$K_1 = 8.3 \times 10^{-9}$ amp meter/volt, and

$K_2 = 1.38 \times 10^{-5}$ (AMU volt-meter)

for linear characteristics, where Q is the total ionization for CH_4, taken as 5.53×10^{-20}(meter)^2.

The number of ions formed in ℓ meters of electron beam path is given by:

$$I_f^+ = QI^- \ell n \quad \text{amps} \tag{19}$$

where I^- is the ionizing electron current, and the ionization density is then

$$J^+ = QI^- \ell n / A_o \tag{20}$$

where A_o is the object area of the ionizing region.

Combining (17), (18), and (20),

$$J^+ = K_1 K_2 \frac{E_i^{3/2}}{M^{1/2}} \ell / A_o \quad \text{amps/m}^2 \tag{21}$$

for linear ion source operation.

Combining with (6), the emitted current is

$$I_s^+ = \frac{A_e}{A_o} K_1 K_2 \frac{E_i^{3/2} \ell}{M^{1/2}} \frac{k_1 \sqrt{I}}{\phi \sqrt{}} \tan^2 \alpha \int_0^{\phi \sqrt{}} \psi(V_r) dV_r \tag{22}$$

or from (7)

$$I_s^+ = K_1 K_2 \frac{E_i^{3/2} \ell}{M^{1/2}} \theta_s \tag{23}$$

From these equations, the limiting linear current from the ion source may be calculated, considering the conditions under which the equations were developed. However, values for electron current and molecular density will arise which can be limited by other parameters of the system such as those imposed by the electron emitter or by the pump. We believe, should it be found that other variables do not limit electron current and density, that operation is a non-linear region of the source characteristic would be possible by proper calibration.

4.23 Alpha Bombardment Source

Alpha bombardment appears to be an attractive ionization method for several reasons; the most important being, in this case, the saving in weight, complexity, and power over conventional electron bombardment techniques. In addition to these, however, an ion source without electron apertures may be more tightly enclosed, thereby increasing the differential pumping between source and analyzer and secondly, the spectra[16] may be somewhat simplified.

While the cross-section for ionization by alpha particles is approximately one-half that by electrons, the number of disintegration which may be concentrated in the desired volume is quite small. To some degree this loss can be recovered by use of a higher pressure. The limiting condition then becomes one of ion-molecule collisions giving rise to combination peaks in the spectra. These

---

[16] C. E. Melton and P. S. Randolph, J. of Chem. Phys. 30, 847 (1959)

are undesirable, both from the greater analytical complexity and the additional information to be transmitted.

Reduction in the volume of information could be gained by selection of peaks. However, this appears to be presumptive in view of the unknown composition of the Martian atmosphere. Therefore, we assume that these spurious peaks should be kept below the level of the smallest constituent to be measured; i.e., less than 10^{-3} of the major peaks.

The fact that this requirement is normally difficult is indicated in the results of Field, et al[17], where, in a cycloidal mass spectrometer, they obtain (ref. 17, Figure 3) in the order of 2×10^{-3} CH_5^+ ions from CH_4 at ion source field strengths of 100v/cm, dropping to 10^{-3} at field strengths of 200v/cm. The field strength in this case appears to control the reaction time of the ion in the source. The indicated density in the ion source for these tests was $n = 3.75 \times 10^{13}$ molecules or approximately 1.8 microns at 200°C. In order to avoid spurious combination peaks, therefore, the ion source density should remain below approximately 2×10^{13}/cc, dependent upon field strength and molecular species.

The effect upon the spectra of various hydrocarbons[16, 18], using 5.1 MEV Alpha particles, indicate that fragmentation of the molecule is reduced in comparison to electron bombardment and thus, the spectra simplified.

---

[17] F. H. Field, J. L. Franklin, and F. W. Lampe, J. Am. Chem. Soc. 79, 2419 (1957)

[18] P. S. Rudolph and C. E. Melton, J. of Phys. Chem. 63, 916 (1959)

The effect upon the spectra of the fixed gases is not known. However, it would be expected that they would tend to respond in a similar manner.

4.23.1 Ionization Density of Alpha Bombardment Sources

Using early data on the passage of alphas through air, approximately a constant 4000 ions/alpha/cm of path length/760 mm Hg are produced if the alpha has an energy greater than 1 MEV. From this, we compute a cross-section of $Q_\alpha \approx 1.5 \times 10^{20}$ meter^2. By comparison with the mass spectrometer data of Melton[16] where he obtains 4×10^{-16} amps of $C_2H_2^+$ from acetylene for 2×10^6 disintegrations/sec at a pressure of 2×10^{-4}mm, this cross-section appears to be in rough agreement if we assume Melton's data refers to the ion current formed in the source.

The number of ions formed in the source per sec. is

$$N_f^+ = Q_\alpha N^\alpha \ell n \qquad (24)$$

where N^α is the alpha flux per sec., ℓ the path length, and n, the molecular density or the formed current is

$$I_f^+ = Q_\alpha q N \ell n \qquad (25)$$

where q is the charge per ion.

Since the ions formed are dispersed throughout the ionizing region, a high field or specially shaped electrode system would be required. As a result of the increased volume from which ions must be drawn, the number lying within given increments of volume, angle, and energy would be expected to be smaller. If we assume a fraction k^1

of the volume lying over the object area A_o, is utilized, the useful current formed is

$$I_f^+ = k' A_o/A_\alpha Q_\alpha q N \ell n \qquad (26)$$

where A is the area through which the alpha flux travels; or the ion "cathode" density is

$$J^+ = k'/A_\alpha Q_\alpha q N \ell n \qquad (27)$$

R. Baldock of Oak Ridge National Laboratory has indicated[19] that the level of alpha flux could possibly be increased by three orders of magnitude without creating problems in handling. This capability is dependent upon methods for coating polonium to prevent high surface migration effects of this material. These methods are now under investigation at ORNL. Limitations would eventually be reached due to self absorption of the alphas in the emitting material and coating.

Considering the factors discussed, if we let

$k^1 = 0.1$, $A_o/A = 0.1$

$Q = 1.5 \times 10^{-20} m^2$, $N = 2 \times 10^9$ disintegrations/sec

$\ell = .01$ m and $n = 3.5 \times 10^{19}$ molec/m^3 (1 μ Hg at 0°C)

and assume singly charged particles, then

$$I_f^+ = 1.7 \times 10^{-14} \text{ a}$$

If we further estimate a transmission efficiency of 10%, we would have a collected current of 1.7×10^{-15} a.

For a dynamic range of 10^4, this implies measurement of current

in the approximate range of 2×10^{-15} a to 10^{-19} a. With 6×10^{18} electronic charges/amp sec., the range is 1.2×10^{4} ions/sec to 0.6 ions/sec. Since the dynamic range of 10^{4} is selected to encompass the largest peak and also to read a 0.1% component to 10% accuracy, the smallest peak expected to be of significance would have the order of 6 to 12 ions/sec. Using as a measure of accuracy, $\sigma = 1/n^{\frac{1}{2}}$, where σ is the standard deviation of n gaussian distributed events, the accuracy may be considered to be approximately 30% when 10 ions arrive during a one second reading.

This is certainly a best limiting case, since statistical variations of the electrons in an electron multiplier, background noise, the confidence limit required for this reading and other variables are not considered. However, in view of the large number of assumptions and a possible discrepancy in cross-section, the values calculated could be in error by two orders of magnitude. Such factors as a special ion source, the increase in pressure that could be tolerated, the practical aspects of using alpha emitting materials as well as the realizable increase in intensity can only be obtained experimentally.

We believe, because of the advantages of this ionization method, that further study should be conducted and that because of the complicating factors, this should be on an experimental basis.

4.30 COLLECTOR SYSTEM

The collection of the ions which are transmitted through the quadrupole filter presents some special problems which must be overcome. These are stated below:

4.31 Collection Efficiency and Harmonics

It has been previously stated that one of the requirements of the quadrupole system was that flat-topped peaks were obtained and that this was dependent upon 100% transmission efficiency of the quadrupole. It is clear that the same requirement must also hold for the collection system. That is, if flat-topped peaks are to be produced, then a 100% efficient collector system must be employed. The radial velocity and radius of an ion at the end of the rods can take on a wide range of values, thereby making the job of collection a difficult one.

It must also be pointed out that the frequencies of the major oscillations in the X and Y directions are $\frac{1}{2}(1-\beta_x)\omega$ and $\frac{1}{2}\beta_y\omega$, respectively. Consequently, only for the frequency condition $\beta_x + \beta_y = 1$ will these frequencies be the same. This means that at only one point on the stability diagram will the X and Y motions cross the Z axis at the same time. At all other values of β_x and β_y, the period of oscillation will be different, thereby creating a more severe condition for the collector to overcome. The worst case occurs when β_x and β_y have values such that both the X and Y motions have maxima at the collection point. It is also clear that because frequency is being scanned over a slightly greater range

than 2:1, all possible conditions will be presented to the collector. If the collector is made too small, a mass peak will be chopped into a series of peaks presenting a spectrum that looks very much like a Fraunhofer diffraction pattern. In order to avoid this unsatisfactory condition, it is necessary to make the collector as large as possible, preferably slightly larger than the rod spacing diameter, so that high angle ions will be collected.

4.32 Electrometer Input Capacity

A second problem at the collector is the effect of quadrupole rf voltage on the electrometer input. Since the electrometer is by nature a very sensitive instrument, even a few micromicrofarads of capacitive coupling is enough to impair operation when a large a-c signal is in the vicinity as is the case with the quadrupole voltage. There are two techniques available for combatting this problem. They are: 1) reduce the capacity between the electrometer and the quadrupole rods, and 2) filter the input of the electrometer.

It has already been stated that the collector radius will have to be large and that it will have to be close to the ends of the rods if all of the ions are to be collected. At the same time, filtering the input to the electrometer would greatly increase the leakage resistance on the input, thereby slowing down the time response of the amplifier. This cannot be tolerated if the specified rate of scan is to be maintained.

4.33 Secondary Emission

Another problem which arises in collecting ions is that secondary

electrons inevitably arise. If they are allowed to escape from the collector, an erroneous current will be read. In conventional systems, this problem is overcome by the use of a small aperture, cage-type collector, or else a magnetic field is present which turns the secondary electrons into tight orbits thus prohibiting their escape. Because of the requirements of a large collector aperture, and that magnetic fields are to be avoided if at all possible, neither of these methods are available and others must be resorted to.

4.34 Adaptation of a Multiplier

It is very possible that in order to improve the sensitivity of the detector system, an electron multiplier will have to be employed. Should this happen, then a new requirement would be placed upon the collector system. In order to have a non-discriminating system, and in order to maintain overall accuracy, the ions must be directed toward the first dynode of the multiplier with nearly uniform energy and angle and this property must be maintained over the entire mass range. These conditions cannot be met unless an intervening structure is placed between the end of the quadrupole rods and the first dynode of the multiplier which imposes uniform conditions on the ions.

4.35 Lens System

The only method which appeared to be useful in solving all of the problems presented by a direct electrometer input or by a multiplier input was the use of a post quadrupole lens system. The requirements

on such a lens system are that it have a large initial aperture so that ions with a large radius are accepted; it must have a strong leakage field out into the quadrupole region so that ions with high radial velocities are captured; and the lens structure must be short so that the overall length of the assembly does not become too great.

The lens which appeared to most nearly satisfy these conditions is the three aperture unipotential lens, often called an einzel lens. In this system, all of the electrodes are flat discs with relatively close spacing so that length is minimized. The three electrodes offered maximum shielding of the electrometer. A high refractive power (i.e., short focal length) is obtained when the central electrode is operated far negative. This is also advantageous since it is compatible with the large leakage field. Because of the complex nature of the surrounding fields and the wide range of initial conditions on the incoming ions, a detailed analysis of the lens system was not entered into, and its characteristics were determined by experiment. The actual design and experimental results are covered in Section 6.30.

4.40 SAMPLE FLOW

For accurate analyses, the flow of unknown samples must be predictable throughout the mass spectrometer. The two most critical areas for this requirement are the sample inlet leak and the pump since in the remainder of the mass spectrometer, the flow is molecular in nature.

4.41 Inlet Aperture

The conventional manner of accurate continuous sampling is to first reduce the pressure by means of a continuous viscous flow pressure dividing system and second, at an appropriate pressure, take a small portion of the flow through a molecular leak into the instrument. By holding temperatures constant, the quantity of each gas flowing into the mass spectrometer is in proportion to its partial pressure in the original mixture. Since this method involves relatively high flow rates and two separate pumping systems, it does not appear to be a feasible approach.

In order to arrive at a solution having a single pumping system maintaining a low pressure within the instrument, the sample must be introduced directly from the atmosphere. Three possible flow types present themselves in this flow range: viscous, non-critical; viscous, critical; or molecular. As will be shown, a viscous, critical leak in the range of interest is non-existent since the flow is essentially free-molecular.

Viscous, non-critical flow may be achieved through a single narrow channel or through a multiplicity of channels such as in sintered materials. The single channel is sufficient to define the characteristics. For isothermal flow in a long capillary channel, the boundary layer almost immediately (in approximately 8 diameters) fills the opening at the entrance and the resulting flow can be expressed as

$$Q_m = \left(\frac{M}{RT}\right) \frac{a^2 (P_1^2 - P_2^2)}{16 \eta L} A \text{ grams/sec} \quad (1)$$

where: Q_m = mass flow (grams/sec.)

M = molecular weight of the gas

R = 8.31×10^7 ergs/°K/mole

T = temperature (°K)

a = radius of the capillary (cm)

P_1 = entrance pressure (dynes/cm^2)

P_2 = exit pressure (dynes/cm^2)

η = viscosity of mixture (poise)

ℓ = capillary length (cm)

A = capillary cross section (cm^2)

For the problem at hand $P_1 \gg P_2$ and thus P_2 is neglected. This also neglects the nature of flow at the exit where in some cases the velocity is equal to the speed of sound thereby causing a series of expanding and contracting shock waves to dissipate the remaining energy of flow. We may further simplify to energy flow in ergs/sec. by multiplying both sides by (RT/M). This is then in terms of pressure times conductance, or:

$$Q_E = P_1 C = \frac{a^2 P_1^2 A}{16 \eta \ell} \qquad (2)$$

First it is observed that the quantity of flow increases as the square of the external pressure. Since internal pressure is proportional to flow for a constant pump speed it is seen that a wider dynamic range would be required for this $P_{in} = P_{ex}^2$ relation than for a linear pressure increase. The second adverse factor is that the internal sample is a function of the viscosity of the mixture. The viscosity of the mixture is a complicated empirical relation

depending upon the relative amounts of the various constituents, and it also varies empirically with temperature.

4.41.2 Molecular Flow

It is apparent that if molecular flow could be achieved directly from the atmosphere, the inlet flow problem would reduce to only a temperature measurement. The number of molecules passing through an aperture A cm^2 per unit time is

$$N_i = \frac{n_i \bar{C}_i A_i}{4} \quad \text{MOLECULES/SECONDS} \tag{3}$$

where n is the density in molecules/cc,

subscript i refers to inlet, and

$\bar{C} = \left(\frac{8RT}{\pi m}\right)^{1/2}$ is the mean molecular speed in cm/sec.

If this flow takes place directly into the ionizing region of the mass spectrometer and the flow out of the source is molecular, then

$$N_s = \frac{n_s \bar{C}_s A_s}{4} = \frac{n_i \bar{C}_i A_i}{4} \tag{4}$$

or the source density

$$n_s = \frac{A_i}{A_s}\left(\frac{T_i}{T_s}\right)^{1/2} n_i \tag{5}$$

Thus if the mass spectrometer is accurately calibrated as a function of density, the density of each species in the atmosphere is known by a knowledge of the temperature ratio T_2/T_s.

In order to determine the requisites of molecular flow we express the Knudsen flow equation[1] of conductance

$$C = \left(\frac{\pi}{128}\frac{D^4\bar{P}}{\eta L}\right) + \left(\frac{1}{6}\sqrt{\frac{2\pi KT}{m}}\frac{D^3}{L}\right)\left(\frac{1+\sqrt{\frac{m}{KT}}\frac{D\bar{P}}{\eta}}{1+1.24\sqrt{\frac{m}{KT}}\frac{D\bar{P}}{\eta}}\right) \text{ C.G.S. UNITS} \tag{6}$$

[1] c.f., Any text on "Kinetic Theory of Gases" such as L. B. Loeb, McGraw Hill p. 295 ff (1934).

as is normally done by

$$C = \frac{1}{L}\left(aP + b\,\frac{1+cP}{1+fP}\right) \tag{7}$$

If L is considered to be an increment of length Δ L and since the flow Q is given as $Q = C\Delta P$, then

$$Q = \left(aP + b\,\frac{1+cP}{1+fP}\right)\frac{\Delta P}{\Delta L} \tag{8}$$

may be integrated[2] to provide

$$Q = \frac{1}{L}\left[\frac{a}{2}P^2 + \frac{bc}{f}P + \frac{b(f-c)}{f^2}\,\ln(1+fP)\right]_{P_2}^{P_1} \tag{9}$$

where P_1 is the entrance pressure and P_2 the exit pressure. This equation covers viscous (non-turbulent) and molecular flow over wide ranges of pressure, channel length and diameter. We may simplify this equation in our case since $P_2 \ll P_1$ by letting the lower integration limit $P_2 = 0$.

From the nature of the original equation the coefficient (a) represents viscous conductance while the coefficient (b) represents conductance in the molecular flow region and (c) and (f) are coefficients effective in the transistor region between viscous and molecular flow.

By manipulation (3) becomes

$$QL = \frac{a}{2}P^2 + bP\left[\frac{c}{f}\left(1 - \frac{\ln(1+fP)}{fP}\right) + \frac{\ln(1+fP)}{fP}\right] \tag{10}$$

---

[2] c. f., Guthrie and Wakerling Vacuum Equipment and Technique, p. 191, McGraw Hill (1949) and Ochert and Steckelmacher, Brit. J. App. Phys. 2, 332 (1951)

or since the following are related numerically: a = .029 bf and c/f = .807; then

$$QL = .058\, bf P^2 + bP\left[.807\left(1 - \frac{\ln(1+fP)}{fP}\right) + \frac{\ln(1+fP)}{fP}\right] \qquad (11)$$

Factoring bP and letting f P = x and bP = y

$$QL = \left[0.058\, x + .807\left(1 - \frac{\ln(1+x)}{x}\right) + \frac{\ln(1+x)}{x}\right] y \qquad (12)$$

where $x = fP = \left(\frac{m}{kT}\right)^{1/2} \frac{D}{\eta} P_1$ (dimensionless) (13)

and $y = bP = \frac{1}{6}\left(\frac{2\pi kT}{m}\right)^{1/2} D^3 P_1$ ergs/sec. (14)

in c.g.s. units.

As $x \to 0$, $\frac{\ln(1+x)}{x} \to 1$, and QL = y which is equivalent to the molecular flow equation

$$Q = \frac{\pi}{3}\left(\frac{kT}{2\pi m}\right)^{1/2} \frac{D^3}{L} \Delta P \qquad \text{ergs/sec (c.g.s.)} \qquad (15)$$

Since, within the brackets of equation (12) we have a function of viscosity and pressure which approaches the value 1 at low pressure, thus we may plot the deviation from molecular flow as a function of x = fP. This is shown in Figure 4.41.

From this characteristic we may then calculate the inlet apertures required for molecular flow. Using air at 10^5 microns Hg at 0°C the aperture length in microns is plotted against aperture diameter in microns with flow in micron - cc/sec. as a parameter in Figures 4.42 and 4.43.

4.42 Differential Pumping

The basic flow system which is under consideration is shown in Figure 4.44.

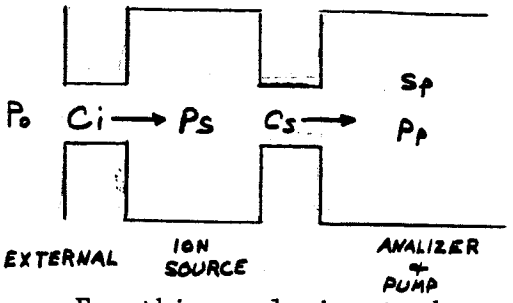

P_0 = outside pressure
P_s = source pressure
P_p = pump and analyzer pressure
S_p = pump speed
C_i = inlet conductance
C_s = source conductance

For this analysis steady state conditions shall be assumed along with a single component sample, and molecular flow at all apertures. There are three flow equations governing this system:

$$P_o C_i = (P_s - P_p) C_s \qquad \text{for } P_o \gg P_s \tag{16}$$

$$(P_s - P_p) C_s = P_p S_p \tag{17}$$

$$P_o C_i = P_p S_p \tag{18}$$

We shall assume that the atmospheric pressure is constant at its surface value. This will place the most severe conditions on the pump system. Then we make use of the molecular flow relation:

$$Q = P_o C_i \quad \mu\text{-cc/sec} \qquad \text{where } P_o \gg P_s \tag{19}$$

Substituting this into equations (16) and (18):

$$Q = (P_s - P_p)\, C_s \quad \mu\text{-cc/sec} \tag{20}$$

$$Q = P_p S_p \quad \mu\text{-cc/sec} \tag{21}$$

One of the primary considerations in the design of an ion source for this particular application is that of high differential pumping.

This implies that the pressure in the ionizing region is high compared to the pressure in the analyzer and the pump. It is not necessary to maintain the entire source at this elevated pressure. In fact it is best to confine this volume to its minimum value which is the ionizing region. The reasons for this are:

1) The minimizing of the surface area of the ionizing region in conjunction with the differential pumping reduces the effect of surface interactions on the background spectrum and at the same time reduces the magnitude of this spectrum.

2) The second important feature of this configuration arises from the relatively poor pumping of inert gases (notably argon). In the pump and analyzer sections the background will become extremely distorted due to the build up of argon but this effect is minimized by the differential pumping of the source.

3) A by product of the differential pumping is improved source sensitivity for a given pump pressure. This improved sensitivity is traded off against the impaired sensitivity due to the necessary restriction of the ion beam. However, this restriction would be forced to a large extent anyway by the small size of r_0 and the ratio r_0/r_e requirements for a 100% transmission efficiency. In other words although source sensitivity could in theory be increased by making the exit aperture larger, a real improvement cannot be obtained because those ions entering the analyzer at larger radius cannot be accepted.

4) Another reason for minimizing the volume of the ionizing region is to improve the time constant of the sample flow system.

The effects of differential pumping can be investigated by defining the following ratio as a fundamental quantity of interest:

$$D = P_s/P_p \tag{22}$$

This quantity can then be substituted into the previous flow equations. A question arises as to which pressure, P_s or P_p should be substituted for. If P_s is removed from the equations then the limitations on the pumping system can be investigated. If P_p is removed, the limitations imposed by source sensitivity can be investigated. Let the first of these alternatives be followed. The following equations result:

$$Q = P_p C_s (D-1) \ \mu cc/sec. \tag{23}$$

$$D = 1 + S_p/C_s \tag{24}$$

Equation 24 is the fundamental relationship which determines the value of differential pumping. If a few typical values of S_p and C_s are assumed the approximate range of D can be determined. The conductance of the source is determined by three apertures:

1) Ion beam exit

2) Electron beam entrance

3) Electron beam exit

It is immediately clear that there are practical limitations to the conductances of these apertures based on the necessity that they

transmit a certain amount of current. In the case of the electron beam, space charge repulsion limits the size of the cross section to a significant value. In the case of the ion beam, practical limitations on the focal properties of the lens system require a significant cross section. The net result is that an extremely low source conductance cannot be obtained. It had been previously thought that the same electron beam could be used for both the ion source and ion pump operations, however, this would require an electron beam exit, further increasing the source conductance. It was therefore decided to use separate electron beams but obtain them from the same filament. In this way the beam can be collected by an anode structure at source pressure. The filament itself, must be in a pumped region of the flow system because of the chemical reactions at the elevated temperature and their affects on the sample analysis.

Based on the calculations of the ion source design it appears that the ion exit aperture can be reduced to about 2 cc/sec. or less. So far as the electron beam entrance aperture is concerned it is not presently known what the limiting value of conductance will be. It will depend upon the effort which goes into the electron gun design and the emission efficiency which must be maintained.

Let it be assumed that a 100μa electron beam is used which has been accelerated through 140v. The perveance of this beam would be about 6×10^{-8} m.k.s. units which is not very high considering values of 2×10^{-6} have been attained. This value therefore appears reasonable.

Then if the minimum radius of the beam is y_0 at an axial distance of $40y_0$, the beam radius is $1.7y_0$. Therefore the problem involves the original focus. This problem has not been thoroughly investigated.

The ion source which was tested had a total source conductance of about 35 cc/sec. which gives a differential pumping factor of about 4.3 for a pump speed of 150 cc/sec. For the same pump speed a conductance of 7.5 cc/sec. is needed if a differential pumping factor of 20 is to be obtained. This value can be attained by using a electron beam entrace aperture 0.100" x 0.030" x 0.010". Careful electron gun design might well make this a reasonable value. The result is that a D = 20 is probably possible with a 150 cc/sec.

From equation (23) it is seen that for D = 20

$$Q = 19P_pC_s \ \mu cc/sec.$$

Then P_p max = $1 \times 10^{-2} \mu$ implies

$$Q_{max} = 1.42 \ \mu cc/sec. \text{ at maximum external pressure.}$$

It appears that this value should be held as closely as possible so that the overall system sensitivity is high enough. There does not appear to be any great difficulties in the flow system provided that the pump is good enough. This will be considered in the next section on pumping.

Let us examine briefly the sample distortion problem.

Let $P_0 = P_{a0} + P_{i0}$ a = active

i = inactive

Then $Q \cong (P_{a0} + P_{i0})C_i = P_{ap}S_a + P_{ip}S_i$

$Q_a = P_{a0}C_i = P_{ap}S_a$

$Q_i = P_{i0}C_i = P_{ip}S_i$

$$P_s = P_p \left[\frac{S_p}{C_s} + 1\right] \tag{25}$$

$$P_{as} = P_{ap}\left[1 + \frac{S_a}{C_s}\right] = P_{ap} D_a \tag{26}$$

$$P_{is} = P_{ip}\left[1 + \frac{S_i}{C_s}\right] = P_{ip} D_i \tag{27}$$

Then

$$\frac{P_{as}}{P_{is}} = \frac{S_i}{S_a}\frac{P_{a0}}{P_{i0}}\left(\frac{C_s + S_a}{C_s + S_i}\right) \tag{28}$$

Let $D_a = 20$ and $\frac{S_i}{S_a} = 0.08$

$S_a = 150$ cc/sec. $\quad C_s = 7.5$ cc/sec.

$$\frac{P_{as}}{P_{is}} = 0.65\,\frac{P_{a0}}{P_{i0}}$$

This is a substantial improvement over a source with no differential pumping which would have a value of: $P_{as}/P_{is} = 0.08\ P_{a0}/P_{i0}$. However, it is clear that this distortion would have to be calibrated. If a triode type pump were used the distortion would be considerably less as can readily be calculated.

4.50 PUMPING

4.51 Theory

The general boundary conditions of this problem dictate that the only practical method for maintaining a working pressure in the mass spectrometer is by using some type of getter-ion pump. There are three important mechanisms at work in such a pump which combine to give effective results:

a. Active gases are pumped by the gettering action of the metal surfaces. These surfaces are conventionally of titanium. At 20°C, the sorption rate of such a surface ranges from 3 liters/sec/cm^2 for N_2 to 12 liters/sec/cm^2 for CO with other values within this range for other active gases. Under varying conditions of temperature and gas composition, the effective gettering action will, of course, vary and, therefore, larger surface areas are needed than indicated by these numbers.

b. Gas molecules are ionized by electron bombardment and are thereby pumped. This is the mechanism by which the chemically inactive gases are pumped. Consequently, if the background of inactive gases is to remain nearly constant, relative to that of the active gases, it is necessary to ionize the inert gases at a rate which will compare favorably with the rate at which active gases are being adsorbed. The active gases are also pumped by the ionization process and therefore the following equations apply:

$$\frac{dp_a}{dt} = \frac{Q_a}{V} = -\left(\frac{s_g + S_i}{V}\right)p_a + \left(\frac{P_{ao} - P_a}{V}\right)C \qquad (1)$$

$$\frac{dP_i}{dt} = \frac{Q_i}{V} = -\frac{S_i P_i}{V} + \left(\frac{P_{io} - P_i}{V}\right) C \qquad (2)$$

where

P_i = inactive gas pressure in pump

P_a = active gas pressure in pump

V = pump volume

S_g = getter pumping

S_i = ionization pumping speed

C = conductance into pump cavity

P_{io} = constant external inactive gas pressure

P_{ao} = constant external active gas pressure

Q = gas flow

Solving these equations and setting $t = \infty$ gives the stable values of P_i and P_a as:

$$P_a(\infty) = \frac{P_{ao} C}{S_g + S_i + C} \; ; \; P_i(\infty) = \frac{P_{io} C}{S_i + C} \qquad (3)$$

then,

$$\frac{P_a(\infty)}{P_i(\infty)} = \frac{P_{ao}}{P_{io}} \left[\frac{S_i + C}{S_g + S_i + C}\right] \qquad (4)$$

It is seen from this that in order to keep the ratio $\frac{P_a}{P_i}$ nearly the same as $\frac{P_{ao}}{P_{io}}$, it is necessary to have:

$$S_i + C \gg S_g \qquad (5)$$

If we assume that this implies:

$$S_i \gg S_g \qquad (6)$$

then using the general flow equation:

$$Q = P_o C \approx P_p S_i \qquad P_p = \text{pump pressure} \qquad (7)$$

and since $P_p \ll P_o$, it is seen that

$$S_i \gg C \qquad (8)$$

and the assumption is seen to be correct. Then,

$$\frac{P_a(\infty)}{P_i(\infty)} \simeq \frac{P_{ao}}{P_{io}} \frac{S_i}{S_a} \qquad S_a = \text{pump speed for active gas} \qquad (9)$$

The result of this is that ion pumping must be the most important agent in the pump if the sample is to remain undistorted. This situation is also aided by differential pumping of the source; however, it appears that the desired ratio of differential pumping may not be achievable and hence, the burden of the sample distortion problem is thrown back on the ion pump.

c. The ionization of a gas molecule does no guarantee that it will be pumped. By some mechanism it must be bound to the surface and remain there. In the case of an active gas, this mechanism is the weak adsorption bond. The pumping speed of this mechanism has already been briefly discussed; however, the capacity of this pumping mechanism must also be considered. The capacity of titanium for N_2 is about 0.05 micro-liters/cm^2.

At a pressure of 5×10^{-5}mm and assuming the sorption rate of a clean surface, it would take about 0.3 seconds to completely saturate the titanium. This value may be inaccurate since the exact conditions for which it pertains are not known. There-

fore, sputtering must be relied upon to continuously lay down a fresh coat of titanium on the cathode. Sputtering of titanium is obtained by allowing ions to impinge upon a titanium surface. The orientation of this surface, with respect to the cathode, is of extreme importance and will be discussed shortly.

The method by which the inactive gases are pumped is also dependent upon sputtering but for a different reason. Inactive gases are pumped by being buried by a new layer of sputtered titanium. The impinging ions penetrate the cathode surface to a depth of of about two molecular layers (the exact depth depending upon the impact velocity), and they must be covered over to a greater depth at some rate such that an appreciable number of them cannot diffuse to the surface. The diffusion rates of inert gases in titanium are not precisely known and therefore, it is difficult to set the necessary sputtering rate. The depositing ion rate, as a function of ion current, is found below:

Atomic volume of T_i = 10.6 cc/gm at. wt.

Therefore,

$$\therefore \frac{6.06 \times 10^{23} \text{ atoms/mole}}{10.6 \text{ cc/mole}} = 5.72 \times 10^{22} \text{ atoms/cc}$$

Taking the two-thirds power:

1.48×10^{15} $\frac{\text{atoms}}{\text{cm}^2\text{-layer}}$ from which it is easily found:

$$l = 4.2 \times 10^{-3} \frac{I^+ \gamma}{A} \frac{\text{Layers}}{\text{Sec}} = \frac{K_1 I^+ \gamma}{A} \qquad (10)$$

A = area in cm^2

I^+ = ion current microamps

r = sputtering factor = $\frac{\text{sputtered atoms}}{\text{ion}}$

This equation can now be applied to find the ratio of ion current to pressure.

The saturation time is inversely proportional to pressure:

$$T_s = K_2/P\mu \tag{11}$$

$P\mu$ = pressure in microns

In order to maintain a clean surface,

$$1 = K_3/T_s \tag{12}$$

where the value of k_2 is not exactly known. Combining these equations with the earlier one yields:

$$\frac{I+}{P\mu} = \frac{A\,K_3}{K_1 K_2 \gamma} \quad \frac{\mu a}{\mu} \tag{13}$$

By the proper choice of k_2 and k_3, and γ which are not accurately known, the value of I^+/P can be brought into close agreement with those values obtained on commercially available getter-ion pumps. The values of these constants necessary to achieve this agreement are conceivably within reason. This result was stated in terms of the theory behind the pumping of active gases; however, the form of the last equation also holds for the pumping of inert gases in a system which makes effective use of sputtering. This fact is evidenced by the experimental data which has been obtained on commercial pumps. It is true that the exact method by which the gas is pumped is somewhat different than in the case of active gases; however, the results are the same.

Each of the mechanisms which has been discussed is of importance in achieving good overall pump characteristics and therefore, the effectiveness of a pump must be considered in the light of these factors.

4.52 Types of Getter Ion Pumps

Commercially available ion pumps are magnetic and therefore are not too desirable for this application. Because magnetic pumps have been proven, it is felt that they should be discussed. Three types of non-magnetic or weak magnetic pumps were also investigated and the results are stated below.

4.52.1 Magnetic

The two types of magnetic pumps which are available are a diode-type, such as the Varion VacIon pump and a triode-type such as the Consolidated Vacuum Corporation Drivac pump. It has been pointed out by Brubaker[1] that the triode-type ion pump is considerably more effective in the pumping of inactive gases (notably argon). The basic reason for this is that the pumping of inactive gases is much more dependent upon the effective use of sputtering than is the pumping of active gases. In a diode pump, the sputtering is extremely ineffective because it is only obtained by the impinging of ions on the cathode surface. This causes titanium to be sputtered back on the surface from which it came. The result is that an inactive gas

---

1 W. M. Brubaker, "A Method for Greatly Enhancing the Dumping Action of a Penning Discharge"

which has very weak adsorption bonds is re-evolved when this takes place. Consequently, the gas is not effectively pumped.

In the case of a triode pump, the majority of the puttering occurs at the grid and this material is deposited on the cathode surface, burying the weakly bonded gases so that they cannot escape. The relative effectiveness of these methods is attested to by the fact that the advertised relative pumping speed of argon in a VacIon pump is 1% that of air, while the advertised value is about 33% of air for the Drivac.

The appeal of the VacIon pump rests solely in the fact that there is one commercially available which could conceivably be flown. Its specifications are as follows:

Speed - 0.15 liters/sec

Weight - 0.42 pounds

Approx. size - 2 inches x 2 inches x 1 inch = 4 cubic inches

Current/pressure - approximately 3×10^3 microamps/micron

Power - 0.15 watts at 1.5×10^{-5}

Larger VacIon pumps are available which obtain an advertised relative pumping speed for argon of 8%. This is accomplished by special machining of the cathode surface. Varian is willing to do this machining on one of its 0.15 liter/sec pumps, so conceivably, a pump could be readily obtained with the specifications given which has a relative pumping speed for argon of 8%. While this is not nearly as high as would be necessary to avoid appreciable sample distortion

during the fall through the Martian atmosphere, it may be necessary to accept such a solution.

Referring to equation (4), it is seen that:

$$\frac{P_a(\infty)}{P_i(\infty)} \cong 0.08 \frac{P_{ao}}{P_{io}} \tag{14}$$

The time constants of this stabilization are:

$$\tau_a \cong \frac{V}{S_a} \qquad \tau_i \cong \frac{V}{S_i} \tag{15}$$

There are two time constant since the gases reach equilbrium independently of each other. If a volume of 1 liter is assumed for the pump and quadrupole, then

$$\tau_a = 66 \text{ seconds} \qquad \tau_i = 830 \text{ seconds} \tag{16}$$

These time constants are so short that sampling could not continue for an appreciable time without severe problems of sample distortion and pressure increase.

If a triode-type pump were used with a relative pumping speed of 30% that of air, it is found that:

$$\frac{P_a(\infty)}{P_i(\infty)} = 0.33 \frac{P_{ao}}{P_{io}} \qquad \begin{aligned} \tau_a &= 66 \text{ Seconds} \\ \tau_i &= 198 \text{ Seconds} \end{aligned} \tag{17}$$

The final pressure will, of course, be lower because of the higher overall pumping speed. The triode pump appears to be only slightly more efficient than the diode as far as the pumping of active gases is concerned, but the fact that it pumps argon so much more effectively makes it a more acceptable unit. At the present time, a small triode pump is not commercially available, but there appears to be no reason that one could not be constructed small enough to

become flight hardware. Because of the slightly more complex structure, a 0.15 l/sec pump might be slightly larger than the VacIon pump of the same speed.

The significant problem associated with either of these types is the magnetic field which is used to maintain the electron orbits. The field strength must be high in order to maintain a high space charge saturation level which, in turn, means a high ratio of ion current to electron current. Several methods were investigated for trapping the electrons without the use of these high fields and are discussed below.

4.52.2 Spherical Electrostatic Field Pump

The first pump considered has an essentially spherical geometry, with the anode at the center and the electrons emitted near the surface of the surrounding cathode. It is found that if the emitted electrons have enough tangential velocity, they will orbit the anode and, having orbited once, will continue to do so until a gas molecule is struck.

There is one difficulty, however, in that being in an inverse square field, any electron starting from a given point and orbiting the anode will return to the same point, with the result that a collision with the emitting structure may occur. An electron orbiting an anode in cylindrical geometry, however, will follow an elliptical path which precesses about the anode at a rate of 254° per orbit. This suggests the possibility of using a basically spherical geometry

with a slight eccentricity to obtain just enough precession so that the electron does not return to the same point from which it was emitted and yet without loss of the Z-axis constraint. (Z-axis defined as perpendicular to the plane of intended orbiting.) Likewise, the orbits may pass above and below an emitter because of the slightly aspherical field.

Figure 4.51 shows a conceptual design for the scheme just described. One point of particular importance is the support of the centrally located anode. This must be accomplished such that the essentially spherical field is maintained. The proposed method makes use of a central conductor for the anode lead which is covered with ceramic insulation. A conductive coating is then deposited on the surface of the insulator with a tapered thickness to obtain the 1/r voltage variation. This coating is then protected by a series of shields so that change in conductivity due to sputtering of the cathode material does not occur.

Thorough investigation of this proposed method revealed several basic problems which appeared to be nearly insoluble. If a precessing elliptical orbit is relied upon to obtain a long path length, it is not certain that the two conditions of enough precession to miss the emitting point on the first orbit and yet not enough precession to cause the orbit to precess the full 360° and return too quickly, can be simultaneously met. In addition, this scheme would require highly eccentric orbits for best results and this causes the average ion impact energy to be low for a given anode potential,

thus reducing the efficiency of the pumping action. The restriction of high eccentricity places a tight restriction on the range of initial conditions which can be tolerated for stable orbits. This means that a crude method of getting the electrons into orbit cannot be relied upon. It was originally thought that the magnetic field created by the filament current might, under the proper geometrical conditions, act on the emitted electrons in such a way that sufficient side energy would be obtained. Another method which was considered was to place a small accelerating electrode near the filament to help the electrons into orbit. In view of the strict requirements on entrance angle, these schemes had to be abandoned. Nothing short of an electron gun would be sufficient. Several orientations of the gun were considered, but in no instance could the question of ultimate return to the emitting point be resolved. Part of the problem lies in the fact that calculation of the orbits for an aspherical system out of the plane of symmetry is quite difficult. This method was abandoned.

4.52.3 Cylindrical Electrostatic Pump

An idea for a cylindrical ion pump was conceived which appeared to have promise. Part of its appeal was that sufficiently accurate calculations could be carried out to determine if the efficiency would be high enough. This pump consists of an appropriately shaped rod (anode) inside a cylcindrical shell (cathode) closed at the ends as shown in Figure 4.52(a). Electrons are emitted from a source as shown. The electrons are directed at some minimum pitch angle α

min. with an angular spread $\Delta\alpha$ above the principle plane which is perpendicular to the central axis. The motion of the electron in the principle plane is made circular by balancing the centrifugal and electrostatic forces. These factors result in an electron trajectory that spirals upward. In order for all electrons to get past the source on the first orbit, it is necessary that α min. be greater than some value which depends on the size of the source.

In order to achieve the necessary efficiency, an electron path length of 1000 cm is desirable. If the pitch angle of the electron trajectory is decreased after it passes the source, the path length will be increased. This can be accomplished by a decelerating region in which the axial component of velocity is decreased. In this region, the central rod and outer shell radii are reduced. The deceleration region is designed so that the axial velocity of the electron with minimum initial axial velocity will be reduced to zero. The weakness of this system is that only those electrons with one particular axial velocity can achieve stable orbits. All electrons with a greater initial axial velocity will still have a residual axial velocity after passing through the decelerating region. This results in lower average path lengths. Those electrons which continue to spiral upward above the decelerating region will be reflected by the curved end of the shell. The pitch angle after reflection will be the same as before reflection, except for the reversal in the axial component of velocity. The electrons then return to the end from which they started and strike the surface.

It is clear that in this type of pump, the electrons have a geometry limited path length as previously discussed.

The detailed calculations are given below. Refer to Figure 4.53 for definitions of parameters.

$$E_r = \frac{\Delta V}{\ln(r_{c1}/r_{a1})} \frac{1}{r} = \frac{K_1}{r} \qquad \frac{\text{VOLTS}}{\text{METER}} \tag{18}$$

In equilibrium:

$$\frac{mV_\theta^2}{r} = eE_r = \frac{eK_1}{r} \qquad V_\theta = \text{orbital velocity} \tag{19}$$

from which,

$$V_{\theta_1}^2 = \frac{e}{m} K_1 \tag{20}$$

Note that this equation is independent of radius.

Let $eV_0 = \frac{1}{2} m v_0^2$ = initial kinetic energy (21)

then, $V_\theta = V_0 \cos\alpha$ = tangential velocity (22)

which results in:

$$V_0 = \frac{1}{2} \frac{K_1}{\cos^2\alpha} \tag{23}$$

which fixes the initial conditions in terms of α, ΔV, and r_c/r_a.

The Z component of velocity in region 1 is given by:

$$V_{z_1} = V_0 \sin\alpha = \sqrt{\frac{eK_1}{m}} \tan\alpha \tag{24}$$

When the electrons pass through the decelerating region, they reach a new axial velocity V_{z_2}:

$$V_{z_2} = \sqrt{V_{z_1}^2 - 2\frac{e}{m} E_z z_1} \tag{25}$$

Where it has been assumed that E_z is constant over the distance Z_1. The limiting condition which is desired is $V_{z2} = 0$, which implies:

$$Z_1 = \frac{1}{2} \frac{m}{e} \frac{V_{z1}^2}{E_z} \tag{26}$$

Only an approximate value of Z_1 is needed to determine if it is short, compared with the total maximum allowable length of the pump. In line with this, an approximate expression for E_z is used:

$$E_z \approx E_r \sin\beta = \frac{K_1}{r_{e1}} \sin\beta \tag{27}$$

where it will be assumed for the moment that K_1 and V_e remain constant.

Substitution for E_z and V_{z1} yield:

$$Z_1 = \frac{1}{2} r_e \frac{\tan^2\alpha}{\sin\beta} \tag{28}$$

As an example, let:

$r_e = 0.5$ cm

$= 30°$

$\tan^2 \quad = 0.335$

$L = 3$ inches

$Z_1/L = 0.10$

This implies:

$\beta = 6.3°$

It is evident that the values of r_{a2} and r_{c2} are not much different than r_{a1} and r_{c2}. Consequently, no particular problems appear to present themselves so far as geometry is concerned.

In region 2 the new equilbrium radius will be:

$$r_{e2} = r_{e1}\frac{V_{e1}}{V_{e2}} = r_{e1}\sqrt{\frac{K_1}{K_2}} = \sqrt{\frac{\ln r_{c2}/r_{a2}}{\ln r_{c1}/r_{a1}}} \qquad (29)$$

This result was obtained by use of the principle of conservation of angular momentum which must hold in a cylindrical system. Since the ratio r_{c2}/r_{a2} is very nearly the same as r_{c1}/r_{a1}, it is implied that $r_{e2} \approx r_{e1}$. This implies that the orbiting electrons will be relatively closer to the cathode in region 2 than in region 1. The result is a relatively lower ion impact energy which is undesirable since sputtering is reduced.

Investigation of the effect of angular spread of the electron beam was carried out by finding the average ratio of path length/axial length as a function of total angular spread. The results are shown in Figure 4.54. These results are for the pump geometry of Figure 4.52(a). A pump with a 3-inch length would have a somewhat shorter effective length (approximately 2 inches) by which to multiply the D/Z ratio. This is due to the ineffectiveness of regions 1 and 2 and the reflecting region of the pump. It can be concluded that only a very narrow beam spread can be tolerated if a 1000 cm path length is to be achieved. Such a narrow spread would be unattainable in actual practice.

A modification of this design was also considered. This was to convert the pump into a double-ended geometry as shown in Figure 4.52(b). In this system, the average path length is not only dependent upon α and $\Delta\alpha$ but also upon the probability of an electron getting past

the electron gun on its return trip.

This probability is easily computed to be:

$$P_{trans} = \frac{r_{e1}}{l} \quad \frac{1}{1+(h/l)/\tan\alpha} \qquad (30)$$

where:

p = transmission probability

r_e = equilibrium radius

l = length of emitting structure

h = height of emitting structure

α = pitch angle

This relation is plotted in Figure 4.56 for two values of h and 1. If p = 0.5, the double-ended gun is exactly equivalent to the single-ended pump of the same dimensions and pitch angle α . It is seen that the higher the value of α , the higher is the probability of transmission past the emitting structure. This requirement is opposed to the requirement of low pitch angle for long path length. It is then expected that there will be an optimum pitch angle. This is borne out in Figure 4.55. An angular spread of 10% because it was felt that for the small emitting structures which are under consideration, a lower value of $\Delta\alpha$ could not be obtained. It is seen from the graph that the maximum value of path length is about 200 cm. Again, a 1-inch effective value for L is assumed. This is not as high as would be desirable.

Space charge effects have not been taken into account in this analysis. In actual operation, a sheath of space charge would exist about a

radius r_e. This would result in space charge saturation of the pump volume. The density of this saturation would be extremely low because there is no Z axis constraint to keep the electrons away from the emitting source. Consequently, it was felt that space charge analysis would not be fruitful and the decision to abandon this design was based upon the analysis presented.

4.52.4 Weak Magnetic Pump

Another new pump which was conceived and studied was a weak magnetic field pump. As was stated earlier, the primary problem with a spherical electrostatic pump is attempting to get electrons into stable orbits which do not return to the emitting point. Since it is the electrostatic field which provides the actual constraining force, it was felt that the B field necessary to flip the orbits would be considerably less than that necessary for constraining the electrons as used in conventional ion pumps. (Conventional pumps employ magnets which have been charged to the highest possible value. This is in the neighborhood of 3500 gauss.)

The principle of operation is shown schematically in Figure 4.57. An electron in an orbit with a pitch angle ϕ will feel a force due to the magnetic field which tends to decrease the angle θ. When the orbit aligns itself perpendicular to the B field, there is no longer any force acting to rotate the orbit out of this plane. Provided that this is a damped system, the electron should remain rotating in this new plane. The force exerted by the B field should be much less than the electrostatic forces so that the distortion of the path set up by the balance of the electrostatic forces is small.

The forces present in this system are

$$F_r = eE_r = \frac{ec\,V_A}{r^2} = -\frac{K}{r^2} \tag{31}$$

V_A = anode voltage

E_r = electrostatic central force field

$C = r_c r_a/(r_c - r_a)$ = geometry factor

and

$$\vec{F}_B = -e\vec{v} \times \vec{B} \tag{32}$$

where $\vec{B} = B_z \vec{e}_z$

In order to set up the equations of motion, let a spherical coordinates system be used as shown below:

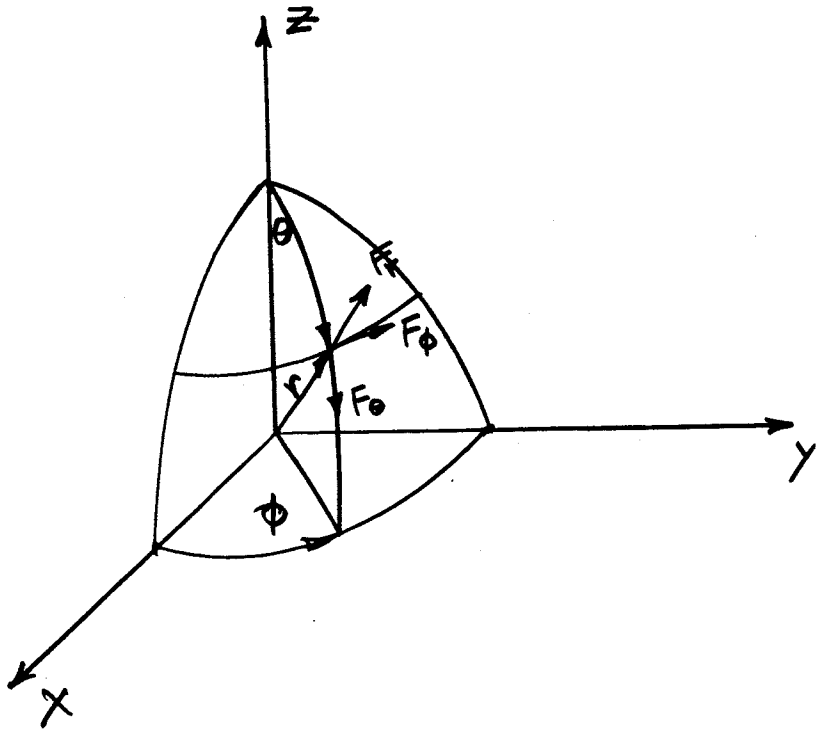

The equations of motion in spherical coordinates are written:

$$F_r = m(\ddot{r} - r\dot{\theta}^2 - r\dot{\phi}^2 \sin^2\theta) \tag{33}$$

$$F_\theta = m(2\dot{\theta}\dot{r} + r\ddot{\theta} - r\dot{\phi}^2 \sin\theta\cos\theta) \tag{34}$$

$$F_\phi = m(2\dot{r}\dot{\phi}\sin\theta + r\ddot{\phi}\sin\theta + 2r\dot{\phi}\dot{\theta}\cos\theta) \tag{35}$$

In order to express F_B, it is necessary to write the velocity in component form:

$$\vec{V} = \dot{r}\vec{e}_r + r\dot{\theta}\vec{e}_\theta + r\dot{\phi}\sin\theta\,\vec{e}_\phi \tag{36}$$

Since ϕ is positive as shown in the sketch, it is necessary to have B pointing in the negative Z direction if a stable orbit in the X-Y plane is to be achieved. Then:

$$\vec{F_B} = eB\{(r\dot{\phi}\sin^2\theta)\vec{e}_r + (r\dot{\phi}\sin\theta\cos\theta)\vec{e}_\theta - (\dot{r}\sin\theta + r\dot{\theta}\cos\theta)\vec{e}_\phi \tag{37}$$

The equations of motion may then be put in their final form:

$$eBr\dot{\phi}\sin^2\theta - \frac{K}{r^2} = m(\ddot{r} - r\dot{\theta}^2 - r\dot{\phi}^2\sin^2\theta) \tag{38}$$

$$eBr\dot{\phi}\sin\theta\cos\theta = m(2\dot{\theta}\dot{r} + r\ddot{\theta} - r\dot{\phi}^2\sin\theta\cos\theta) \tag{39}$$

$$-eB(\dot{r}\sin\theta + r\dot{\theta}\cos\theta) = m(2\dot{r}\dot{\phi}\sin\theta + r\ddot{\phi}\sin\theta + 2r\dot{\phi}\dot{\theta}\cos\theta) \tag{40}$$

These equations would be rather difficult to solve as they stand and therefore, if any use is to come out of them, they will have to be simplified. Let us restrict the range of solution to values of near 90°; that is, the orbit is nearly perpendicular to the magnetic field. Let θ' be defined such that $\theta = 90° - \theta'$ then:

$$\begin{aligned} \sin\theta &= \cos\theta' \approx 1 \\ \cos\theta &= \sin\theta' \approx \theta' \\ \dot{\theta} &= -\dot{\theta}' \quad ; \quad \ddot{\theta} = -\ddot{\theta}' \end{aligned} \tag{41}$$

At the same time, let it be assumed that:

$$\begin{aligned} \dot{r} &= \ddot{r} = 0 \\ \dot{\phi} &= \omega = \text{const} \Rightarrow \ddot{\phi} = 0 \end{aligned} \tag{42}$$

What is implied by these statements is that when the orbit is nearly aligned with the X-Y plane, the radius is nearly constant and the angular frequency of the rotation is nearly constant. Both of these assumptions appear to be valid on a physical basis. Making use of them, the equations of motion become:

$$eBr\omega - \frac{eK}{r^2} = -mr\dot{\theta}^2 - mr\omega^2 \tag{43}$$

$$eBr\omega\theta' = -mr\ddot{\theta}' - mr\omega^2\theta' \tag{44}$$

$$eBr\dot{\theta}'\theta' = 2mr\omega\dot{\theta}\theta \tag{45}$$

If we now disregard all second order terms in θ' and $\dot{\theta}'$, the final result is:

$$eBr\omega - \frac{eK}{r^2} = -mr\omega^2 \tag{46}$$

$$\ddot{\theta}' + \left[\omega^2 + \frac{eB\omega}{m}\right]\theta' = 0 \qquad (47)$$

First, let us look at these equations for B = 0. Then:

$$\frac{eK}{r^2} = mr\omega^2 \quad \text{and} \quad \ddot{\theta}' + \omega^2\theta' = 0 \qquad (48)$$

The first of these equations is simply the force balance equation for circular motion in a central force field.

$$\omega^2 = \frac{eK}{mr^3} \qquad (49)$$

The second equation is simply the equation of motion for an orbit which is tilted in such a way that varies as the particle goes around the anode. When the B field is then included, the meaning of the equations does not change. All that happens is that the angular frequency ω changes because the B field has pulled the orbit out to a new radius. It is therefore seen that the equation as stated is of little value, since we are looking for a damped sinusoidal solution for θ'.

The problem appears to be that in linearizing the differential equations, the damping factor is lost. If an attempt is made to regain it, the equations immediately become impossible to solve. A very approximate expression for the flipping frequency was obtained by the following approximate analysis.

$$\omega_f = \sqrt{\frac{mB}{I}} \qquad (50)$$

is the expression for the flipping frequency of a magnetic galvanometer. Even though this is an undamped system, an approximate

value for the rate at which a stable orbit is approached should be obtainable.

m = magnetic moment = iA

I = moment of inertia

$$\omega_f = \sqrt{\frac{e\omega B}{2m \sin\theta}} \qquad (51)$$

Assume $\sin\theta \approx 0.35$ which might be a reasonable value for a flip from $\theta = 45°$ to $\theta = 0°$.

In eq. (46) if it is assumed that

$eBr\omega \ll eK/r^2$ then:

$$\omega^2 \approx \frac{eK}{mr^3} \qquad (52)$$

Letting $\omega_f \approx \omega$ as a reasonable value of sufficiently fast flipping.

$$B = 0.7\sqrt{\frac{m}{e}\frac{K}{r^3}} \qquad (53)$$

Let K = 3000v x 0.005 m

r = 0.02 m

$\frac{m}{e} = 5.7 \times 10^{-12}$

B = 70 gauss (54)

If $\omega_f = \omega$ at 70 gauss then perhaps only a 20 gauss field or so would be needed to flip 45° in one revolution.

It is now necessary to check the assumption made on the negligible effect of the magnetic field on the radius of the orbit. This cannot be done using eq (46) alone because both of the variables ω and r appear. In addition, conservation of energy is also used:

$$E = PE + KE = \text{const.} \tag{55}$$

$$PE = eV = ecVa\left(\frac{1}{r_a} - \frac{1}{r}\right) \tag{56}$$

$$KE = \frac{1}{2}mv^2 \qquad \frac{1}{2}mv^2 = \frac{ecVa}{2r} \tag{57}$$

$$E = ecVa\left(\frac{1}{r_a} - \frac{1}{2r}\right) = E_a + E_r \tag{58}$$

If r_o is the initial radius and injection into the system is made such that a circular orbit would be followed in the absence of a B field, then $E = E_a + E_{r_o} = \text{const.}$ When the final orbit is obtained:

From which: $$\omega^2 = \frac{2eK}{m r^2}\left[\frac{1}{r} - \frac{1}{2r_o}\right] \tag{59}$$

Substituting this into eq. (46) and solving for B

$$B = \frac{51(\eta - 1)}{\sqrt{\eta^3(2-\eta)}} \text{ gauss} \tag{60}$$

where: $\eta = \frac{r_{final}}{r_o}$ $\qquad r_o = 1.2\text{ cm};\ cV_a = 15$

From this equation it is found that

$\eta = 1.1 \Rightarrow B = 4.5$ gauss

$\eta = 1.5 \Rightarrow B = 19.5$ gauss

$\eta = 2 \Rightarrow B = \infty$

It is seen that the field will have an appreciable effect upon the size of the orbit, however, this does not impair the operation.

Now a few words must be said about some of the practical aspects of the pump operation. The most important of these is the actual pump geometry. Since reasonable accuracy is needed to get electrons into

orbit with the right velocity and position, it is clear that an electron gun is necessary. Since in the final design only one filament is proposed, it will be necessary to funnel electrons into the pump chamber through a relatively long nozzle. It will require a good design to obtain a high efficiency for such a gun. The other principle physical object in the pump cavity is the anode, and even more important, its support post. The orientation of the gun with respect to the anode support may have a great effect upon the operation. In Figure (4.58) several possible orientations are shown. In configuration (a) the gun is at 90° to the magnetic field. This creates a problem since the radius of curvature of a 1000v electron at right angles to a 20 gauss field is about 5 cm. Either the electron gun would have to be built with this in mind or else the barrel would have to be effectively shielded. If shielding were employed, care would have to be taken that it did not distort the magnetic field so badly that proper orbiting was not achieved. Another disadvantage of this geometry is that the orbiting electrons come fairly close to the barrel of the gun and enough of a perturbation might be encountered to cause a collision. This situation is partially remedied in configuration (b). Here the gun is rotated part way around the imaginary circle which constitutes the first orbit. In this position the bulk of the barrel is swung down away from the final orbiting plane. At the same time, the tip of the barrel moved closer to this plane, so that some sort of optimum position must be experimentally arrived at. In configuration (c), the

gun is parallel to the magnetic field so the magnetic effects are eliminated. Actually, there will probably be a component of B which is not aligned with the z axis so total elimination of these effects will not be achieved. The second difference in the configuration is that the anode support is at 45° to the plane of the final orbit. It had to be moved to this new position to avoid a collision on the first orbit; however, the post will now effect the final orbits since it is closer to their plane and no longer symetrically located with respect to it. In choosing between (b) and (c) it is a matter of weighing the distortion of the electrostatic field against the distortion of the magnetic field (if the gun is shielded). Because of the new orientation of the gun, circular orbits can no longer be obtained since the tip of the barrel would have to lie in the final orbit plane, a condition which is not acceptable. If an elliptical orbit is followed, the eccentricity must be kept low enough that a collision with the cathode is avoided. Circular orbits appear to be more desirable since the path can lie nearer the anode over its total length than in the case of an elliptical orbit. This means higher sputtering efficiency.

Since stable orbits are obtained in this device, the ion current formed must be a function of the space charge density which can be maintained. If the volume fills with a space charge cloud, the operation and resulting electron motion will be severely altered.

The precise calculation of these effects is a difficult task. Again, experimental test is the only practical means of determining the necessary information. One thing is certain, the space charge will be higher the more difficult is made the means of escape for the trapped electrons. Two guides are clearly set forth: First, the initial radius and velocity of the electrons must be adjusted so that they cannot reach the cathode. Second, the gun barrel and anode post must be well shielded to minimize the area of the escape route. A shielded pump is shown in Figure (4.58)(d). The fact that the B field stretches the orbit aids in preventing the electrons from returning to the gun barrel.

A few general comments can be made about the space charge distribution. The outer boundary of the cloud is determined by energy considerations. If it is desired to fill the entire volume then the total initial energy of the electrons relative to anode potential should be set equal to eV_A . In the space charge free case, the proper position fro the electron gun would be $r_o = \frac{1}{2} r_c$, if a circular orbit is initiated. In the presence of space charge, the field distribution is modified but the gun potential must be set for the non-space charge case so that stable orbits will result and allow for space charge build up. The fact that the initial radius is far from the anode should not hinder a high sputtering rate since it is anticipated that the entire volume will become filled with space charge.

The magnetic field will not play a major roll in maintaining the space charge density. The rotating charge mass should line up with its axis of rotation parallel to the Z axis. Then it is seen that the central force field will do most of the containment in the Z direction. There appears to be no reason why a sufficiently high space charge density could not be obtained.

4.53 Pump Speed

In any of the systems which have been discussed, the restrictions placed upon the initial conditions of an electron are much more severe than in the case of a strong field magnetic pump because the trapping mechanism is much more refined. For this reason, a well directed electron beam must be used as the source of electrons rather than the Penning discharge which is used in magnetic pumps.

If we assume that a cathode system emits a current, i_c, of energy, qVe, and that a fraction, f_{ic}, goes into a useful orbiting path, then three limiting conditions upon the length of this path can be specified:

Case 1: The electron path length is limited to an average value S_1 by the pump structure and that reactions with gas molecules cause a negligible loss.

Case 2: The electron path length is limited by the mean free path in the gas; i.e., the dimensions of the structure have no part in determining average path length.

Case 3: The electrons go into a well trapped orbit such that the space charge of a circulating beam produces the limiting current.

Let:

S_n = ionization probability as a function of gas density in ions per electron per centimeter of path length per molecule per cc.

n = molecular density in molecules/cc

s = path length in cm

I^+_f = positive ion current formed

Then: (63)

$$I^+_f = S_n f_{ic} s n$$

For Case 1: (64)

$$I^+_{f_1} = S_n f_{ic} s_1 n$$

For Case 2: (65)

$$I^+_{f_2} = S_n f_{ic} \lambda_e n$$

where λ_e is the electron mean free path in centimeters. In this case, since λ_e is a linear function of 1/n, it is apparent that the ion current will be independent of pressure. In Case 1, however, the ion current is directly proportional to pressure.

For Case 3: Each electron removed from a trapped orbit by collision is replaced by an electron from the emitter so that the space charge limited condition is maintained. If N_e electrons are in orbit with an average velocity v_e then:

$$S i_{sc} = e N_e v_e$$

where e is the electronic charge and i_{sc} is the equivalent space charge current.

Then: (66)

$$I^+_{f_3} = S_n e N_e v_e n$$

N_e is calculated for space charge limited conditions by the solution of Poisson's equation for the geometry of interest. In this case,

the cathode current is unimportant provided that $i_e > I^+_{f_3}$. This must be true since all of these cases assume that when an ionizing collision takes place the resulting electrons are scattered out of the system and are not utilized. These calculations will be altered if either electron produces additional ionization or if non-ionizing inelastic collisons change the probability function. Neither condition is considered.

Now that I^+_f has been expressed, the pumping speed can then be calculated. If Qn is the gas flow of an ion pump in molecules per second, the pumping speed, S_p in cc/sec., is given by:

$$S_p = Q/n_o$$

where n_o = molecular density under conditions of dynamic equilibrium

If it is assumed that each molecule ionized is a molecule removed, then,

$$S_p = I^+_f/qn$$

q = average charge per ion

As previously discussed, the number of molecules pumped is actually related to the number of active sites available for absorption and, for rare gas atoms, the rate of deposition of sputtered material relative to the diffusion rate of the gas. Thus, the number of atmos of getter material relative to the diffusion rate of the gas. Thus, the number of atoms of getter material sputtered per ion and

the geometric configuration will govern the number of active sites, while the geometry and impact energy will govern the burial and release of absorbed molecules. Consequently, let:

$$S_p = \frac{\phi I_f^+}{qn}$$

where ϕ = F(Vion, geometry, gas being pumped)

It would be extremely difficult to calculate a value for ϕ, so rather than attempt this it will be estimated from the available data on diode and triode pumps. Then for the different electron path cases the pumping speeds are found to be:

$$S_{p1} = \frac{\phi S_n f_{ic} S_1}{q} \tag{67}$$

$$S_{p2} = \frac{\phi S_n f_{ic} \lambda_e}{q} \tag{68}$$

$$S_{p3} = \frac{\phi S_n e N_e V_e}{q} \tag{69}$$

The electron mean free path can be obtained by assuming stationary target molecules and a collision area $\pi d^2/4$ per molecule where d is the molecular diameter. Thus:

$$\lambda_e = \frac{4}{n\pi d^2}$$

For a gas consisting of N_2 molecules:

$$\lambda_e = 9 \times 10^{14} / n$$

Typical values of Sn for nitrogen are:

Ve = electron energy volts	Sn = ionization probability ions/electron/cm/molecule/cc
30 ev	1.5×10^{-16}
100 ev	3.2×10^{-16}
1000 ev	0.93×10^{-16}
2000 ev	0.56×10^{-16}

Writing equation (25) (70)

$$S_{p_2} = \frac{9 \times 10^{14} \phi S_n f_{ic}}{nq}$$

But

$$p = nkT \Rightarrow S_{p_2} = \frac{2.5 \times 10^{-2} \phi S_n f_{ic}}{pq} \quad \text{at } 0^\circ C$$

It is seen that under these assumptions, the pumping speed will decrease inversely with pressure for the free path limited condition. As a means of comparison, the electron mean free path is 1000 cm when p = 2.5×10^{-5} mm at 0°C. Consequently, above this pressure, the pumping speed of a device having a geometry limited electron path of 1000 cm would fall off as pressure continued to rise.

As an example for Case 2, let:

$\phi = 1$ $f_{ic} = 10^{-4} a$ $V_e = 1000$ v. $p = 10^{-5}$ mm

Then $S_{p_2} \approx 150$ cc/sec = 1.5 cc/sec-μa

This implies that 100 microamps useful current at 1000 cm path length would be required in a geometry limited system for a pumping speed of 150 cc/sec.

4.54 Pump Power

In a conventional magnetic getter ion pump, the major portion of power consumption is accounted for by the ion current which falls through a high voltage and strikes the cathode. In such a pump power is proportional to pressure. In the Vac Ion® 0.15 liter/sec. pump, the ion current is: 3×10^3 μa/μ.

At 1×10^{-5} mm: $I^+ = 30$ μa

The voltage difference between the ionizing region and the cathode is about 3 kv. Therefore $P = 3 \times 10^3 \times 30 \times 10^{-6} = 0.09$ watts

This is clearly a reasonable value for compatibility with the system under consideration.

In a pump which requires an electron gun, the considerations are somewhat different. Let us consider a geometry limited system. In such a system the power can be divided into four parts. The first is the filament power necessary to obtain electron emission. It is proposed that the same filament be used for both the ion source and pump requirements. The additional filament current required for an extra 100 to 200 μa of emission is relatively small when compared with the total current necessary to achieve emission. Therefore, this power will be lumped with the filament power. The other power losses occur in the electron gun and in

the current flow to the anode and cathode of the pump. The power loss in the electron gun is:

$$P_G = (1-f) i_c V_0 \tag{71}$$

The power loss to the anode is:

$$P_A \cong f i_c (V_A - V_0) \quad \text{(neglecting electrons from ion formation)} \tag{72}$$

The power loss to the cathode is:

$$P_c = I^+ \bar{V}_i \tag{73}$$

where $\bar{V}_i$ is the average potential of the ion immediately upon being formed. These expressions may be related to one another by the pump speed calculations which were carried out in the previous section.

From eq. 64 and 67:

$$I^+_f = S_n f i_c S_1 n \tag{74}$$

$$= \frac{q S_p n}{\phi} = \frac{K_q S_p P}{\phi} \quad \text{where } n = K_p$$

$$P_c = \frac{K_q S_p P \bar{V}_i}{\phi} \tag{75}$$

Also from eq. 67:

$$f i_c = \frac{q S_p}{\phi S_n S_1} \quad \text{from which} \tag{76}$$

$$P_a = \frac{f q S_p}{\phi S_n S_1} (V_A - V_0) \quad \text{and} \tag{77}$$

$$P_g = \left(\frac{1-f}{f}\right) \frac{q S_p}{\phi S_n S_1} V_0 \tag{78}$$

Several observations can be made at this point.

a. Only cathode power is greatly effected by pressure, being proportional to it.

b. Cathode power is also proportional to pump speed.

c. However, Pa and Pg are only proportional to ic. Therefore, improving the pumping speed by increasing S_1 will only increase P_c. Now substituting some typical numerical values:

$\phi = 1.0$
$S_n = 0.93 \times 10^{-16}$
$q = e = 1.6 \times 10^{-13}$
$K = 3.6 \times 10^{16}$ at 0°C for N_2
$S_p = 150$ cc/Sec
$p = 1 \times 10^{-5}$ mm
$f = 0.5$
$V_a = 5$ kv
$V_o = 1250$ v.)
$V_i = 2500$ v.) (Based on spherical pump geometry with $V_c/V_a = 4$)

$P_c = 0.0216$

$P_a = 0.485$

$P_g = 0.322$

These numbers are very approximate and are only intended to show that the presence of the electron gun accounts for the majority of the power required. The value P_c is less than the power dissipated in the Vac Ion pump primarily because the value ϕ is higher in the pump assumed here. ϕ was assumed to be unity because a triode configuration is contemplated. Brubaker[2] has reported that this is a reasonable value for this type of geometry.

The values for P_a and P_g are high and it must be remembered that a space charge limited pump such as the weak B field pump will

2 W. M. Brubaker, "A Method for Greatly Enhancing the Pumping Action of a Penning Discharge"

operate more efficiently. However, because it requires an electron gun it cannot operate as efficiently as the Penning discharge type.

4.60 DETECTORS

There are basically two types of detectors which can be employed. The first is a broad class of electrometer amplifiers and the second is electron multipliers. Electrometers may be classified as linear and non-linear. Both types are discussed.

4.61 Electrometer Amplifiers

4.61.1 General Electrometer Amplifier

The block diagram of a general electrometer amplifier is shown in Figure 4.61.

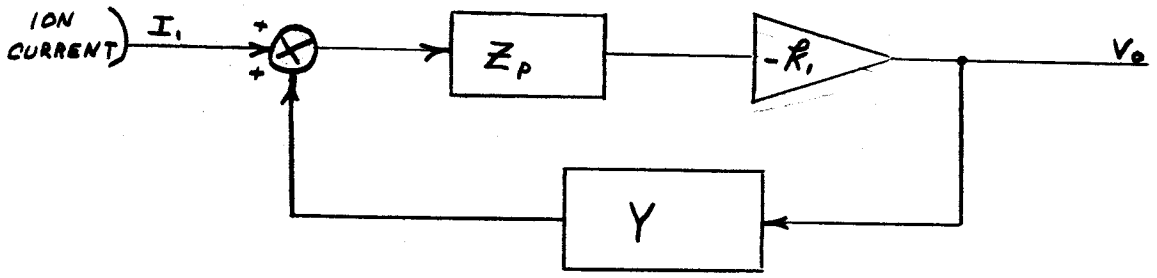

Figure 4.61

GENERAL ELECTROMETER AMPLIFIER

where: k_1 = gain of forward loop linear amplifier.

Z_p = parallel combination of input impedance to ground and feedback circuit impedance excluding attenuators.

Y = total susceptance of feedback circuit.

Of importance in the system is the ratio of voltage out to input current known as the transfer impedance Z_{21}.

$$Z_{21} = \frac{V_o}{I_1} = -\frac{1}{Y}\left[\frac{1}{1 + \frac{1}{K_1 Z_p Y}}\right]$$

for a typical amplifier, $K_1 Z_f Y >> 1$

Therefore:

$$Z_{21} = \frac{V_o}{I_1} = -\frac{1}{Y}$$

The circuit for a basic electrometer amplifier is shown in Figure 4.62.

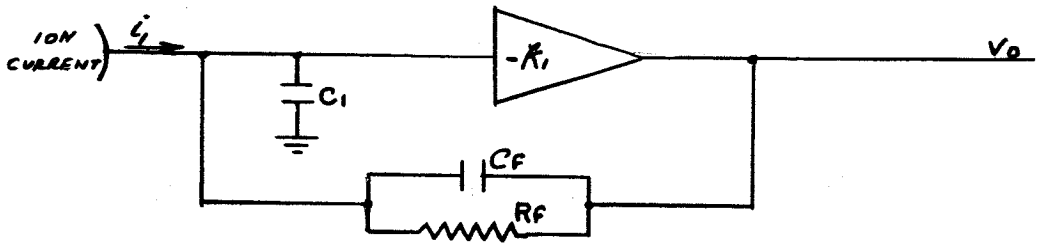

Figure 4.62

BASIC GENERAL ELECTROMETER AMPLIFIER

Where C_1 is the unavoidable total input capacitance to ground, R_f is a very large resistor whose value is generally of the same magnitude in ohms as is the reciprocal of the input current in amperes, and C_f is the unavoidable capacitance associated with the feedback resistor, R_f. For this circuit:

$$Z_p = \frac{\frac{1}{C_1 + C_f}}{S + \frac{1}{R_f (C_1 + C_f)}}$$

$$Y = \frac{1}{R_F} + C_f S$$

$$Z_{21} = \frac{-K_1}{C_1 + [K_1+1]C_f}\left[\frac{1}{S + \frac{K_1+1}{R_f(C_1+[K_1+1]C_f)}}\right]$$

where "S" represents the Laplace operator. For $K_1 >> 1$ and $k_1C_f >> C_1$ which is true in a typical amplifier:

$$Z_{21} = \frac{V_o}{I_1} = \frac{-1}{C_f}\left[\frac{1}{S + \frac{1}{R_f C_f}}\right]$$

For a current step input $I_1(t) = I_u(t)$, the D-C voltage level which the output approaches is

$$V_o(DC) = \lim_{T\to\infty} V_o(t) = \lim_{S\to 0} S Z_{21} \frac{I}{S} = -I A_f$$

and the time constant with which it approaches this value is

$$\tau = R_f C_f$$

These equations show that the output will be related to the input by the factor R_f. If R_f is a constant resistance, the output is directly proportional to the input. If R_f varies in some known manner, the output will vary with the input in the same known manner. As an example of how this principle will be used, if R_f varies logarithmically so will the output as compared to the input current. It might also be noted that if the resistance of R_f is of the approximate magnitude in ohms as is the inverse of the input current in amperes, the output voltage will be approximately one volt.

The time constant which is equal to R_fC_f is unfortunately very long if the input currents are small and any practical output voltage range is used. The state of the art is such that the capacitance C_f of the feedback element can not be made small enough to give reasonable time constants.

Two methods which have been devised to decrease the output time constant will be discussed. The first method will be applicable only to linear output (directly proportional to input) amplifiers. The second method is applicable if the feedback element R_f is not constant and is the method used in the experimental logarithmic electrometer amplifier developed for the study.

4.61.2 **Linear (Output Directly Proportional to Input) Amplifier**

A system which will give an output voltage directly proportional to input current with a fast response is shown in Figure 4.63 where R_f is a resistor of constant value.

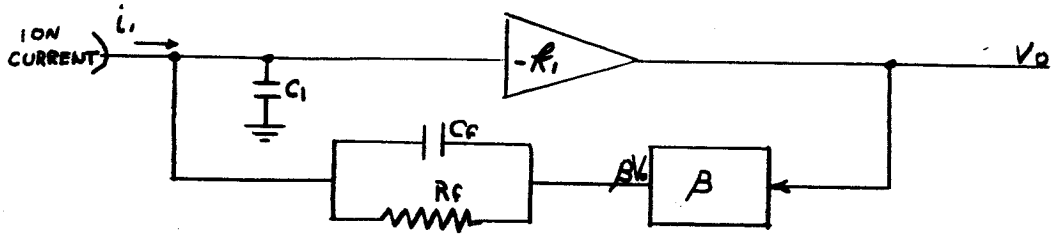

Figure 4.63

FAST LINEAR ELECTROMETER AMPLIFIER

The equations for this circuit are:

$$Z_p = \frac{\frac{1}{C_1 + C_f}}{S + \frac{1}{R_f(C_1 + C_f)}}$$

$$Y = \beta\left[\frac{1}{R_f} + C_f S\right] = \beta\frac{1}{R_f}\left[1 + R_f C_f S\right]$$

To improve the response time, β is made equal to $(1 + R_f C_f)^{-1}$ through the use of the circuit shown in Figure 4.64.

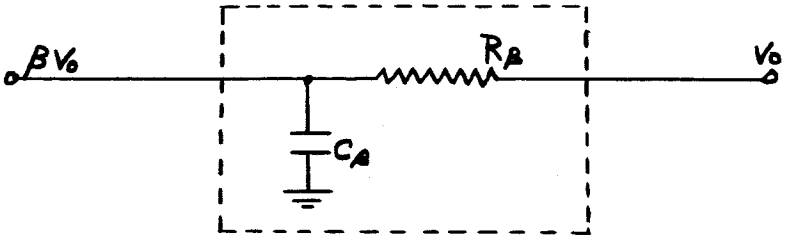

Figure 4.64

β COMPENSATING NETWORK FOR A LINEAR AMPLIFIER

If C_β is made relatively large and $R_\beta C_\beta$ is made equal to $R_f C_f$, then

$$\beta = \left[1 + R_\beta C_\beta\right]^{-1} = \left[1 + R_f C_f\right]^{-1}$$

and

$$Y = \frac{1}{R_f}$$

the transfer impedance is given by

$$Z_{21} = -\frac{k_1}{C_1 + C_f}\left[\frac{1}{S + \frac{k_1}{R_f(C_1 + C_f)}}\right]$$

For $k_1 >> 1$ which is true for practical amplifiers:

$$Z_{21} = \frac{V_o}{I_1} = \frac{-k_1}{C_1 + C_f}\left[\frac{1}{S + \frac{k_1}{R_f(C_1 + C_f)}}\right]$$

For a current step input $i_1(t) = I_u(t)$, the d-c voltage level which the output approaches is

$$V_o(DC) = \lim_{t \to \infty} V_o(t) = \lim_{s \to 0} S Z_{21} \frac{I}{S} = I R_f$$

and the time constant with which it approaches this value is

$$\tau = \frac{R_f (C_1 + C_f)}{k_1}$$

It is seen that this network reduces the time constant by a factor approximately equal to the gain of the forward loop linear amplifier. However, it must be realized that the time response cannot be extended beyond that which effects due to material polarization (dielectric hysteresis) may dictate.

4.61.3 Controlled Non-Linear Amplifier

A system which will give output voltages which are not proportional to input currents but has a known relationship with a fast response is shown in Figure 4.65. This is the type of system built for the present study.

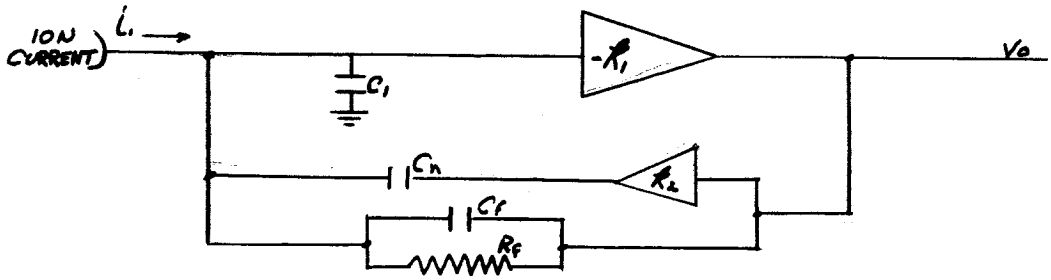

Figure 4.65

CONTROLLED NON-LINEAR AMPLIFIER

The equations for the circuit are:

$$Z_p = \frac{\frac{1}{C_1 + C_f + C_n}}{S + \frac{1}{R_f (C_1 + C_f + C_n)}}$$

$$Y = \frac{1}{R_f} + \frac{1}{C_f S} + K_2 \frac{1}{C_n S}$$

$$Z_{21} = \frac{\frac{K_1}{C_1 + C_f + C_n + K_1 K_2 C_n + K_1 C_f}}{S + \frac{K_1 + 1}{R_f (C_1 + C_f + C_n + K_1 K_2 C_n + K_1 C_f)}}$$

In order to have a fast response with a large value of R_f, $k_1 \gg 1$ and $k_2 = - C_f/C_n$.

Under these conditions:

$$Z_{21} = \frac{V_o}{I_1} = \frac{-k_1}{C_1 + C_f + C_n} \left[\frac{1}{s + \frac{k_1}{R_f(C_1 + C_f + C_n)}} \right]$$

For a current step input $i_1(t) = I_u(t)$, the d-c voltage level which the output approaches is

$$V_o(DC) = \lim_{t \to \infty} V_o(t) = \lim_{s \to 0} \; s Z_{21} \frac{I}{s} = -I R_f$$

and the time constant with which it approaches this value is

$$\tau = \frac{R_f (C_1 + C_f + C_n)}{k_1}$$

This time constant is nearly the same as that for the linear amplifier. It can be made quite small by using a high gain forward loop amplifier k_1. Polarization effects at the input will be the limiting factor on the time response. The d-c relationship between output voltage and input current will be governed by R_f.

4.62 Electron Multipliers

Very little investigation was done in the area of electron multipliers. The reason for this is that a multiplier would probably only find use in conjunction with an extremely low sensitivity ion source such as the alpha source which is discussed in Section 4.24.

In such an application, the multiplier would be used as a pulse amplifier to amplify single electrons which arrive at its input to a pulse of electrons at the output. These pulses are then fed into a counter. Since the primary effort of this program was directed toward electron bombardment sources, it was felt that pulse counting techniques were inappropriate since the sensitivity level is too high.

When applied as an amplifying stage in an analog system, the multiplier becomes less desirable. The principle problem appears to be that of maintaining gain stability during the six month transit to Mars. It is unlkiely that the dynode surfaces would remain unaffected during such a long time period. This implies that the multiplier would have to be calibrated before entering the Martian atmosphere. At the same time, a relatively high sensitivity logarithmic amplifier would have to follow the multiplier and therefore, the weight and power would be greater than in the case of a logarithmic electrometer discussed in the previous section.

It was decided that study beyond the scope of this contract would be necessary to prove the feasibility of an electron multiplier as an analog instrument in this application.

5.0 COMBINED SYSTEM ELEMENTS

Now that the individual components of the system have been discussed in detail, they may now be brought together to obtain the general relationships for the system as a whole. In carrying out this operation, there are two important determining factors which should be considered; 1) the power, weight, and size requirements, and 2) the performance standards of resolution, sensitivity, and accuracy. The choice of the final operating conditions should, if possible, be compatible with both of these areas. It is felt that the most logical way to attack this problem is to let the performance specifications be the independent variables and the power, weight, and size be the dependent ones. The principal reason for this is that the theoretical treatment of the former group is more readily accomplished than the latter.

The following logic is used: The accuracy and available data bits require that an absolute minimum peak top width to base width ratio of 50% is essential. Even this requirement implies that some form of selected data technique be employed or else that a synchronized mass scan is used, thereby placing severe requirements on the quadrupole power supply. From Figure 4.14 it is seen that a 50% (t/b) ratio implies an (V_e/V_o) ratio of about 0.03 at a resolution

of 25, and $\gamma = \sqrt{\frac{V_I}{V_{ac}}} \sin\alpha = 0.01$. In addition, if this resolution is to be obtained at the operating point indicated in the figure, then Eq(24) Sec4, relating V_{ac}/V_I to the system geometry must be complied with.

The choice of V_I/V_{ac} will then determine the exit angle requirements on the ion source in order to maintain γ at the assumed maximum value of 0.01. On the other hand, V_I/V_{ac} may be implied by r_0/η and r_0 may be implied by the transmission characteristics. Then V_I can be set by the source sensitivity required and a value for V_{ac} results. This, in turn, sets the theoretical power consumption of the quadrupole LC circuit.

The combination of the analytical expressions expressing these relations would be a tedious task and it seems that the only way that a solution can be obtained is to apply one's feel for the problem to set some of the parameters and then determine what the remaining ones must be. If $\alpha = 3°$ for a double aperture thermal ion source, then $V_I/V_{ac} \leq 1/27.5$. From the standpoint of power considerations and the necessity of using a transistorized r.f. supply, it appears that $V_{ac} = \sim 300$v. is a maximum allowable value implying a V_I of 10.9v. . It is doubtful that a high enough ion source sensitivity or the required exit angle can be obtained at such a low injection voltage.

If an $\alpha = 2°$ is assumed, then $V_I / V_{ac} = 1/12.1$ is implied or $V_I = 24.8$ at $V_{ac} = 300$. This operating condition appears much more likely of attainment than the first, however, a 2° angle appears to be somewhat ambitious.

It is readily seen that the limited number of data bits available puts a tight squeeze on the variables V_I, V_{ac}, and α which is independent of the other system variables and only depends upon the additional requirement that the r.f. electronics be transistorized. Should more bits become available, these requirements could be relaxed.

Another approach which might be contemplated is to increase the allowable value of γ. Careful examination of eq. (39) Sec. 4, and confirmation by numerical calculation indicates that doubling γ would more than half the required r_e / r_o ratio. At best, it would be 0.015, which for $r_o = 0.200"$, (which appears to be a maximum value) $r_e = 0.003"$. This is possibly an acceptable value and might be forced by the differential pumping requirements anyway. With $\gamma = 0.02$ and $\alpha = 3°$ then $V_I / V_{ac} = 1/6.9$. This is getting to be a reasonable value. Now $V_I = 25v.$ implies $V_{ac} = 173v.$ which can be tolerated by the electronics.

With $V_{ac} / V_I = 6.9$ eq. (24) Sec. 4, says that the r_o / ℓ ratio is 0.07 which implies $\ell = 2.87"$ for $r_o = 0.200"$. The indication here is that the length of the quadrupole rods can probably be reduced from the value of 6" which has been anticipated. It

must be remembered, however, that the analytical accuracy, eq. (24) Sec. 4, is in question and, therefore, it cannot be taken for granted that the rods would be shortened. What is implied, however, is that an accurate analysis should be performed on the 1% peak height resolution to determine its quantitative dependence upon V_{ac}/V_t and r_o/l. Assuming that the rods could be shortened, and that the volume and weight of a 6" quadrupole with an is reasonable, then it appears that optimum values for could be determined such that the valume remains constant.

Now let us examine the next area of importance: sensitivity, and see what the interelations are which determine this quantity. If a logarithmic electrometer amplifier is used, then the detectible limit cannot be pushed much below 1×10^{-13} amps without a corresponding increase in time constant or a redesign of the amplifier to produce more gain. The first alternative is intolerable and the second must be viewed with some skepticism since a great deal of effort would probably be required to produce a reliable, working instrument. At the same time, more power would be required for the extra amplifying stage. Let us assume that the second alternative is not followed either. It has also been assumed that the analyzer pressure can operate as high as 1×10^{-5} mm and that a pressure range of 10:1 is encountered over the sampling range so that the analyzer pressure would vary from 1×10^{-6} mm to 1×10^{-5} mm. Investigation of the inlet

flow requirements indicate no problem in accommodating these pressures and ion pumping is certainly feasible in this range. The pressure in the ion source is then D times the analyzer pressure where D is the differential pumping ratio. Then

$$(I^+_T)_{min} = SDI^- \times 10^{-3} \text{ amp.}$$

where S = source sensitivity in amps/μ-μa

I = emission current (μa)

The detectible limit is 0.1% of I^+_t and so

$$i_o = SDI^- \times 10^{-4} = 10^{-13} \text{ amp.}$$

This equation is plotted in Figure 5.01. The dotted lines mark off the region that is applicable to the present problem, assuming a pumped filament. At a differential pumping ratio of 20, the required source sensitivity is 5×10^{-11} amps/μ-μa which was exceeded in the experimental source under conditions of negative exit aperture bias and is only a factor of five above the value attained with the exit aperture at ground. It is true that these sensitivities were attained for an r_e of 0.010", but as is stated in the conclusions of the experimental work, it should be possible to attain the higher sensitivity at a lower value of . It should also be mentioned that rather than fight the differential pumping problem of D of 10 could be accepted if the emission current was increased to 200 μa. This would not require too great an increase in filament power. There would be the added problem of getting 200 μa into the source region. This approach would only be practical if an ion pump is used which pumps argon at a reasonable

rate with respect to air (1/3 or better). The differential pumping ratio could be greatly improved if a completely enclosed electron beam and filament were used. If this were done, the only flow path would be the ion exit aperture. The conductance of this aperture can probably be made as low as 2 cc/sec. which would yield a differential pumping ratio of 76 for a 150 cc/sec. pump. This would have two significant affects. First, the total ion current would easily be high enough to meet the detector requirements. Second, the argon distortion problem would be essentially eliminated. But, you can't get something for nothing. In this case, sample distortion occurs due to chemical reaction with the filament. In addition, the background level would be much higher, thus defeating one of the purposes of a high differential pumping ratio. This still might be the most practical approach, although time would have to be spent in analyzing the sample distortion for different known gas mixtures.

The conclusion reached is that there is a high probability that the necessary conditions can be met to achieve the resolution, accuracy, and sensitivity required. The problem of argon pumping may not be completely solved, but with two scans, enough data should be available that the effects of the sample distortion can be accounted for. The weight and power considerations are discussed in Section 8.

6.0 EXPERIMENTAL DESIGN

After a preliminary theoretical investigation was completed, several areas were found in which experimental verification was necessary. The design of these experiments is discussed below. The construction techniques which were employed on these experimental assemblies were not intended to be representative of actual flight hardware. The principle guide followed in the design and fabrication was to build the components as quickly and inexpensively as possible while still allowing for the testing of the pertinent characteristics which would apply to actual space hardware.

6.10 QUADRUPOLE ANALYZER

The principal parameters which must be determined in the design of the analyzer are the rod spacing radius r_o, and the rod length l. It will be assumed for the time that the entrance aperture radius r_e is associated with the collector design. It was decided to make r_o as small as possible and l as long as possible, compatible with the package size limitations. The reasons for this were that a small r_o implies a small overall analyzer diameter and should save weight as well as power. The maximum length was deemed necessary to minimize tails on the peaks. It was found later that in the frequency range which the analyzer will be operating that r_o may be increased with a small increase or possible decrease in power.

It was decided that the maximum allowable rod length would be six inches. The addition of the ion source and collector would increase the overall length to eight or nine inches. It was felt that this was a reasonable maximum length. The minimum allowable r_o was determined from the standpoint of the minimum rod diameter at which the necessary tolerances could be maintained and at which the 6 inch rods could stand the vibration requirements. Based on these considerations r_o was set at 0.100 inches making the rod diameter 0.232 inches.

The layout of the quadrupole is shown in Fig 6-11. The rods are supported from the sides so that the analyzer could be assembled separately from the source and collector units and yet still allow for a close spacing between the ends of the rods and these assemblies. The completed analyzer is shown in Fig 6-12. The rods and outer shell were fabricated of 303 stainless steel. The quadrupole voltages are fed in thru standard Coors feed thrus. These are much bulkier than necessary. The only difficulty encountered in the fabrication was met in aligning the rods so that they did not have a twist. This can be taken care of in the final system by the use of an aligning slot at each end of the rods.

From eq.(24) of section 4.1 the voltage ratio Vac/V_1 necessary for negating the effects of tails can be computed. For $m/\Delta m = 25$ $Vac/V_1 = 3.8$. For the actual operation of the instrument it was decided to operate at a higher Vac than is implied by this result. Therefore tails should not be a problem.

It was decided to set Vac = 125v. which for V_1 = 25 sets Vac/V_1 = 5 which should be high enough to prevent appreciable tails. With r_o and Vac determined the necessary frequency range can then be expressed by the use of eq. (23) Section 4.1. This range turns out to be 2.3 megacyles to 4.7 megacyles. With the frequency range determined it is only necessary to know the value of the quadrupole capacity and the size of the inductor can be found. The capacity of the analyzer by itself was measured and found to be 33 p.f. It was estimated that an additional 17 pf. would be acquired when the source, collector and the external wiring were added and so C = 50 p.f. was used. This sets L = 22 microhenries. This chain of calculations shows the logic diagram discussed in Sec 3.0 is supposed to work.

6.20 ION SOURCE

There were two goals in mind in designing the experimental ion source. The first was to determine the sensitivity which could be obtained from a non-magnetic source. The second was to experimentally demonstrate the effects of differential pumping, and the resulting restrictions on the sensitivity. A parabolic electron beam type as discussed in Section (4.2) was chosen. It was decided that because of relatively low injection energy and high ion beam density desired and the small space available that a thermal imaging source would be designed. Another factor which aided in reaching this conclusion was the increased difficulty encountered, greater investigation required, in the design of a perfect imaging system.

The design of the experimental source was based on the limiting values of detector sensitivity and analyzer pressure. If the minimum desirable detector current is $1x10^{-13}$ amps and H_2O is assumed to be 0.1% of the total composition then the total ion source current must be $1x10^{-10}$ amps at the operating pressure. If the minimum analyzer pressure is $1x10^{-7}$ min Hq and the differential pumping ratio is 20 the pressure in the ion source will be $2x10^{-6}$ min. The ion current formed can be approximately expressed as:

$$I^+ = 10\ I^-\ p\ l \qquad (1)$$

where:

l = beam length in cm.

p = pressure in min Hq

I = electron beam current

In the case at hand, if the first aperture below the electron beam has a radias r_a then $l = 2\ r_a$ and:

$$r_a = \frac{1}{20}\ \frac{I^+}{I^-}\ \frac{1}{P} \qquad (2)$$

Inserting the values stated above and assuming an electron beam current of 100 μa:

$$r_a = \frac{10^{-10}}{10^{-4}} \times \frac{1}{20x2x10^{-6}} = \frac{10^{-6}}{4x10^{-5}} = 2.5x10^{-2}\ \text{cm.}$$

Expressed in inches r_a = 0.010". This was the value used. The source was then designed with the goal of getting all of the ion current which passed the first aperture out through the exit aperture.

The theoretical sensitivity of this source is:

$$S = \frac{I^+}{I^-_p} = \frac{1\text{x}10^{-10}\text{a}}{100 \text{ ua x2x } 10^{-3}\,\mu} = 5\text{x}10^{-10}\,\frac{\text{a}}{\mu\text{-}\mu\text{a}}$$

This is a reasonable value to try to obtain from a thermal imaging source.

Several source configurations were theoretically investigated. The one which was decided upon was the double aperture source which is shown schematically in Fig. 6-21. The following relationships can be established:

$$V_I = V_a + K_1 V_r \qquad (3)$$

$$V_a = V_I - K_1 V_r \qquad (4)$$

$$V_o = 2V_r (1-K_1) \qquad (5)$$

$$V_e = V_o - (K_1) V_r \qquad (6)$$

Where V_e = equivalent Kinetic energy voltage of electrons at the minimum in the trajectory.

From equations (5) and (6)

$$V_r = \frac{V_e}{1-k_1} \qquad (7)$$

Another relation which may be determined by the requirements for a parabolic path is:

$$K_1 d_1 = d_1 - \tfrac{1}{2} X_o \equiv Y \text{ min} \qquad (8)$$

It was decided to let

$X_o = 0.200"$ and $K_1 d_1 = 0.040"$.

The most efficient ionization potential is nominally 70 volts. Therefore $V_e = 70v$. Substitution of these valves into eqs. (7) and (8) yields: $V_r = 98v$. $d_1 = 0.140"$ $K_1 = 0.286$

If V_I is set at 25v. then from equation (4):

The focal length of a single aperture lens can be expressed as:

$$f = \frac{4V_c}{E_2 - E_1} \tag{9}$$

Applying the equation to the accelerator aperture it is found:

$$f_1 = \frac{112\, d_2}{-3 - V_L - K_2 98} \tag{10}$$

where $K_2 = d_2/d_1$

It is clear that if a positive focal length is to be obtained the voltage on the lends must be negative. Applying eq. (9) to the second aperture:

$$f_2 = \frac{4(25 - V_L)d_3}{V_L(1+K_3) + 3K_3} \tag{11}$$

where $K_3 = d_3/d_2$

In order to transmit all of the ions it is necessary that the following relation is approximately true:

$$\frac{r_a}{r_2} = \frac{f_1}{f_1 - d_2} = \frac{1}{K_4} \tag{12}$$

In addition, if a small exit angle is desired then the most practical solution is to attempt to get zero angle. A well known relation of optics is:

$$\frac{1}{X_1} + \frac{1}{X_2} = \frac{1}{f} \tag{13}$$

In the case at hand $X_1 = -(f_1 - d_2)$, $X_2 = \infty$

and $f = f_2$ then $f_2 = -(f_1 - d_2) = -K_4 f_1$ (14)

Combining these aspects of the problem leads to the following difining relations. From eqs. (10) and (12):

$$d_2 = \frac{-3 - V_L - 112(1 - K_4)}{700} \tag{15}$$

From eqs. (11), (12) and (14):

$$K_3 = \frac{\alpha_K V_L}{(4-\alpha_K)V_L - (3\alpha_K + 100)} \qquad (16)$$

where $\alpha_K = K_4/(1-K_4)$

By the use of eqs. (15) and (16) the following values were computed:

Independently Chosen			Dependently Determined		
K_4	r_2*	V_1	d_2	K_3	d_3
0.5	0.005"	-50v.	0.067"	0.198	0.013"
0.5	0.005"	-100v.	0.139"	0.248	0.035"
0.5	0.005"	-200v.	0.201"	0.285	0.057"
0.2	0.002"	-200v.	0.154"	0.058	0.012"
0.2	0.002"	-500v.	0.582"	0.063	0.037"

*For r_a = 0.020"

The results of this work indicate that a well focused beam can be obtained at a reasonable source size and reasonable voltages. It was decided to use an r_2 of 0.005" since it was felt that this radius would be sufficient to give a high enough differential pumping action. For an r_2 = 0.010" and a length of 0.050" C = 7.34 $\frac{cc}{sec.}$ In the final design the radius of this restriction was not maintained constant but started at 0.010" and opened up to 0.020". This was done to prevent a grazing incidence for the ion beam which might cause adverse effects. This restriction was followed by another one in the exit aperture which was 0.020" long

and 0.020" in radius. The net speed of these two restrictions was about 15 cc/sec. This would not be low enough to produce a high differential pumping ratio if the pump speed were only 0.150 l./sec., but since the tests were carried out on an experimental vacuum system with a speed of at least 5 l/sec. the differential pumping would be quite high. The source calculations show that there seems to be no practical reason why an $r_2 = 0.002"$ could not be employed and therefore the flow through the ion exit aperture could be made quite small. The real problem was encountered in the electron beam entrance and exit apertures. The indicated flow through these was so high that it was decided to use a closed anode and eliminate the exit aperture all together. It had been thought originally that the ion source electron beam could be used in the ion pump also but this plan had to be altered because of the ion source conductance required. If an electron beam entrance aperture is used with a length of 0.100", width of 0.060" and thickness of 0.020" the conductance of the aperture will be 27.6 cc/sec. It is readily seen that this conductance is considerably larger than the conductance of the ion exit aperture. In the interest of time a readily available standard filament and mounting used. For this reason special electron beams focusing could not be employed to cut down the size of the electron beam aperture. This mounting consists of a straight wire filament with a cupped shield directly behind it. The shield is connected to a feed thru pin so that its potential can be adjusted for optimum focusing. In fact it was

decided to use a slot with a width of 0.100" and in the course of fabrication it was found necessary to shorten it to a length of 0.080". The resulting conductance is considerably higher than allowable for the necessary differential pumping.

The layout of the experimental ion source is shown in Fig. 6-21. The high pressure region of the source was inclosed by ceramic rings between the repeller and accelerator and between the accelerator and negative lens. The sample is brought in through a tube located in a hole in the side of one of the ceramic rings. The exit aperture was facricated with a snout which protrudes into the analyzer section. The inside dimensions of the snout were such that the maximum angle which could be transmitted is 7°. The exit aperture was insulated from ground and connected to a feed thru pin so that it could be put at any voltage desired. The spacing between the lens and exit aperture was reduced from the theoretical value of 0.057 inches to 0.030 inches to increase the value of E_3. This was felt necessary because of the thickness of the lens electrode (0.050"), while the theory assumes zero thickness. The disassembled source is shown in Fig. 6-23.

A simple filament test fixture was fabricated to determine the percent of total emission which could be focused through a slot 0.100" long, 0.030" wide and 0.010" thick. The conductance of this slot is 5 $\frac{cc}{sec.}$ A straight wire 5 mil rhenium filament was

mounted on a standard filament support and centered in a grove 0.020" wide and equally deep. The accelerator plate with the slot in it was mounted on ruby insulators and clamped to the cathode block with a 0.010" spacing. A collector was mounted behind the accelerating plate to collect those electrons which were transmitted thru the slot. The fixture was mounted to a 1" thick Teflon base and pins were forced through under sized holes to make the electrical connections. The Teflon base is mounted to the vacuum system with an O ring seal and is held there by the external air pressure when the test chamber is evacuated. The experimental assembly is shown in Figs 6-24 and 6-25.

6.30 COLLECTOR

The collector assembly consists of a three aperture Einzel lens system and a double collector bucket. The first aperture plate in the lens was permanently grounded while the second two electrodes were connected to Coor's feed thrus. The radius of the aperture of the first electrode was set equal to r_0 and the electrode was placed as close as possible to the end of the quadrupole rods to insure a 100% collection efficiency. The dual collector consisted of an inner and outer collector, the purpose being to test the focal properties of the lens system. The rear end of the collector housing is fitted with a flange which fastens to the vacuum system. The drawing of the collector is shown in Fig 6-31 and the assembly is shown in Fig 6-32. Figs 6-33 and 6-34 show the assembled ion source, analyzer, and collector layed out in the proper orientation with respect to each other.

6.40 QUADRUPOLE POWER SUPPLIES

The operation of the quadrupole mass filter requires the use of d-c and radio frequency voltages. The parameters of the experimental quadrupole were such that approximately 500 volts peak-to-peak were required from the R.F. supply. The output coil of the R.F. power supply was center tapped to provide approximately 250 volts peak-to-peak on each of the poles. Scanning of the mass range of 12 to 50 could be accomplished by varying the amplitude of the voltage or frequency or both. The required frequency range, with a constant voltage, was found to be 2.3 to 4.75 megacycles. The combination of a-c and d-c voltages was arranged in such a manner that the ratio of the voltages remained essentially constant during the scanning process. The level of the d-c voltage was made adjustable around a nominal value approximately 16 percent of the R.F. voltage. The output of the d-c supply was approximately 20 volts.

6.41 R.F. SUPPLY

Several types of oscillators were investigated in order that the most efficient and reliable system could be determined. RC and RL phase shift oscillators were found to be very stable but inefficient. In addition, the high voltage developed across the active element would make the use of transistors difficult. As a result of these problems, an LC oscillator appeared to be most satisfactory. Since the quadrupole structure is effectively a capacitance, it was used as part of the LC circuit.

In an effort to increase efficiency and reliability, a push-pull

circuit was chosen. The distinct advantages of this approach is that the required output voltages are divided between two transistors thus reducing the requirements placed on the individual transistors.

The R.F. oscillator circuit is shown in Figure 6.41.

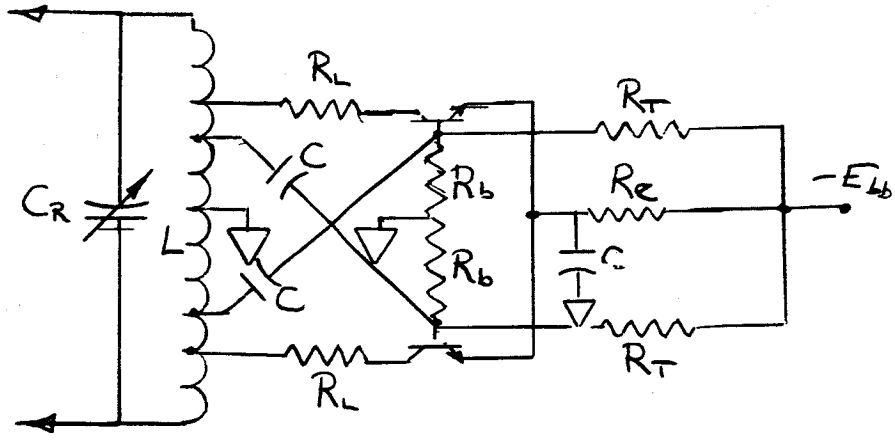

R.F. OSCILLATOR
Figure 6.41

The inductor L, the variable capacitor C, and the capacity of the quadrupole determine the frequency. The inductance of the coil was 17 microhenries. The capacity of the quadrupole was found to be 33 picofarads. The variable capacitor, C_R, ranged from 14 to 432 picofarads. The combination of these values provided a tuning range of 1.8 to 5.6 megacycles.

The two 2N1893 transistors used are capable of high frequency operation and are rated at 50 volts between the collector and emitter. The maximum voltage developed between the collector and emitter will

be the supply voltage, E_{bb}, which has a value of 28 volts d-c. The collectors are isolated from the tank circuit through small load resistors, R_L, which serve to stabilize the circuit. Auto-transformer action in the tank coil is used to step up the output voltage to the required level.

The resistors R_b and R_T from a voltage dividing network which establishes the proper base bias. The values of these resistors were kept sufficiently low so that changes in base current did not appreciably effect the operating point. This latter consideration contributes substantially to greater temperature stability.

The emitter resistor, R_e, provides a degree of negative feedback and acts so as to establish temperature stability. The additional capacitors in the circuit serve as d-c blocking capacitors.

The required oscillator feedback is accomplished by connecting the transistor bases to tops on the tank coil. An effort was made to operate the transistors in the class B region to effect efficient operation. With the particular transistors used it was found necessary to establish the bias in the class A or class AB region. The use of more recently developed transistors could permit more stable operation in the class B region with a corresponding increase in efficiency.

The amplitude of the output voltage of the experimental oscillator was found to vary slightly with changes in frequency. This change was found to have a negligible effect on the performance of the

quadrupole as long as the ratio of the a-c and d-c voltages was held constant. This change in amplitude can be taken into consideration in the design of the scanning system. An alternative approach would require the addition of a feedback stage designed to hold the oscillator amplitude constant with some decrease in the overall circuit efficiency.

During the experiments, it was found that adequate shielding of the tank circuit was necessary to maintain a sinusoidal waveform. Since the required power varies greatly with the Q of the circuit, the shielding must be such that the circuit Q is not degraded. It has been determined that copper or silver should be used as shielding material since it is possible that the use of aluminum can reduce the coil Q by as much as 50%. A shield thickness of approximately 5 mils has been found to provide sufficient thickness at the operating frequencies.

In order that the quadrupole could be adjusted properly during the experiments, it was found necessary to determine the equivalent circuit of the configuration. It was found that the quardrupole was essentially capacitive with 33 picofarads across the rods and 26 picofarads from each rod to the center common. The equivalent circuit appears in Figure 6.42. Additional stray capacity will be added by the connecting leads. This capacity has been taken into account by the increased frequency range of the oscillator.

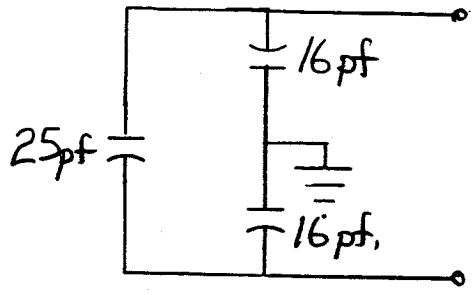

QUADRUPOLE EQUIVALENT CIRCUIT

Figure 6.42

6.42 D-C SUPPLY

Since the ratio of the a-c and d-c voltages must be held nearly constant, it was determined that the simplest and most efficient approach to a d-c supply involved the rectification of the RF voltage. Using this approach, the output of the d-c supply will always be proportional to the a-c voltage.

The d-c supply used was a simple half wave rectifier operating from a voltage derived from the tank circuit. RC filtering was used. The level of the d-c voltage was adjustable by means of a potentiometer. Two such power supplies were required to provide the necessary voltages for the quadrupole rods. The power supply circuit is shown in Figure 6.43. Balancing of the d-c voltages was accomplished by varying the positions of the power supply taps.

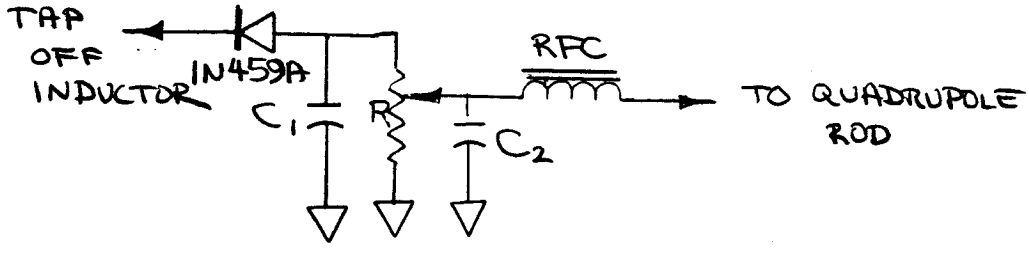

ONE SIDE QUADRUPOLE D-C SUPPLY

Figure 6.43

A power supply capable of controlled balancing against ground is shown in Figure 6.44.

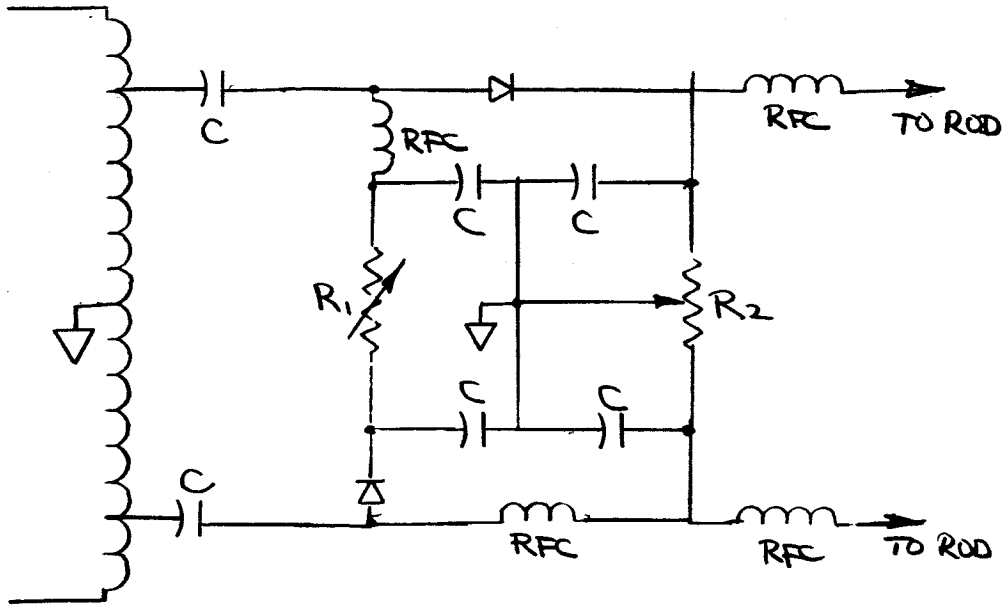

MODIFIED D-C QUADRUPOLE SUPPLY

Figure 6.44

This circuit is connected in such a manner that only two adjustments are required to establish a balance between the voltages. Potentiometer, R_1 establishes the d-c output level. R_2 varies the power supply center point so that equal voltages may be supplied to both sets of rods. A supply of this type was used on the quadrupole mass filter built by the Bell and Howell Central Research Laboratories and proved to be successful.

Figure 6.45 shows the schematic diagram of the complete power supply system. A photograph of the experimental unit is shown in Figure 6.46.

6.50 MASS SCANNING SYSTEM

The ability of the quadrupole mass spectrometer to detect a spectrum of molecules with different mass numbers is dependent upon changing the voltage or RF frequency supplied to the quadrupole elements. It has been determined that varying the RF frequency would be most desirable.

Since certain data sampling methods become more simplified if the mass numbers are sampled linearly with time, the variation of frequency with respect to time was investigated. The relationship between frequency f and mass number m is given by:

$$f = \left[\frac{V_{AC}}{k}\right]^{\frac{1}{2}} \frac{1}{m^{\frac{1}{2}}} \quad (1)$$

Where

$$k = \frac{\pi^2 R_o^2 Q}{e}$$

Several methods may be used to change the frequency to effect the mass number scan. All these methods require a change in the capacitance of the tank circuit in the RF and d-c quadrupole supply.

A small motor using 1 watt or less may be used. This motor may be of a constant speed type which through a cam or similar arrangement would vary the capacitor giving the desired frequency variation with time. It is also possible to use a servo system which would sample the frequency and through a feedback arrangement and shaping circuit allow the frequency to be changed in the desired manner. A different application using a motor would involve the use of a stepping relay which would step to the desired mass positions.

This latter type should require less power.

A very promising method of changing capacitance to vary frequency would require a digital selection of capacitances. Although many mass peaks would need to be investigated, the capacitors could be efficiently utilized so as not to require a large number of capacitors. Smaller steps of capacitors could be reconnected between larger capacitor additions. This method would reduce the power consumption, weight, and perhaps size.

Two other possibilities are:

a) The use of a clock spring and escapement to drive the variable capacitor.

b) The use of a voltage variable capacitor and gated logic system to select the proper voltage level.

Both of these methods present difficulties which should be overcome and will require further study.

6.60 FILAMENT EMISSION REGULATOR

Factors such as power supply variations, temperature changes, and variations in filament resistance result in unstable filament emission. Since the mass spectrometer ion source requires constant electron emission if quantitative results are required, the emission of the filament must be regulated.

The unit which was constructed for use on the experimental quadrupole mass spectrometer was based on the design used on a satellite mass spectrometer system developed by Consolidated Systems Corporation. With extended use, this regulator has been shown effective and reliable.

A circuit diagram of the filament emission regulator constructed is shown in Figure 6.61. The 2N441 transistor is a power unit and will have essentially all the filament current flowing through it from the 3 volt source. There are two inputs to the system. One is the actual total electron emission and the other is a regulated reference voltage which is kept constant at approximately 20 volts. By adjustment of the 15 k potentiometer, the current flowing into the base of the 2N543 transistor from the regulated reference can be adjusted to a desired value. This value is that which gives a current very nearly equal to the proper total electron emission. Under these conditions there will be no base current into the 2N543 transistor since all the current from the regulated reference will flow as total electron emission. Should the total electron emission tend to either increase or decrease, this change will be sensed and

amplified by the 2N543 and 2N540 transistors. The change is then applied to the 2N441 power transistor which will then decrease or increase the filament current in a direction so as to correct for the total electron emission change. The 1N459 diodes are used to eliminate transient fluctuations.

The disadvantage of the unit built for the study is its high power consumption. It will consume approximately 2.3 watts. This power is essentially all lost through the 2N441 power transistor. The case of the emission regulator is used as a heat sink to dissipate the energy which was converted to heat.

The breadboard emission regulator is shown in Figure 6.62.

The power loss in this type of emission regulator is high. For this emission it would be desirable to use a phase controlled or switching type emission regulator for which efficiencies approach 90%. During this program no work was done in this area but previous experience with this type of regulator indicates that it would be applicable to the problem at hand. The principle of operation would be much the same with the exception that the output transistor would operate in the switching mode. The regulated reference and total electron emission would then be compared and used to control the duration of the "on" portion of the output transistor. In this way the only power lost in the output transistor would be due to the saturation voltage and cut off current.

6.70 LOGARITHMIC ELECTROMETER AMPLIFIER

The output of the quadrupole mass filter is in the form of a positive ion current in the range of 10^{-15} to 10^{-8} amperes. It is necessary to construct a special purpose amplifier to sense this very small current and to give a proportional or calibrated output between +5 and 0 volts representing the ion current. Because of the wide current range, and the need to distinguish between the smallest ion currents, it is desirable to have an output which is most sensitive to currents in the 10^{-14} ampere range.

This may be accomplished by using a linear electrometer amplifier; the output of which is fed into another amplifier whose function is to compress data at the high current end, usually in a logarithmic fashion. Another and more efficient method is to build one electrometer amplifier whose output is logarithmic. The electrometer amplifier discussed in this section is of the latter type.

In order to measure the small ion currents, it is necessary to keep the input impedance of the amplifier extremely high. With high input impedance, the time constants will in general be very high. It then becomes necessary to provide a feedback loop in the amplifier to increase the time response. To measure all the mass number peaks between 12 and 50 sampled during the time alloted, it is estimated that the amplifier time constant should be at most a few tenths of a second.

As discussed in section 4.61.3, Controlled Non-Linear Amplifier, the

d-c response of a non-linear amplifier is dependent on the feedback resistor R_f. Since a logarithmic amplifier is preferable, a feedback resistor, R_f, with logarithmic characteristics must be used.

6.71 Logarithmic Feedback Element, R_f

Because of the very high resistance needed for R_f, it was necessary to consider vacuum devices with linear characteristics. The possible range of resistance needed is 10^8 to 10^{15} ohms. It was found that the CK5886 electrometer tube when used as a diode would best fulfill this need. The CK5886 gives best logarithmic response when used as a diode between the cathode and control grid. The circuit and biasing used to give best diode results is shown in Figure 6.71.

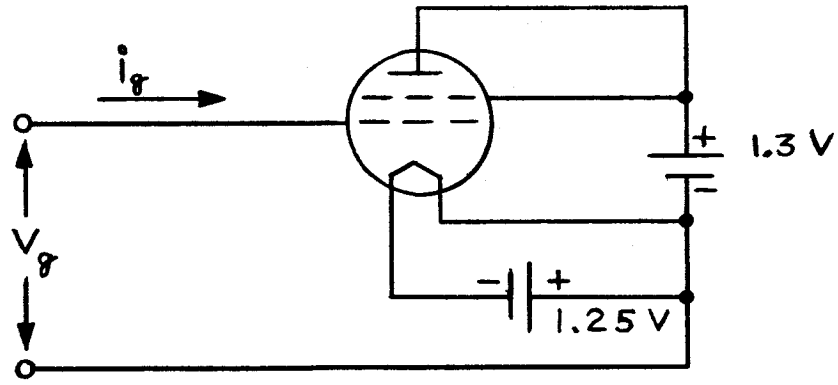

CK5885 VACUUM AS LOGARITHMIC R_F

Figure 6.71

The feedback element values are related to this circuit by

$$R_f = \frac{V_g}{I_g}$$

C_f= grid to cathode tube capacitance.

A curve was plotted for Vg vs. Ig for a wide range of currents. The

plot was made on semi-log paper and is shown on Figure 6.72. Characteristics of two tubes are shown. A very sensitive electrometer amplifier was used to make the measurements.

The results of the investigation on the CK5886 tube were very encouraging and showed the characteristics to be very close to logarithmic to a current of 10^{-15} amps. These same characteristics were investigated by Bell and Howell Central Research Laboratories for currents down to 10^{-12} amps on many CK5886 tubes. The characteristics were logarithmic in each case.

The tube capacitance (C_f) was measured and found to be in the 2-3 pf range.

6.72 Logarithmic Amplifier Developed For Study

It has been found that to effectively sample all the peaks while descending through the Martian atmosphere, a time response of at most 300 m sec. is needed. For sensitivity approaching 10^{-14} amperes the following values are effective:

$$C_1 = 3pf$$

$$R_f = 5 \times 10^{13}\ \Omega$$

$$C_f = 3pf$$

$$C_n = 3pf$$

Solving for k_1 from the time constant equation given in section 4. 61.3, Controlled Non-Linear Amplifier.

$$k_1 \geq \frac{R_f(C_1 + C_f + C_n)}{\tau} = 1500$$

The forward loop gain of a satellite mass spectrometer electrometer amplifier built by CSC is between 1600 and 2000. Since this amplifier has proven to be very reliable and has the appropriate gain with low power consumption, it was decided to use its basic principles for the forward loop amplifier.

The circuit diagram for the logarithmic amplifier constructed for the study is shown in Figure 6.73. A CK5886 electrometer tube together with a CK6281 tube and two 2N1234 transistors are used as the forward loop amplifier. The RC pi network at the plate of the CK5886 amplifier is a constant 30° phase shift circuit for increased stability of the amplifier. A CK5886 tube used as a diode together with a parallel resistor R_p serve as the logarithmic feedback element R_f with C_f being the capacity of the tube. R_p limits the sensitivity and should be made larger if a current sensitivity of 10^{-14} or 10^{-15} amperes is desired. The JFD 0.8 to 10 pf variable capacitor serves as the neutralization capacitor C_n. Transistor 2N929 serves as amplifier k_2 and inverts the signal as required. Since C_n can be made closely equal to C_f, the gain of k_1 is approximately minus one. The 910 pf capacitor is parallel with the 250K pot functions to reduce the high frequency loop phase shift.

For study purposes, the amplifier was adjusted for a dynamic range of 10^{-8} to 10^{-13} amperes. The output was set at +5.0 volts at 10^{-13} amperes in, and 0 volts at 10^{-8} amperes in. The procedure used to align the amplifier is given as follows:

1. Adjust "Screen Pot" to obtain +8.1 volts CK5886 screen grid to ground.

2. Short the input to ground with a very short lead and adjust "Input Offset Pot" to give an output voltage close to zero.
3. With maximum current (10^{-8} amp) input, adjust "Zero Adjust Pot" to give zero output.
4. Adjust "Feedback Pot" for proper output (+5 volts) with input of minimum current (10^{-13} amps).
5. Adjust neutralization capacitor C_n for best time response.

A photograph of the logarithmic electrometer amplifier developed and constructed for this study is shown on Figure 6.74.

6.73 Polarization Effects

Dielectric hysteresis at the logarithmic amplifier input has played a most important role. Because of the high impedance at the input, polarization effects using ordinary support materials were most troublesome. After some investigation and discussion with Bell and Howell Central Research Laboratories, it was determined that a single teflon standoff support would be the material with the least polarization. Though the effects were greatly reduced, the polarization was still appreciable. Through the use of a copper ground plane and the elimination of any input standoff supports, the polarization effects were reduced so that reasonable time constants were achieved. The input components were placed in close proximity to reduce input capacity and to form a solid support without the need of an input standoff. It should also be noted that the input should be directly coupled with a short lead which is not connected to a

shield through any insulating material.

It is felt that the polarization effects can be reduced even more by a more thorough investigation of input components with low dielectric hysteresis.

The polarization effects at very low currents will effect linear amplifiers as well and appear to serve as the fundamental time response limitation to very small current inputs.

6.74 Input Shielding

By reducing input capacitance it is possible to improve the output response time. Therefore, input shielding is very important. All input leads were shielded from the remainder of the circuit. It is also important to note that the input capacitance of the CK5886 electrometer tube can be reduced by shielding it from the rest of the circuit. This was not done on the study model but is a factor which should improve response.

6.75 Simulated Current Step Inputs

In order that the response of the electrometer might be properly tested, a current input source was needed which would simulate the ion current input.

To test d-c response of the logarithmic amplifier, a voltage was applied to a hi-meg resistor in series with the input. This very high resistance effectively controlled the current input. However, several different resistors were needed since the voltage range

would be impractical if it alone were varied over the required current input range.

So that the amplifier response to a step input of current could be observed over the entire d-c range without changing components, other methods were investigated.

The method which was used in the study was a modified triangular wave input. A voltage waveform which was triangular with the bottom clipped off was introduced through a small coupling capacitor C_T. During the clipped portion of the wave the input was zero but at the moment the slope of the wave began it applied a step input of current of magnitude:

$$i_1(t) = -aC_t \left\{ 1 + \left[\frac{C_1 + C_f}{C_1 + C_f + C_t} - 1 \right] e^{- \frac{t}{R_f (C_1 + C_f + C_t)}} \right\}$$

where a is the slope of the triangular wave. It can be seen that it was necessary to keep C_T very small so that it would not appreciably effect the time constant. Unfortunately, when the triangular wave changed slope the electrometer gave meaningless data. However, the clipped portion of the wave was made long enough to overcome any of these unfavorable transients. The input and output of the amplifier using this method is shown in Figure 6.75.

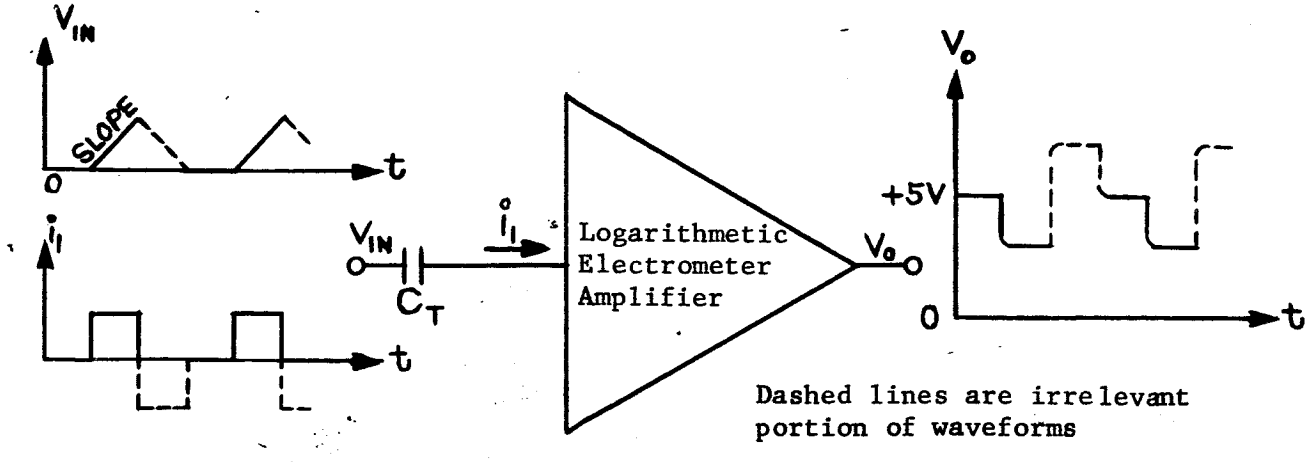

Figure 6.75 Simulated Current Step Input

The input slope was calibrated by placing a known current into the amplifier and adjusting the slope of the triangular wave to give the same output. By determining several values, a slope vs. input current curve was constructed.

Another method which may be used in the future involves the use of a phototube acting as a current source with light impinging on it at regular intervals.

6.80 WEAK MAGNETIC FIELD PUMP

It was decided that of all the ion pumps that were theoretically statied the weak magnetic field pump was the most promising since it offers space change limited operation, while at the same time the possibility of a great improvement in magnetic leakage field over the conventional ion pumps. A Schematic diagram of the experimental design is shown in Fig 6-81. The vital parts of the pump were mounted in a vacuum housing which mounted to the vacuum system. The cathode was fabricated of Titanium sheet stock and mounted to the base flange on three ceramic standoffs. It was decided to test a Triode configuration since this is the only possible means of obtaining efficient pumping Argon. The grid structure consisted of a stack of rings held together by Titanium rods and mounted to the base flange on ceramic standoffs. Because of the low sputtering efficiency of Titanium it was decided to intersperse copper and Titanium rings. Electrical connections were made to the cathode and grid by spring clips mounted on pins which entered the vacuum housing thru Coors feed thrus. The anode was mounted on a 1/16 inch rod which also extended from a feed thru. This rod was shielded by a ground potential cylinder which slipped over it and seated in the feed thur recess. All ceramic surfaces were shielded so that they could not be coated with sputtered material. The pump assembly is shown in Fig 6-82.

The cathode and grid structures were fabricated with a cylindrical geometry rather than the spherical geometry which was theoretically studied. This was done in order to expediate fabrication. The operation of the pump should not be affected by this change since the voltage distribution is determined primarily by the anode geometry.

The electron gun used to inject electrons into the pump cavity was designed using the space charge beam principles of J. R. Pierce.* The calculations are not presented here. There is a primary focusing action between the cathode and the accelerator which was designed to accept a 200 μa beam with a perveance of 2.2×10^{-6}. A secondary focus is obtained a lens action at the accelerator - barrel (?) boundary. This lens acts like an equidiameter cylindrical lens. The focal length of this lens was adjusted to equal the length of the barrel.

The gum was fabricated from 303 stainless steel except for the envelope which was facricated of 416 SS. The electron gum is mounted to a base flange and inserted into a 2" diameter tube. This tube is then mounted to the base flange of the ion pump. The drawing is shown in Fig 6-83 and the assembly is shown in Fig 6-84.

*"Theory and Design of Electron Beams."
J. R. Pierce. Bell Telephone Labs Series.
Van Nostrant Press.

6.90 INLET APERTURE

The desire to have a molecular inlet leak in the presence of a large pressure drop necessitated the investigation of methods for fabricating sub micron apertures. These are discussed below.

6.91 PRELIMINARY INVESTIGATION

6.91.1 Laser Beam Techniques

One possible way of making a sub micron hole is by burning it in a thin sheet of material with a laser beam. This technique has been used for 1 μ to 10 μ diameter holes but the sub micron range has not to our knowledge been investigated. It is difficult to control the beam's size at one micron and the exact position of the beam is also difficult to control. Holes can be drilled in various materials up to a few thousandths of an inch thick. The hole cross section usually varies over its length. This technique appeared promising but was not experimentally investigated.

6.91.2 Quartz Fibre Technique

Quartz fibres with submicron diameters are comercially available. One of these fibres could be used as a die around which a submicron hole could be formed. A jeweler's drill could be used to make a 1 mil hole in a thin metal plate. A submicron diameter quartz fibre would then be placed in the hole (this in itself would be

a difficult task.) The metal would then be melted around the quartz and the hole would close down to the diameter of the fibre. As the metal is cooled it should pull away slightly from the quartz and the fibre would be removed. In theory this sounded like a plausible method but the reduction of this operation to practice would undoubtedly pose some severe problems. This method was not experimentally persued.

6.91.3 Electron Microscope Techniques

A conversation was held with Dr. R. H. Willens of the California Institute of Technology concerning the use of an electron microscope for burning submicron holes. The substance of the conversation follows:

It is common practice to burn holes in various materials with an electron microscope. The primary use of such holes is aligning the electron beam. Hole sizes range down to 0.01 μ. The electron beam area is greater than 1 μ in diameter but submicron holes can be formed due to the non uniform beam intensity by turning on the beam for short periods of time. It was indicated that a single hole in the size range that was desired might be difficult to make and therefore it may be necessary to use a group of smaller holes. A second problem which was anticipated was that extremely thin materials must be used in order to obtain good results. The material should not be over 0.1 μ thick. This is slightly thinner than necessary for molecular flow but could be built up by evaporating metal on the

foil to build up the thickness. Thicknesses can be accurately controlled by this technique. The foil with the submicron hole must then be mounted over a larger hole (on the order of 10 μ) in order to support it.

A third problem which would be encountered is that holes which are burned in metal films are irregular in shape and their size is difficult to control. This problem may be combatted by making the hole in collodium, evaporating metal on the collodium surface and then dissolving the base material. This technique may offer an additional advantage in that it should be easier to make a single hole in collodium film. Electron microscope techniques offer the advantage of being able to see what you are doing, since an optical microscope cannot resolve such small distances.

Based upon this conversation it was decided to investigate electron microscope techniques for making the inlet leak. The services of Dr. Willens were engaged.

6.92 RESULTS OF DR. WILLENS WORK

Presented here are the reports which Dr. Willens submitted.

6.92.1 Progress Report

Progress on the investigation of making holes between 0.25 μ and 0.5 μ

in diameter and between 0.1 μ and 1 μ in length is discussed.

There are three main considerations involved in making a small hole in a thin foil for the purpose of a small leak - a reproducible method of producing holes, attaching the foil to the main body of the spectrometer through a vacuum seal, and a support fixture for the thin foil so it can take one atmosphere of pressure without failure. Preliminary calculations revealed that the foil would have to be supported over its entire area except for a small hole where the flow controlling leak hole is located. The size of the hole in the support piece should be less than 10 μ in diameter if the stress level is to be maintained below 10,000 psi, for a foil thickness of 0.2 μ, under a load of one atmosphere. A desirable form for the finished product would be as shown below.

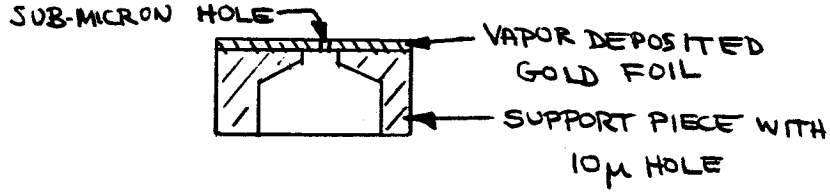

The vacuum seal to the system could then be made by clamping the support piece against a metal gasket.

Methods for Making Holes

1. Holes in low melting point metal by electron beam.

   (a) Place 200 A film of collodium over 5 μ hole in Pt support piece.

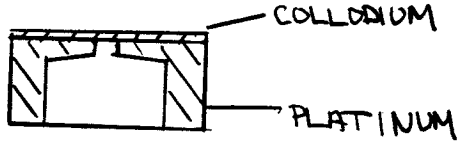

   (b) Evaporate 400 A Bi on lower side of Pt, then remove collodium by acetone wash.

   (c) Place in electron microscope and attempt to melt hole in the Bi with beam.

   (d) Vapor deposit Au on top side of Pt, propogating hole and then remove Bi with acid.

Observations

Six samples prepared by this method.

The making of holes in the bismuth was extremely difficult due to the fact that an oxide layer was difficult to puncture, i.e., the metal would melt away and leave the oxide. By rapidly raising the beam current, it was possible to puncture holes. Unfortunately one hole never appeared, rather several at one time. The best sample prepared had three holes in the 5 μ circle approximately .3μ x .3μ, .4μ x .6μ, and 1.2μ x .4μ. This method was abandoned.

2. Holes in collodium (Br) film by electron beam. (similar to first method.)

   (a) 200 A film on Pt support piece with 5 hole

   (b) Bombared in electron microscope to make holes

   (c) Evaporate 500 A Au on lower side

   (d) Remove collodium film with acetone wash.

   (e) Evaporate gold on top side.

Observations

12 Attempts - could not produce only one hole in 5 μ circle again and size of holes was uncontrollable.

3. Shadow holes of latex spheres

   (a) Make 250 A collodium support films on Pt supports, grids and glass plates.

   (b) Spray 0.34 μ latex spheres on collodium films with nebulizer.

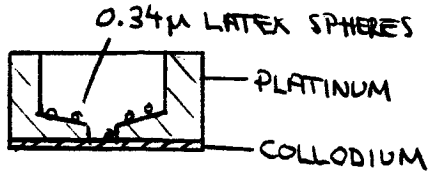

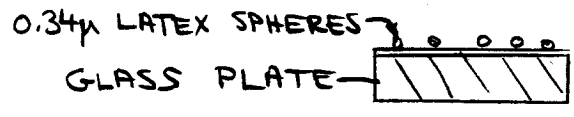

(c) Evaporate 500 A silver.

(d) Wash away or dissolve latex spheres.

(e) Dissolve collodium

(f) Evaporate gold on silver progating hole.

(g) Remove silver with acid.

Observations

a) Twelve 200 mesh grids were prepared by this method. There where perfect holes within the grid squares in the evaporated silver foil. There was approximately one hole per 1000 u^2. An electron micrograph of one of these holes is shown in Figure 1. Figure 2 shows two of these holes (from different areas) after evaporating 0.12 μ of gold on top of the silver.

b) Ten Pt supports were prepared by this method. The Pt supports had various size support holes ranging from 10 μ to 100 μ. The density of latex spheres was so low that only one was found in a 100 μ hole.

c) Two glass plates were prepared by this method. The observations were the same as a).

Conclusions

The shadowing of latex spheres has been shown to be a convenient and reproducible technique for producing sub-micron holes in thin foils. Although 0.34 μ latex particles were used in these experiments, the latex spheres can be obtained with various diameters. (0.19, 0.26, 0.37, and 0.56 μ spheres are on order.) Due to the fact that only a very small amount of solution with 0.34 μ spheres was on hand, the density of sub-micron holes was low. This made the probability of finding a hole within the aperture of the support piece quite low. Once a hole is located within the aperature hole it will be very easy to alter its flow characteristics by either vapor depositing more gold to increase the hole length or electropolishing to increase the hole diameter. (The strong electric field at the edge of the hole results in rapid removal of the metal from this area.)

This technique is applicable to make a filter for the instrument. In this case smaller latex spheres would be used to make several thousand holes in a 1/8" diameter foil. Since there would be hardly any pressure drop across the filter, the support of the foil can be accomplished by a 200-mesh screen grid.

Tentative Work for the Future

A gold foil, 0.8 μ thick, with a high density of holes will be made by the method of shadowing latex spheres. This gold foil will be positioned over a support piece with a 10 μ hole until one of the smaller holes is within the region of the 10 μ aperture. The gold foil and the support piece will then be diffusion bonded. The thickness of the gold foil will then be increased by vapor deposition. Thickness measurements will be made on a secondary sample by the x-ray absorption technique.

Figure 6-91 shows an electron-micrograph of a 0.337 μ hole in a 0.05 μ silver foil at 80,000 magnification. The left hand insert shows the same hole. The insert at the right shows the results of evaporating gold on two holes to a depth of 0.1 μ.

6.92.2 Final Report on the Making of Sub-Micron Holes

As stated in the previous report, the shadowing of latex spheres was found to be a convenient and reproducible technique for producing sub-micron holes in thin foils. The final method chosen may be described as follows:

(a) Several hundred angstroms of Victawet (wetting agent) is evaporated on a glass slide.

(b) Sub-micron latex spheres are sprayed on the coated slide with a nebulizer.

(c) Approximately 500 to 1000 A of gold is evaporated on the glass slide. The spheres leave shadow holes in the gold on the glass surface.

(d) The spheres are removed by an air stream and a wash in benzene and acetone.

(e) The gold foil, while still on the glass, is cut into small squares and then detached from the glass by stripping on to a water surface.

(f) A piece of the gold foil is lifted off the water surface by a platinum support piece (a disk 0.079" in diameter by 0.021" high) with a 10 μ hole in the center.

(g) The gold foil is diffusion bonded to the platinum support.

(h) The thickness of the gold foil is increased by vapor deposition.

The final product will be as shown below:

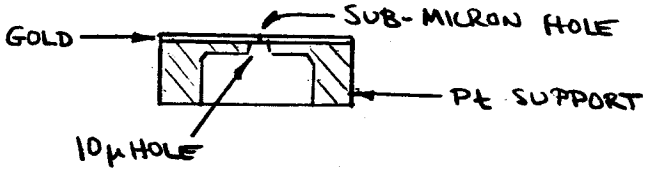

Observations

Many gold foils were prepared by this method using 0.34 μ diameter latex spheres. Due to the fact that only a very small quantity of spheres (2 drops of less than a 5% solution) was available, the density of sub-micron holes in the gold foil was very low (approximately one hole in 1000 μ^2). This made it quite difficult to locate

one of these holes over the 10 μ hole. After many attempts a successful location was made and the previously described procedure was carried to completion. Figure 6-92 shows an electron-micrograph of the sub-micron hole located on the platinum support. The thickness of the gold foil is 0.21 μ as determined by x-ray absorption.

Filter for the Flow Limiting Aperature

To prevent the plugging of the sub-micron hole by a large particle, a foil with many holes smaller than the flow limiting hole was made by the previously described procedure. In this case, 0.26 μ latex spheres were used. There was a sufficient quantity of this size sphere available so there was no trouble in producing a foil with a high density of holes. Figure 6-93 shows an electron-micrograph of the filter. The density of holes is approximately 8 million per cm^2. This foil is mounted on a platinum support disk with a 200 μ hole. There are approximately 2400 sub-micron holes in the 200 μ opening in the platinum support piece. Since there is hardly any pressure drop across the filter, it can be supported by this larger size aperature.

Mounting of the Flow Limiting Hole and Filter

Figure 6-94 schematically shows the mounting of the hole and filter to the spectrometer housing. The vacuum seal is made by a gold

gasket. A 200 mesh copper grid is placed at the entrance to the spectrometer as a coarse particle filter and another placed between the foil filter and the flow limiting hole as a precaution in case a pressure surge breaks the filter. Figure 6-95 is a photograph of the 200 mesh copper grids and the filter and the flow limiting foils mounted on their platinum support pieces.

7.0 EXPERIMENTAL RESULTS

The experimental results are classified in four sections: Mass Spectrometer (including ion source, collector, and quadrupole supply); Logarithmic Electrometer; Weak Magnetic Ion Pump; and Emission Test. There was no experimental data taken on the inlet leak or emission regulator.

7.10 MASS SPECTROMETER SYSTEM

The mass spectrometer system test was begun with an investigation of the ion source properties. The first experiment consisted of varying the potential between the filament and repeller and recording the electron current which was transmitted through the slot in the repeller. This current was collected at the accelerator which was maintained at repeller potential. Several runs were made at progressively higher shield voltages (The shield is mounted behind the filament). The results of this experiment are shown in Figure 7.12. It can be seen that as the shield was taken more negative the electrostatic field lines close in around the filament and restrict the emission thus boosting the filament current for the same total emission. At the same time this action had the dual effect of increasing the maximum transmitted current and shifting the maxima so that they occur at higher and higher values of $\Delta V_{FIL-REP.}$ Both of these effects are desirable since they combine to produce

a higher electron beam transmission efficiency at the proper accelerating voltage. The correct operating value for ΔV FIL-REP is 140v. as determined in the source design. Therefore the shield potential was maintained at -600 volts for the remainder of the tests.

The second experiment performed was to measure the electron current collected at the anode as a function of the repeller-accelerator voltage. The results of this experiment are shown in Figure 7.13. The anode was positioned to accept the electron current at a nominal ΔV REP-ACC of 101v. It is seen that the anode position appears to be adequate. The sharp spike at the left edge of the anode current peak is unexplained. The negative accelerator current is the result of secondary emission. Neglecting the previously mentioned spike the transmission efficiency of the electron beam aperture is 42%, which is not too bad considering that no design work was done in this area.

A third ion source test was the determination of the electron beam thickness. This was doen by measuring the energy distribution of the ions coming out of the source and collected at the collector. The results of this test are plotted in Figure 7.14. The general slope to the plot is due to a superimposed leakage current arrising from the fact that the electrometer detector was grounded through a bucking power supply. It is seen that the electron beam is 31 volts wide in the region above the accelerator aperture. There are two reasons for this. First, ΔV REP-ACC is 91 volts instead of the design value of 101 volts thus shifting the minimum point of the

parabolic trajectory away from the central axis. This was done because the greatest source sensitivity was obtained for this reduced value of ΔV REP-ACC. This is accounted for by the fact that a decrease in ΔV REP-ACC brings the electron beam closer to the accelerator. The second, and more important, factor is that there is evidently a wide dispersion of angles coming from the entrance slot. It was hoped that varying the shield voltage would improve this but no positive results were obtained.

Next the focal properties of the ion source were investigated by measuring the total ion current at the collector as a function of accelerator and negative lens voltages. In order to accomplish the collection of the ion current the quadrupole rods are biased to act like a thick lens. This mode of operation appears to be applicable to the measurement of total current under flight conditions. The results are shown in Figure 7.15. The quantitative accuracy of this particular test is doubtful because it was later found that ion current from the vacuum system ionization gauge could get to the collector. This problem was solved by taking all future readings with the ionization gauge turned off.

The maximum value of ion source sensitivity with the exit aperture (A_3) grounded was found to be 1.0×10^{-11} amps/μ - μa. It was also found that when the aperture electrode was taken negative the sensitivity increased. In this mode of operation the maximum ion source sensitivity was found to be 6.5×10^{-11} a/μ- μa for V_{A3} = -165v. This indicates that the leakage field up through the long aperture

in the negative lens is much weaker than the theory predicted. This is due to the length of the aperture being so great (0.050"). as V_{A3} is increased the leakage field increases and a higher sensitivity is obtained.

An experiment was run measuring the collected ion current to both collectors as a function of the voltage on the central electrode with the rear electrode grounded.

The results indicated that all of the ion current was collected for voltages less than -150v. The maximum sensitivity given earlier was measured at V_{ei} = -168v.

The conclusions which must be reached is that the experimental source sensitivity is too low. The following improvements are suggested:

1) Place the electron beam as close to the accelerator aperture as possible.
2) Improve the electron gun design in order to cut down on the beam spread.
3) Go to a spherical source instead of a parabolic one to obtain focusing in two directions.
4) Make the flow restricting aperture in the exit plate instead of the negative lens. In this way the lens electrode can be made thinner and the focal properties improved.

It is felt that these improvements can increase the source sensitivity to a value which is near the predicted theoretical value. It should also be pointed out that the design sensitivity was based on

the assumption that H_2O would register 1×10^{-13}a. at an analyzer pressure of 1×10^{-7}mm, two decades below the probable maximum allowable pressure. Actually the pressure variation over the sampling range should not exceed one decade and therefore if the maximum analyzer pressure is held at 1×10^{-5}mm the measured source sensitivity for V_{A_3} grounded is only a factor of 5 lower than necessary value. The adoption of the recommended changes should bring up the sensitivity to the necessary level even if the flow restricting aperture is cut to a diameter of 5 mils. which is probably necessary in order to achieve the assumed differential pumping ratio of 20.

The quadrupole RF and d-c supply operated within the design range and functioned adequately so that data could be taken on the quadrupole mass filter.

Frequency range of the supply was 1.92 to 5.75 megacycles and would develop 300 volts peak-to-peak on each side of common. This was accomplished with a 30 volt d-c source and it is anticipated that the voltage and frequency range necessary can be achieved with a 28 volt d-c source. The d-c output was of the appropriate magnitude and appeared to follow the RF magnitude well. However, the exact variation of the V_{d-c}/V_{a-c} ratio was not determined.

With some shielding of the RF tank circuit a waveform which was very nearly sinusoidal was achieved. It is anticipated that an essentially ideal sinusoidal waveform can be achieved if it is found necessary.

No effort was made to closely regulate the amplitude of the RF voltage since the possibility exists that this variation may be taken into account in the mass scanning method. Consequently the RF voltage amplitude varied approximately 15% over the frequency range. This variation was reproducible during the experiment. Due to quadrupole mass filter sensitivity considerations and the need to assure a given voltage level after the 6 month flight is completed there is a strong possibility that a feedback stabilization circuit may be required.

The test of the quadrupole analyzer was carried out once the ion source characteristics had been determined. The first thing which became apparent was that the ratio r_e/r_0 was not large enough. This is understandable when its value of 0.1 is checked on Figure 4.13. It is found that at the designated value of resolution ($m/\Delta m = 25$). that a pointed peak will be obtained. Unfortunately at the time the ion source was fabricated we did not have this pertinent design data and therefore the proper value of r_e/r_0 could not be chosen. The affect of the variation of V_{d-c}/V_{a-c} is shown in Figure 7.16. It is seen that the necessary resolution can be obtained but with a pointed peak shape.

The effects of varying the quadrupole voltages while keeping a-c to d-c ratio constant is shown in Figure 7.17. The a-c voltages indicated are peak-to-peak and therefore twice as great as V_{a-c}. It is seen that the peak broadens as the voltages are lowered and the apikes on the peak become noticably worse. This is to be expected

as was pointed out in the theoretical discussion.

An interesting observation may be made from studying the data shown in Figure 7.18. In this experiment the entire ion source was taken negative with respect to the quadrupole rods. When this is done the ions are apparently slowed as soon as they come out of the ion source and the effect upon the peak shape is exactly the same as if the injection energy were decreased in the ion source relative to the exit aperture potential. The further the ion source is taken negative the better becomes the resolution and the spikes on the peaks subside. It should also be noticed that the peak height does not vary appreciably over this range.

The possible implications of this experiment are that a relatively high voltage ion source may be employed while at the same time maintaining a low injection voltage (V_I). The use of a higher voltage source inplies that greater source sensitivity can be obtained as was pointed out in the general discussion of ion sources.

The recommended changes and investigations based on these experiments with the quadrupole analyzer are:

1) The rod spacing should be increased to $r_0 = 0.200"$ to allow for a lower r_e/r_0 ratio. As discussed in section 4.12.4 the quadrupole power should not change appreciably.
2) The entrance aperture radius should be adjusted to obtain 100% transmission efficiency.
3) The effects of biasing the source negative should be studied further to find out the full range of usefulness of the new technique.

4) Study effects of the Einzel lens further to determine if the collection efficiency is 100%. (This was not determined in the present experiments).

7.20 LOGARITHMIC ELECTROMETER AMPLIFIER

The logarithmic amplifier discussed in section 6.70 was constructed and adjusted as given in the aligning procedure of section 6.72.

An appropriate current was applied to the amplifier through a high megohm resistor. The resistor was changed from 10^{10} ohms to 10^{12} ohms in order to cover the needed range with a practical voltage source. The logarithmic electrometer amplifier input-output data was taken for the various input currents after steady state conditions had been reached. This d-c response data was then plotted. The results are shown on Figure 7.21. It was very encouraging to note that the amplifier characteristic was very close to the ideal logarithmic line even at low currents. This would indicate that the logarithmic characteristics might hold at currents below 10^{-13} amperes. The arrows at the data points indicate whether the data was taken while increasing or decreasing the input current. It is seen that some dielectric hysteresis is evident at lower currents. As indicated in section 6.73 there are methods which should improve this condition.

The effect of varying the neutralizing capacitor, C_n, is shown on Figure 7.22. The input was the modified triangular type discussed in section 6.75 giving a step function input. It can be seen that

C_n is very effective in controlling the time response. The three charts indicate the overdamped, critically damped, and underdamped cases effected by different values of C_n.

With the neutralizing capacitor, C_n, adjusted to give critical damping at 10^{-8} amperes input, the triangular wave slope was adjusted to give +5.0 volts out at 10^{-13} amperes and 0.0 volts out at 10^{-8} amperes. The wave shapes showing this zeroing are shown on Figure 7.23 (Runs #2 and #3).

By determining the triangle wave slope which corresponded to known input currents, the output response was recorded. This data is shown on Figure 7.24 for six different simulated step input currents (Run #4 through #9). It was noted that for larger input current steps, the output dropped from the established level. It is felt that this is an effect which can be attributed to a large time constant associated with the triangular wave input method. It was encouraging to note that the time constant was approximately 100 milliseconds and that the final d-c level was effectively reached in approximately 500 milliseconds.

The data from Runs #4 through #9 (Figure 7.24) was used to make a triangular wave input calibration curve shown on Figure 7.75. Using this calibration curve to associate triangular wave slope with input current, the logarithmic electrometer amplifier response with stepped current inputs was plotted. This graph is shown on Figure 7.26 The linear, ideal logarithmic, and actual response are shown. The actual followed the ideal logarithmic line very closely and in fact

deviated only slightly even at 10^{-13} amperes. This again shows the probability of a continued logarithmic response at even lower currents.

Difficulties encountered in attaching the amplifier to the experimental quadrupole prevented a system evaluation.

7.30 WEAK MAGNETIC ION PUMP

When weak magnetic ion pump was initially tested no positive results were obtained. The pump was removed from the vacuum system and ground shields were placed around the anode support rod and the electron gun barrel. When the pump was replaced and tried again a positive result was obtained. For 21 a of emission current going to the anode 3 a of ion current was registered at the cathode at a pressure of 4×10^{-6}mm with a magnetic field of 195 gauss. This current varied with pressure and was therefore confirmed to be ion current. The Vac Ion® 0.150 cc/sec. pump requires about 12 a of ion current for a pumping at 4×10^{-6} mm and therefore this value of ion current should give a pumping speed of 50 cc/sec. A stable pumping speed was not measured but several factors accounted for this. First, there was no readily available means of determining the pumping speed under the experimental conditions which prevailed. Second, the electromagnet which was used got extremely hot when operated at 195 gauss and therefore the outgassing equilibrium of the vacuum chamber was altered. The heating was probably excessive enough to cause the internal pressure to rise by virtue of the perfect gas law. Third, the magnetic field had a slight effect upon

the ion gauge indication. Fourth, and perhaps the most important, is the fact that the cathode and grid geometry which was tested was probably very far from ideal. The major problem is that the surface area of the cathode is too large for the amount of ion current which impinges upon it. At the same time it would also be advisable to increase the number of rings used in the grid stack and perhaps run some verticle grid members. These changes would increase the sputtering action greatly and therefore improve the overall pumping action. A fifth factor which must be considered is that over half of the rings in the grid stack were fabricated with copper. It has been decided that this was probably not a very good idea even though the sputtering efficiency is higher. It would be desirable to test the pump with all titanium grids.

Further investigation is in order in the following areas:

1) Investigate the effects of improved shielding and electron gun placement on the lowering of the magnetic field necessary to obtain efficient operation.
2) Improve the electron gun design to obtain higher emission efficiency.
3) Investigate improved cathode and grid geometries and all titanium system as indicated above.
4) Solve the differential equations of motion on a digital computer to determine the theoretical value of B necessary to obtain fast flipping.
5) Study methods for obtaining a more controlled experiment so that pumping speed measurements can be accurately made.

6) Solve the space charge distribution problem to determine the theoretical limitations on ion current.

7.40 EMISSION TEST

The results of the emission test indicate a high emission efficiency through a small slit which is long compared to its width cannot be obtained unless considerable effort is expended in the design. It was also concluded that the magnetic field created by the filament current was deflecting the electron beam away from the aperture.

8.0 CONCLUSIONS

Based upon the results of this study program the following conclusions have been drawn. They include a proposed breadboard design, expected performance, power, weight, and recommended studies.

8.10 PROPOSED BREADBOARD DESIGN

The proposed breadboard design is shown in Figure 8.11. The principal changes from the experimental units and other important features are:

1) r_0 has been increased to 0.200" to improve transmission efficiency.
2) A spherical ion source replaces the parabolic source which was tested. This should increase the ion source sensitivity.
3) The quadrupole rods are fabricated of stainless steel tubing rather than solid round stock to decrease weight. Pump out holes are drilled in the back sides of the rods.
4) All flanges were eliminated in favor of welded seals for lightness. The final sealing weld is indicated.
5) The ion source filament and ion pump electron gun filament were combined. Emission is focused in two opposite directions from the same filament. The emission regulator would control the ion source emission and a simple grid type emission control would prevent the pump emission from increasing

too far. Once space charge saturation is reached in the pump subsequent fluctuations in electron beam should not affect the pumping speed; therefore, close regulation is not needed.

6) A single collector replaces the double collector which was only for experimental purposes.

7) The quadrupole voltage feed throughs are moved farther toward the collector and to be compatible with the packaging of the electronics. The feed throughs are also smaller than on the experimental voltages.

8) The quadrupole rods are mounted on ceramic stand offs which slip inside the ends of the tubes. The entire assembly, including the Einzel lens stack and ion source is clamped together and held there by screws which pass through the exit aperture plate and are attached to the envelope structure.

9) The envelope is 0.050" wall stainless steel tubing.

10) The cathode of the ion pump becomes the outer shell for this part of the unit. Since the same filament is used for the electron gun and the ion source the voltage relationships dictate that the cathode be electrically isolated from ground. This is done through the use of a ceramic ring which joins the pump and ion source. The ring performs a second function in that all of the source and electron gun voltages are fed to their proper connections by means of eleven pins seated around the ring. The pump cathode will have to be coated to prevent arcing.

11) The anode and grid voltages are fed in through separate feed throughs.

12) Permanent magnets are used to supply the magnetic field for the weak magnetic field ion pump. The cathode shell is fabricated of magnetic stainless and thereby provides a flux return path. An additional shielding should be necessary.

13) The electronics modules along with the mass spectrometer and pump are mounted in a light magnesium support structure and a unified package is obtained.

14) A large volume is allowed for the r.f. inductor and shield so that it can be made as efficient as possible.

15) The sample inlet leak assembly is mounted in a small flange which comes out of the side of the ion source. There must be a small break-off assembly to open this aperture when sampling is begun. This is not shown in the conceptual drawing.

8.20 EXPECTED PERFORMANCE

The study indicates that it should be possible to meet all the design specifications provided that some leeway is given on the power specification. Some specific problem areas still remain to be dealt with including the improvement of the ion source sensitivity, improving the design of the weak magnetic field pump; improving the electron gun design, and regulating the quadrupole supply voltage (so that a synchronized scan can be used).

As has been previously indicated, there are alternate approaches to

most of these problems and it is therefore felt that the overall performance in terms of resolution, sensitivity, and accuracy can be maintained at or above the level called out in the work statement. A sustained effort in the breadboard phase would be necessary to realize this goal.

8.30 EXPECTED POWER

The expected average power requirements for the proposed breadboard are presented here:

a)	Quadrupole power and power supply loss (averaged over the scan)	1.2 watts
b)	Stepping Motor for scan and drive power	1.0
c)	Filament (including emission regulator and power converter)	5.2 - 3.9
d)	Logarithmic Electrometer	0.4
e)	Electrometer Power Supply	0.4
f)	Source Power Supply	0.1
g)	Ion Pump power (includes supply loss) Electron Gun power (includes supply loss)	0.7
h)	Regulator Reference power supply	0.1
	TOTAL	9.1 - 7.8 watts

These estimates were arrived at as follows:

a) The power required by the quadrupole coil was calculated from the theoretical value assuming:

$$C_{min} = 50pf.$$

Q_{avg} = 150*

r_0 = 0.200"

V_{ac} = 173v. (as required by the considerations of Section 5.0)

Then an oscillator conversion efficiency of 50% was assumed. This should be obtainable under conditions of class B operation.

b) The scan drive power was crudely estimated and should be high because of the relatively short duty cycle (~10%). It is also possible that a clock spring and escapement could be used but this must be investigated.

c) The filament power was estimated by extrapolating available data on 7mil and 5mil rhenium wire filaments to the case of 3mil wire which would be used. The 5.2 watt value assumes the use of a conventional emission regulator, such as built in this study program, in conjunction with an efficient power converter system upon which we have data. It is a saturating core type, but a third core is used for the feedback and the transformer carrying the main load does not saturate. This reduces the losses considerably over other more conventional types. The 3.9 watt value is based upon the use of a phase controlled or switching type regulator. This type of system has not been thoroughly investigated as has the d-c regulator but the approach is a feasible one.

---

*This value appears attainable based on the work of Norton Bell of Bell and Howell Research Center whose consulting services were relied upon.

It should be pointed out that the standard emission regulator was designed to work directly from batteries. If it works from a power converter which in turn is fed by a regulated power source it could be underdesigned to obtain higher efficiency.

This power was estimated for a total filament current of about 200 μa. It is also estimated that the additional power required for more emission is approximately 10^{-3} watts/μa at the filament.

d) The power estimate for the logarithmic electrometer was taken directly from a measurement of the experimental unit.

e) Power converter efficiencies of 50% are not too difficult to achieve even on well regulated systems.

f) The ion source power was estimated on the basis of the expected voltage and current requirements and assuming a low conversion efficiency.

g) The power required to operate the weak magnetic field pump was estimated from the calculations carried out for a geometry limited pump. It was assumed that the space charge limited pump would be three times as efficient as the geometry limited pump and with the power converter losses included and a small safety factor, the value came to 0.7 volts. This efficiency would require the ion pump to work at 10 μa of emission current for an electron gun efficiency of 50%. If the electron gun efficiency can be improved the demands on the pump can be lessened. This value of electron current does not appear to be unreasonable in view of the experimental

results obtained thus far, since it is anticipated that the suggested improvements in pump design will improve the I^+/pI^- ratio.

h) The regulator reference power is based on data acquired on a unit which has been flight tested and is in fact higher than is necessary.

8.40 EXPECTED WEIGHT AND SIZE

The expected weight and size of the proposed breadboard design are given below:

		Weight	Size
a)	Quadrupole mass filter, ion source, collector assembly, and pump	3.0 lb.	44 cu. in.
b)	Filament Supply	0.25	20
c)	Emission Regulator	0.2	—
d)	Logarithmic Electrometer	0.5	25
e)	Quadrupole Power Supply and Coil	0.8 —	20 50
f)	Scan System	0.4	
g)	Electrometer Supply	0.25	20
h)	Pump and Electron Gun Supplies	0.3	20
i)	Regulator Reference	0.2	10
j)	Ion Source Supplies	0.4	25
k)	Break-off Device	0.5	(External)
l)	Structure and Potting	1.0	5 (Structure only)
	TOTALS	7.8 lb.	239 cu. in.

It is seen that the proposed breadboard design will not meet the weight requirement; however, it appears that it may meet the volume requirement. The majority of the weight is due to the electronics. Careful design would be required to meet the weight specifications which are listed here. There may be some instances in which power supplies can be simplified over conventional design, thereby saving weight.

8.50 RECOMMENDED STUDIES

The results of this study program indicate that the following areas should be concentrated on in any future effort.

8.51 Emission System

The largest single power loss occurs in the emission system. Therefore, this area should receive a great deal of attention, to be divided over: low temperature emitters, electron gun design, and high efficiency emission regulation. Electron gun design is also important in obtaining a high differential pumping ratio.

8.52 Pumping

As indicated in the experimental results additional tests and theoretical work should be carried out on the weak magnetic field pump. If the expectations are not realized, then efforts should be directed toward the design of a miniaturized triode type Penning discharge ion pump. In the event this is necessary, some effort should also be directed toward the study of magnetic shielding techniques.

8.53 Ion Source Improvements

As indicated in the experimental results, there are some improvements which can be made in the present ion source design. Axial potential plots should be employed to obtain optimum focal characteristics. These should raise the sensitivity to a level that is compatible with the rest of the system.

8.54 Inlet Leak

The sample inlet leak which was constructed by Dr. Willens should be tested to see how nearly molecular flow is attained. In addition, the possibility of condensation effects should be examined.

8.55 Quadrupole Tests

Further data should be taken on the quadrupole analyzer to examine the detailed aspects of peak tails, transmission efficiency, and biasing of the source with respect to the quadeupole rods.

8.56 Quadrupole Supply

Methods should be studied for closely regulating the voltage level over the full frequency range so that synchronous scan techniques can be employed. Also the effects of better transistors should be analyzed. Some investigation of high Q coils might also be considered, including the possible application of a ferrite core material.

8.57 Pump out and Resealing

Since it would be desirable to have the mass spectrometer pump out in space, it will be necessary to investigate techniques for resealing the mass spectrometer before it enters the Martian atmosphere.

8.58 Logic

In view of the minimum number of data bits which are available and the demands that this makes on the mass spectrometer operation, it seems reasonable to direct some more effort toward a logic system for efficient use of the bits which are available.

8.59 Packaging Techniques

In order to hold weight to a minimum, it will be necessary to employ optimum packaging techniques. These should be investigated.

8.60 Alpha Source

It has been pointed out that the alpha ion source has the advantages of a high differential pumping capability and not using a power consuming electron emission system. This type of source was not experimentally investigated during this study program because it was felt that a more conventional electron bombardment source could be developed more rapidly. It is still believed that the alpha source should be investigated when time allows. Since counting techniques would be used to monitor the output of an alpha ion source system, they should be thoroughly investigated. If this technique is ultimately used, it would then become advisable to weigh the relative merits of the electron gun type ion pumps against the strong magnetic field types since, if the latter were used, the filament and emission system could be eliminated altogether. The saving in power would be truly significant, although this improvement is partially offset by the problems encountered with the magnetic field; however, the result should be an improved system.

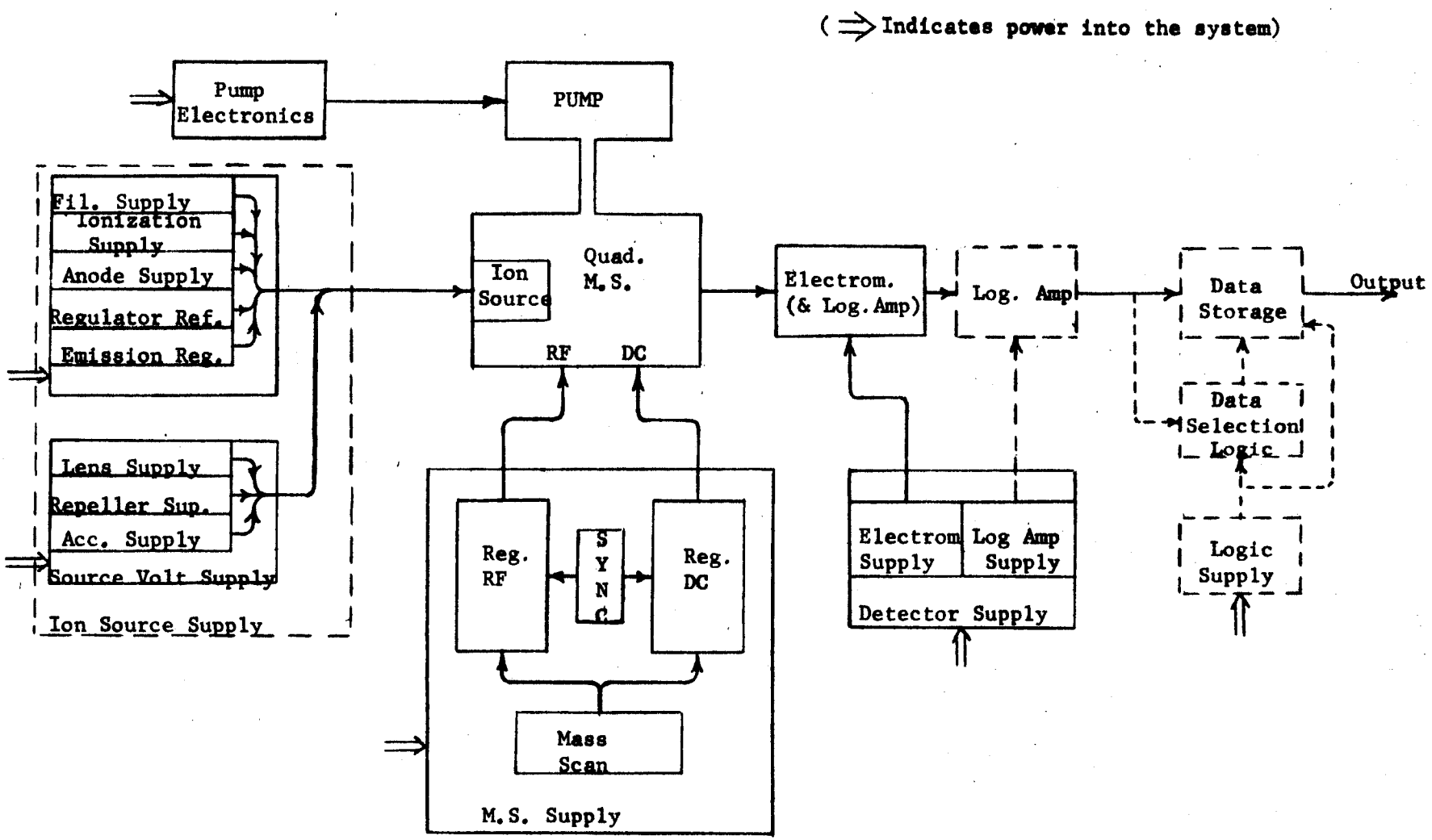

MARTIAN MASS SPECTROMETER SYSTEM

Figure 1.21

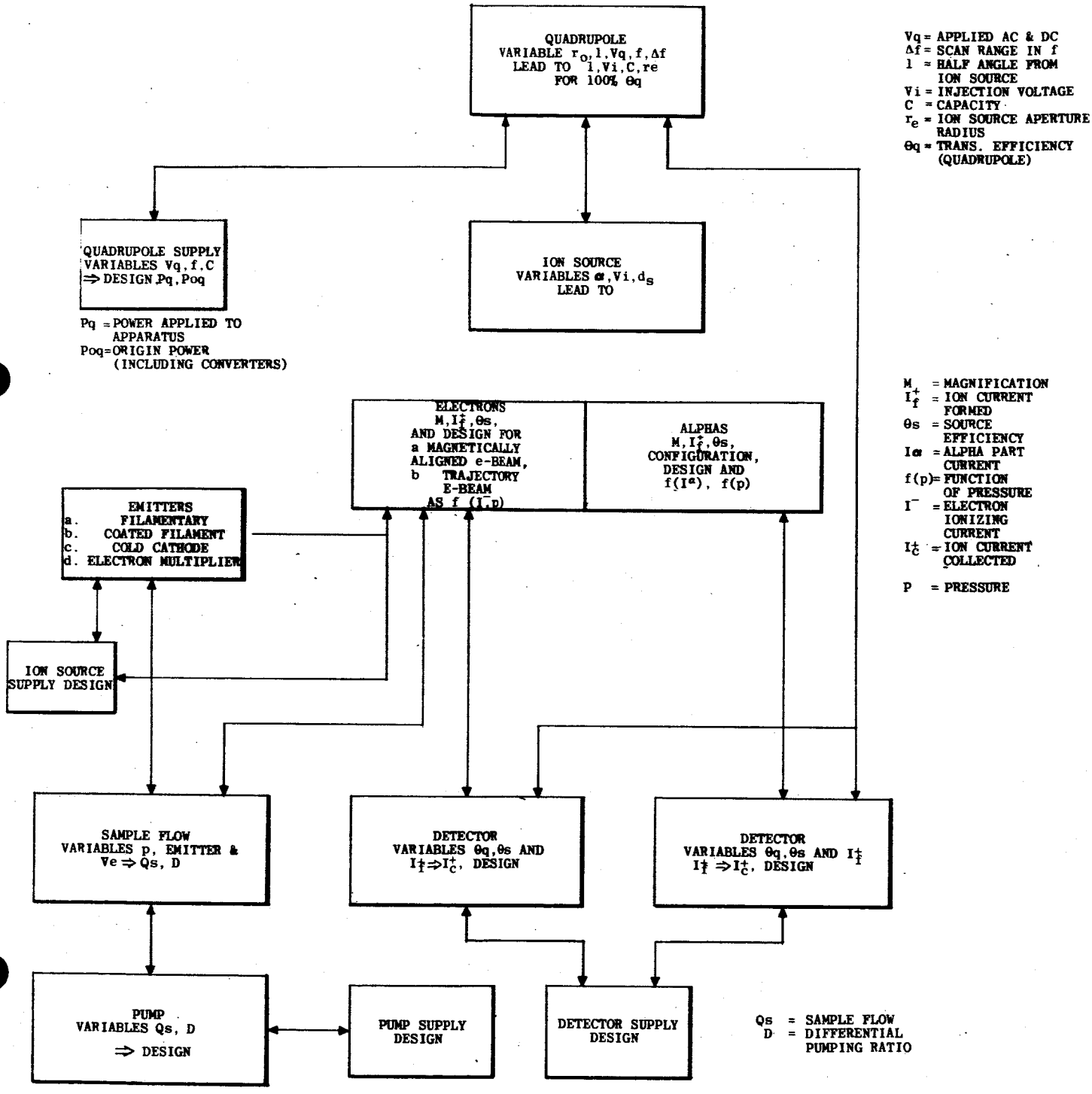
QUADRUPOLE
VARIABLE r_o, l, Vq, f, Δf
LEAD TO l, Vi, C, re
FOR 100% θq
Vq = APPLIED AC & DC
Δf = SCAN RANGE IN f
l = HALF ANGLE FROM ION SOURCE
Vi = INJECTION VOLTAGE
C = CAPACITY
r_e = ION SOURCE APERTURE RADIUS
θq = TRANS. EFFICIENCY (QUADRUPOLE)
QUADRUPOLE SUPPLY
VARIABLES Vq, f, C
⇒ DESIGN, Pq, Poq
ION SOURCE
VARIABLES α, Vi, d_s
LEAD TO
Pq = POWER APPLIED TO APPARATUS
Poq = ORIGIN POWER (INCLUDING CONVERTERS)
ELECTRONS
M, I_f^+, θs,
AND DESIGN FOR
a MAGNETICALLY ALIGNED e-BEAM,
b TRAJECTORY E-BEAM
AS f (I, p)
ALPHAS
M, I_f^+, θs,
CONFIGURATION,
DESIGN AND
f(I^α), f(p)
M = MAGNIFICATION
I_f^+ = ION CURRENT FORMED
θs = SOURCE EFFICIENCY
$I\alpha$ = ALPHA PART CURRENT
f(p) = FUNCTION OF PRESSURE
I^- = ELECTRON IONIZING CURRENT
I_c^+ = ION CURRENT COLLECTED
P = PRESSURE
EMITTERS
a. FILAMENTARY
b. COATED FILAMENT
c. COLD CATHODE
d. ELECTRON MULTIPLIER
ION SOURCE SUPPLY DESIGN
SAMPLE FLOW
VARIABLES p, EMITTER & Ve ⇒ Qs, D
DETECTOR
VARIABLES θq, θs AND I_f^+ ⇒ I_c^+, DESIGN
DETECTOR
VARIABLES θq, θs AND I_f^+
I_f^+ ⇒ I_c^+, DESIGN
PUMP
VARIABLES Qs, D
⇒ DESIGN
PUMP SUPPLY DESIGN
DETECTOR SUPPLY DESIGN
Qs = SAMPLE FLOW
D = DIFFERENTIAL PUMPING RATIO

FIGURE 3.10

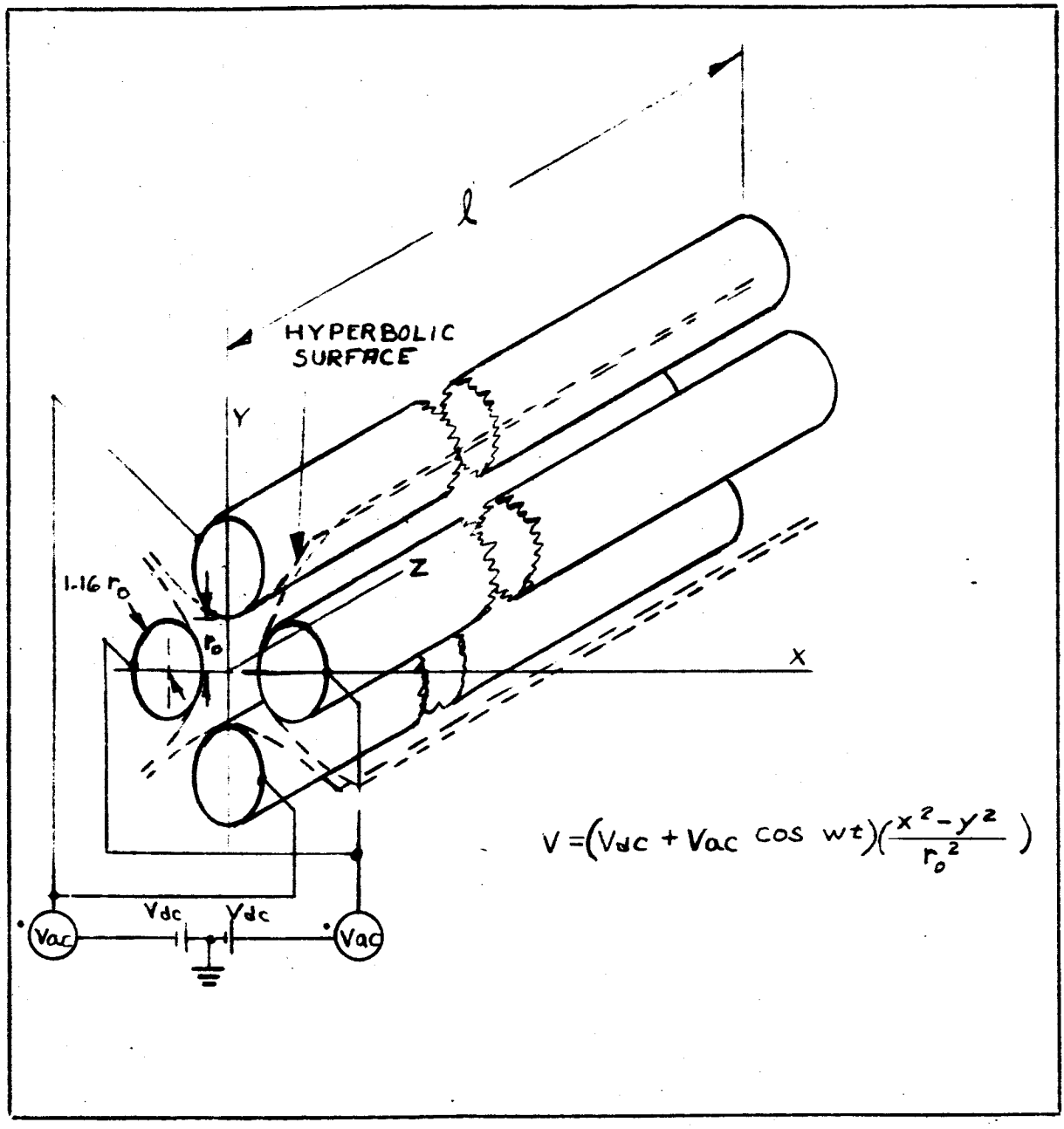

QUADRUPOLE MASS FILTER

FIG 4.11

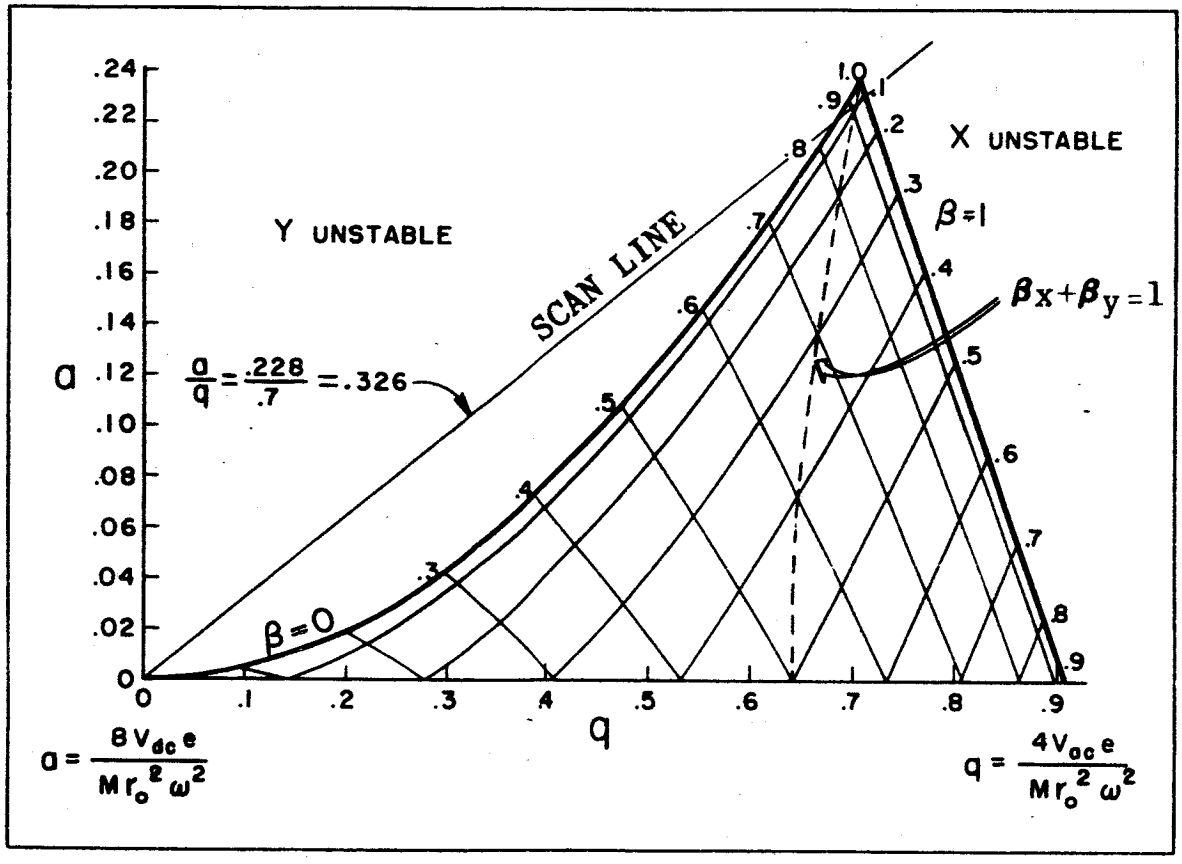

STABILITY DIAGRAM FOR BOTH X AND Y

FIGURE 4.12

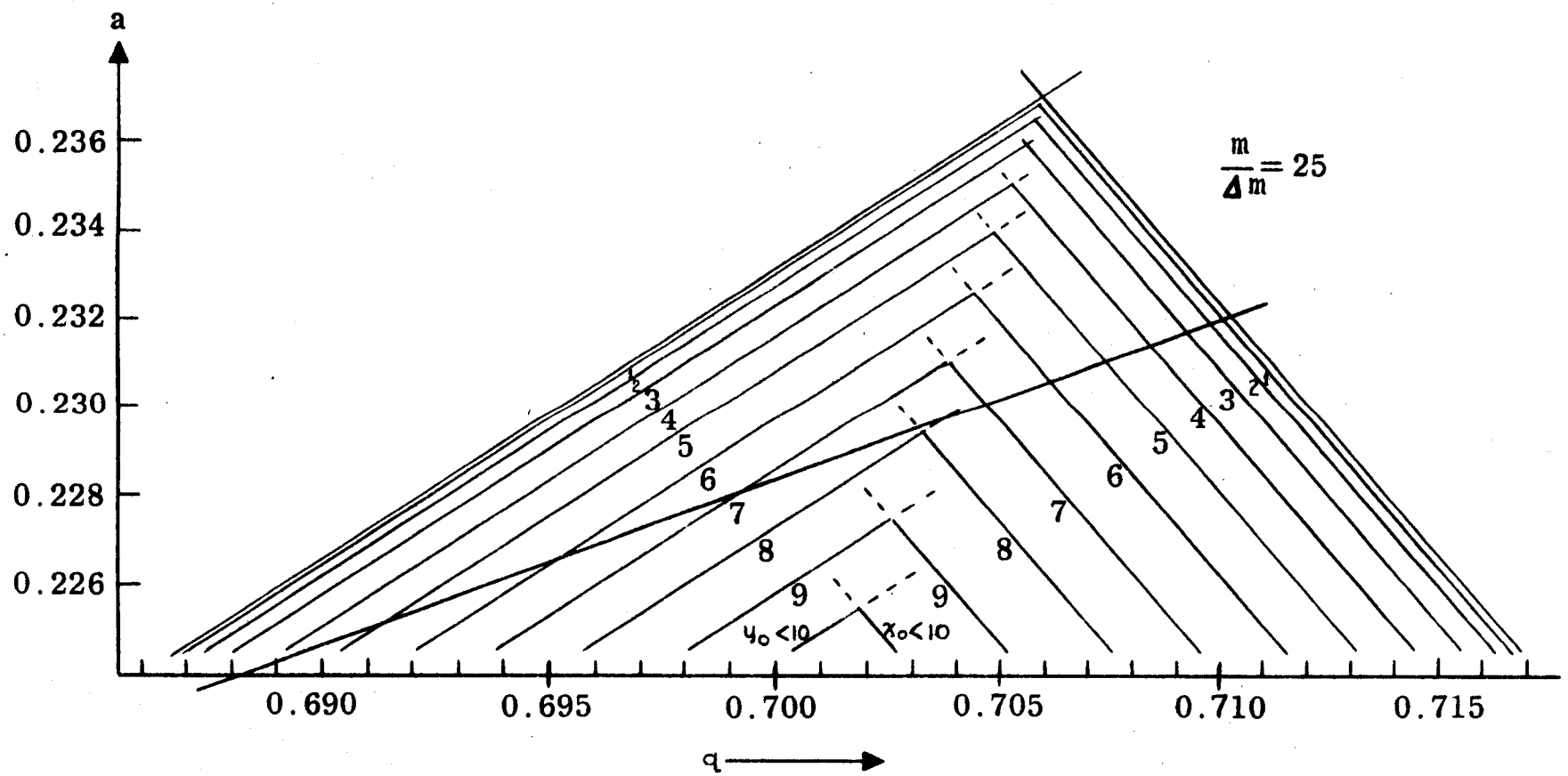

TRANSMISSION TENTS

FOR $X_0 = Y_0 = 0$

AND $r_0 = 100$

FIGURE 4.13

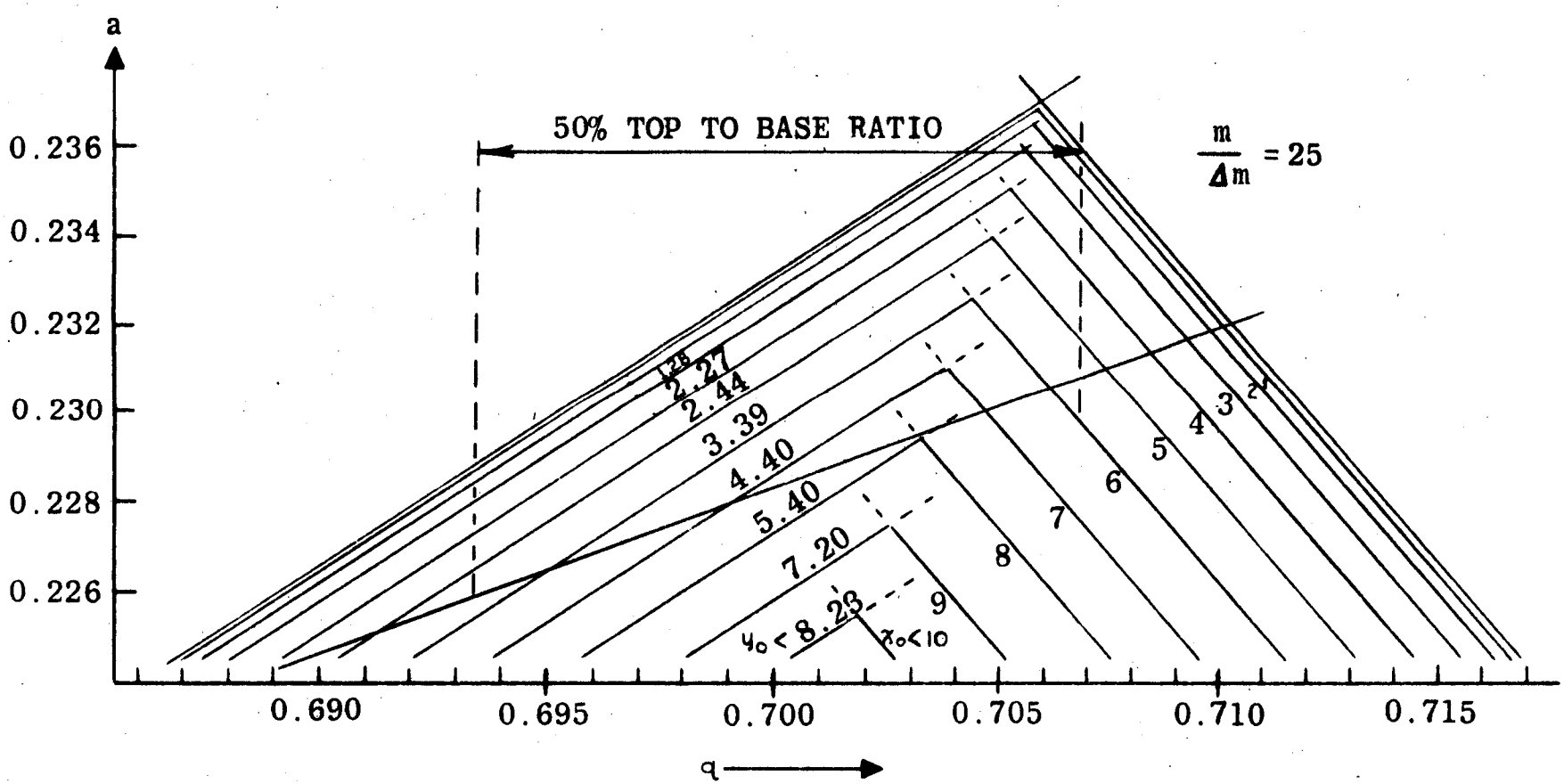

TRANSMISSION TENTS

FOR $X_0 = Y_0 = 0$

AND $r_0 = 100$

$\alpha = 0.010$

FIGURE 4.14

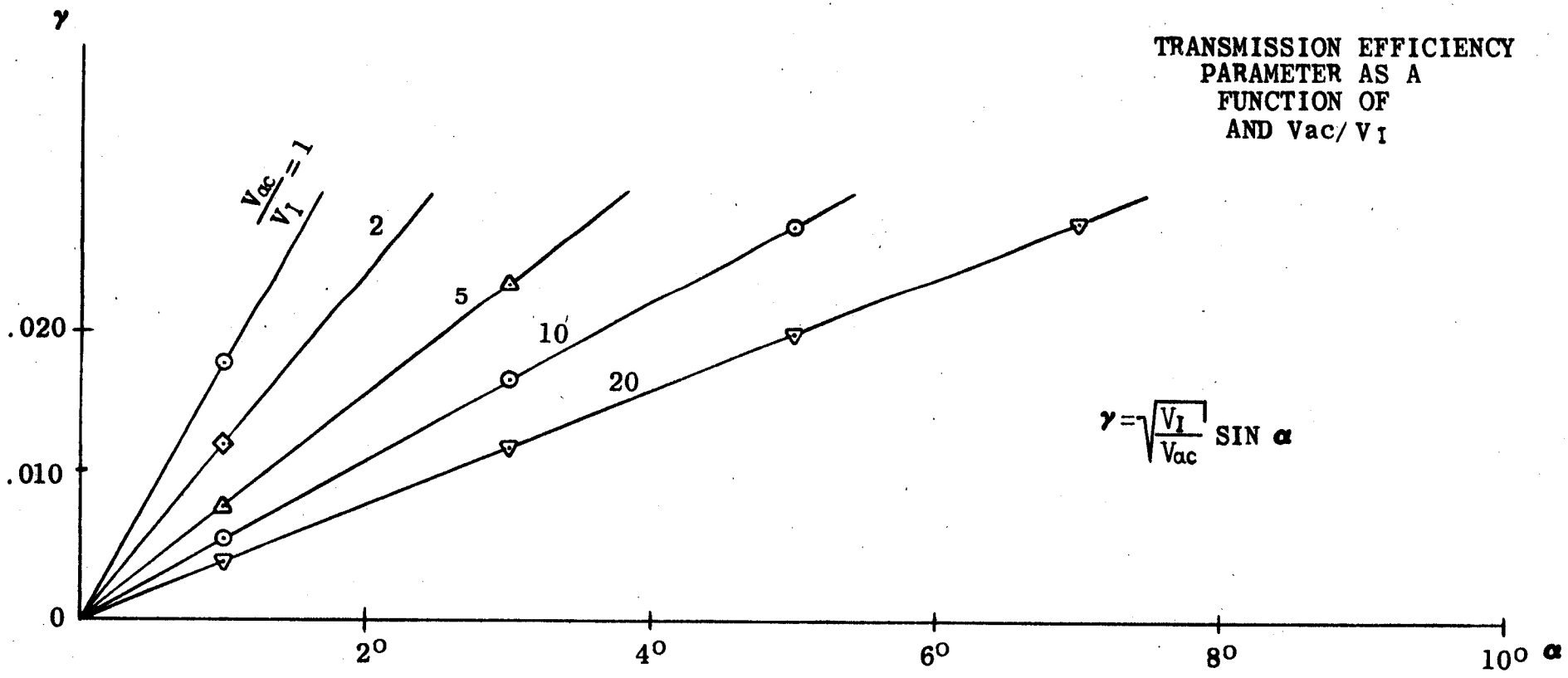
γ
TRANSMISSION EFFICIENCY PARAMETER AS A FUNCTION OF AND Vac/ VI
Vac/VI = 1
2
5
10
20
.020
.010
0
2°
4°
6°
8°
10°
α
γ = √(VI/Vac) SIN α

FIGURE 4.15

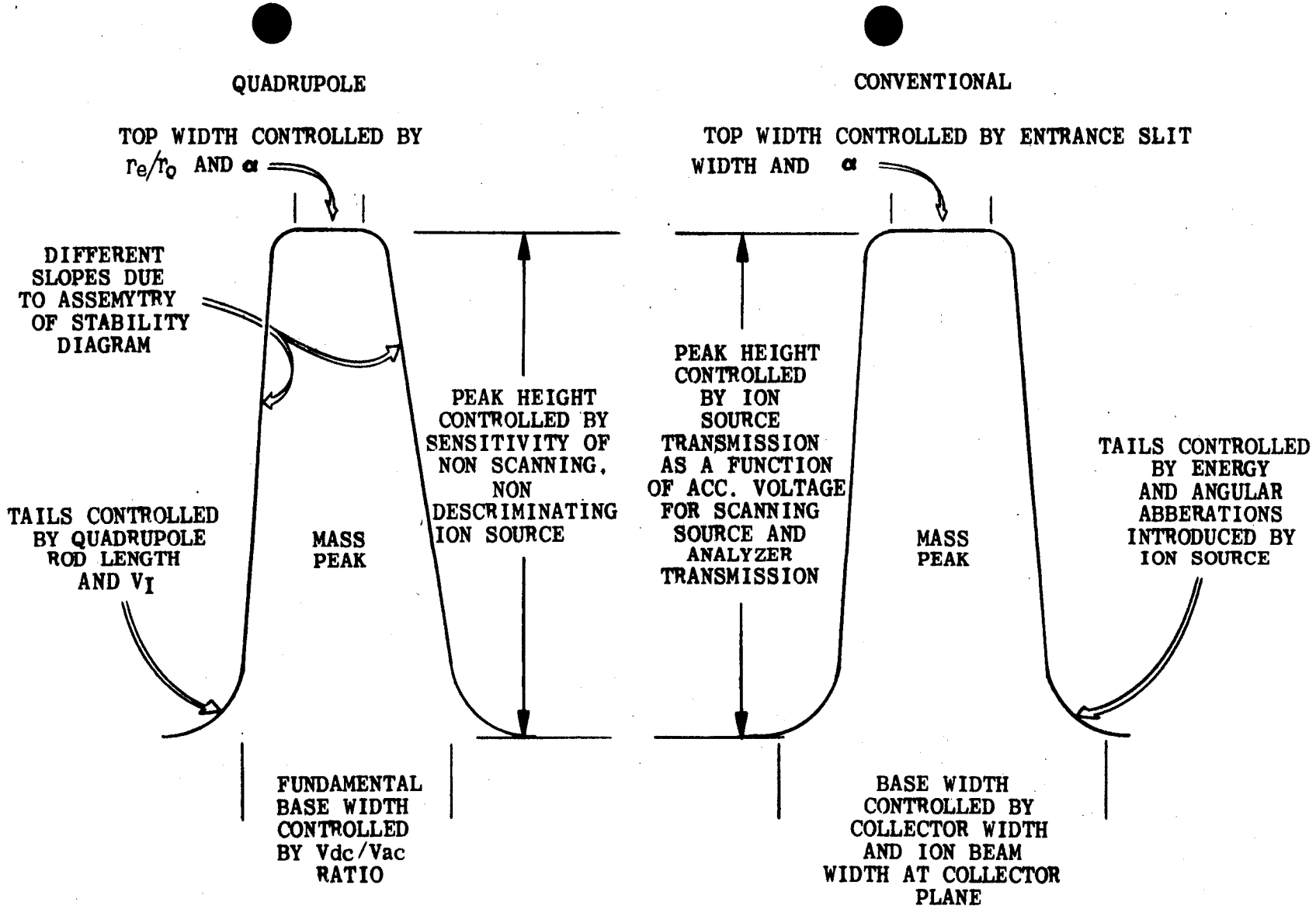

COMPARISON OF CONTROLLING FACTORS
OF PEAK CHARACTERISTICS

FIGURE 4.16

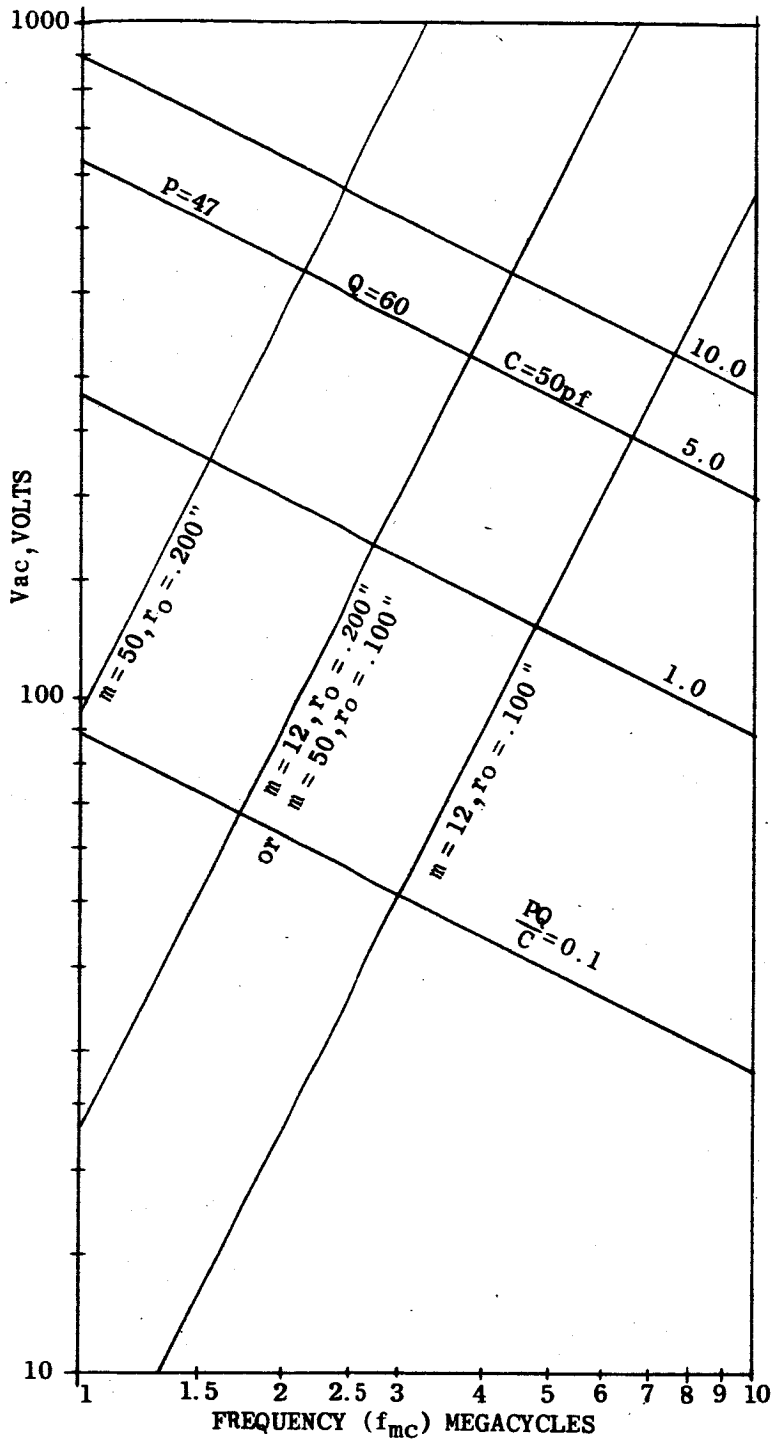

QUADRUPOLE VOLTAGE, FREQUENCY, MASS
AND POWER RELATIONS

FIGURE 4.17

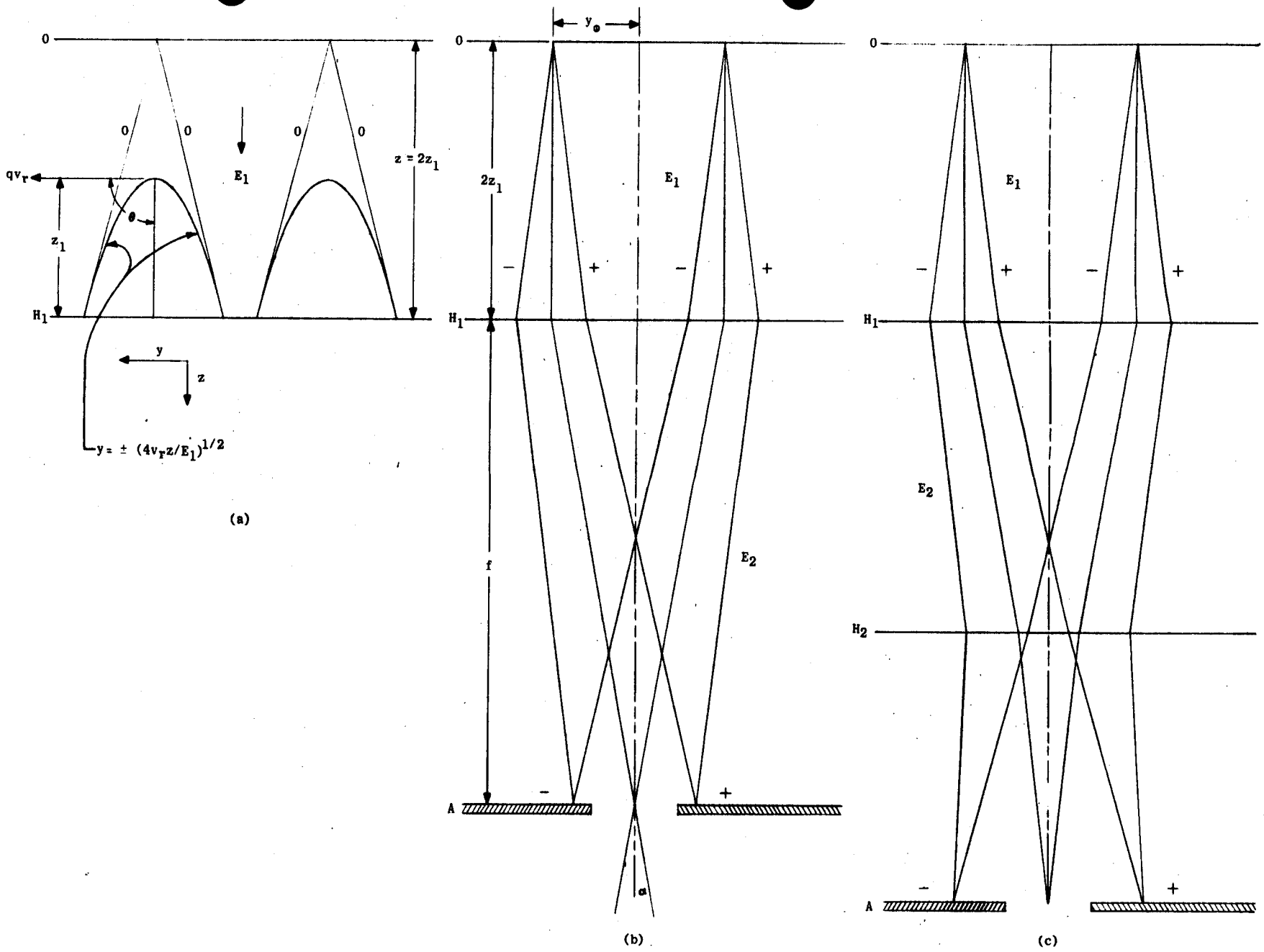

ION SOURCES WITH THERMAL IMAGE

(a) LIGHT OPTICAL ANALOG
(b) SINGLE THIN LENS
(c) SAME AS (b) INCLUDING EXIT DIVERGENCE.

FIGURE 4.21

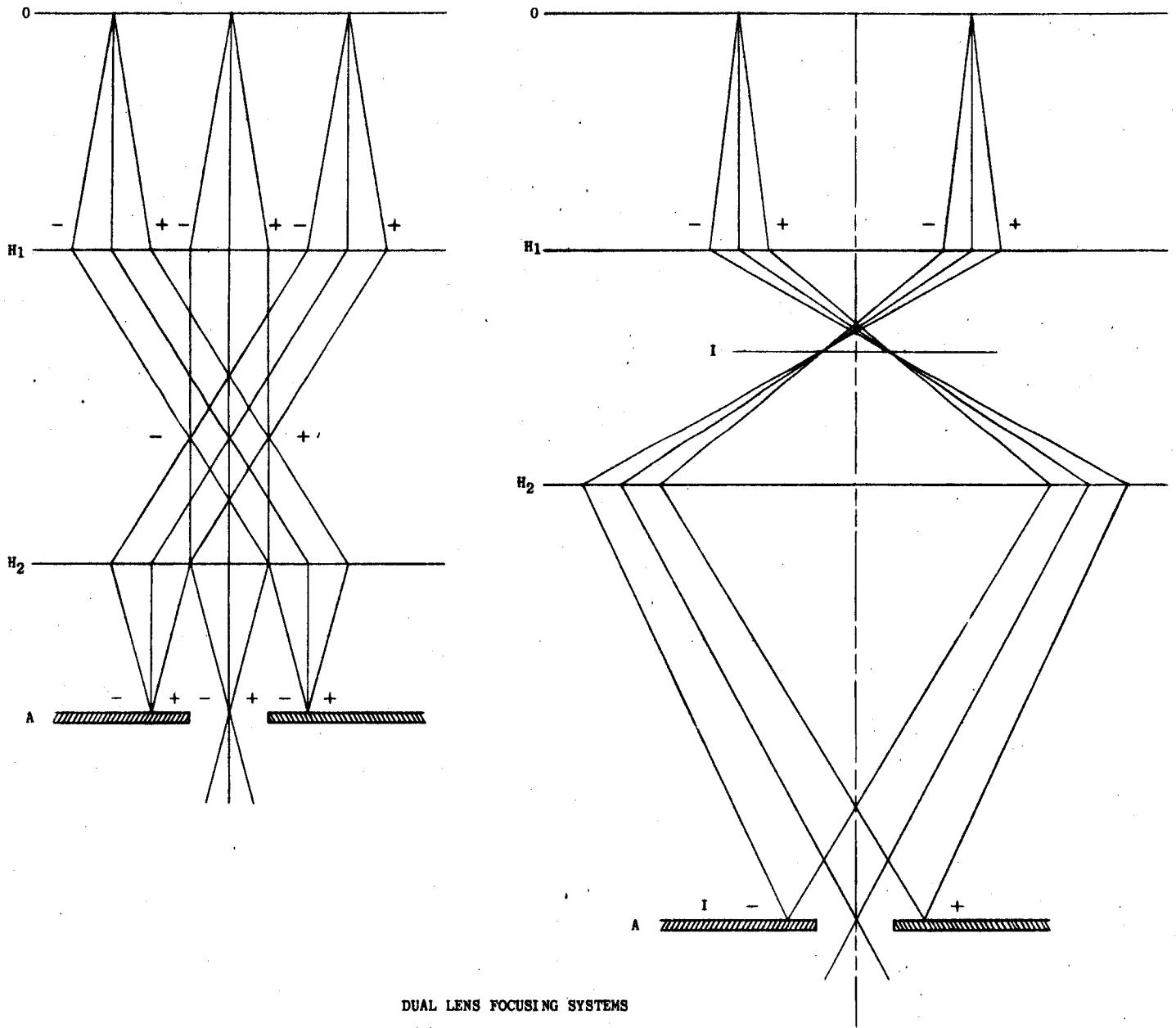

DUAL LENS FOCUSING SYSTEMS

(a) TRUE IMAGE LENS
(b) VARIABLE IMAGE LENS

FIGURE 4.22

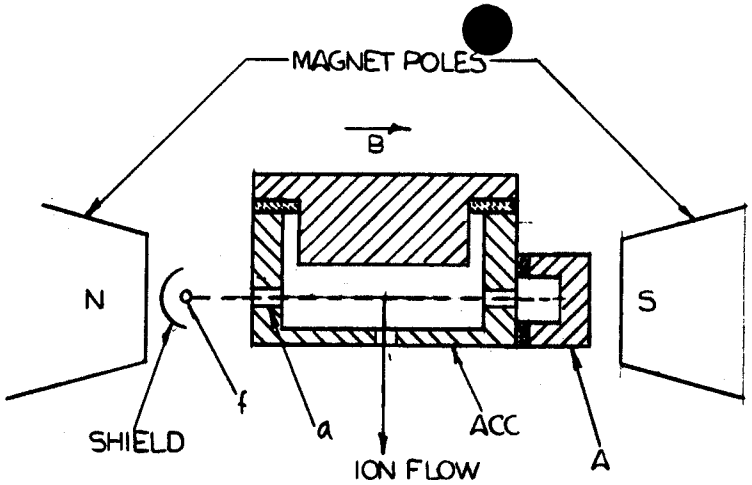

(a)

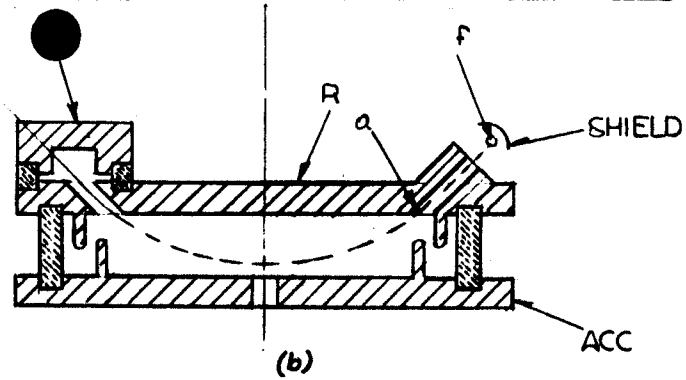

(b)

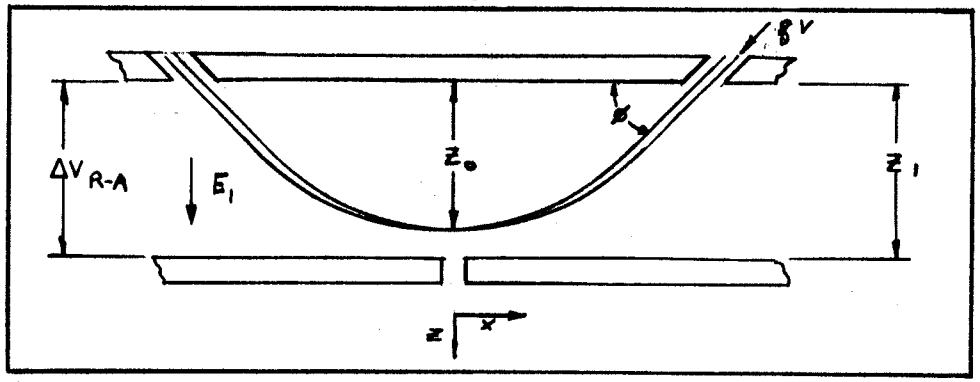

PARABOLIC TRAJECTORY

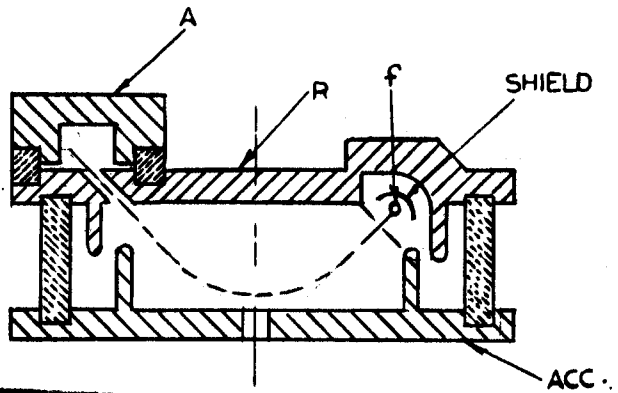

(c)

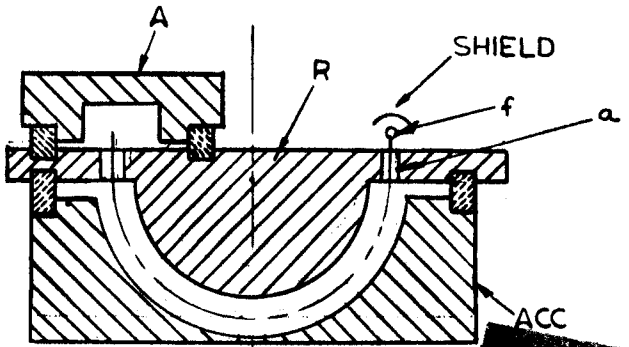

(d)

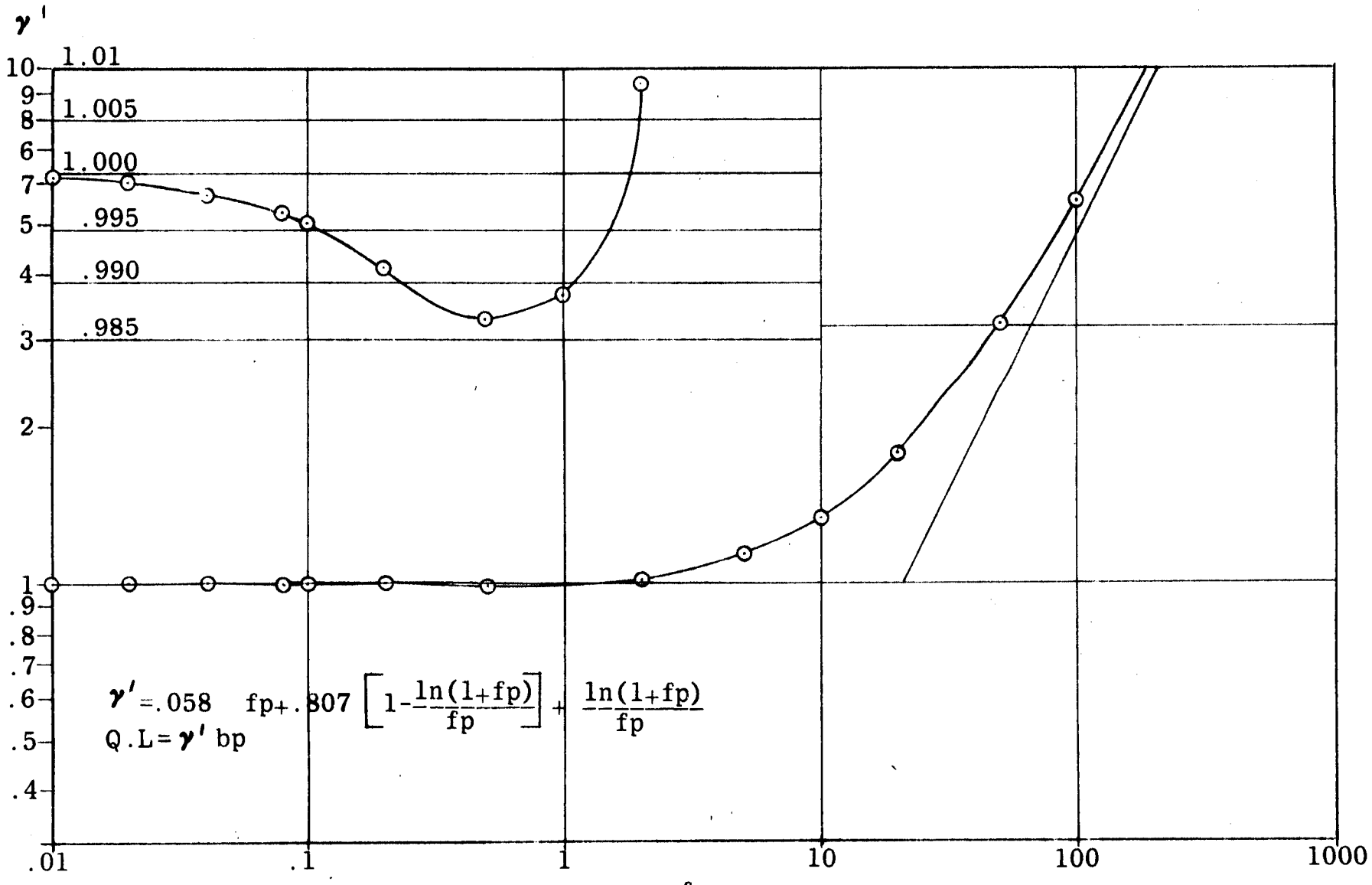

FIGURE 4.41 OVERALL PLOT - LOG LOG

INSET PLOT - SEMI LOG

PROJECT NOTE #12

$Q\ L = 1.91\ D^4 + 9.170^3 + D^2\ \ln\ 1 + 2.53D$
FOR $P_a = 10^5 \mu$ Hg

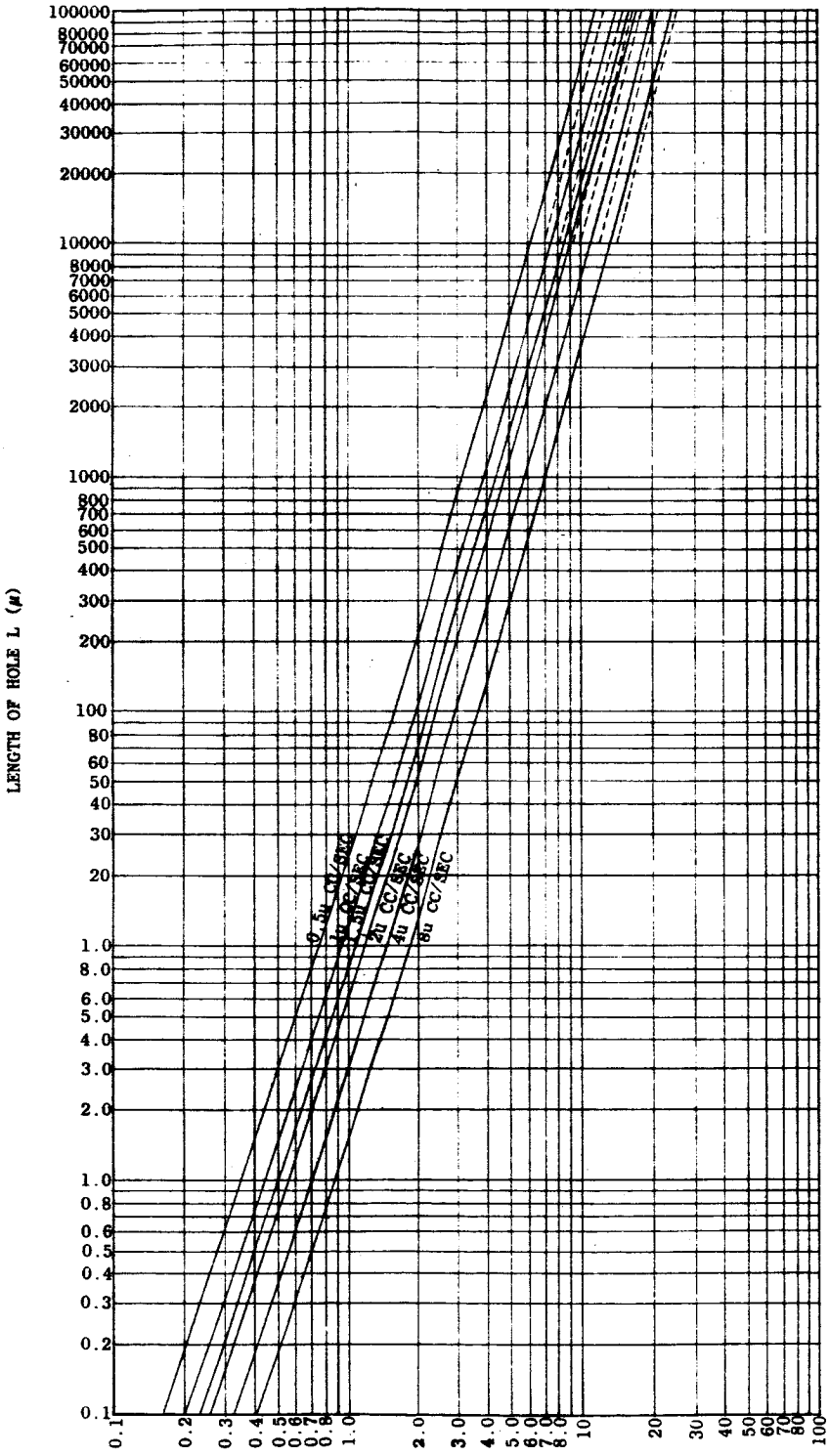

FIGURE 4.42

PROJECT NOTE #10

$Q \; L \;\; 11.86D^3$

FOR $P_a = 1.043 \times 10^5 \mu$

FOR P

= 50 mm λ = 1 u
=100 mm λ = .5 u
=150 mm λ =.33 u

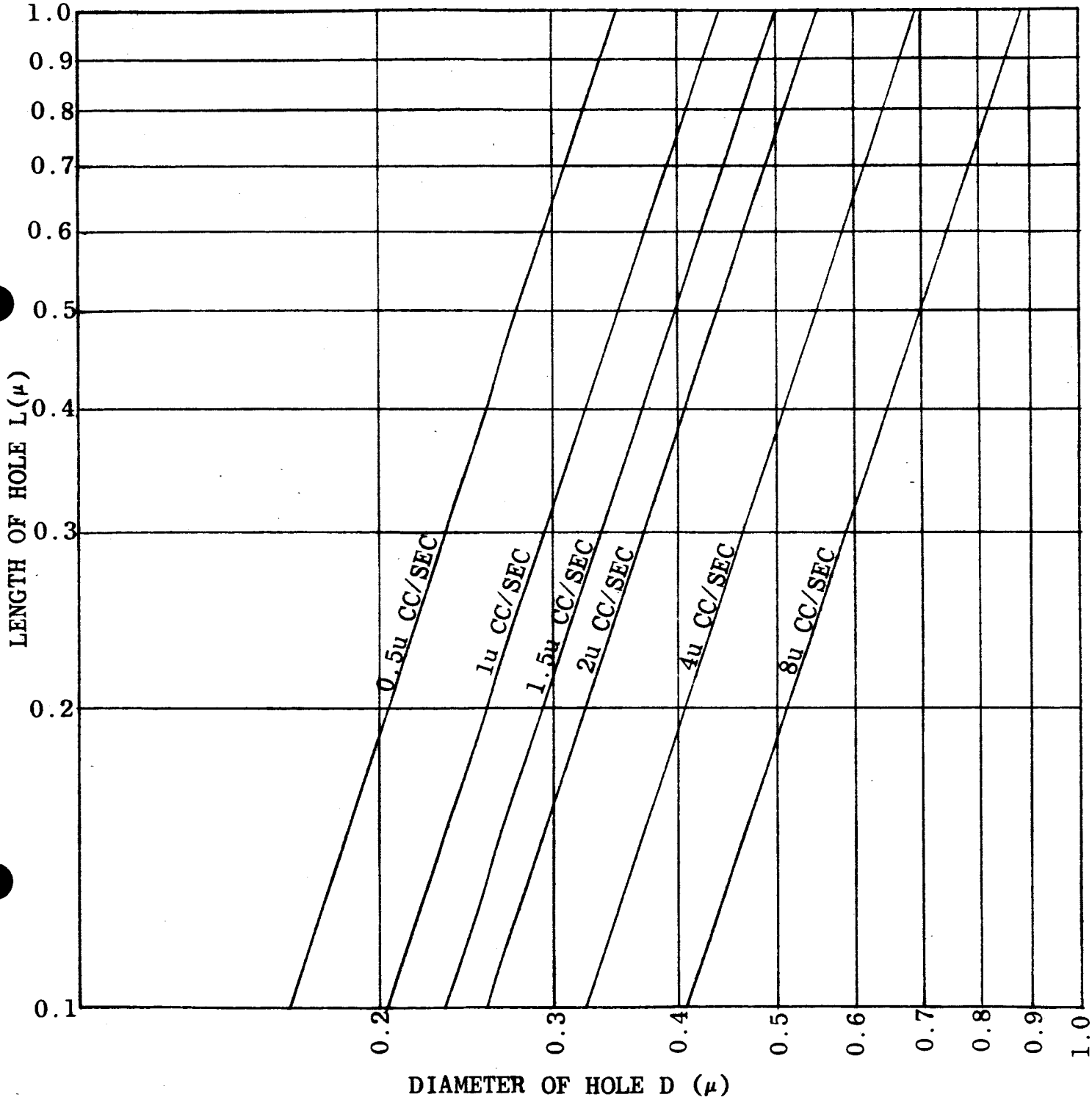

FIGURE 4.43

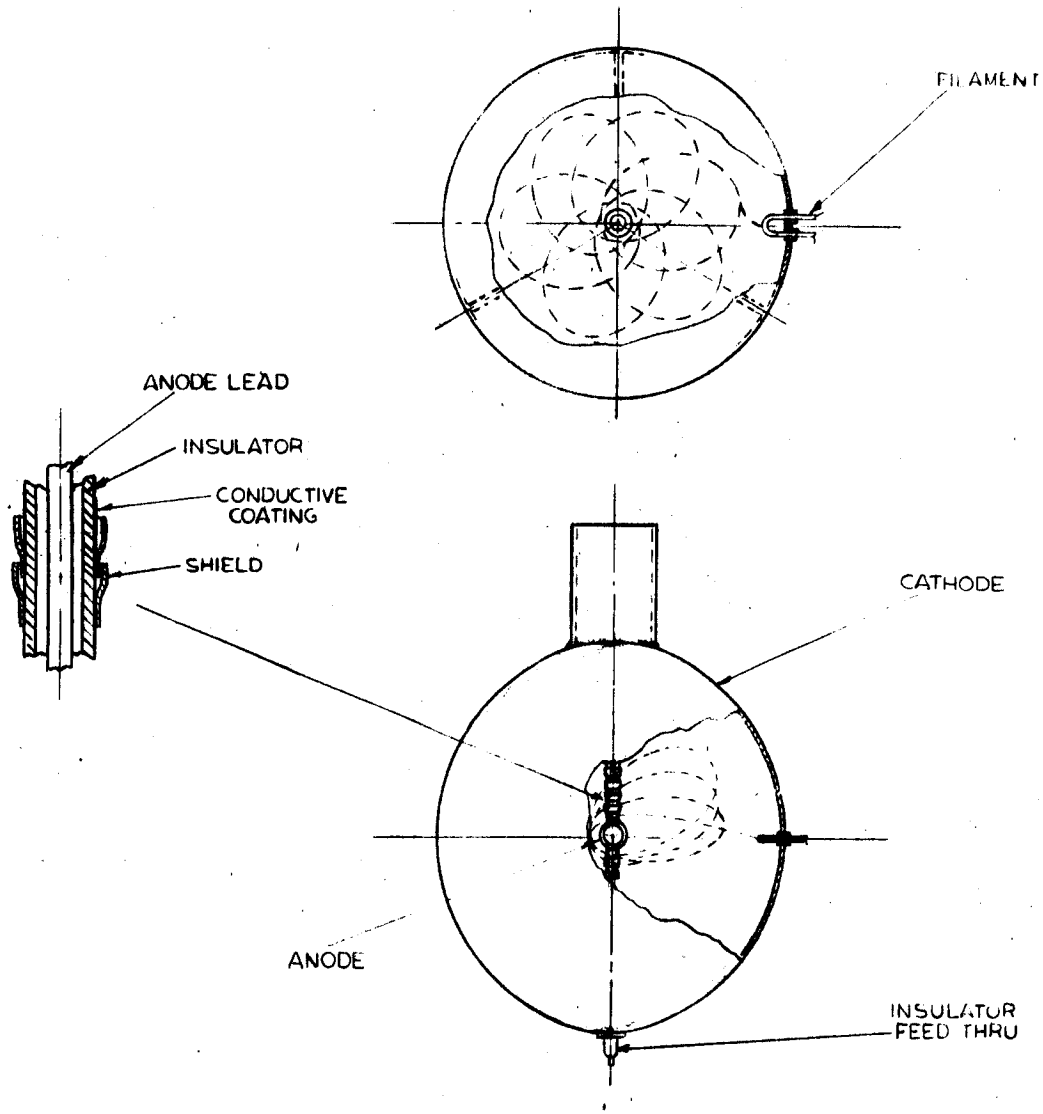

CONCEPTUAL DRAWING OF ION PUMP

FIGURE 4.51

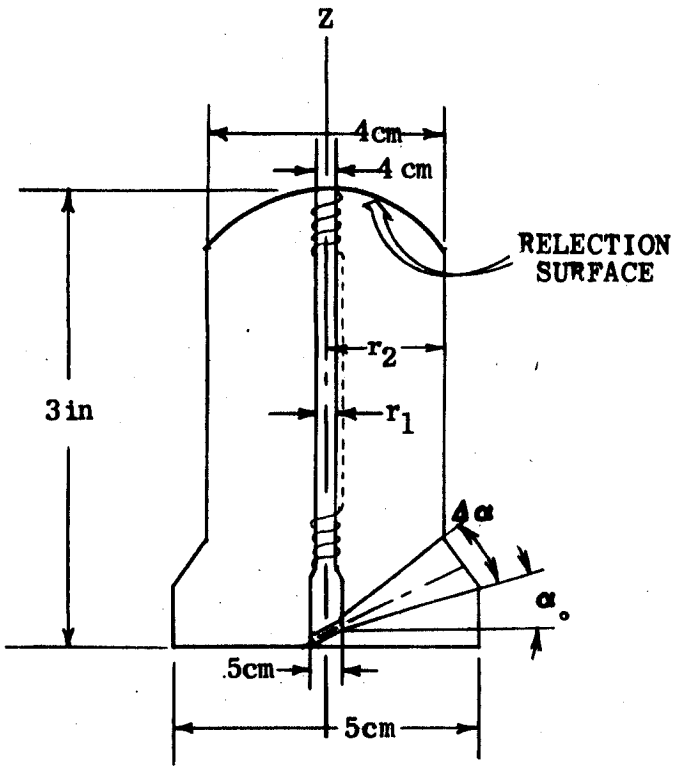

SINGLE ENDED ELECTROSTATIC
IONIZATION PUMP
FIGURE 4.52(a)

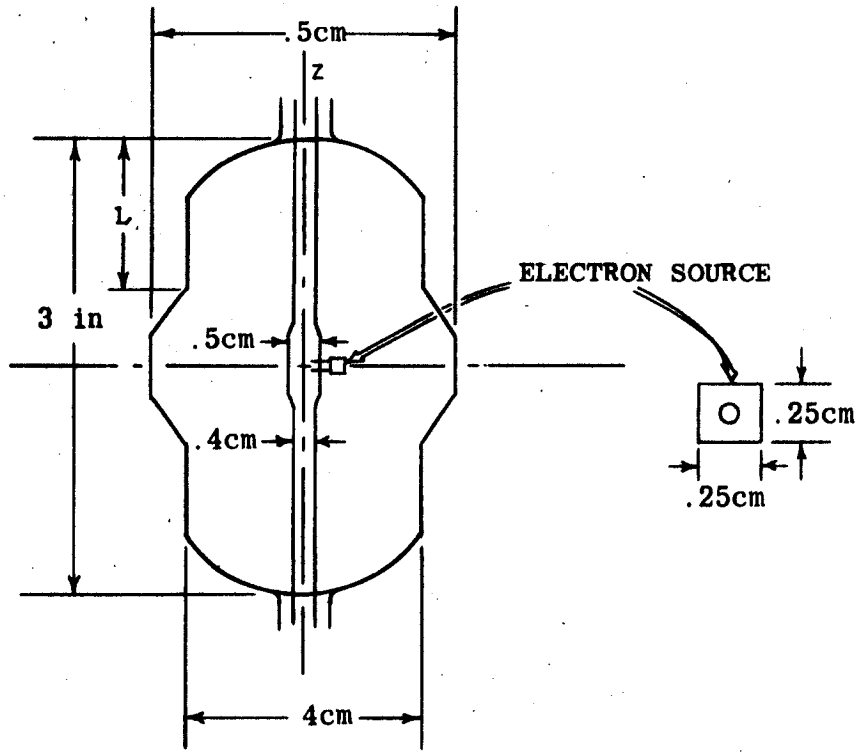

DOUBLE ENDED ELECTROSTATIC
IONIZATION PUMP
FIGURE 4.52 (b)

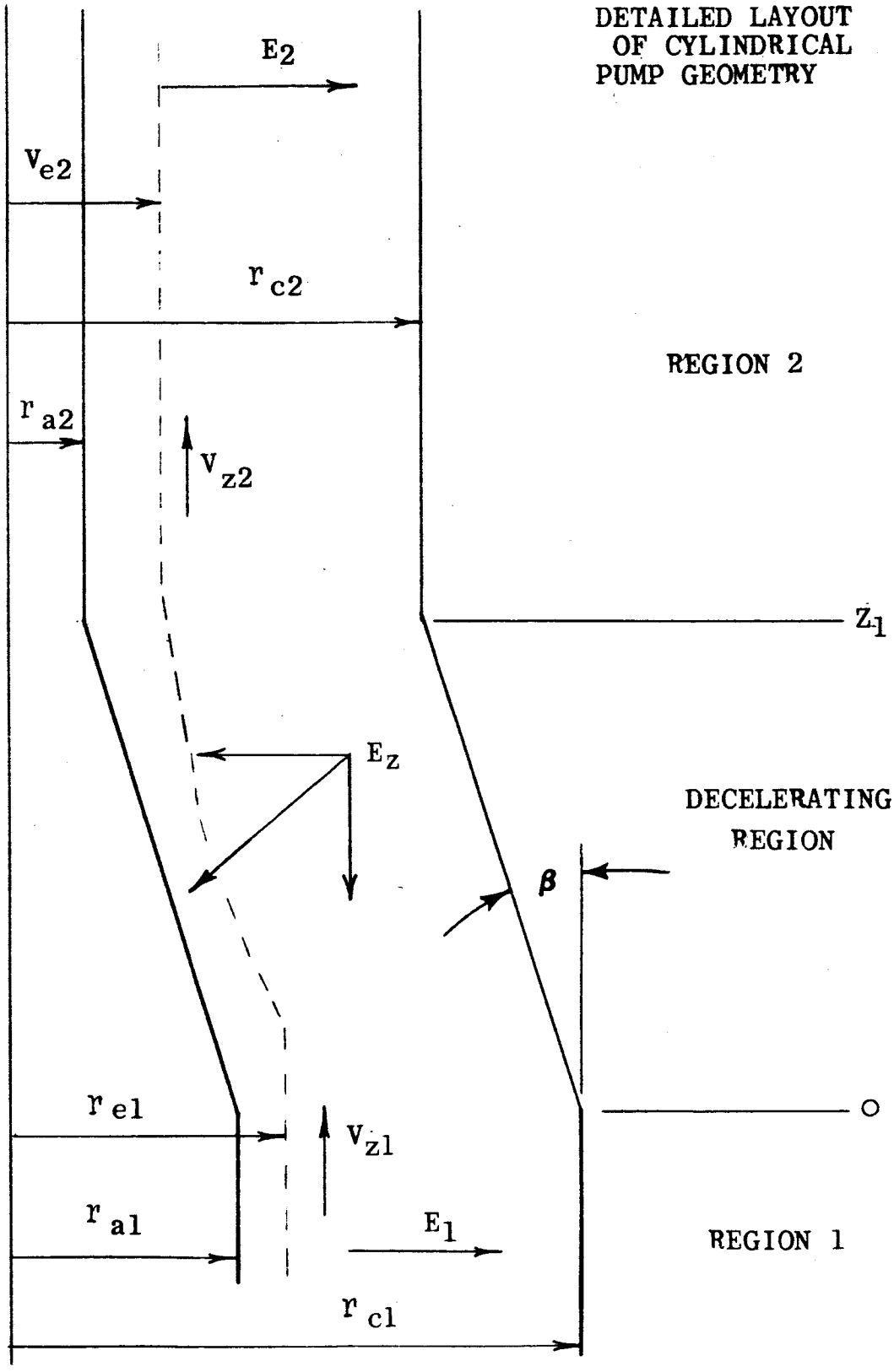
DETAILED LAYOUT
OF CYLINDRICAL
PUMP GEOMETRY
E2
Ve2
rc2
REGION 2
ra2
Vz2
Z1
Ez
DECELERATING
REGION
β
O
rel
Vzl
ral
El
REGION 1
rcl

FIGURE 4.53

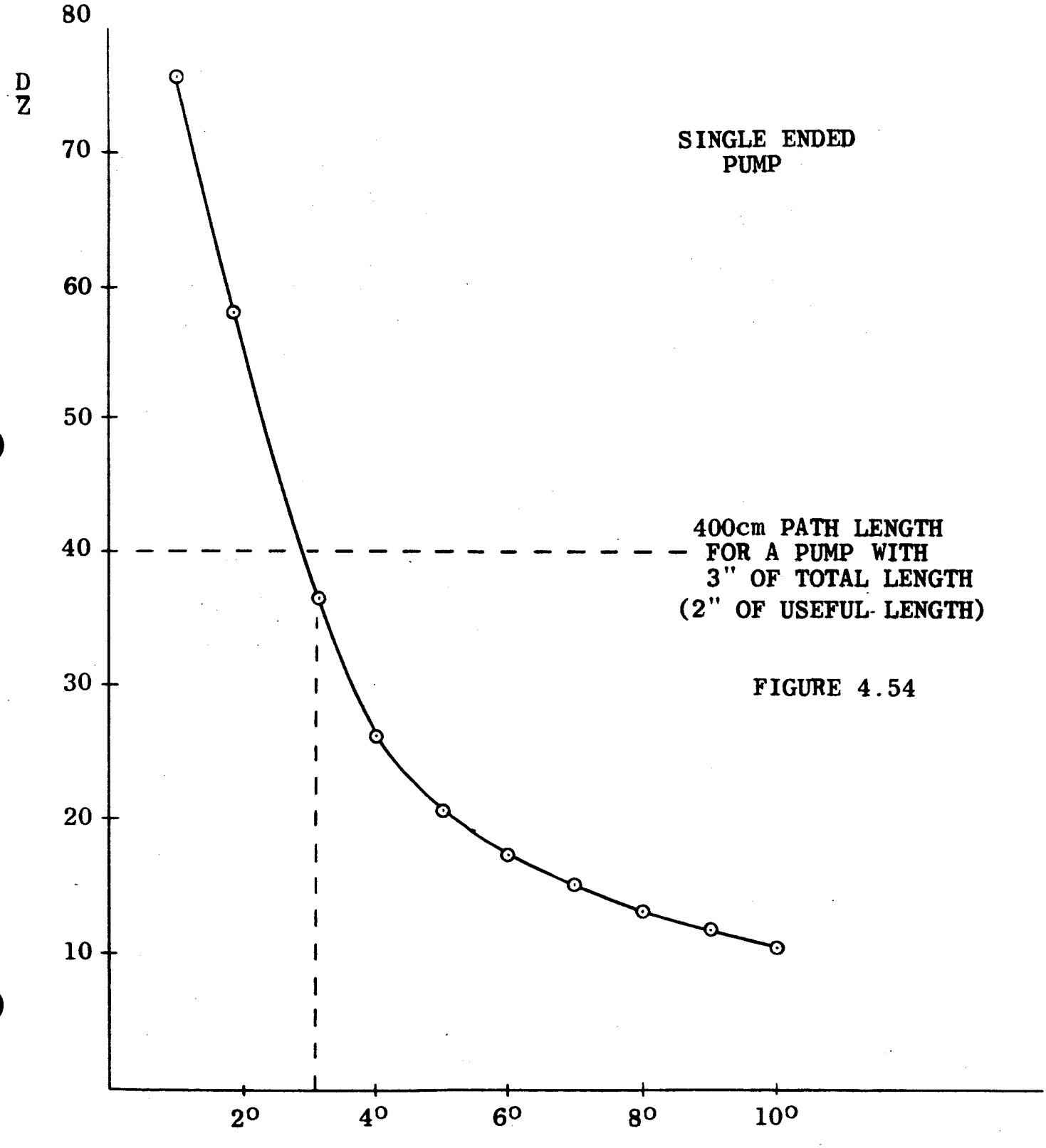

FIGURE 4.54

PATH LENGTH PER Z DISTANCE AS A FUNCTION
OF ANGULAR SPREAD

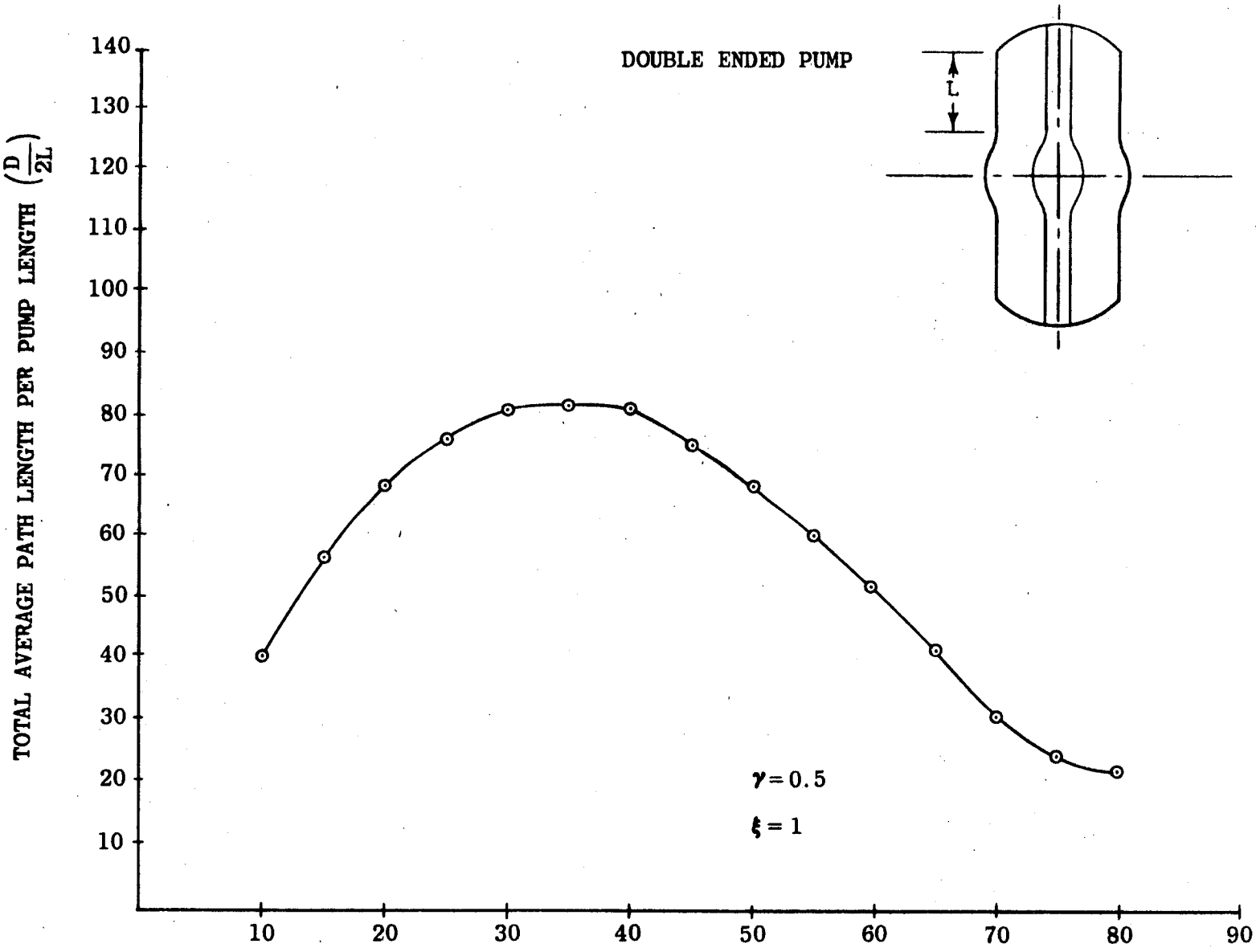

PLOT OF TOTAL AVERAGE PATH LENGTH
AS A FUNCTION OF ANGLE $\Delta\alpha = 10^{\circ}$
FIGURE 4.55

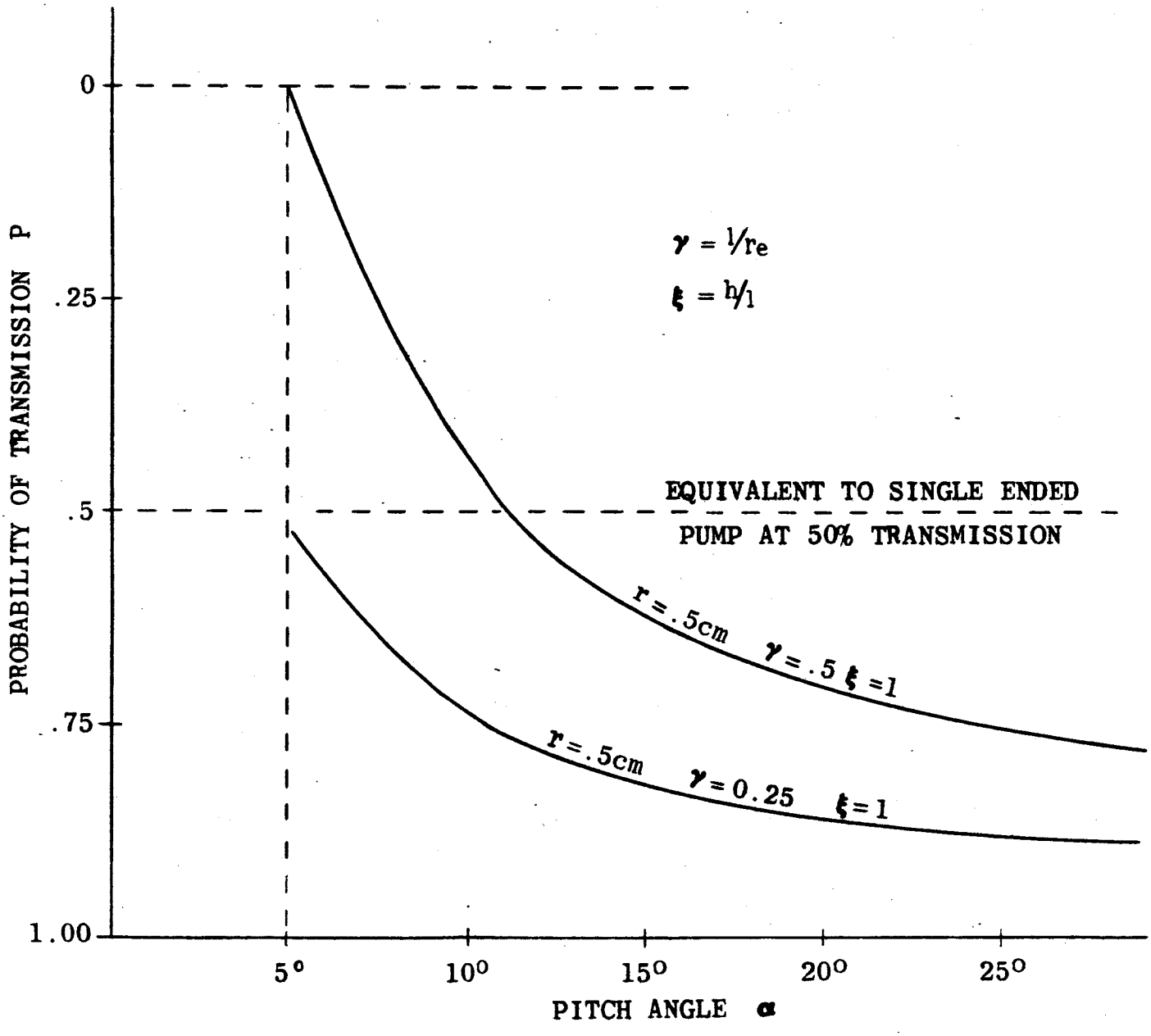

PROBABILITY OF TRANSMISSION VS PITCH ANGLE
FIGURE 4.56

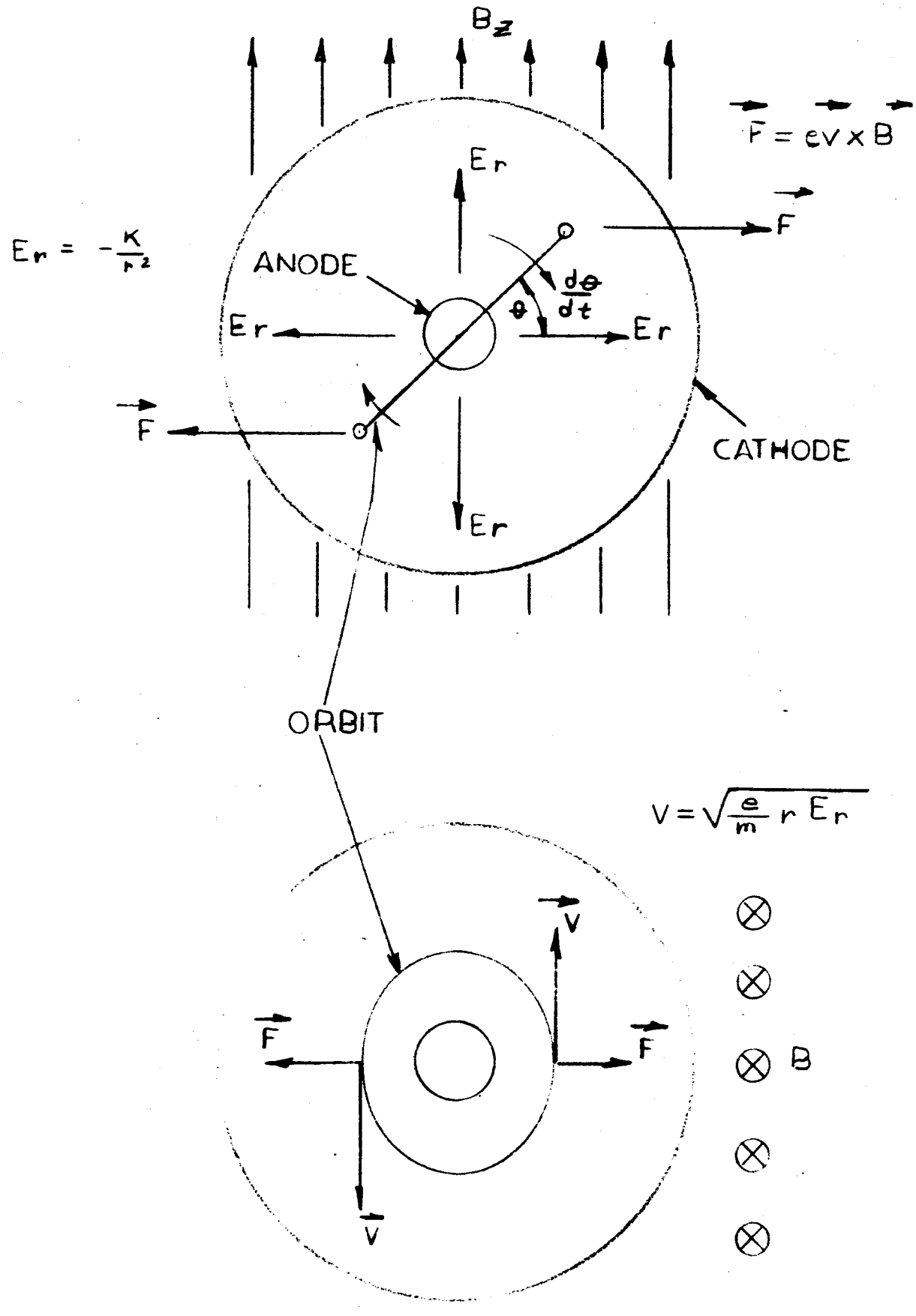
B_z
$\vec{F} = e\vec{v} \times \vec{B}$
$E_r = -\frac{K}{r^2}$
E_r
ANODE
$\vec{F}$
$\frac{d\theta}{dt}$
θ
E_r
E_r
$\vec{F}$
CATHODE
E_r
ORBIT
$V = \sqrt{\frac{e}{m} r E_r}$
$\vec{V}$
$\vec{F}$
$\vec{F}$
B
$\vec{V}$

FIG 4.57

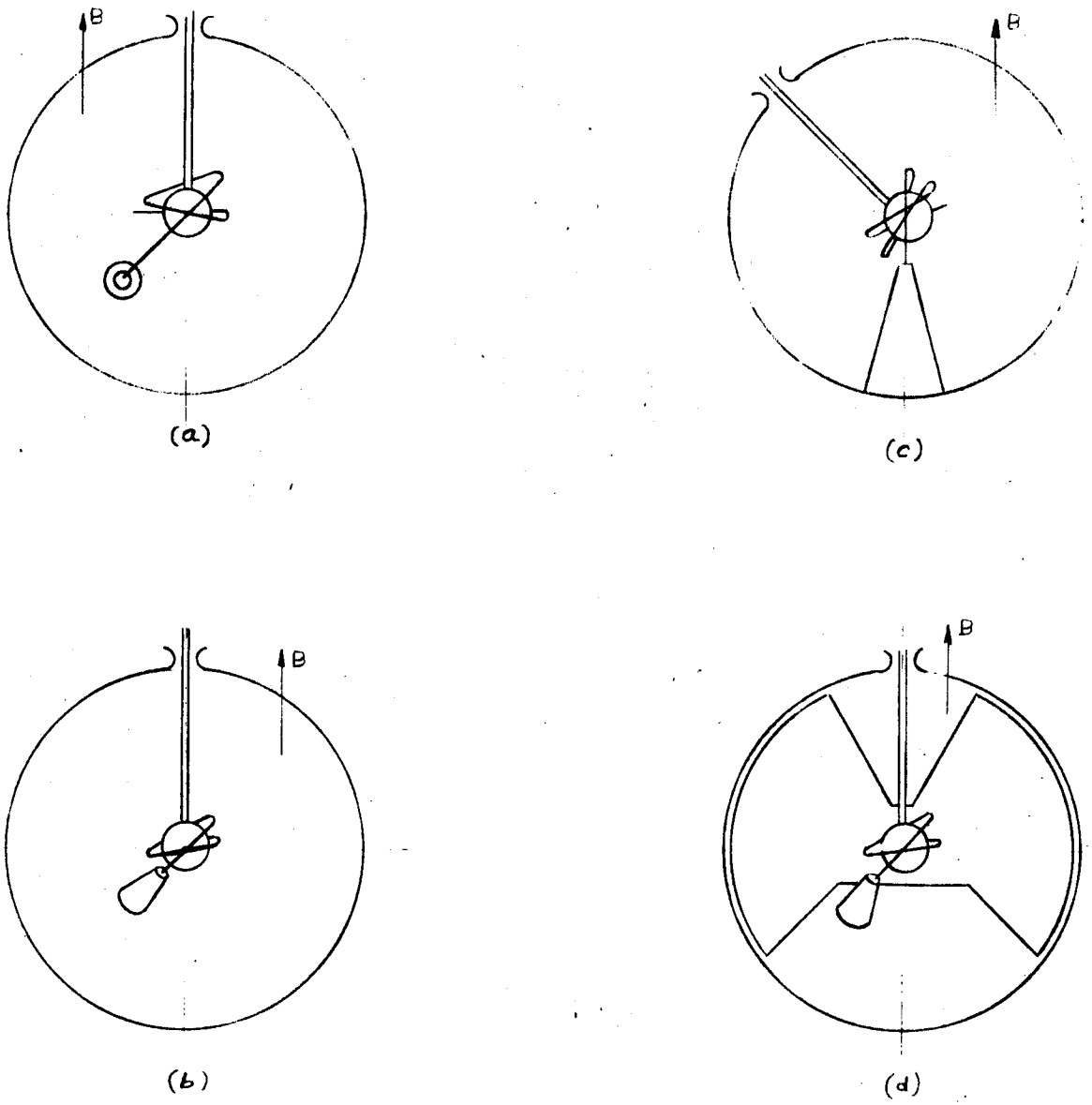

FIG 4.58

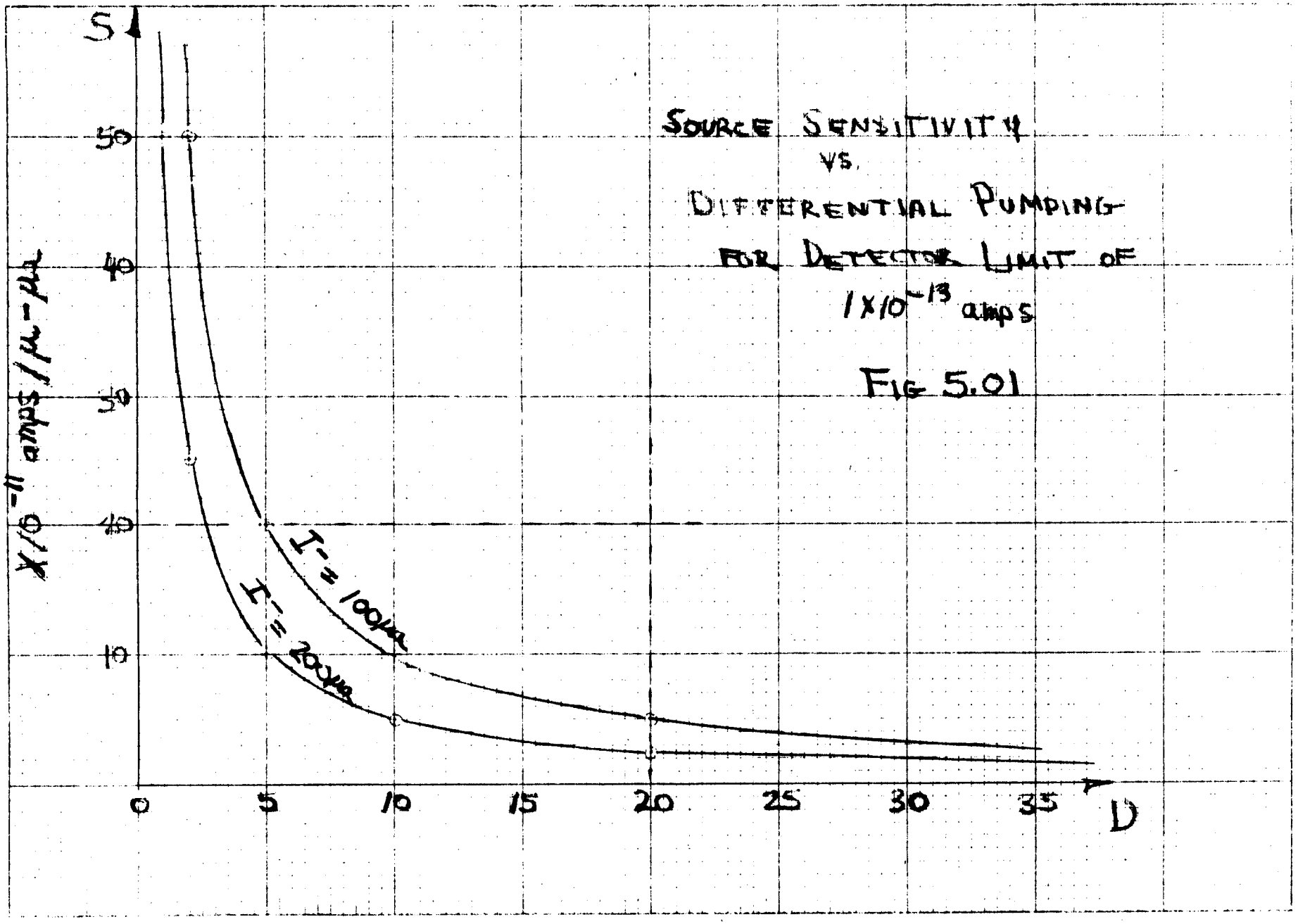

SOURCE SENSITIVITY
VS.
DIFFERENTIAL PUMPING
FOR DETECTOR LIMIT OF
1×10^{-13} amps

FIG 5.01

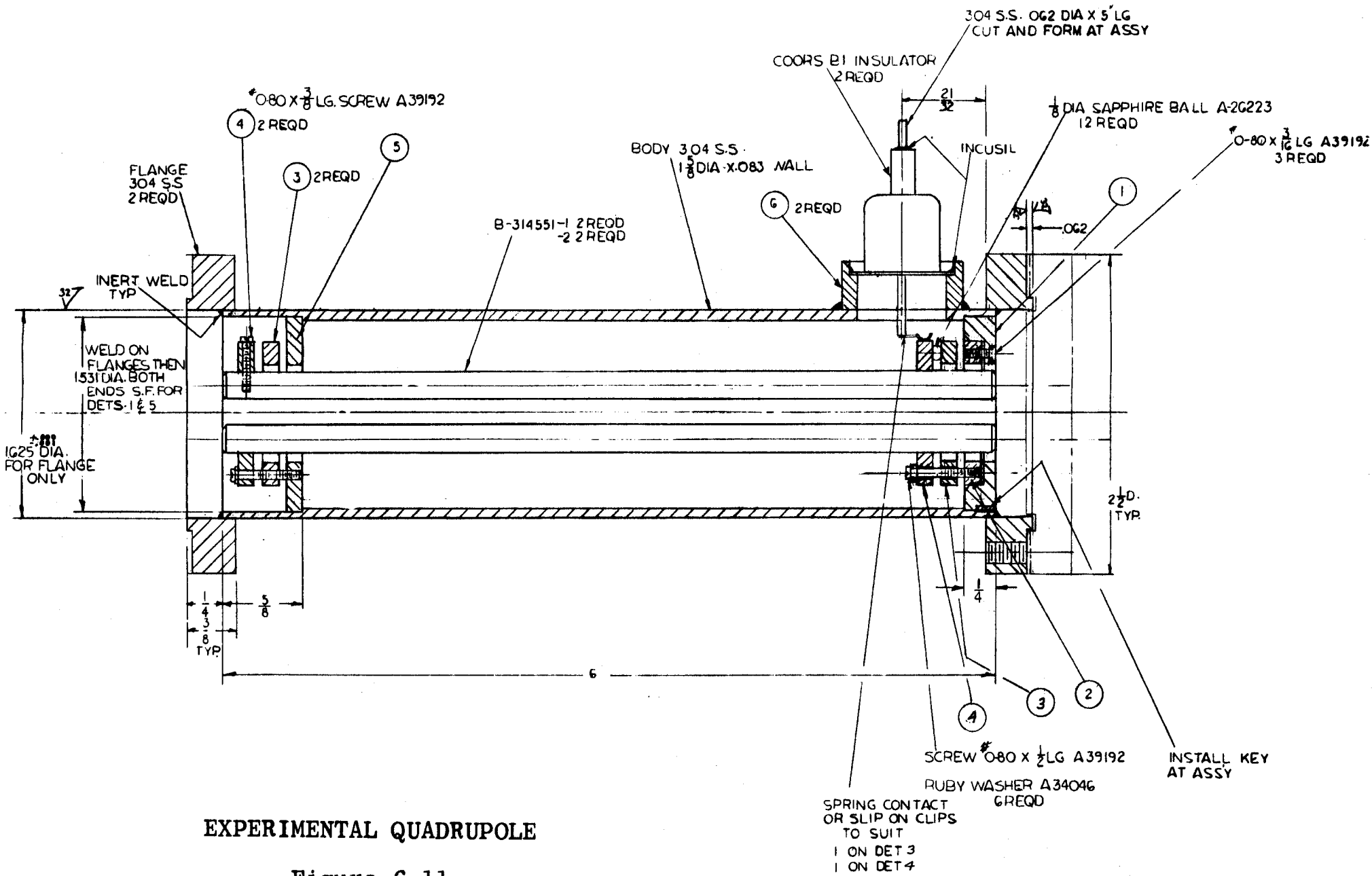

EXPERIMENTAL QUADRUPOLE

Figure 6.11

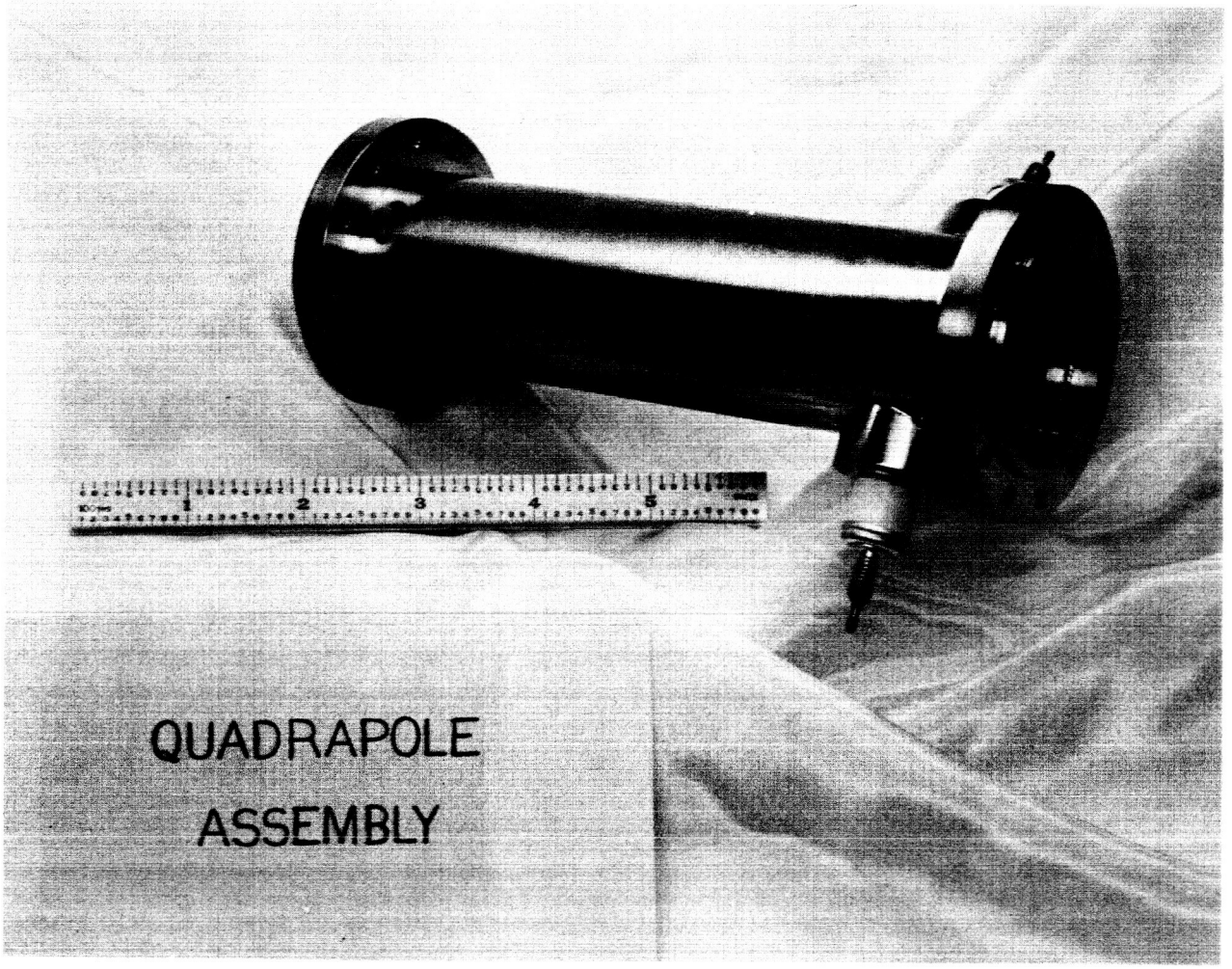

QUADRUPOLE ASSEMBLY

FIGURE 6.12

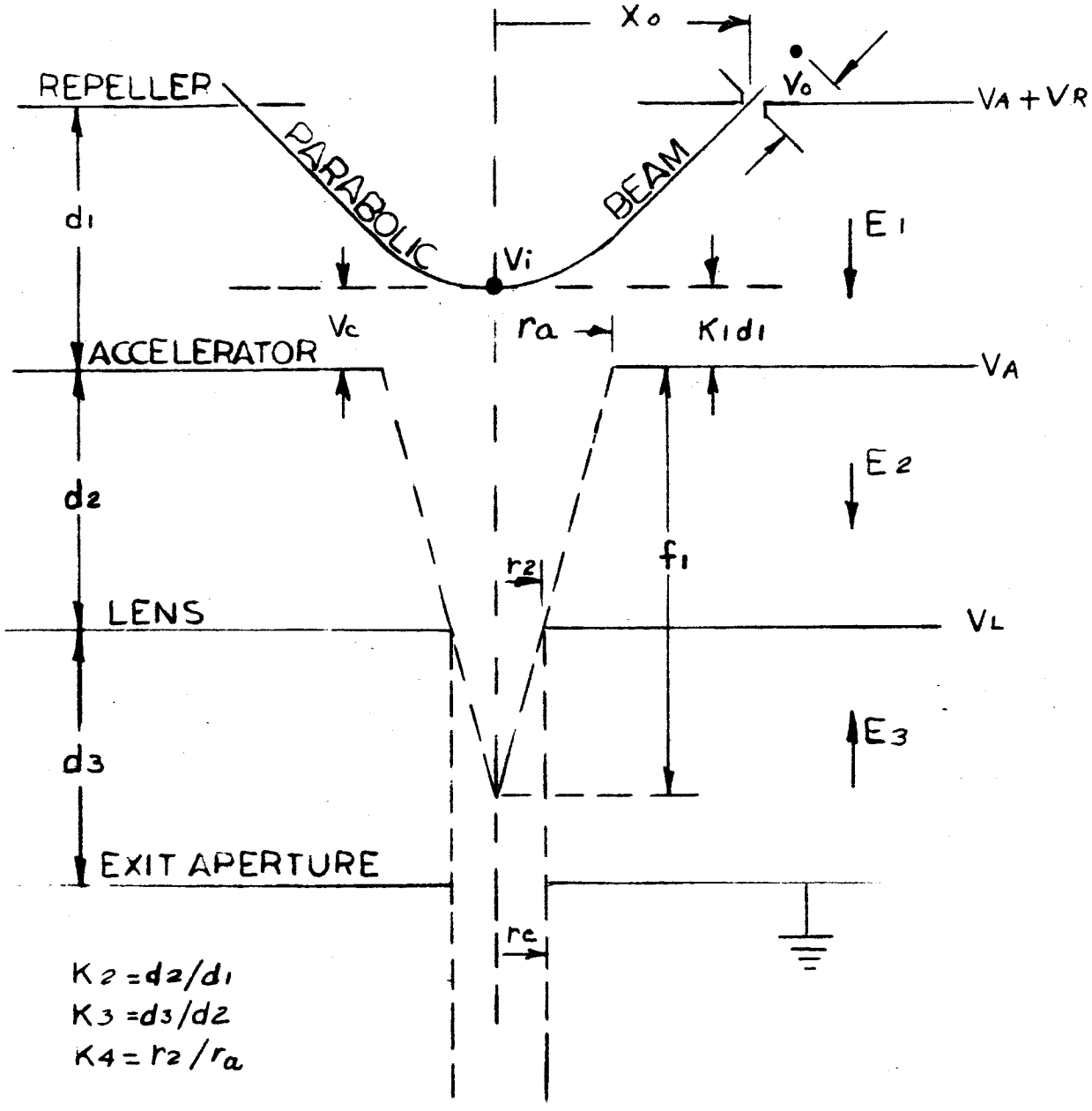

DESIGN FACTORS OF EXPERIMENTAL ION SOURCE
FIG 6.21

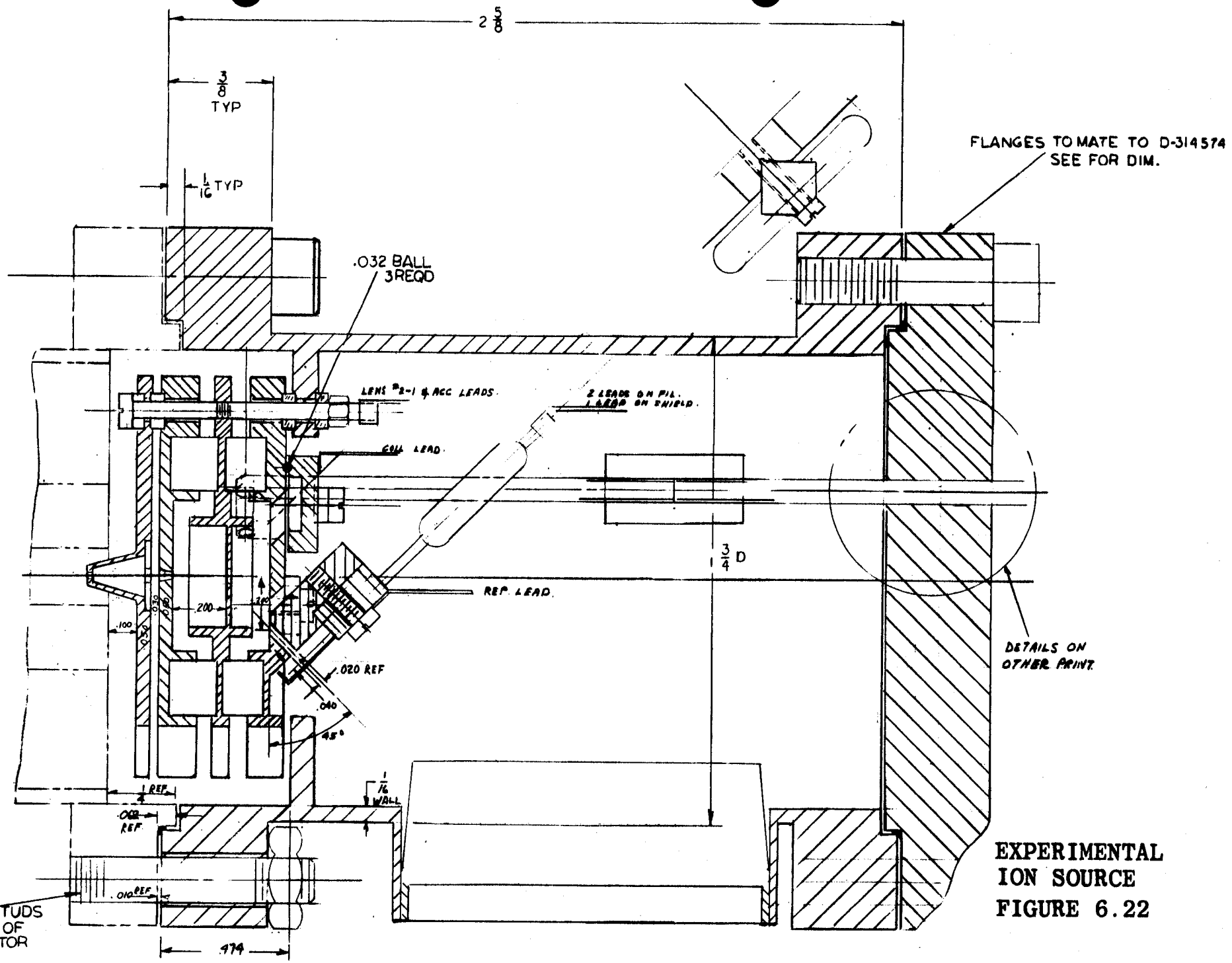

EXPERIMENTAL ION SOURCE FIGURE 6.22

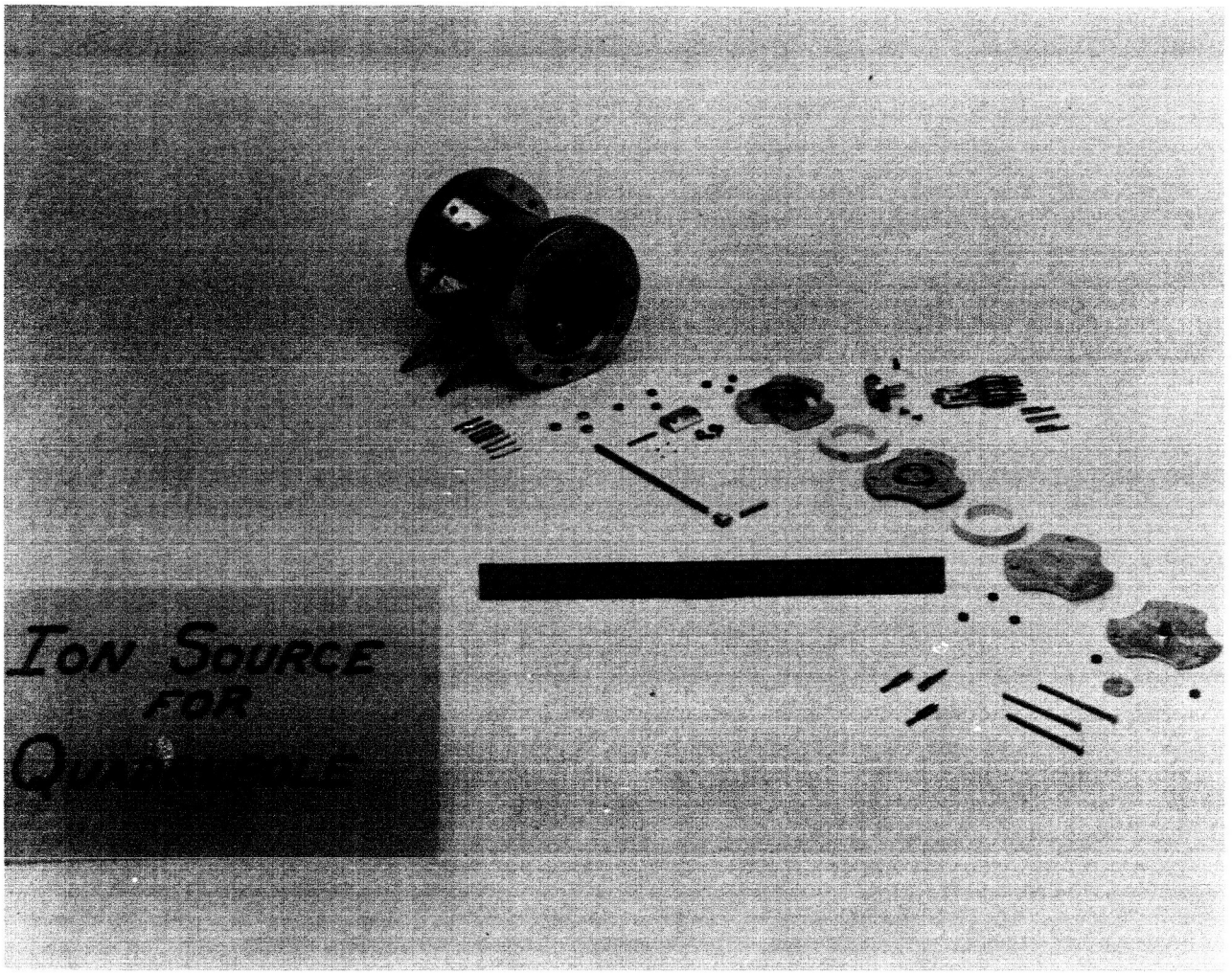

ION SOURCE FOR QUADRUPOLE

FIGURE 6.23

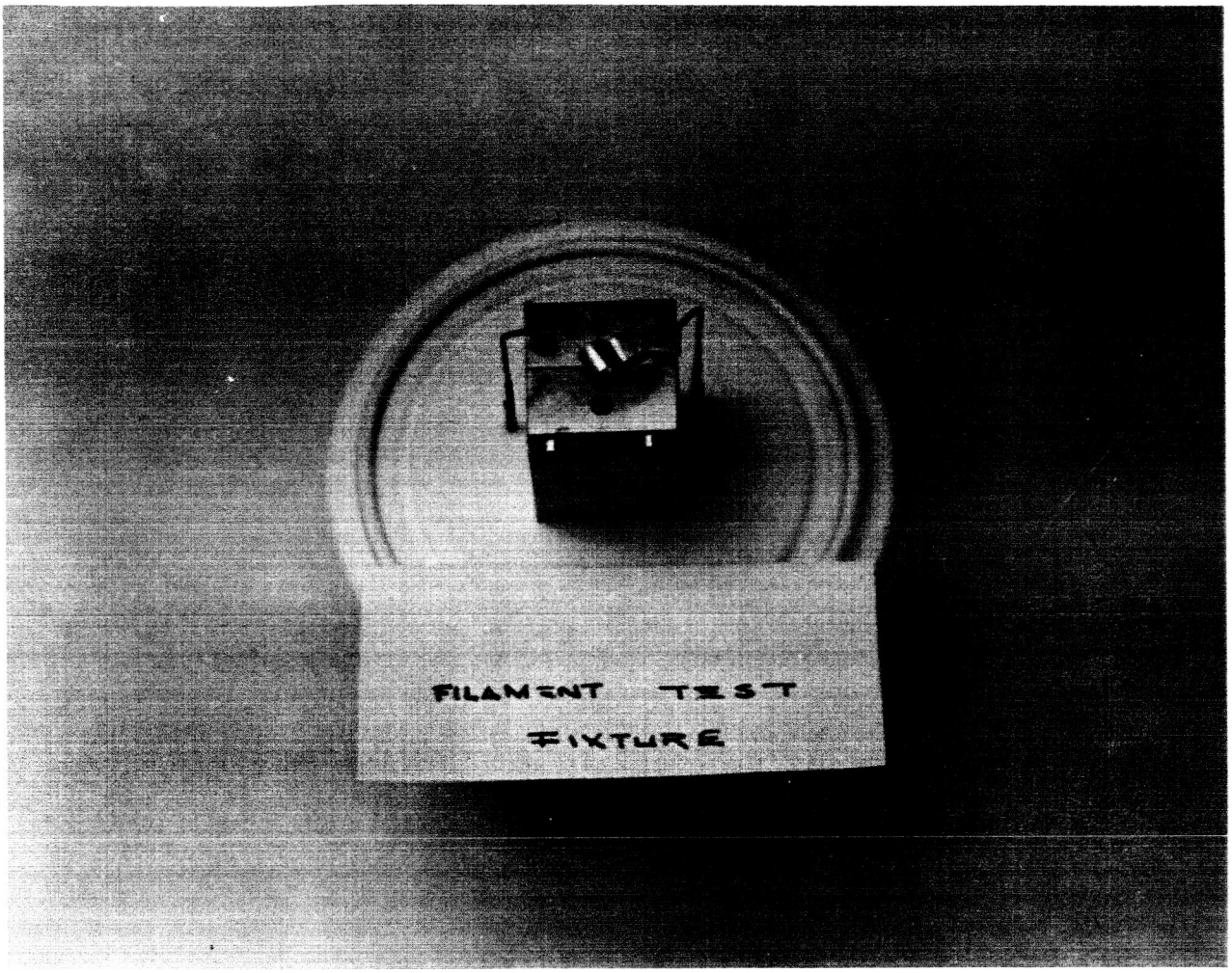

FILAMENT TEST FIXTURE

FIGURE 6.24

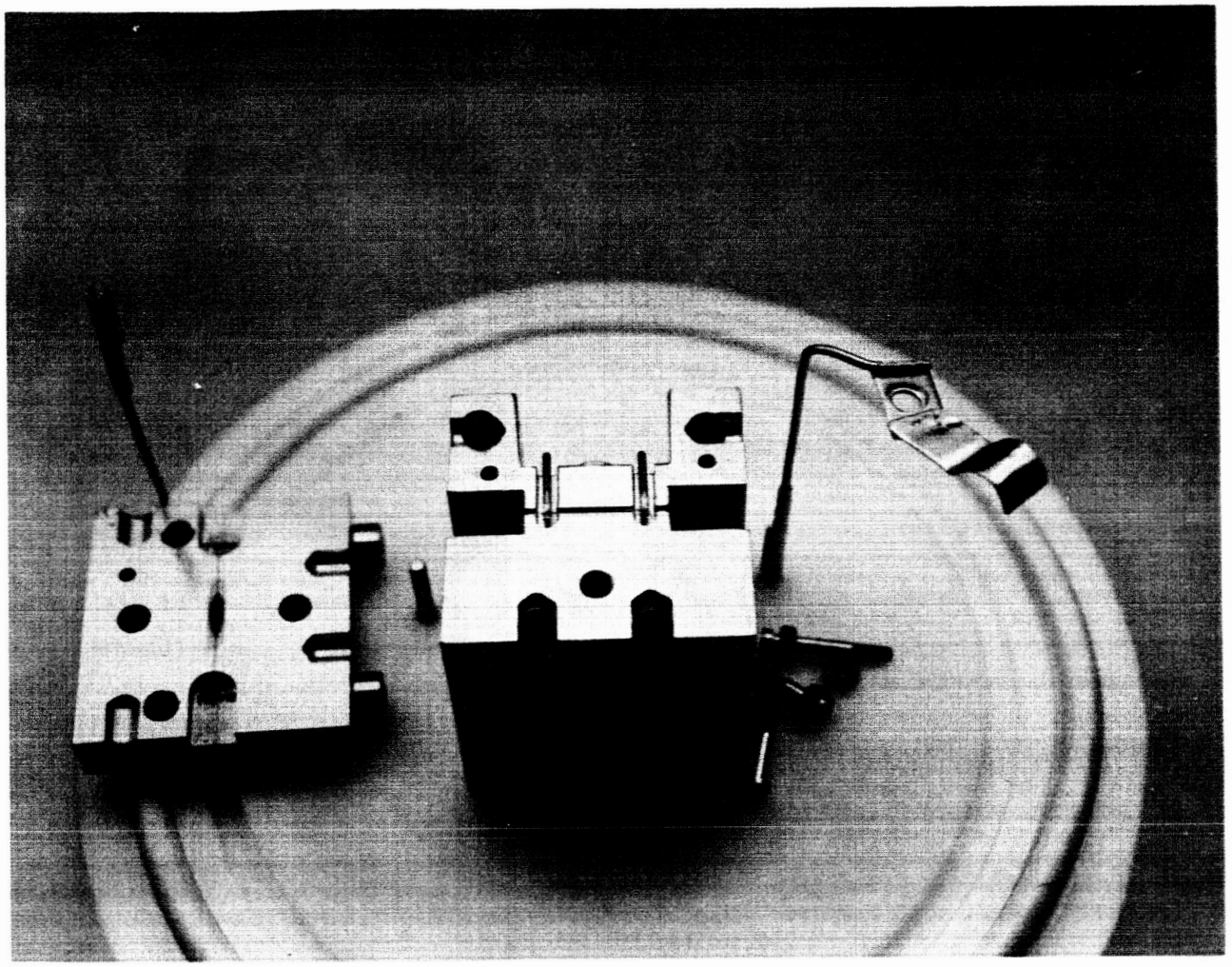

FILAMENT TEST FIXTURE SHOWING THE ACCELERATOR PLATE WITH CONDUCTING SLOT (AT LEFT); CATHODE BLOCK WITH FILAMENT MOUNTED IN GROOVE (CENTER); AND COLLECTOR (AT RIGHT).

FIGURE 6.25

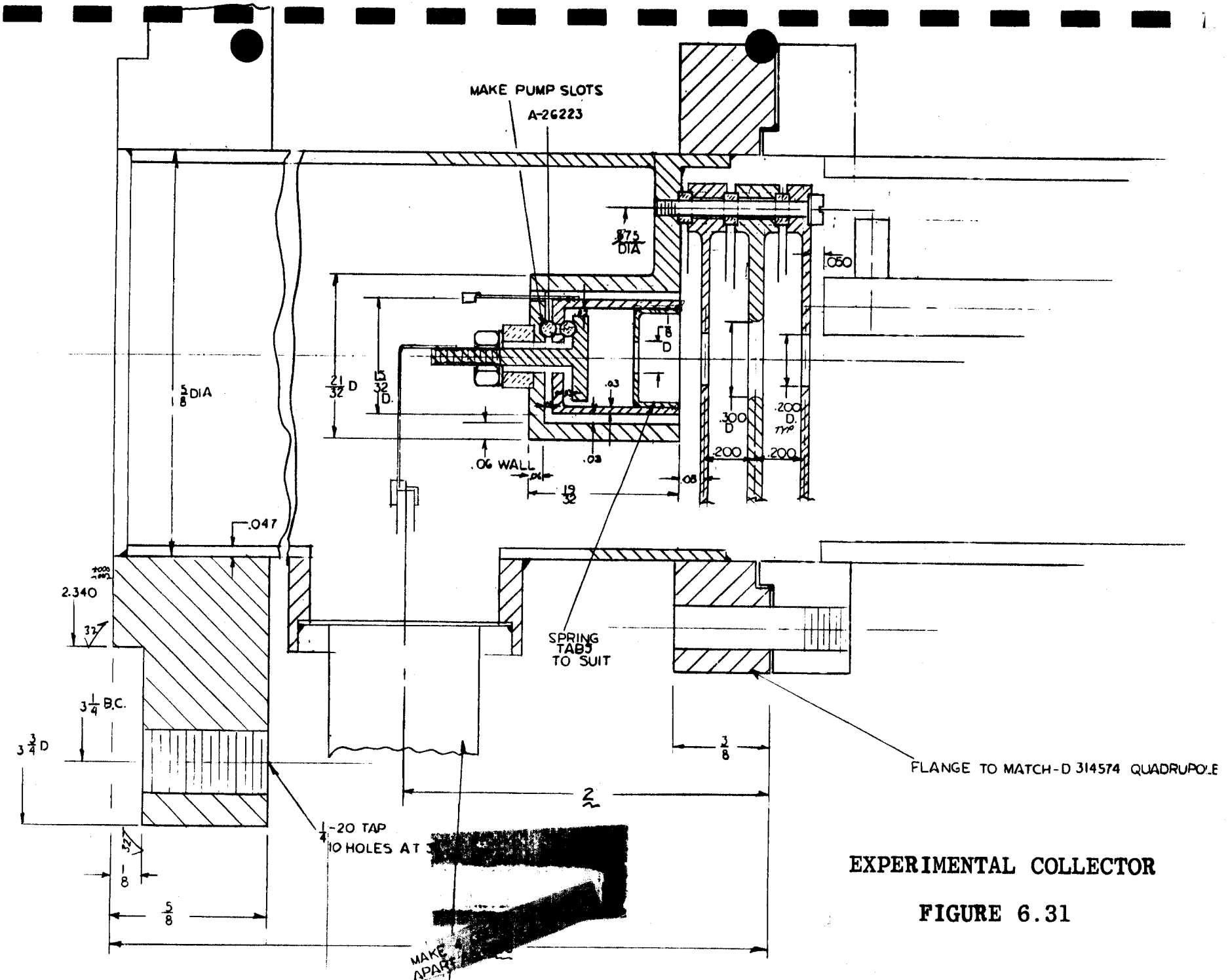

EXPERIMENTAL COLLECTOR

FIGURE 6.31

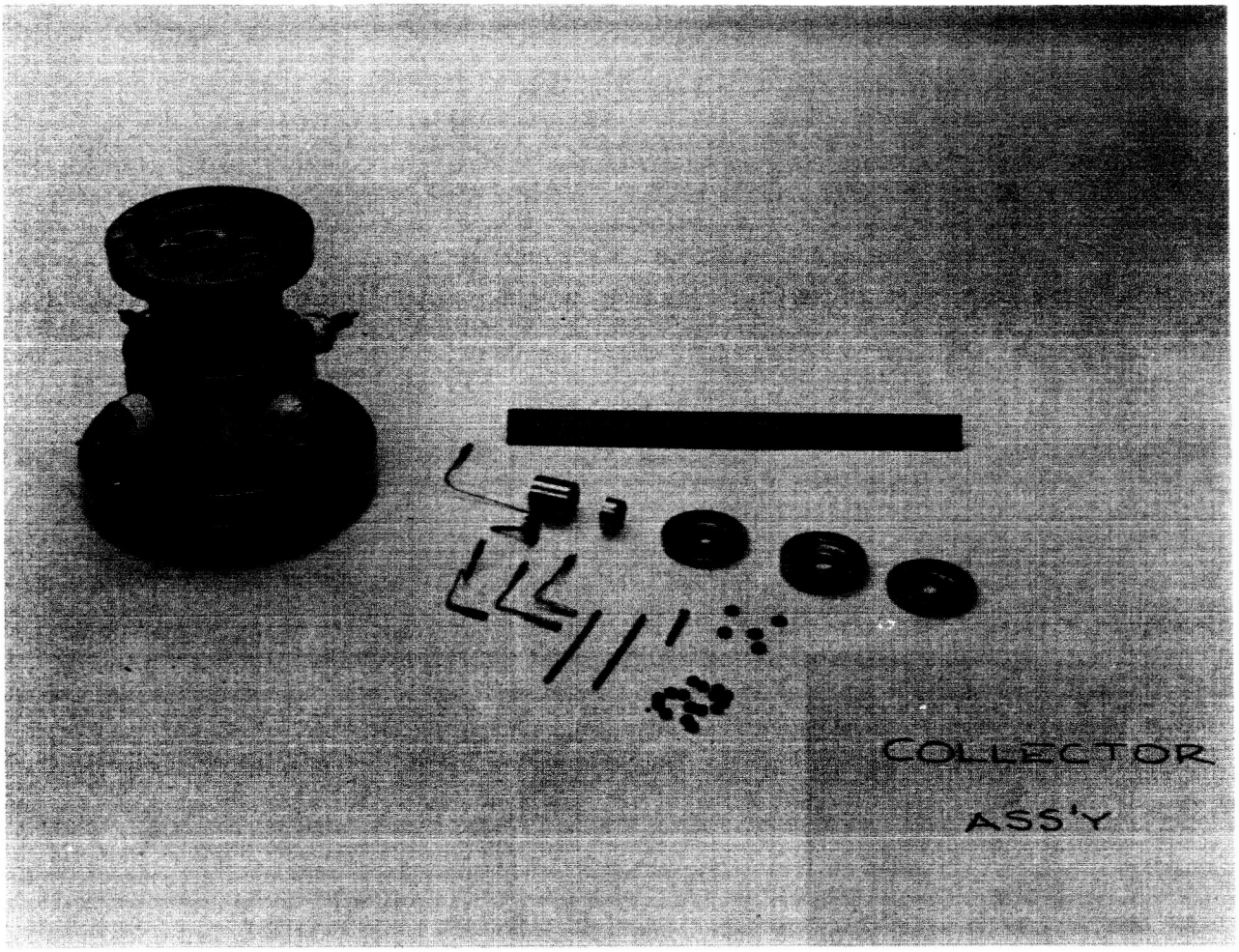

COLLECTOR ASSEMBLY

FIGURE 6.32

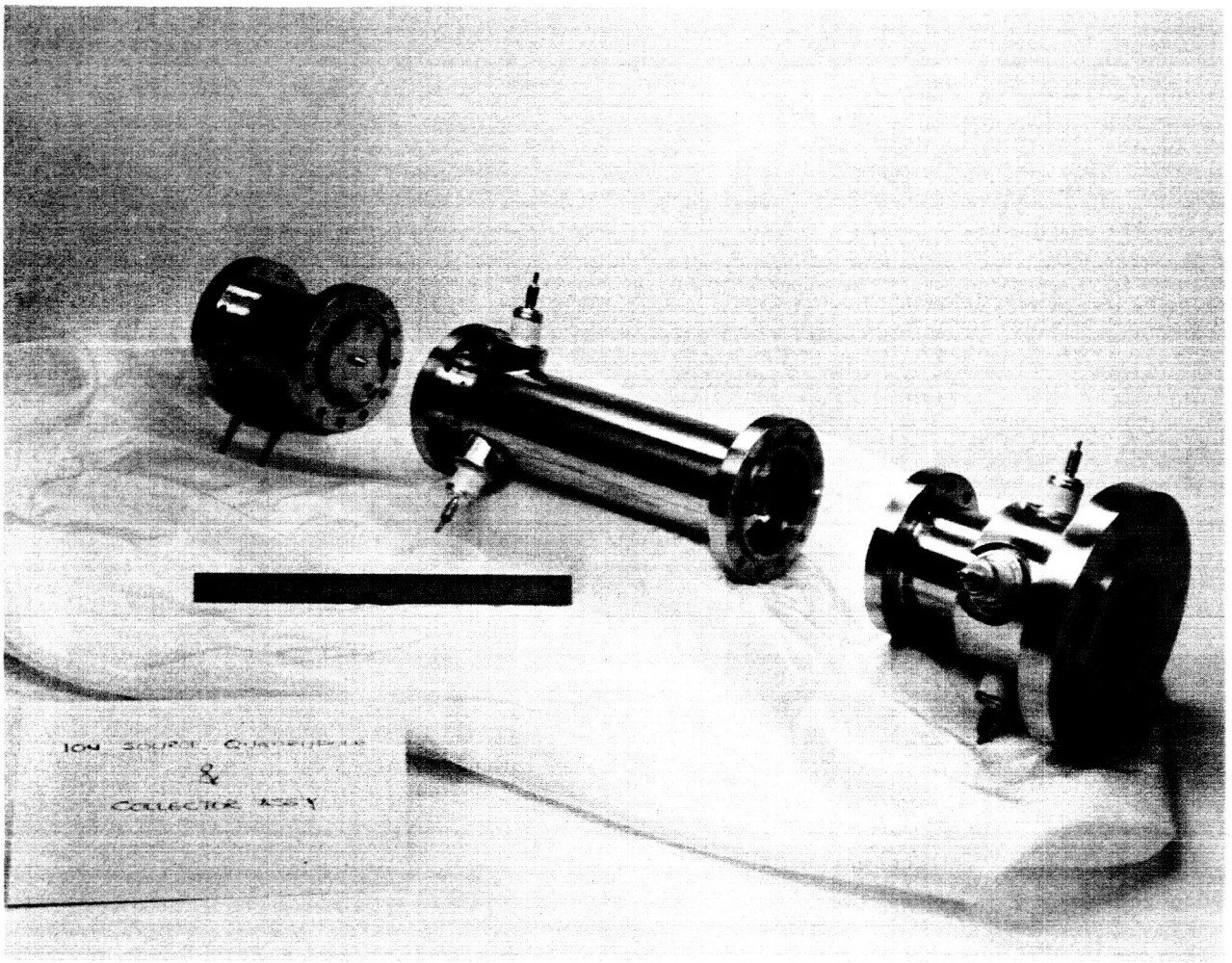

ION SOURCE, QUADRUPOLE, AND
COLLECTOR ASSEMBLY

FIGURE 6.33

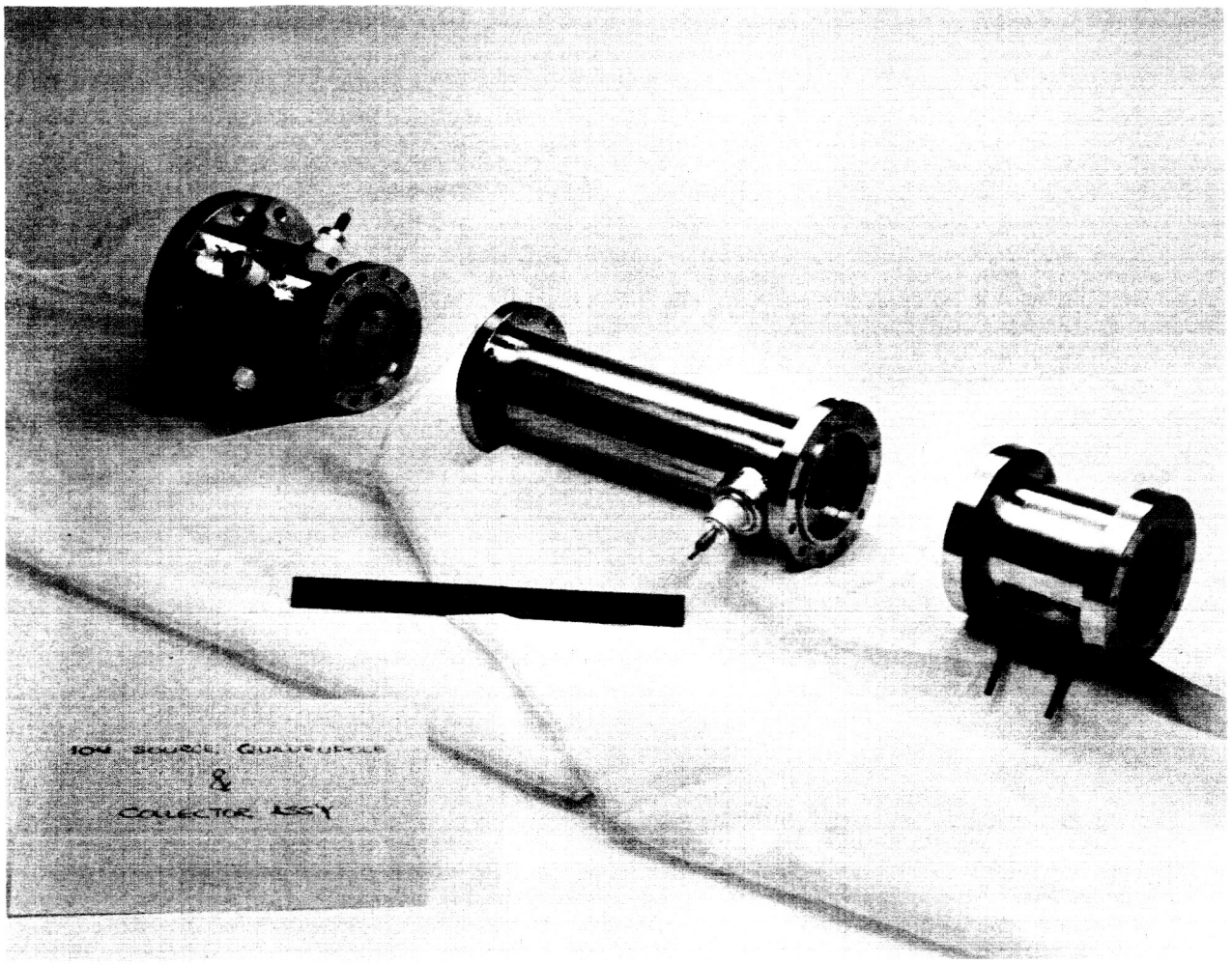

ION SOURCE, QUADRUPOLE AND
COLLECTOR ASSEMBLY

FIGURE 6.34

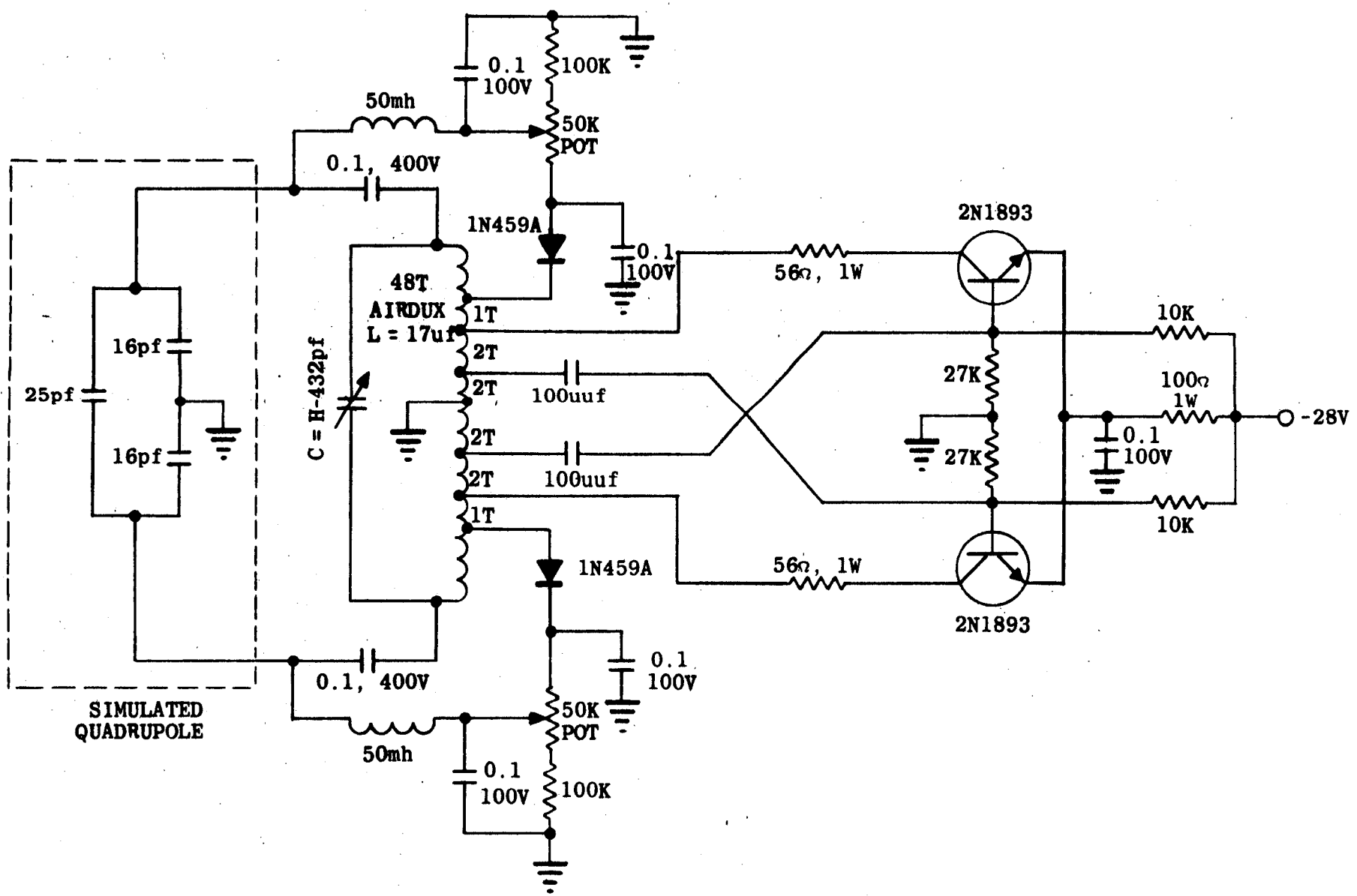

FIGURE 6.45

RF & DC QUADRUPOLE SUPPLY

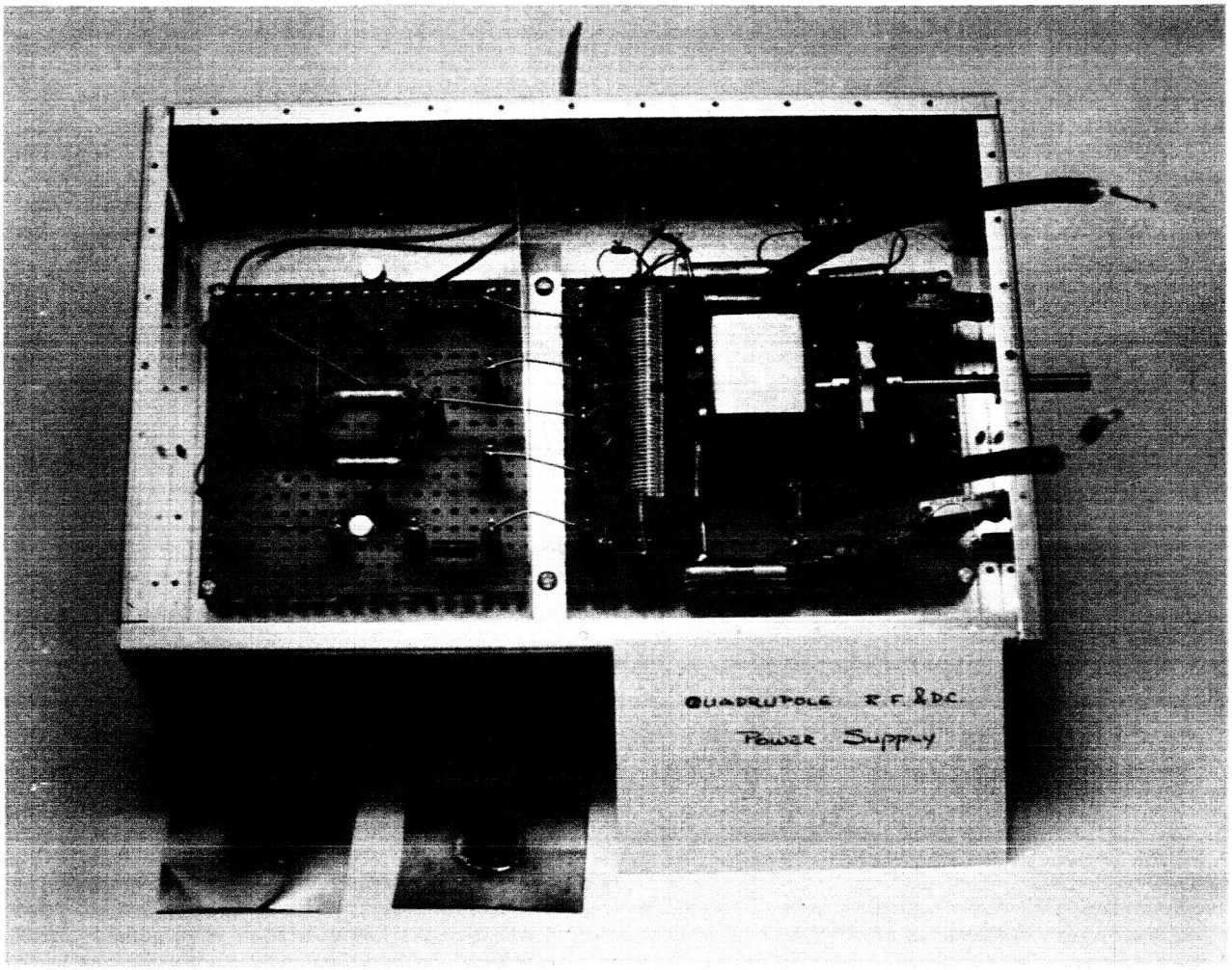

EXPERIMENTAL VERSION OF THE QUADRUPOLE R.F. AND D.C. SUPPLY SHOWING OSCILLATOR, COIL, VARIABLE CAPACITOR AND D.C. TRIMPOTS

FIGURE 6.46

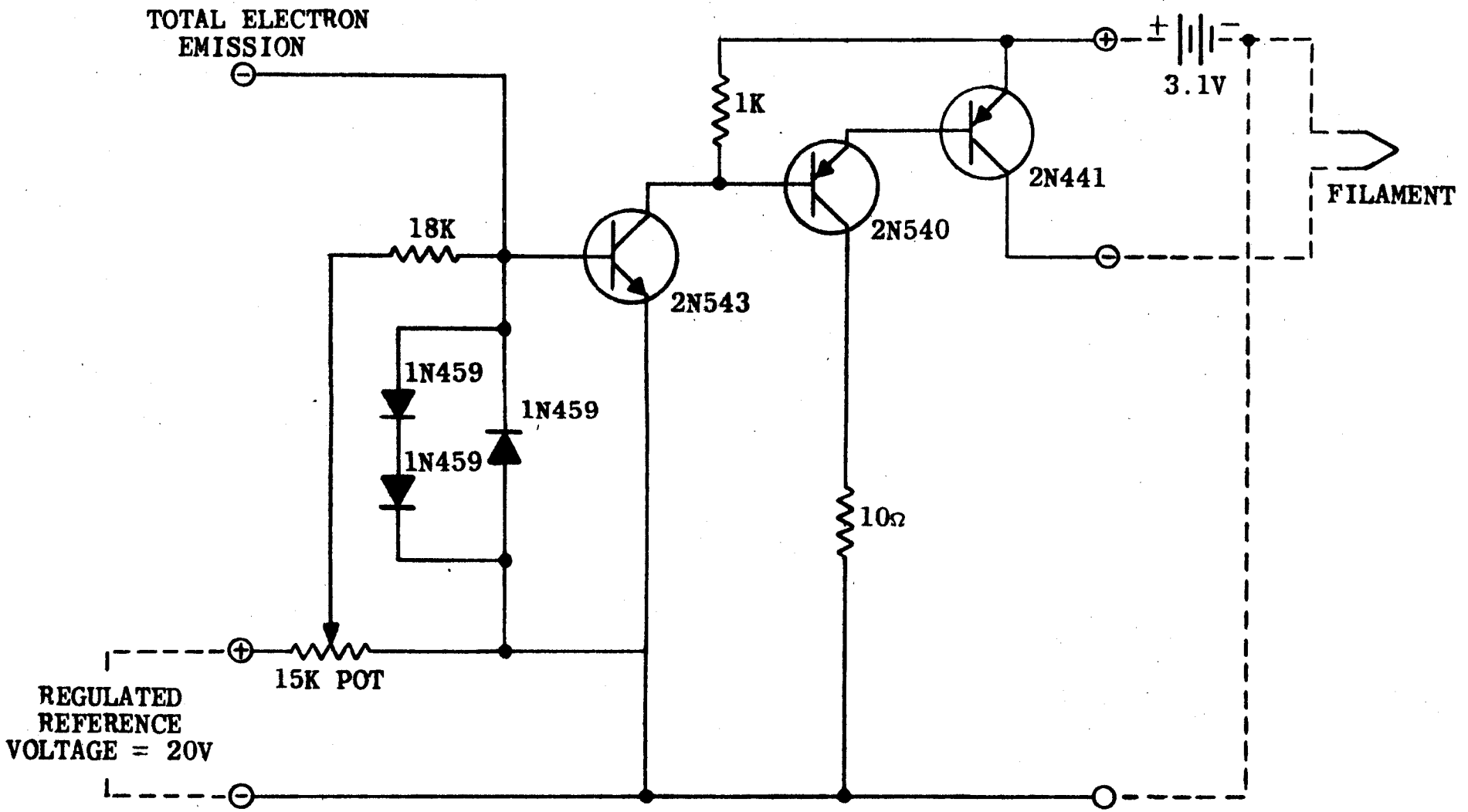

FILAMENT EMISSION REGULATOR
FIGURE 6.61

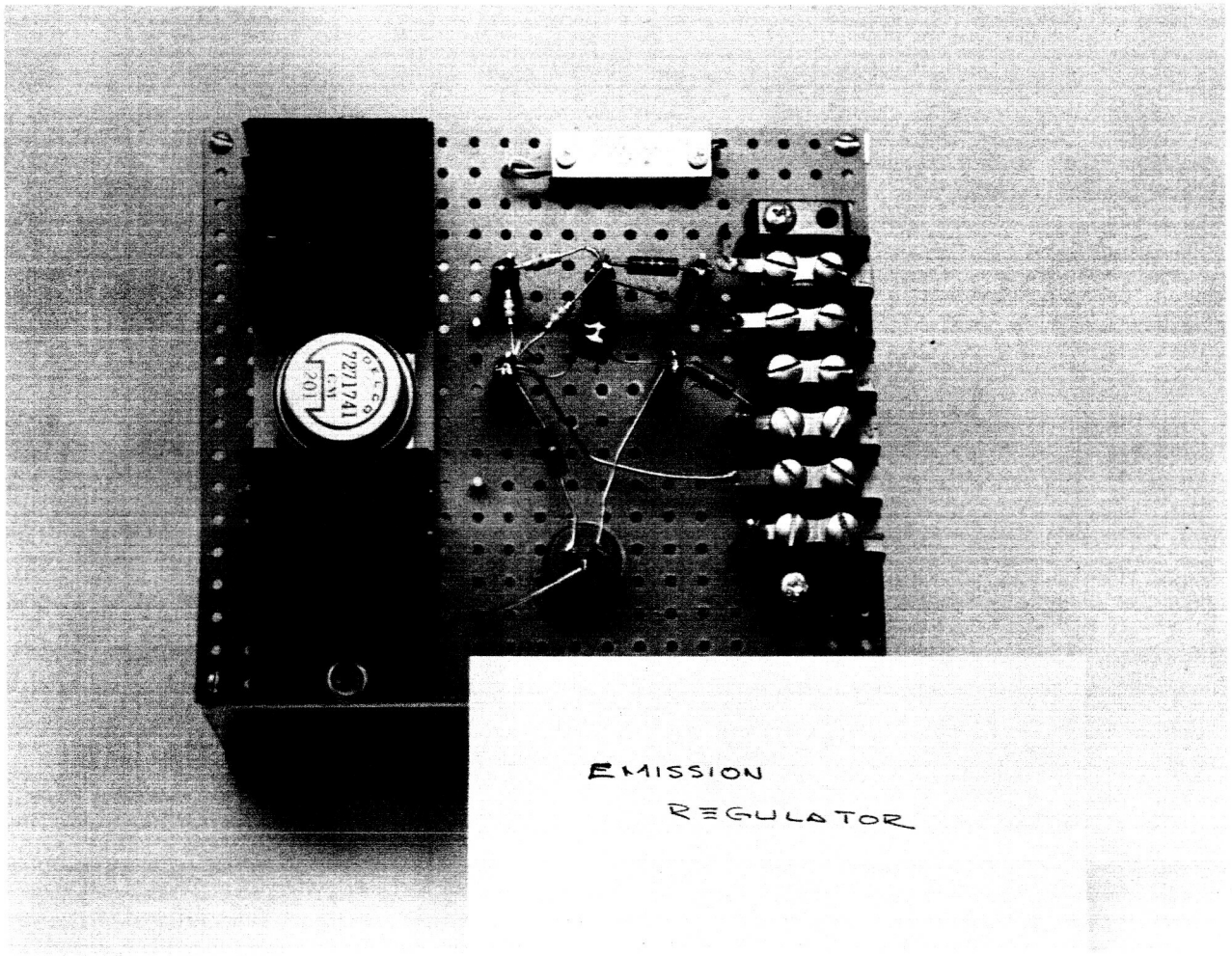

EMISSION REGULATOR

FIGURE 6.62

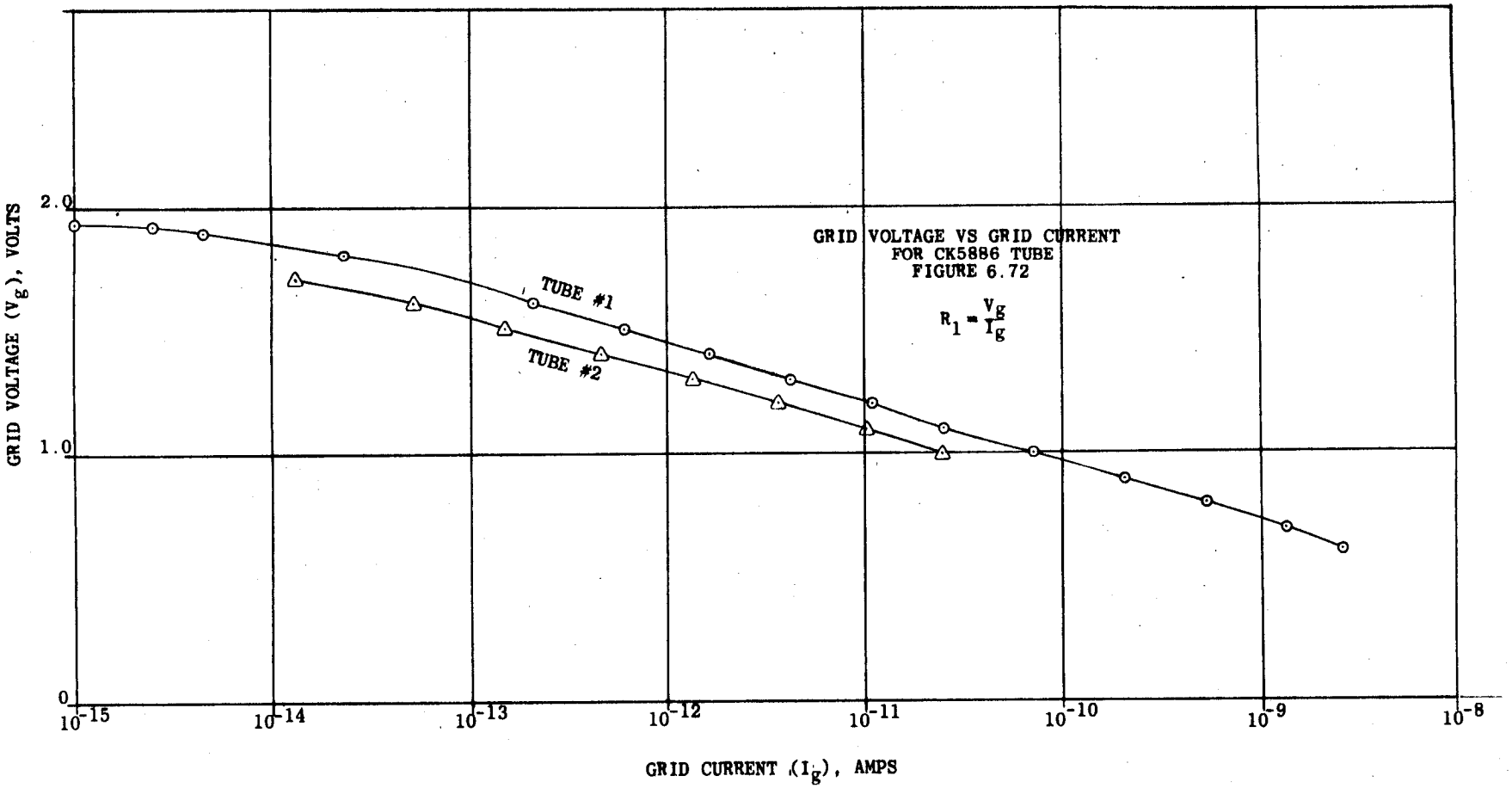
GRID VOLTAGE VS GRID CURRENT
FOR CK5886 TUBE
FIGURE 6.72
$R_1 = \frac{V_g}{I_g}$
TUBE #1
TUBE #2
GRID VOLTAGE (V_g), VOLTS
2.0
1.0
0
10^{-15}
10^{-14}
10^{-13}
10^{-12}
10^{-11}
10^{-10}
10^{-9}
10^{-8}
GRID CURRENT (I_g), AMPS

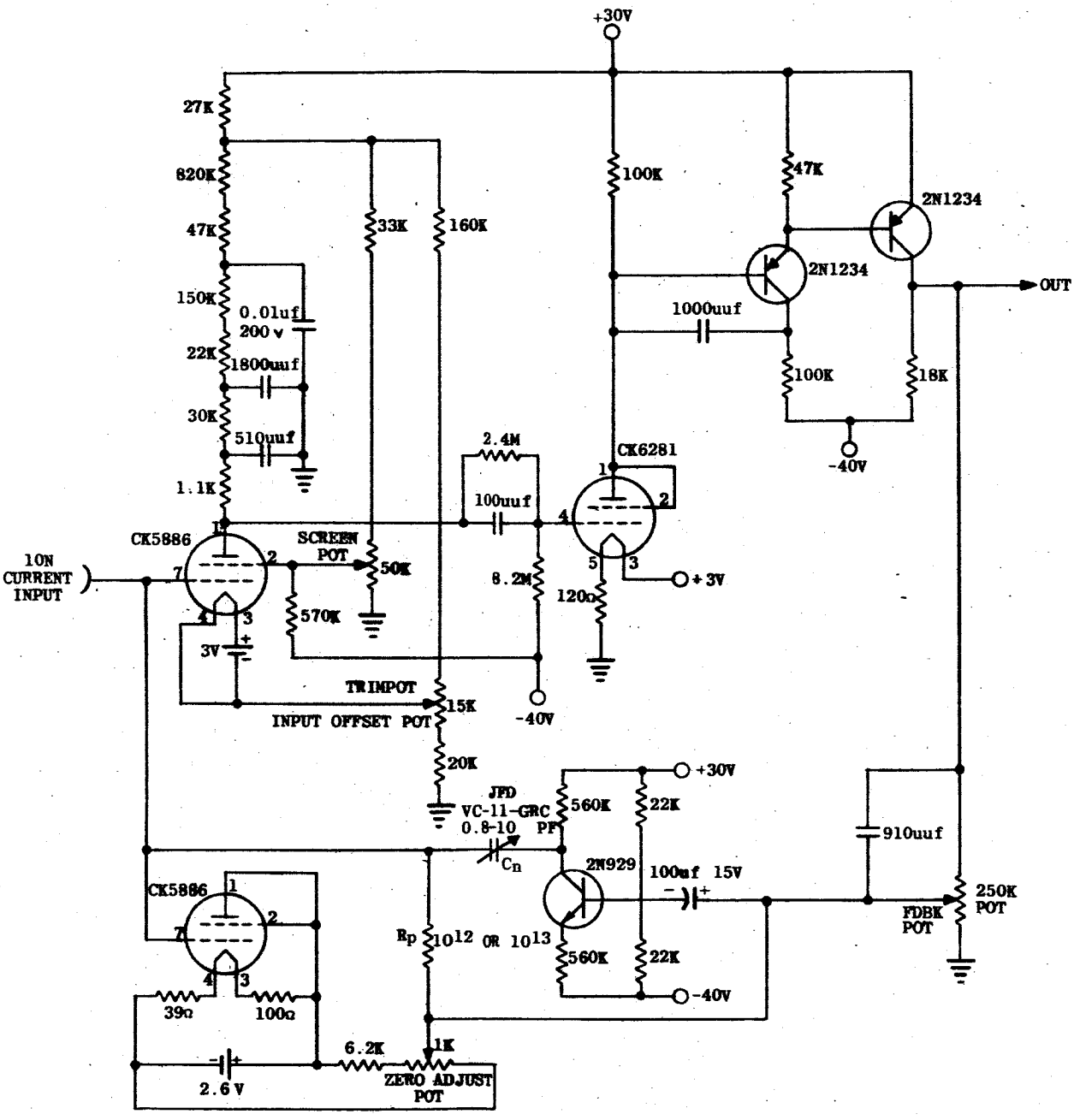

LOGARITHMIC ELECTROMETER AMPLIFIER

FIGURE 6.73

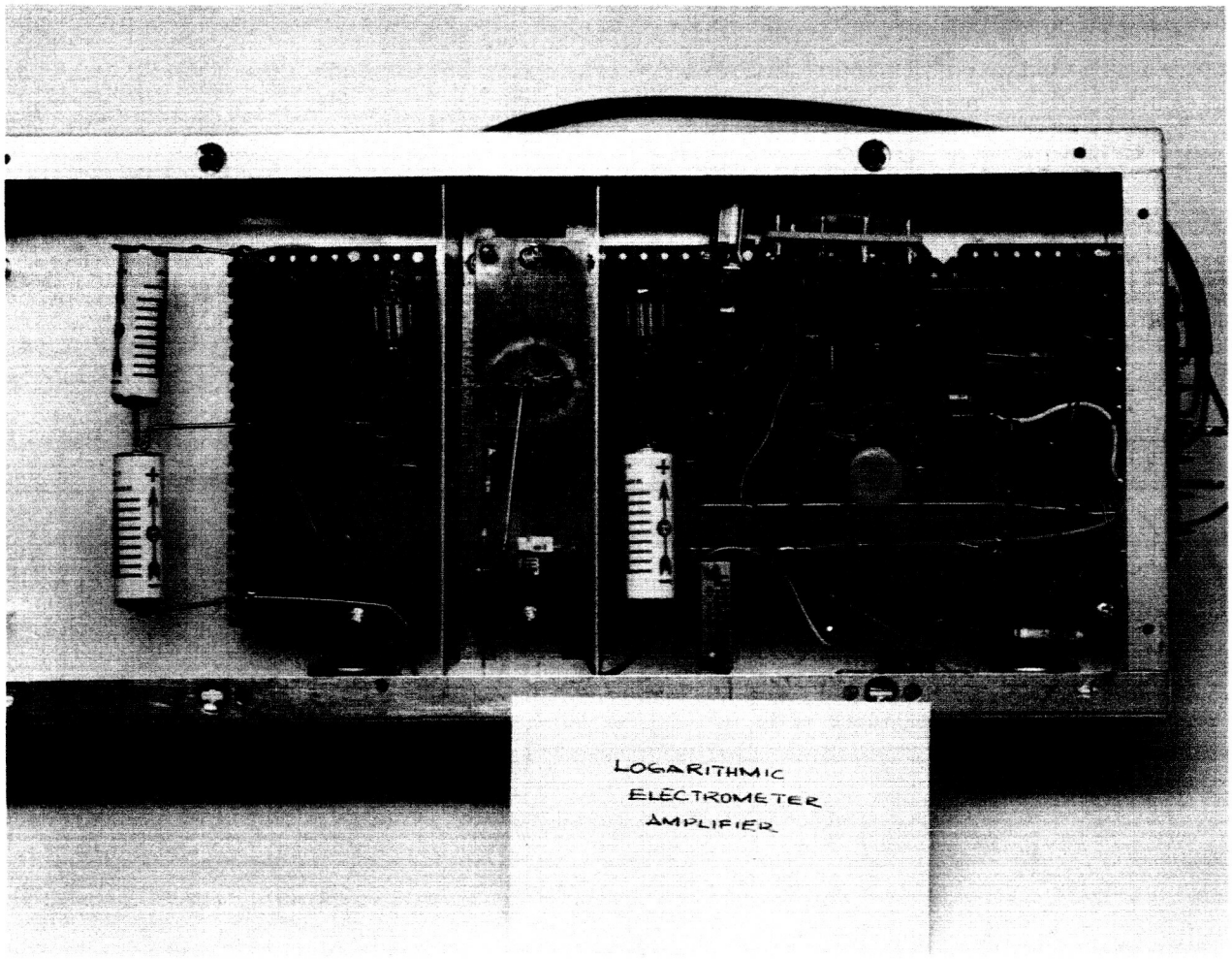

LOGARITHMIC ELECTROMETER AMPLIFIER

FIGURE 6.74

REVISIONS					
SYM	ZONE	DESCRIPTION	DFTMN	DATE	APPROVED

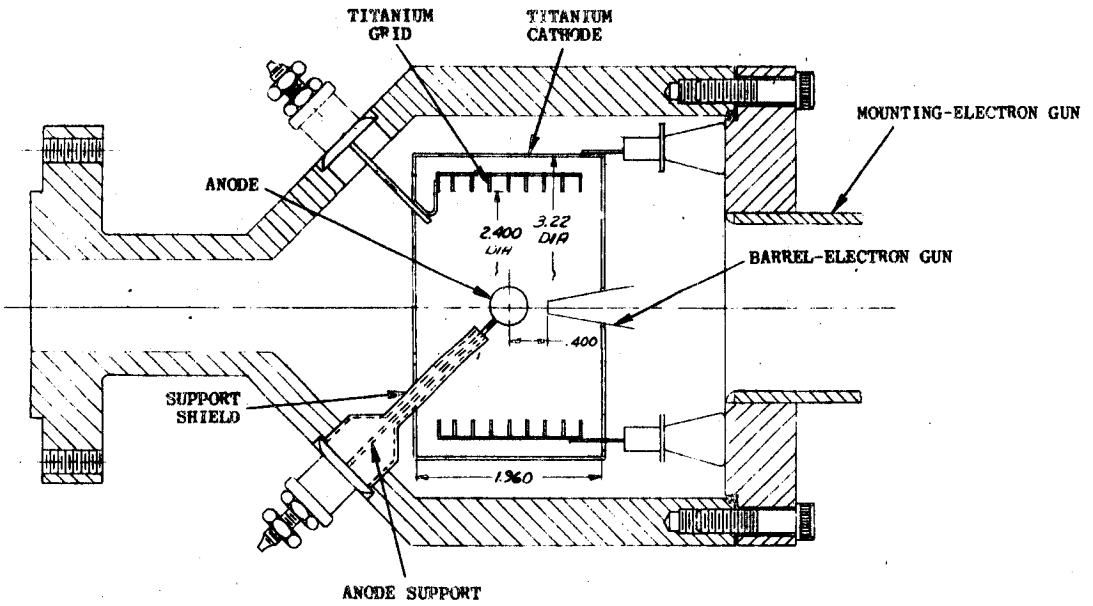

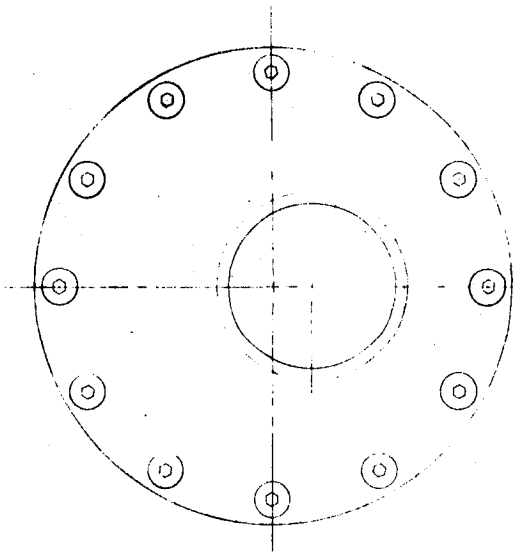

FIGURE 6.81

PART NO.	CODE	DESCRIPTION

REQD/ASSY

LIST OF MATERIAL OR PARTS LIST

TOLERANCES UNLESS OTHERWISE SPECIFIED
ANGULAR FRACTIONAL DECIMAL

UNLESS OTHERWISE SPECIFIED DIMENSIONS ARE IN INCHES

1. BREAK ALL SHARP CORNERS .010 MAX.
2. SURFACE ROUGHNESS 63 MICROINCH R.M.S. MAX.
3. DIAMETERS TO BE CONCENTRIC WITHIN .010 T.I.R.
4. FILLET RADIUS .010 MAX.
5. THREADS-CLASS 2

MATERIAL

DO NOT SCALE DRAWING

DRAWN BY D.McANDREW 8-30-62

CHKD BY

DESIGN

PROJ ENG

41-3494-9

CONSOLIDATED SYSTEMS CORPORATION MONROVIA CALIFORNIA
AN ASSOCIATE COMPANY OF
ALLIS-CHALMERS - BELL & HOWELL - CONSOLIDATED ELECTRODYNAMICS

EXPERIMENTAL GETTER ION PUMP

CODE IDENT NO.	SIZE	
08114	C	315042

SCALE FULL SHEET

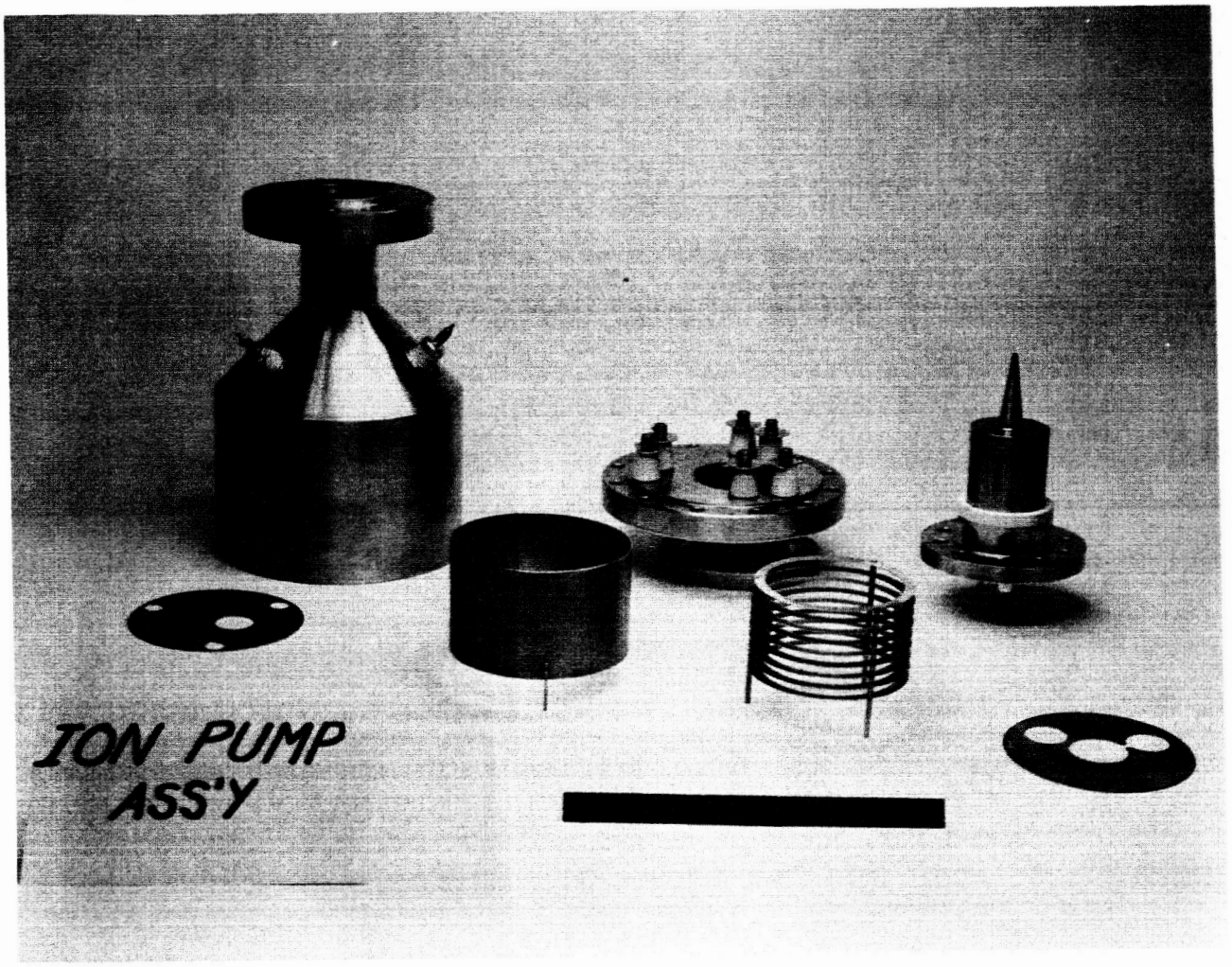

ION PUMP ASSEMBLY

FIGURE 6.82

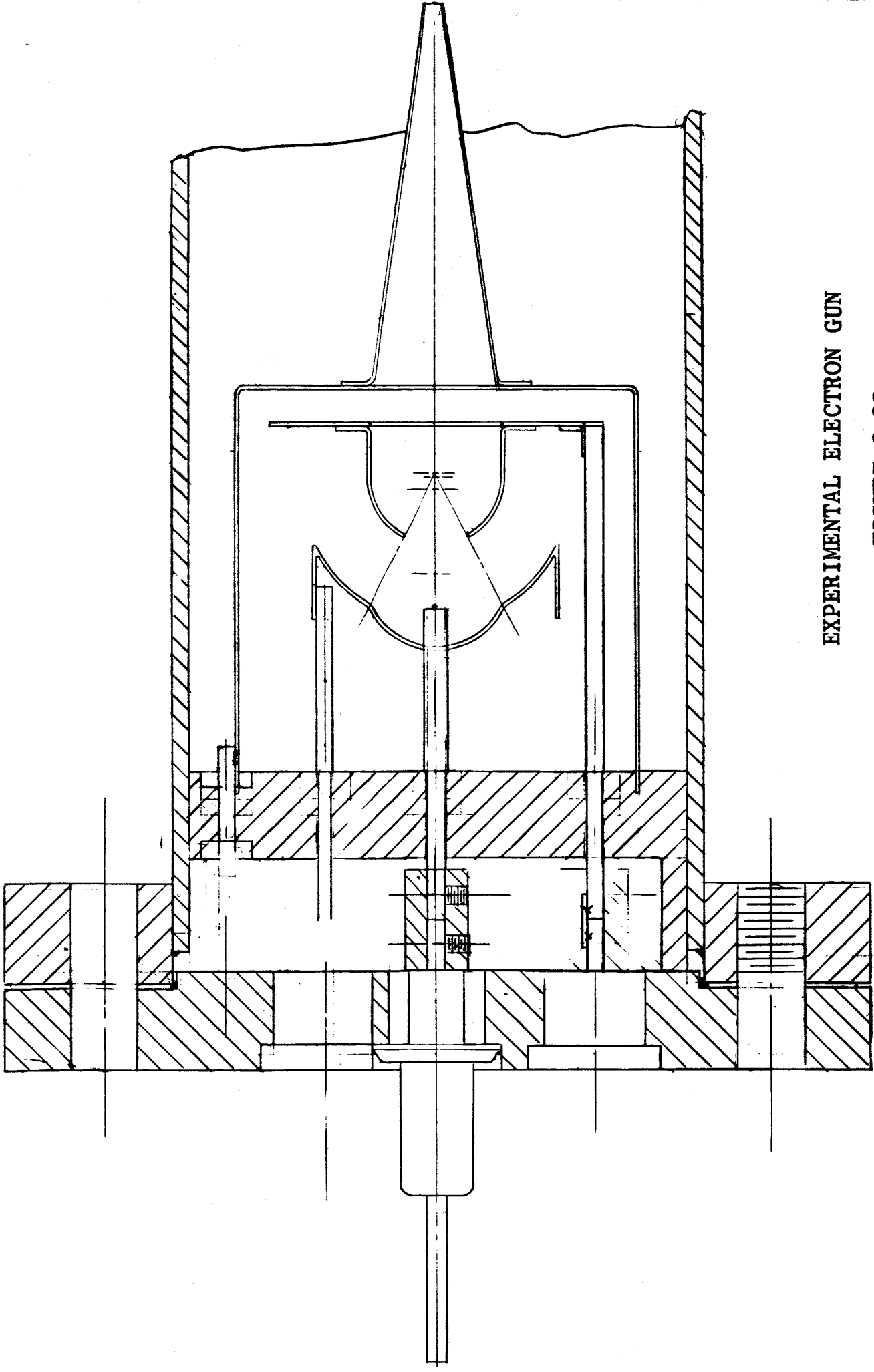

EXPERIMENTAL ELECTRON GUN

FIGURE 6.83

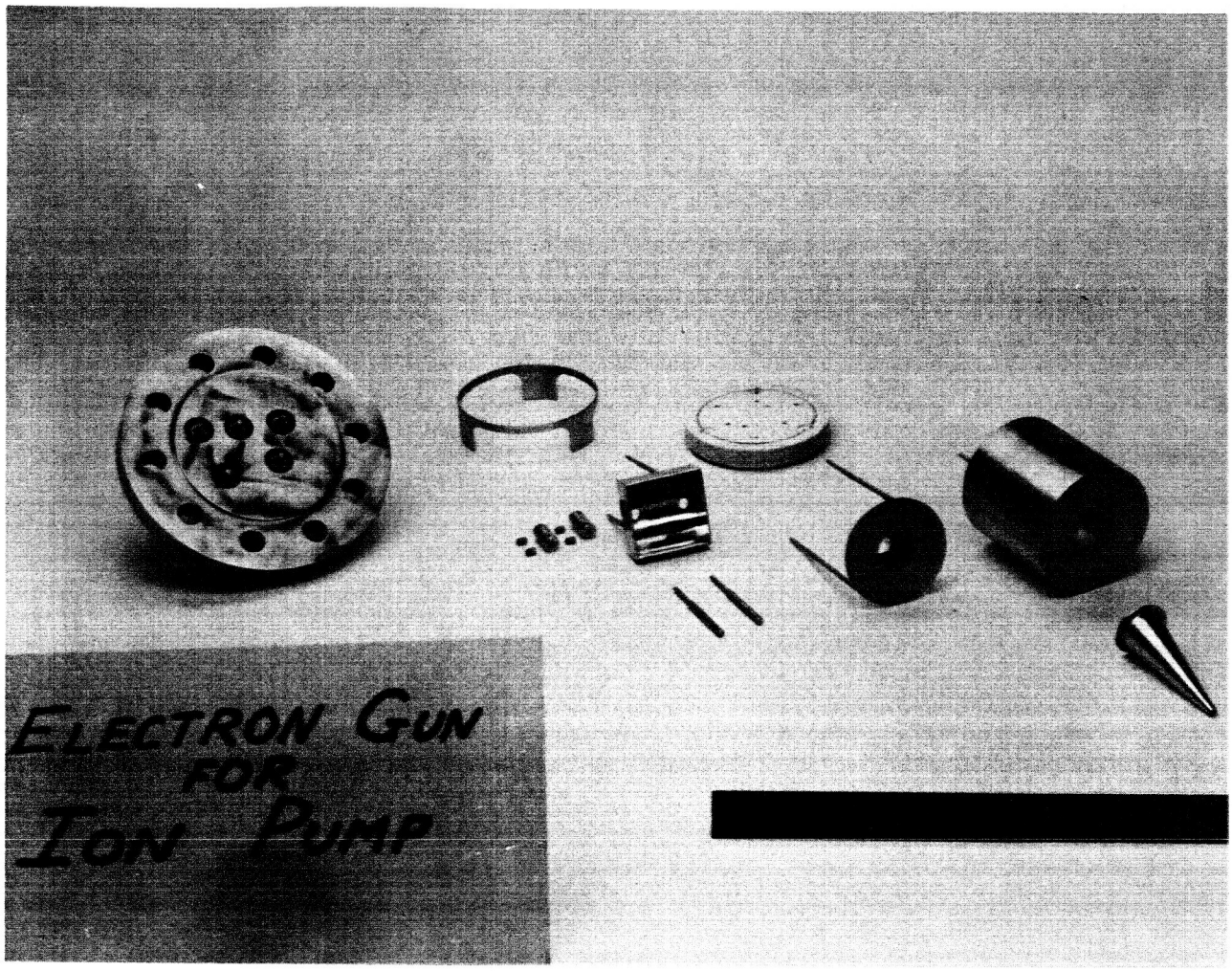

ELECTRON GUN FOR ION PUMP

FIGURE 6.84

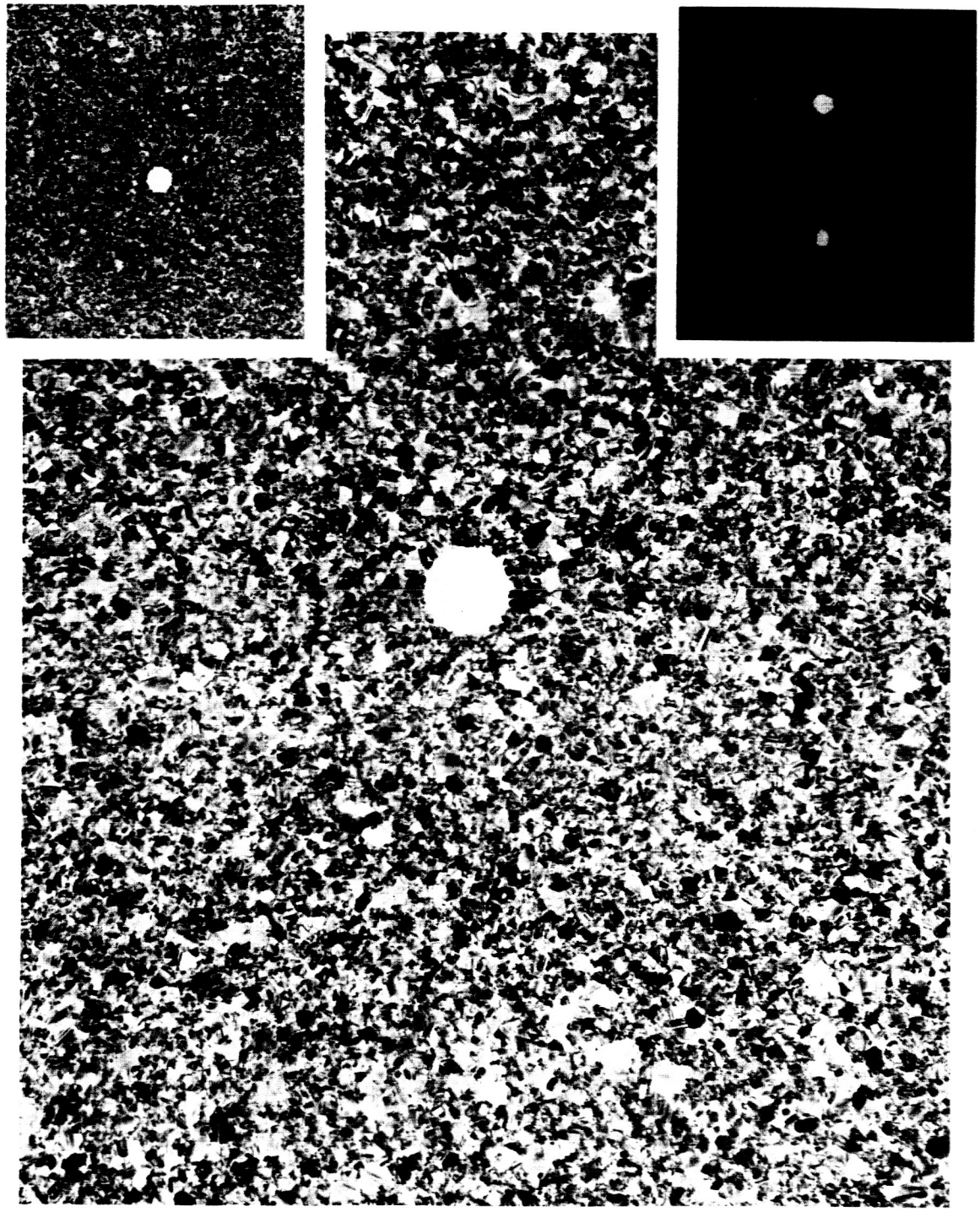

ELECTRON-MICROGRAPH OF 0 337 MICRON HOLE
IN SILVER FOIL. INSERT SHOWS CLOSING OF
HOLES BY EVAPORATION OF GOLD TO 0.1 MICRON

FIGURE 6.91

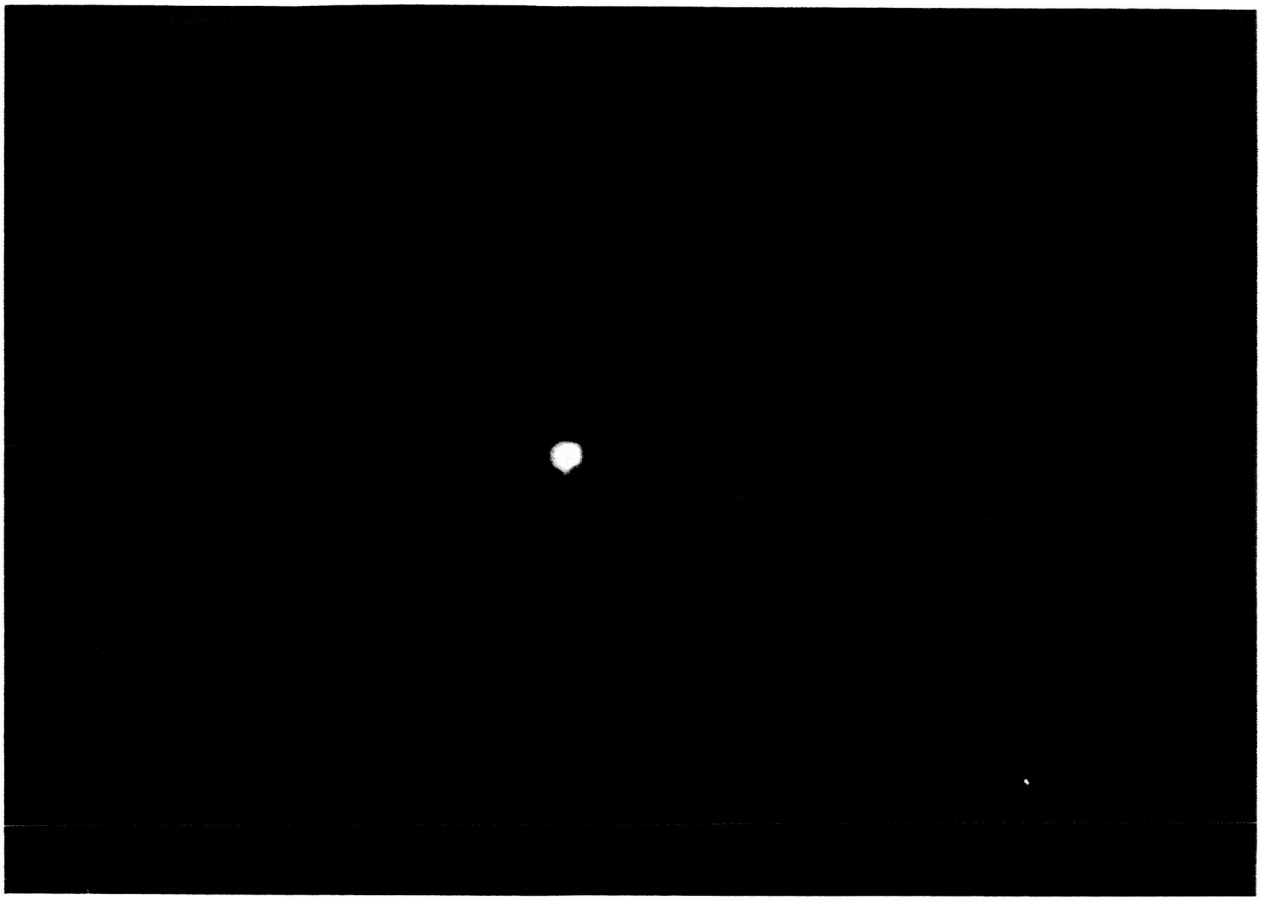

ELECTRON-MICROGRAPH OF SUB MICRON HOLE IN
GOLD FOIL 0.21 MICRON THICK

FIGURE 6.92

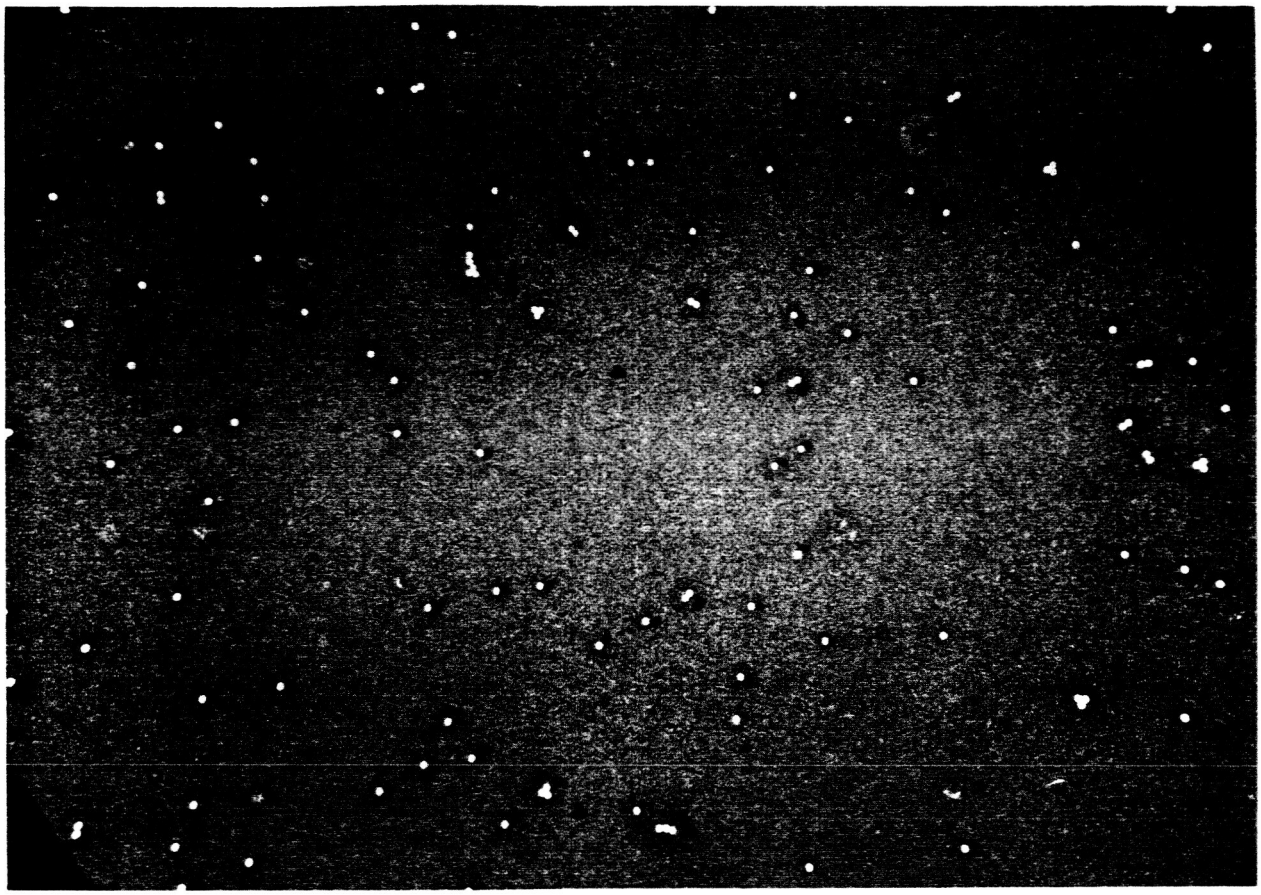

ELECTRON MICROGRAPH OF SUBMICRON FILTER HOLES

FIGURE 6.93

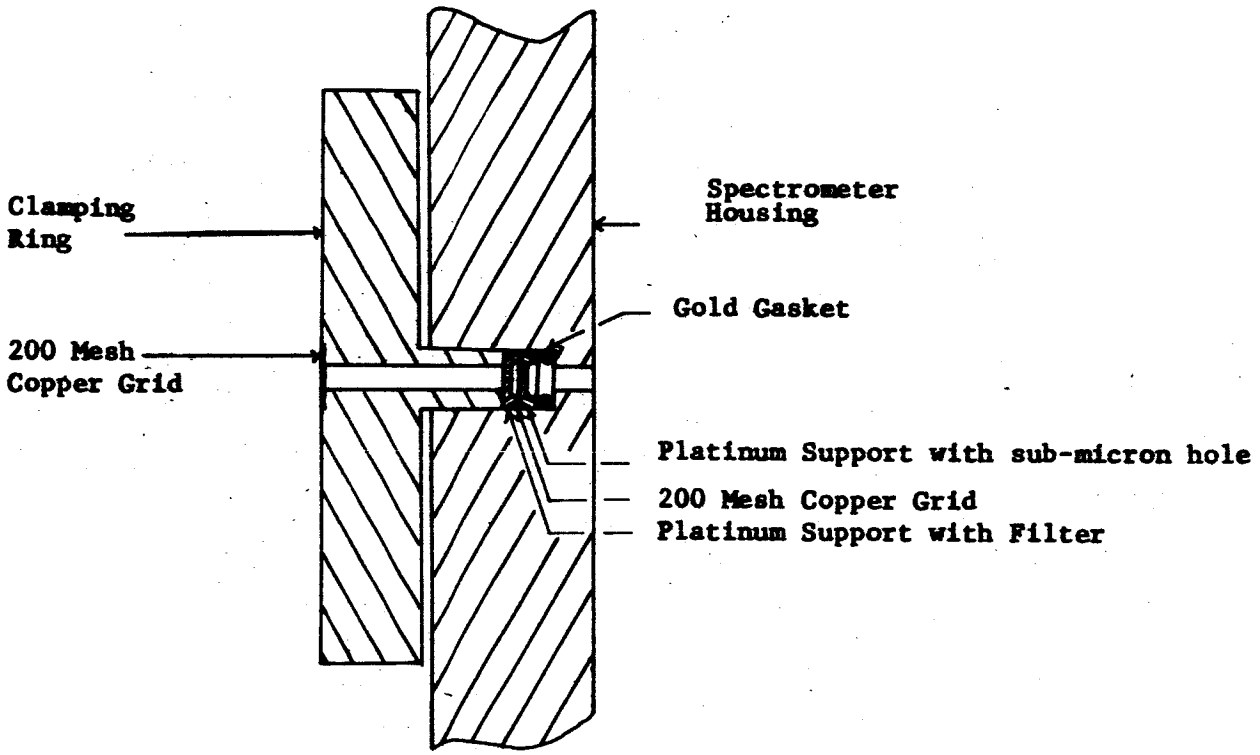

SCALE 4:1

Figure 6.94

MOUNTING OF INLET LEAK

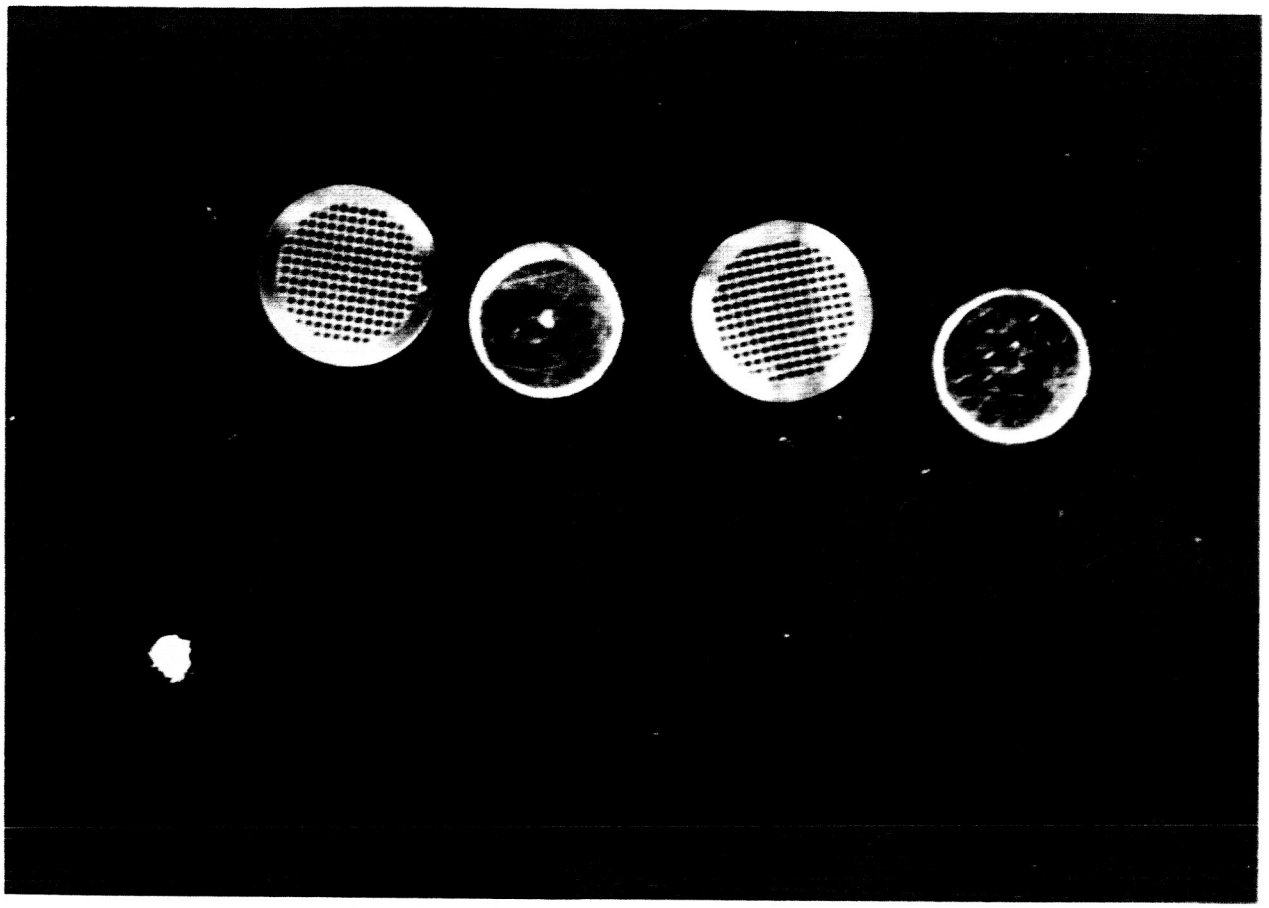

COMPONENTS OF INLET LEAK ASSEMBLY

a) 200 MESH COPPER GRID
b) FILTER ON PLATINUM SUPPORT
c) 200 MESH COPPER GRID
d) SINGLE INLET LEAK APERTURE IN GOLD FOIL, MOUNTED OVER PLATINUM SUPPORT

FIGURE 6.95

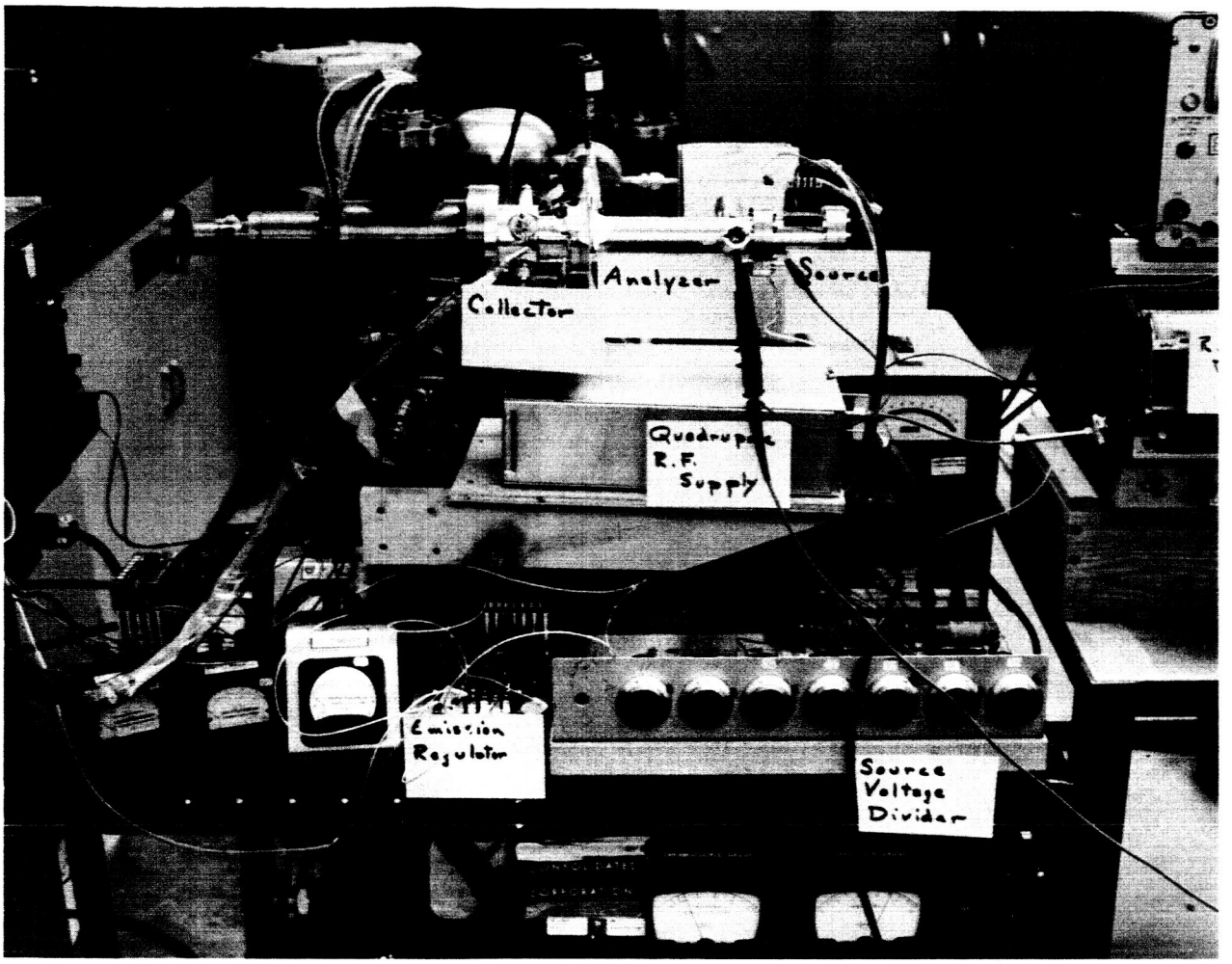

EXPERIMENTAL TEST SET UP OF QUADRUPOLE MASS SPECTROMETER, ION SOURCE AND COLLECTOR WITH SUPPORT ELECTRONICS

FIGURE 7.11

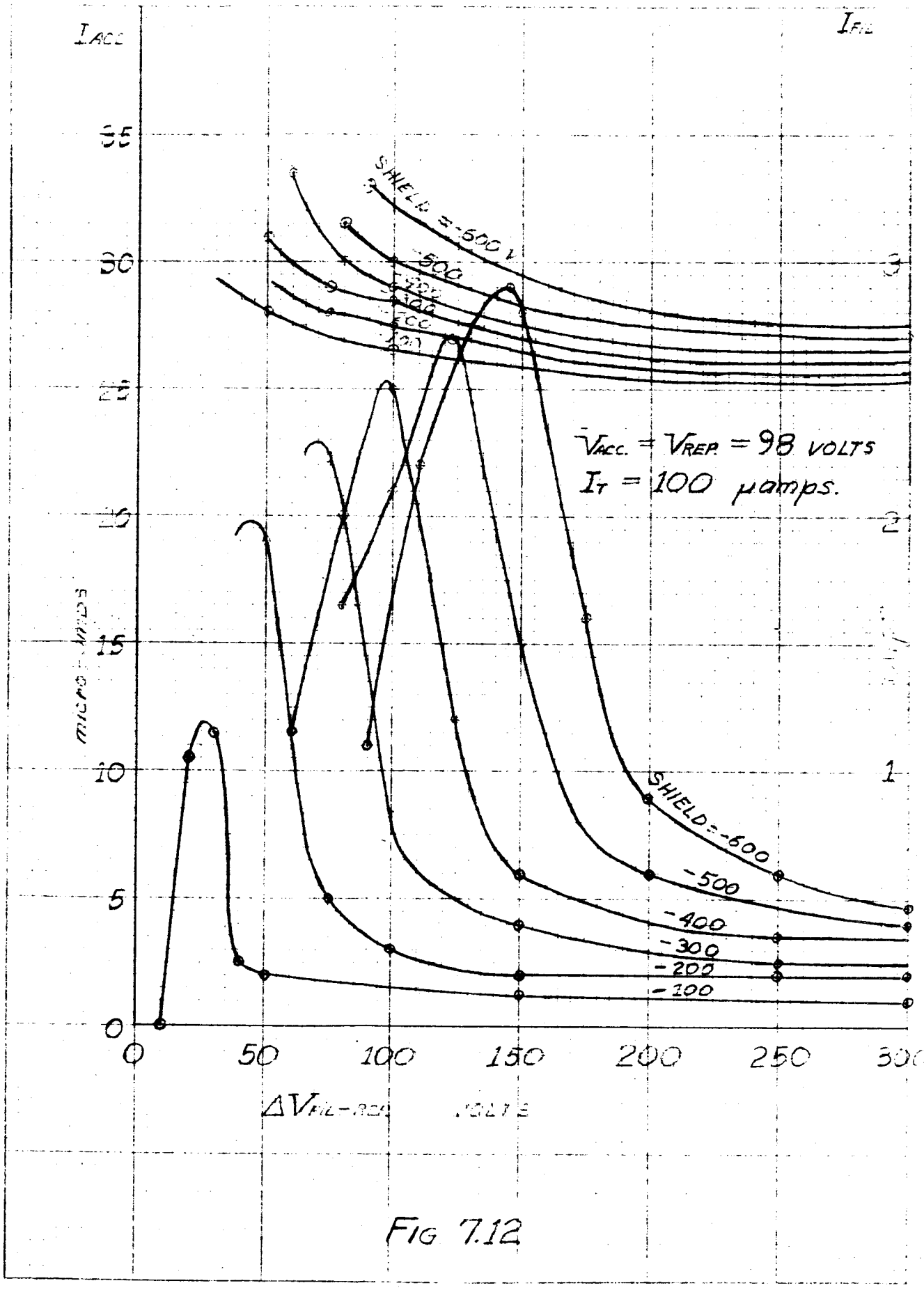
I_{ACC}
I_{FIL}
35
30
25
20
15
10
5
0
3
2
1
0
50
100
150
200
250
300
SHIELD = -600 V
-500
-400
-300
-200
-100
$V_{ACC.} = V_{REP.} = 98$ VOLTS
$I_T = 100$ μamps.
SHIELD = -600
-500
-400
-300
-200
-100

FIG 7.12

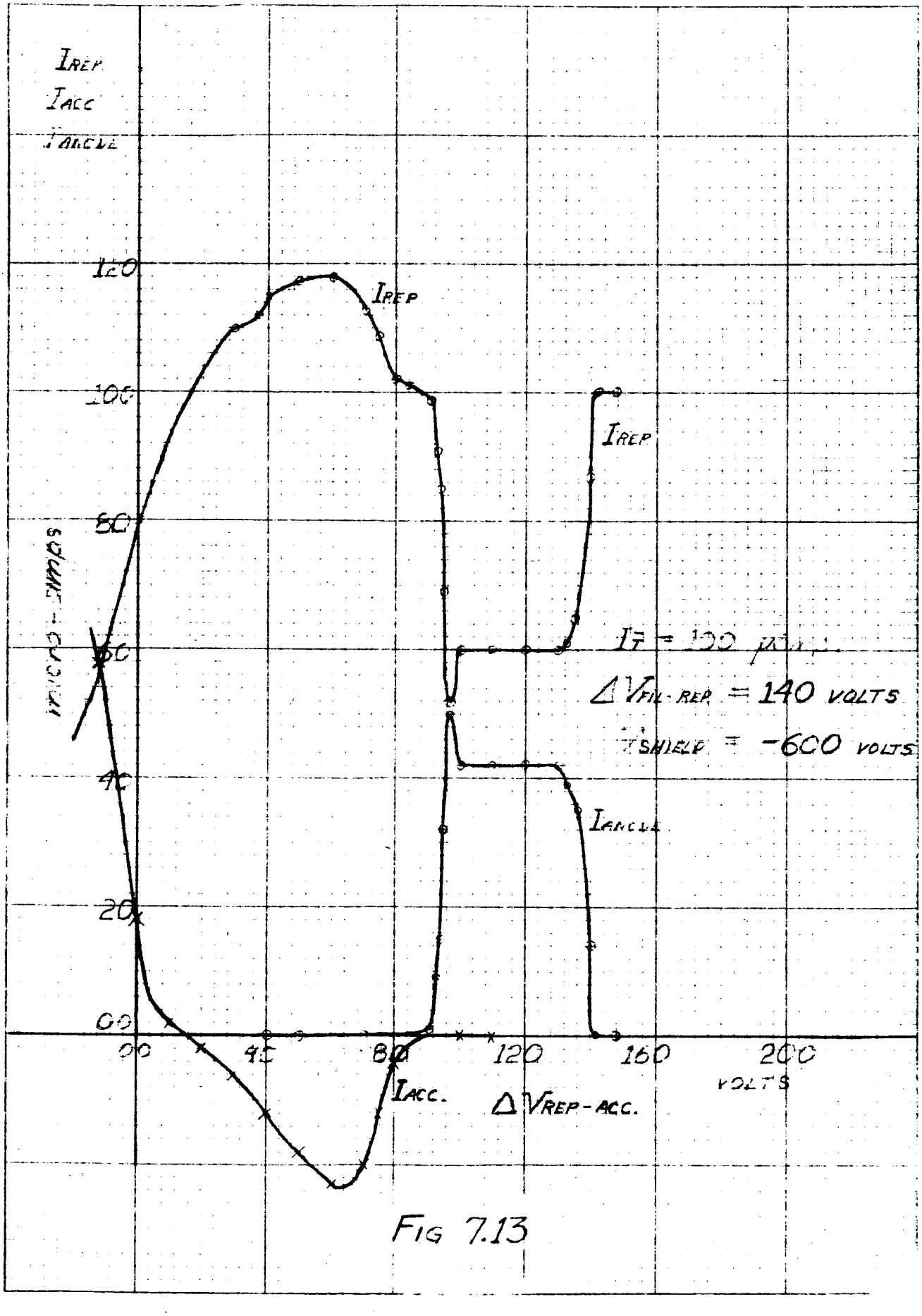
IREP
IACC
IARCLE
120
100
80
60
40
20
00
MICRO-AMPS
IREP
IREP
IT = 100 μA
ΔVFIL-REP = 140 VOLTS
VSHIELD = -600 VOLTS
IARCLE
00
40
80
120
160
200
VOLTS
IACC.
ΔVREP-ACC.

FIG 7.13

Ion Suppression Characteristic of Faraday Cage Collector

Fig 7.14

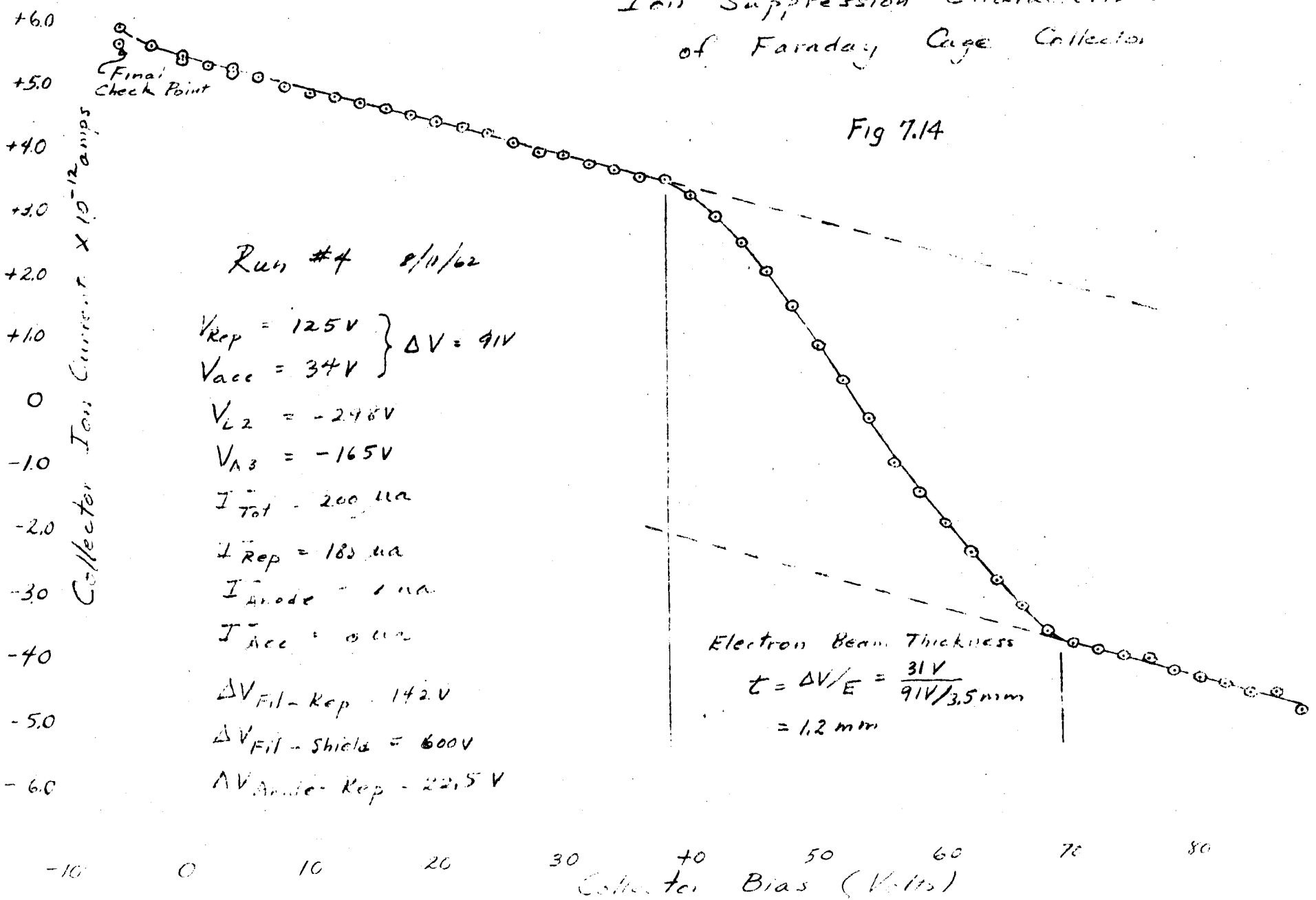

Run #4 8/11/62

V_{Rep} = 125 V
V_{acc} = 34 V
} ΔV = 91 V

V_{L2} = -246 V

V_{A3} = -165 V

I_{Tot} = 200 ua

I_{Rep} = 185 ua

I_{Anode} = 1 ua

I_{Acc} = 0 ua

$\Delta V_{Fil-Rep}$ = 142 V

$\Delta V_{Fil-Shield}$ = 600 V

$\Delta V_{Anode-Rep}$ = 22.5 V

Electron Beam Thickness

$t = \Delta V / E = \frac{31\ V}{91\ V / 3.5\ mm}$

= 1.2 mm

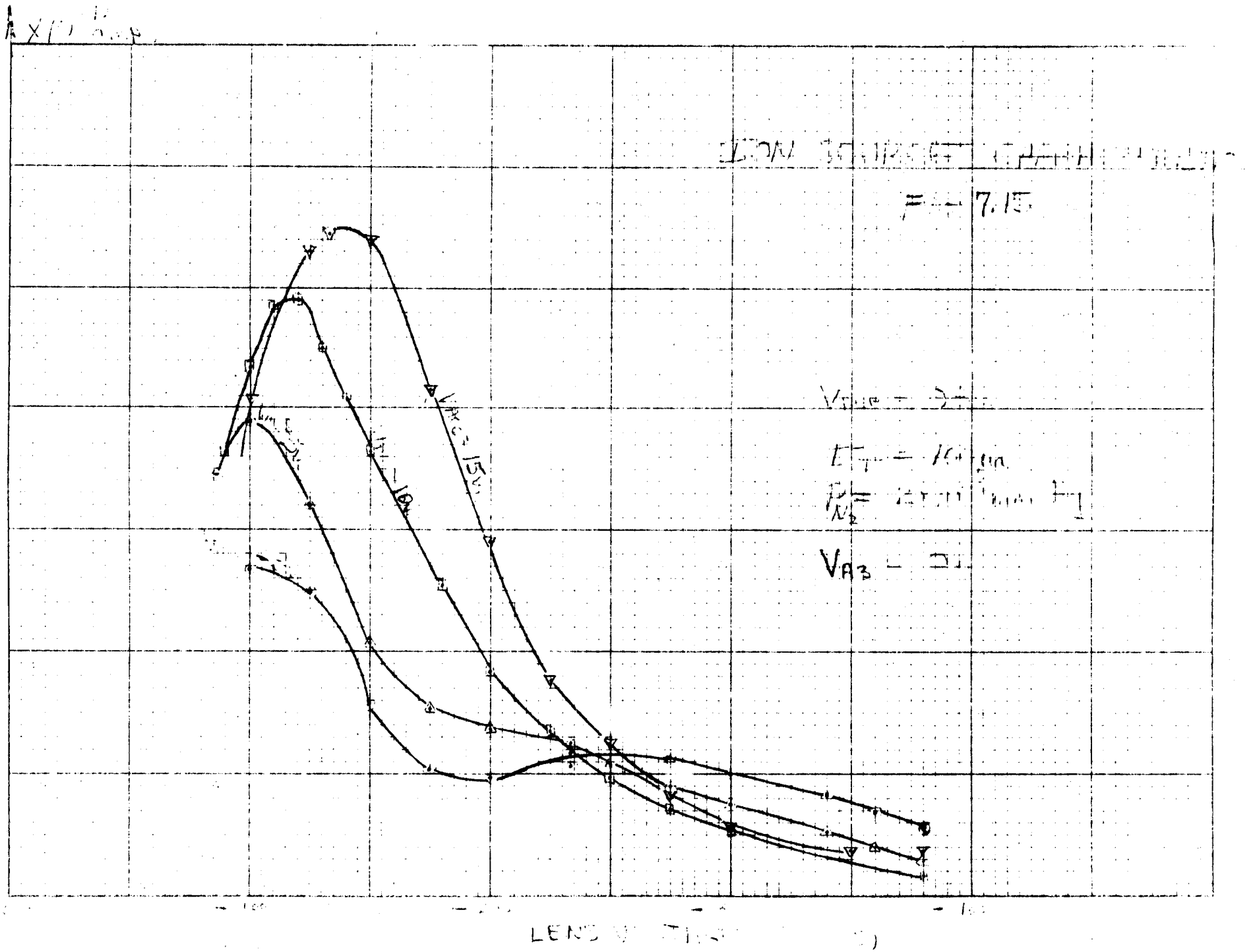

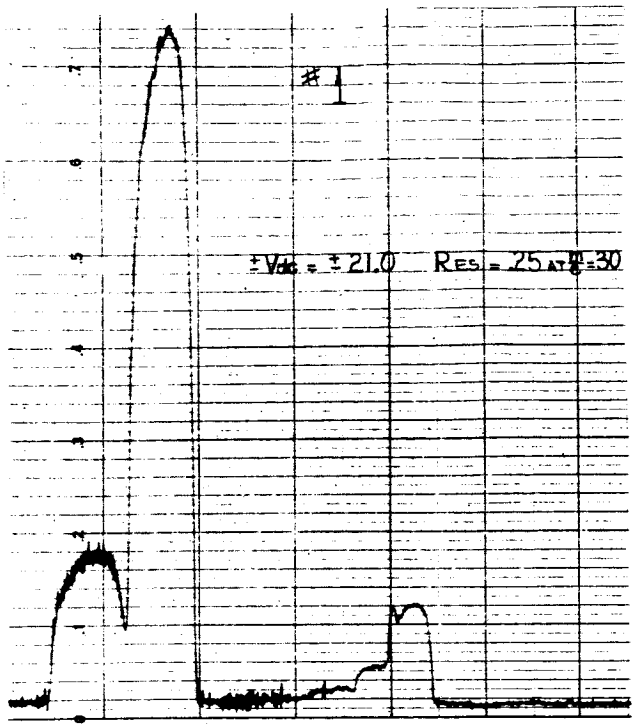

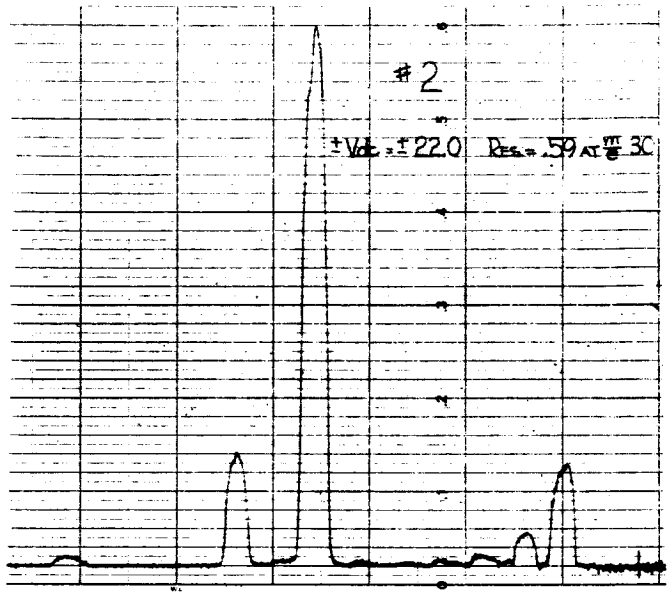

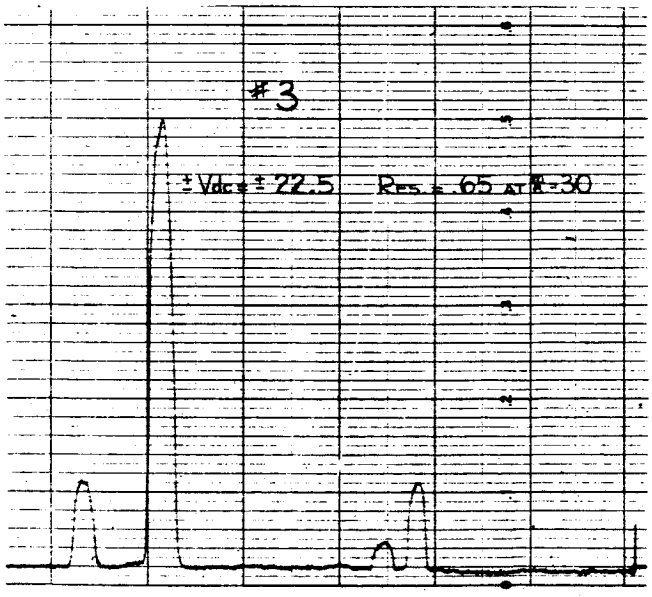

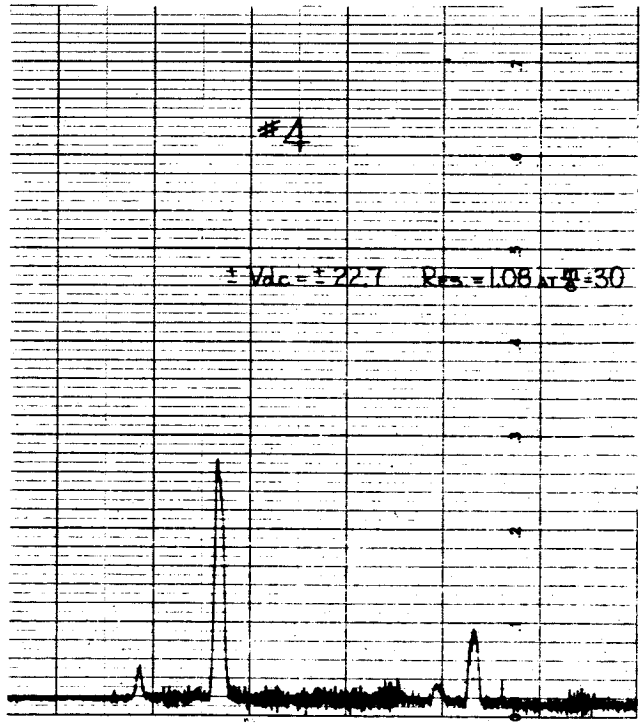

VARIATION OF Vdc/Vac RATIO

GROUND ADJUST NEGATIVE
P= 5×10^{-5} m.m.
I_A = 70μa
$.1 \times 10^{-10}$ AMPS FULL SCALE
$I_T^+ = 3 \times 10^{-12}$ a

V_{REP} = 112 V
V_{LENS} = -82 V
V_{A3} = -25 V,
V_{ACC} = 10.8 V
Δ V_{RA} = 101 V

FIGURE 7.16

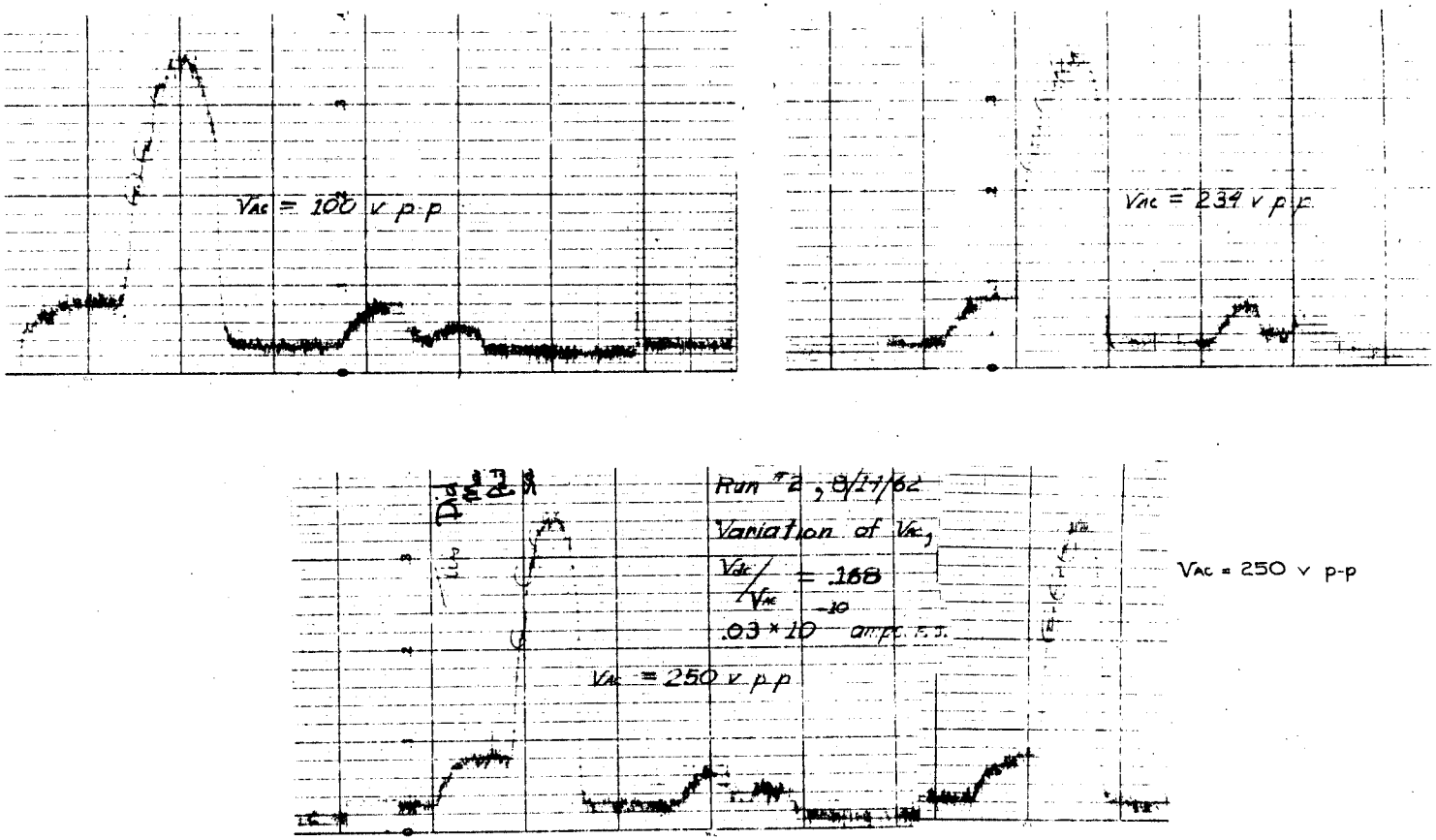
V_{ac} = 100 v p-p
V_{ac} = 239 v p-p
Run #2, 8/17/62
Variation of V_{ac},
V_{dc}/V_{ac} = .168
.03 × 10 amps F.S.
V_{ac} = 250 v p-p
V_{ac} = 250 v p-p

FIGURE 7.17

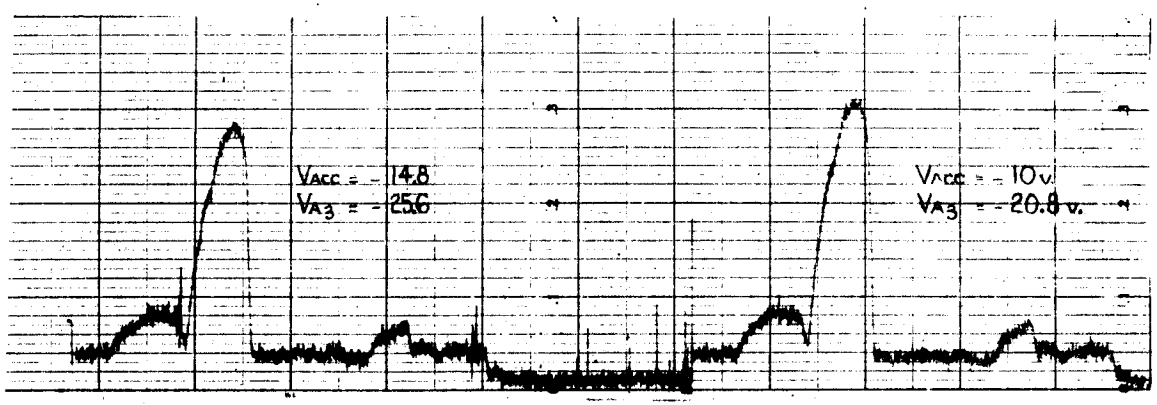

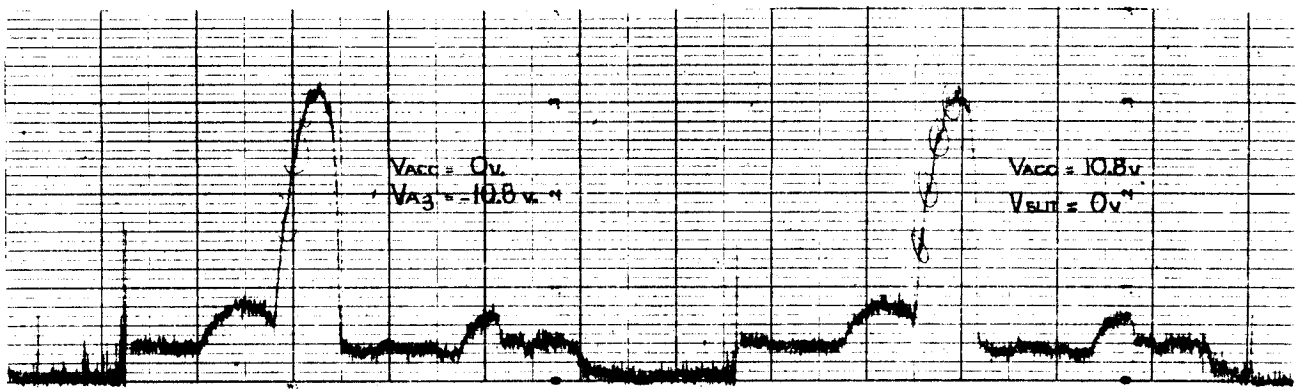

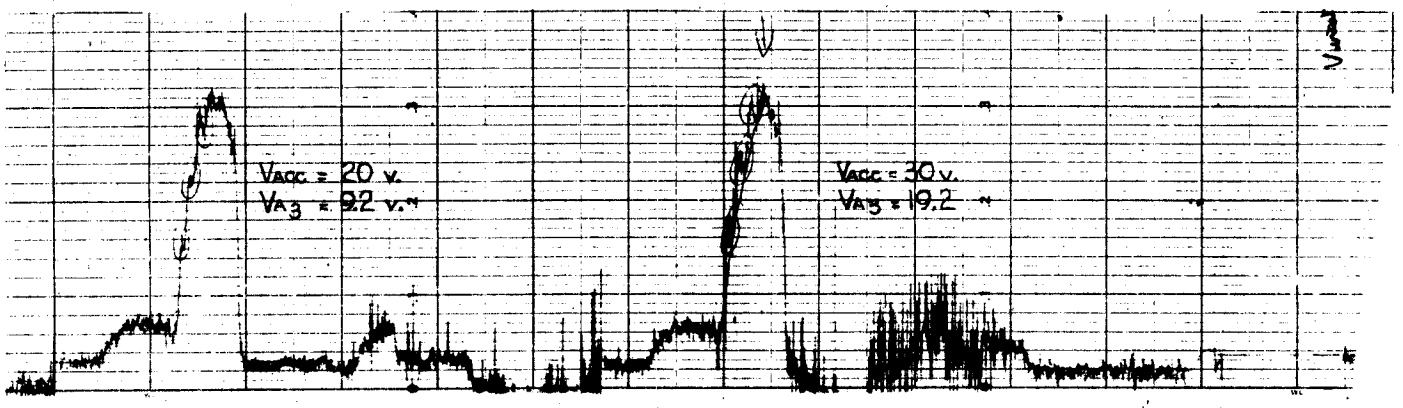

VARIATION IN SOURCE TO QUADROPOLE POTENTIAL
FIGURE 7.18

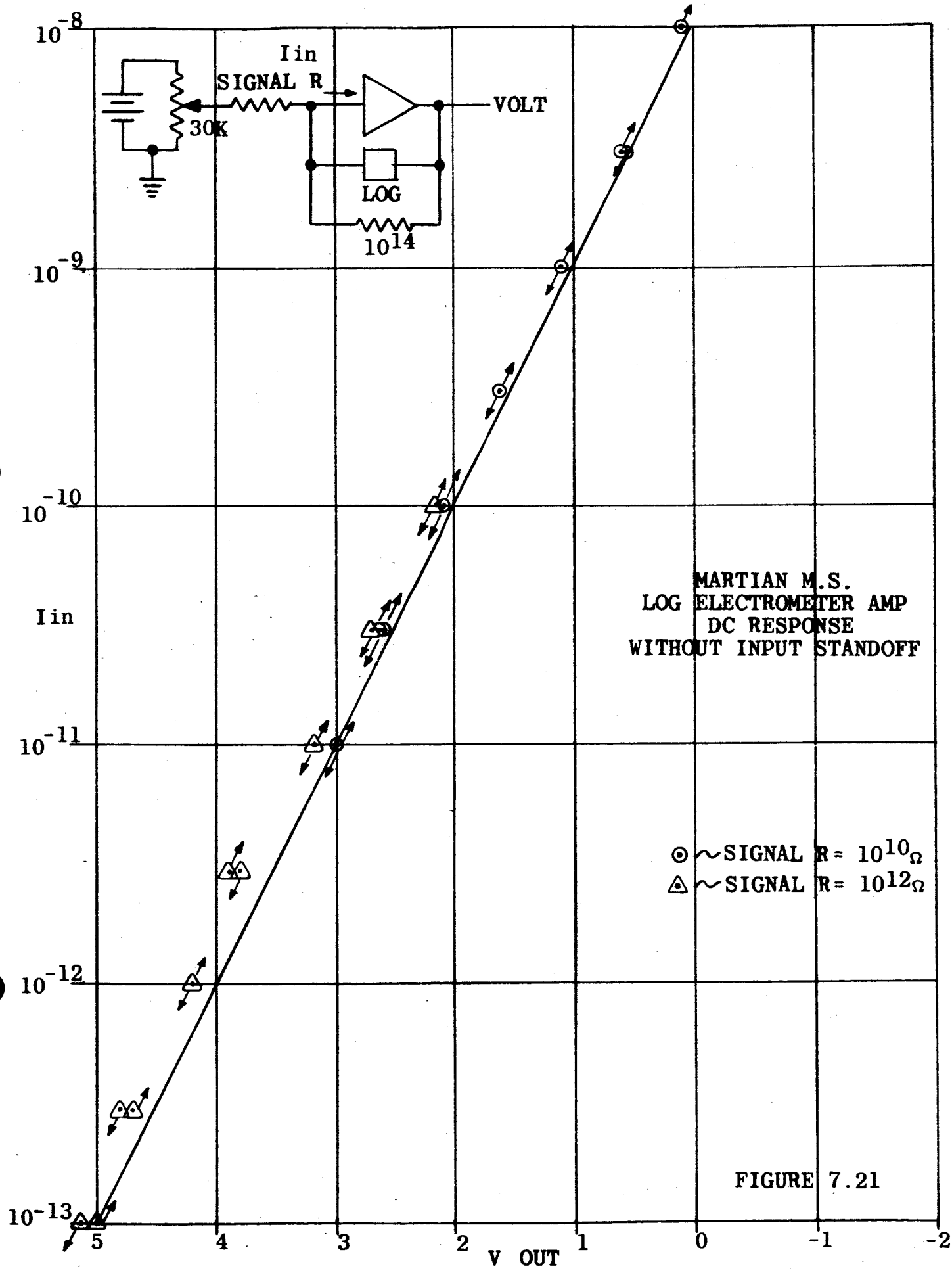
Iin
SIGNAL R
30K
VOLT
LOG
10^{14}
10^{-8}
10^{-9}
10^{-10}
10^{-11}
10^{-12}
10^{-13}
Iin
MARTIAN M.S.
LOG ELECTROMETER AMP
DC RESPONSE
WITHOUT INPUT STANDOFF
⊙ ~ SIGNAL R = $10^{10}\Omega$
△ ~ SIGNAL R = $10^{12}\Omega$
5
4
3
2
1
0
-1
-2
V OUT

FIGURE 7.21

GNW
JHS
8-3-62

EFFECTS OF ADJUSTING C_n ON THE LOG ELECTROMETER

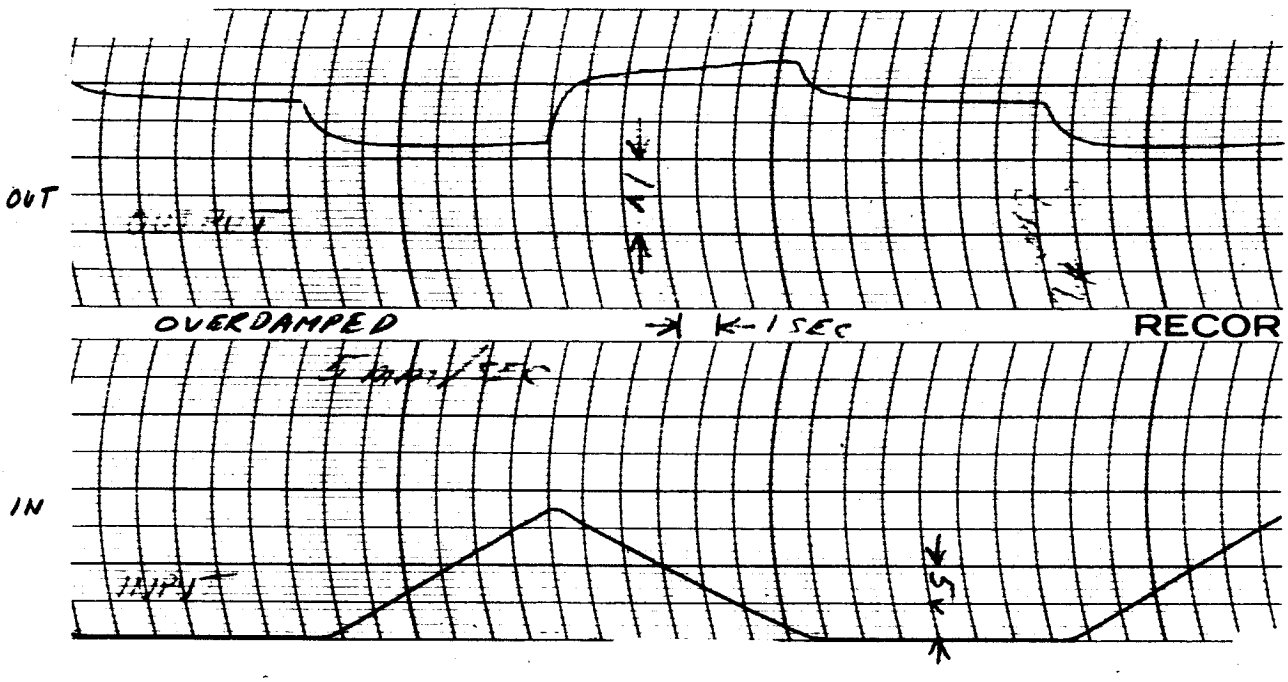

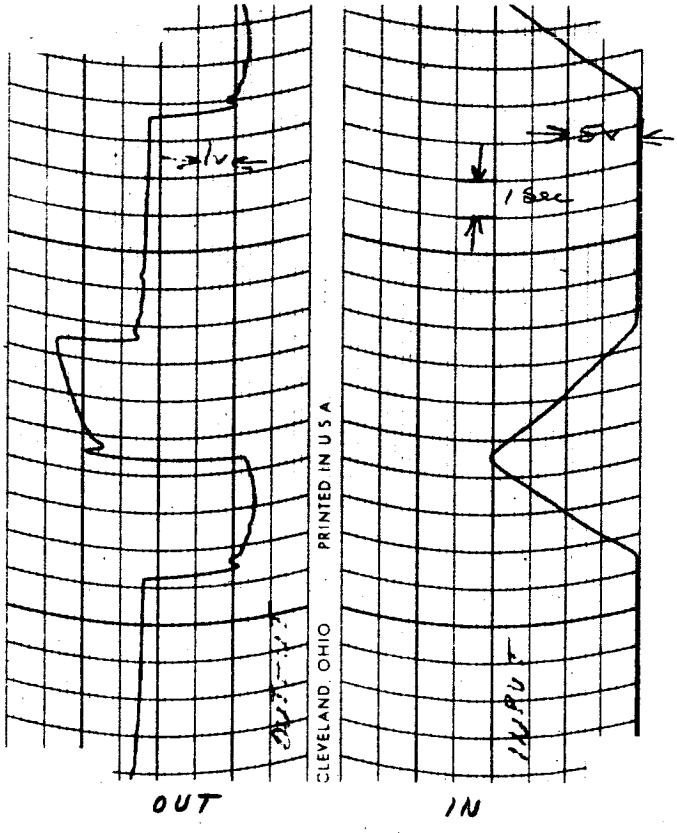

CRITICALLY DAMPED

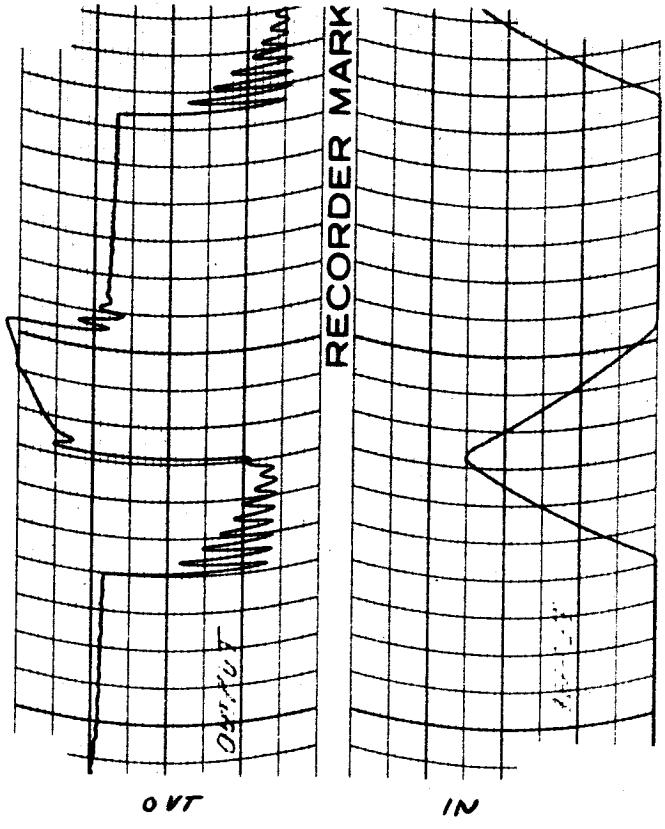

UNDER DAMPED

Figure 7.22

ELECTROMETER OUTPUT RECORDING

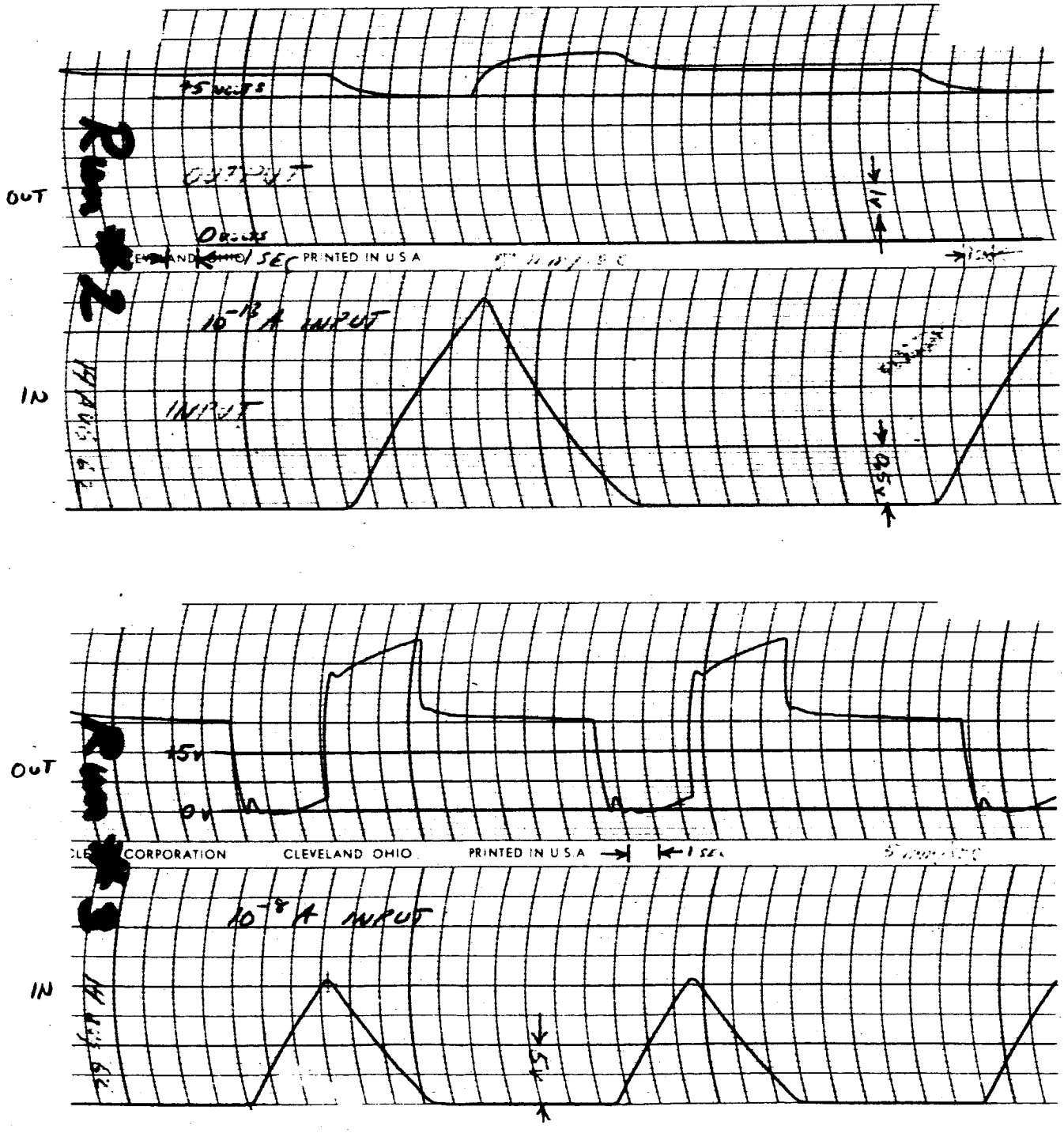

Figure 7.23

GNW
JHS
8-16-62

Log Electrometer AC Response

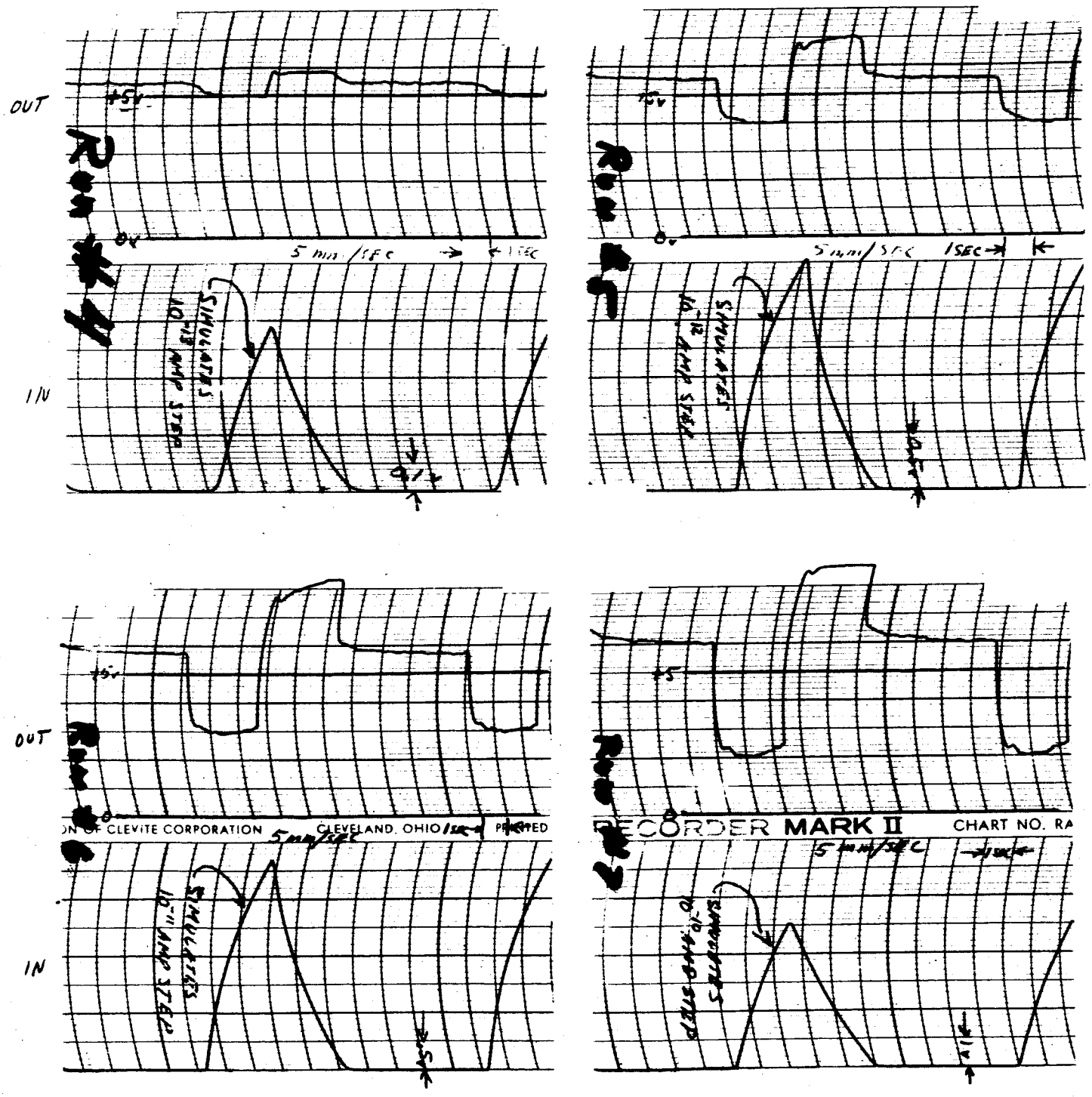

Figure 7.24

UHS
8-16-62

LOG ELECTROMETER AC RESPONSE

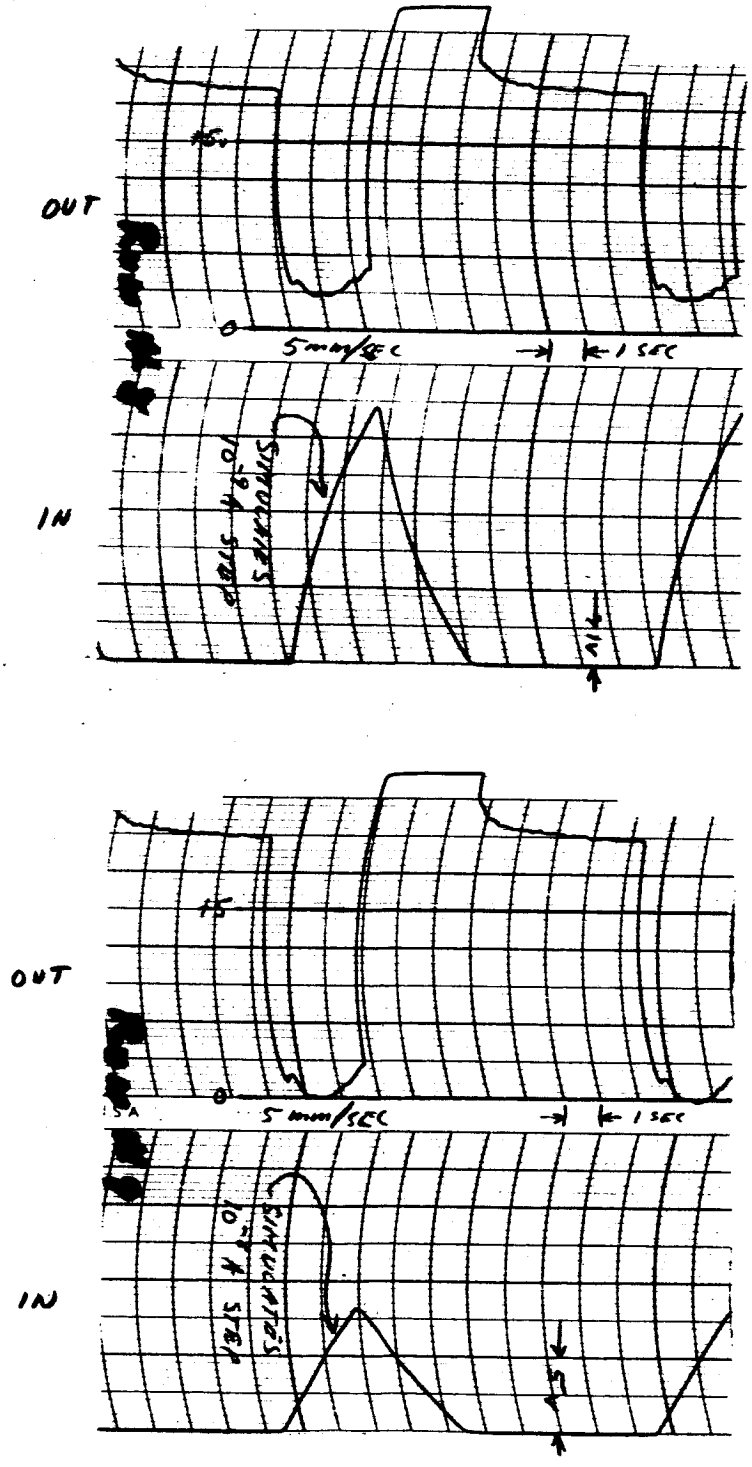

Figure 7.24

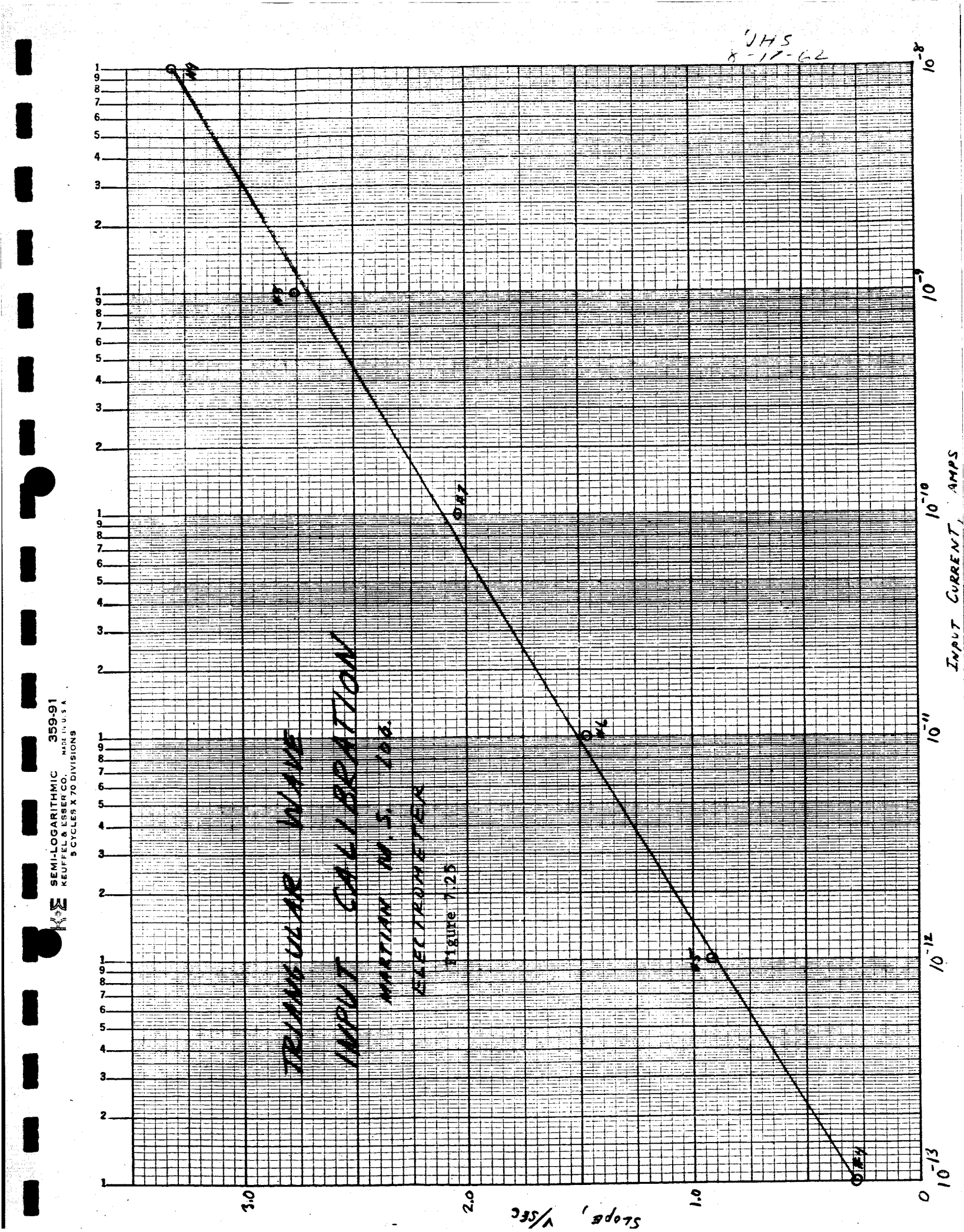
JHS
8-17-62
TRIANGULAR VOLUME
INPUT CALIBRATION
MARTIAN W.S. 108
ELECTRON METER
Figure 7.25
SEMI-LOGARITHMIC 359-91
KEUFFEL & ESSER CO. MADE IN U.S.A.
5 CYCLES X 70 DIVISIONS
Slope, V/sec
3.0
2.0
1.0
0
Input Current, AMPS
10^-8
10^-9
10^-10
10^-11
10^-12
10^-13

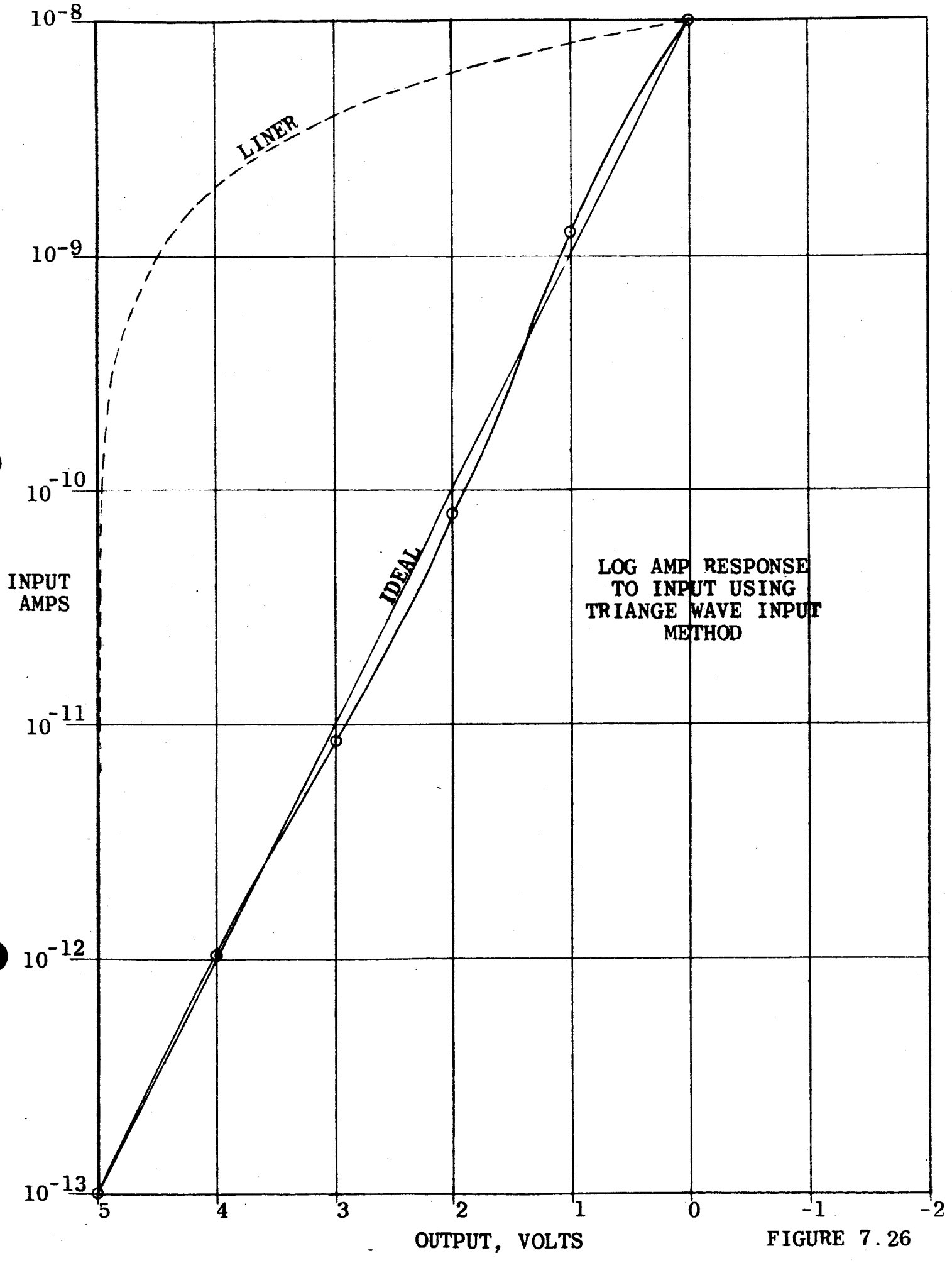
10^{-8}
10^{-9}
10^{-10}
10^{-11}
10^{-12}
10^{-13}
INPUT AMPS
LINER
IDEAL
LOG AMP RESPONSE TO INPUT USING TRIANGE WAVE INPUT METHOD
5
4
3
2
1
0
-1
-2
OUTPUT, VOLTS

FIGURE 7.26

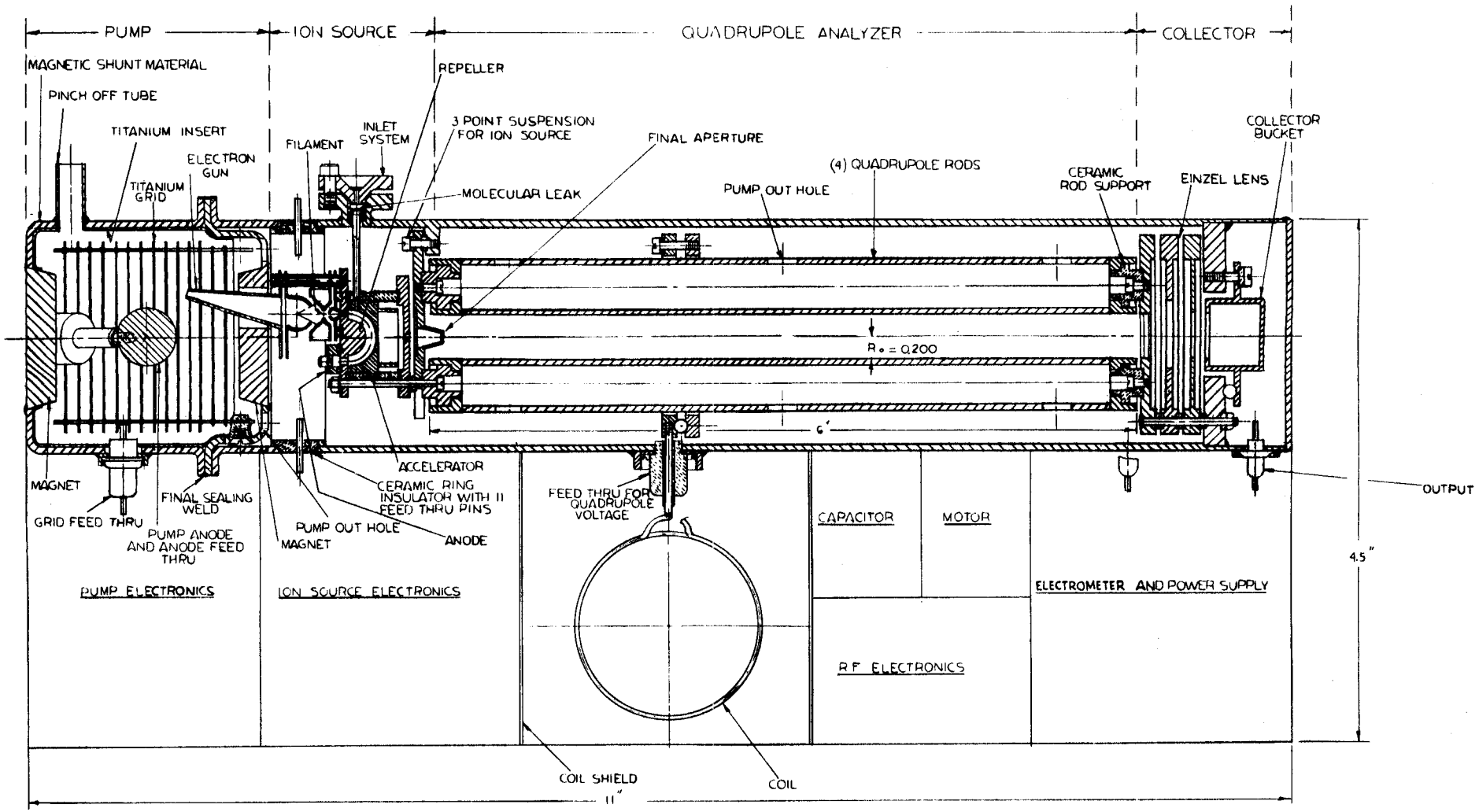

CONCEPTUAL DRAWING OF BREAD BOARD
MASS SPECTROMETER

FIG 8.11